CRANFIELD INSTITUTE OF TECHNOLOGY

School of Mechanical Engineering

Ph.D. THESIS

Academic Years 1974 - 1976

N.K. RIZK

STUDIES ON LIQUID SHEET DISINTEGRATION IN AIRBLAST ATOMIZERS

Supervisor: PROFESSOR A.H.LEFEBVRE

October, 1976

SUMMARY

The work in this thesis has been devoted to studying the influence of liquid film thickness on the characteristics of airblast atomizers. The research was carried out using two special atomizers that were both designed to produce flat liquid sheets which were atomized by high velocity air streams acting on both sides of the sheet. The liquid was injected through sintered plates in the first design, while the film issued from a variable gap slot in the second design.

The investigation was divided into the following phases :

(1) The different stages of the sheet disintegration were observed and recorded by means of a photographic technique which employed a very fast flash of 0.2 microsecond duration to allow detection of the formation of the short life ligaments on the atomizing edge. Various liquid solutions were used to ascertain the changes which might accompany the mechanism of disintegration due to the variation of the main liquid properties namely viscosity, surface tension and density. Also the effect of air velocity and sheet thickness were considered.

(2) Due to the importance of studying all the factors affecting the drop distribution of sprays from the viewpoint of evaporation and the problem of exhaust smoke, a set of experiments were conducted, and the corresponding drop distributions were obtained, by a photographic technique which had the advantage of not disturbing the spray.

(3) In the third phase the thickness of the liquid sheets were measured experimentally by a needle contact device and the results were compared with the thickness determined from some flow models and from theoretical analysis. The effects of air and liquid properties and a characteristic dimension of the atomizer were used to derive a dimensionally correct expression which could predict the thickness of the sheets encountered in airblast atomizers.

(4) The performance of the airblast atomizer was examined under the various conditions of air velocity and liquid flow rate for a predetermined sheet thickness which was kept constant by adjusting the slot gap width of the atomizer. Consequently, the influence of liquid sheet thickness on mean drop size was determined.

(5) It was considered essential to study the effect of air pressure for both liquids of low and high viscosity. Therefore air pressure was varied between 1 and 7.5×10^5 N/m^2 (about 1 to 7.5 atm) and the corresponding values of S.M.D. were measured.

All the measurements of mean drop size were carried out using the light scattering technique, and after careful consideration of the results obtained on the effects mentioned above, the following equation was derived :

$$S.M.D. = 0.5 \left(\frac{\sigma_l^{0.6} \rho_l^{0.25}}{\rho_a^{0.85} V_r^{1.2}} \right) (t)^{0.4} \left(1 + \frac{W_l}{W_a} \right)^{0.85} +$$

$$0.107 \left(\frac{\eta_l^2}{\sigma_l \rho_l} \right)^{0.45} (t)^{0.55} \left(1 + \frac{W_l}{W_a} \right)$$

in S.I. units

which is dimensionally consistent and covers wide ranges of air and liquid properties and film thicknesses.

ACKNOWLEDGEMENTS

The author would like to record his sincere appreciation of guidance, assistance and great interest given to him at every stage of this work by Professor A.H.Lefebvre.

The useful suggestions of Professor R.S.Fletcher and all the academic staff of the S.M.E. are gratefully acknowledged.

He wishes to express his gratitude to the supporting staff of the School of Mechanical Engineering and in particular to Mr. F.W.Pearman, Mr. D.C.Beattie and Mr. R.Wilson who provided every assistance possible. Thanks are also due to Mr. H.D.Bambury for his continuous help.

A special word of thanks to Mr. B.Hunt and the staff of the Photographic Department for their kind co-operation.

Many thanks to Mrs.Steen for her neat typing of this thesis.

CONTENTS

APPENDICES

LIST OF TABLES

LIST OF FIGURES

LIST OF PLATES

NOMENCLATURE

A	=	Cross section area of channel, cm^2
A.F.R.	=	Air/fuel mass flow ratio
A.L.R.	=	Air/liquid mass flow ratio
D	=	Diameter, cm
d_{32}	=	Volume to surface area mean diameter, micron
$\frac{dP}{dZ}$	=	Pressure gradient in direction of flow, N/m^3
$\frac{dv}{dX}$	=	Volume distribution
f	=	Friction factor
G	=	Mass flux, Kg/m^2s
$I(\theta)$	=	Intensity of light at angular displacement θ radiant
l	=	Prefilmer perimeter, cm
M.M.D.	=	Mass median diameter ($\simeq$ 1.2 S.M.D.), micron
n	=	Number of drops, the diameter of which is X
P	=	Pressure, N/m^2
$\frac{\partial P}{\partial n}$	=	Pressure gradient in direction normal to the stream line, N/m^3
Q	=	Volume flow rate, m^3/s
q	=	Distribution parameter in Rosin-Rammler equation
r	=	Photomultiplier traverse distance corresponding to 1/10th $I(\theta)$
R_e	=	Reynolds number = $\frac{\rho VD}{\eta}$
S	=	Periphery of channel, cm
S.M.D.	=	Sauter mean diameter, micron = $\frac{\Sigma nX^3}{\Sigma nX^2}$
t^+	=	Dimensionless film thickness = $\frac{u_* \rho_l t}{\eta_l}$
t	=	Liquid film thickness, cm
u	=	Velocity, m/s
u_*	=	Friction velocity = $(\tau_o/\rho)^{\frac{1}{2}}$, m/s
U.L.D.F.	=	Upper limit distribution function

V = Velocity , m/s

v = Volume fraction of drop material occurring in drops of diameter less than X

W = Mass flow rate, gr/s

W_e = Weber number = $\frac{\rho V^2 D}{\sigma}$

X = Droplet diameter, micron

$\bar{X}$ = Size parameter in Rosin-Rammler equation, micron

y = Distance measured from solid boundary in the liquid film, cm.

GREEK SYMBOLS

σ_l = Liquid surface tension, N/m (= 10^3 dyn/cm)

ρ = Density, Kg/m^3 (= 10^{-3} gr/cm^3)

η = Absolute viscosity, Kg/ms (= 10^3 centipoise)

ν = Kinematic viscosity, m^2/s (= 10^3 centistokes)

μ = Micron ($1\mu = 10^{-3}$mm)

θ = Angular displacement of monochromatic light beam, rad

λ = Wavelength, Angstroms

ε = Energy associated to droplets, Nm

α = Fraction of channel area occupied by gas phase

τ = Shear stress, N/m^2

ϕ = Parameter in Lockhart-Martinelli model

χ = Curvature of streamline, m^{-1}

δ = Parameter related to standard deviation in ULDF

SUBSCRIPTS

a	=	Air
e	=	Equivalent
g	=	Gas
H	=	Homogeneous
i	=	Interface
l	=	Liquid
m	=	Maximum
o	=	Wall
TP	=	Two phase

CHAPTER 1

INTRODUCTION

CHAPTER 1

INTRODUCTION

In recent years the need for more efficient and reliable gas turbine engines for both aircraft and industrial installations has led to intensive research in this field to establish the main design rules for the different components of the gas turbine engine. Now the development of combustion chamber performance depends largely on the factors affecting combustion within the chamber itself. The rate of heat release, the aerodynamics of the chamber, ignition and fuel injection are some examples of these important factors.

The function of the fuel injector, which is the main concern of the present work, is to deliver finely atomized and uniformly distributed fuel to the primary zone of the flame tube in order to enhance the rate of heat release and obtain fairly uniform outlet temperature traverse. Also, in order to satisfy the new legislation on pollutions control, special attention must be given to the quality of atomization. The most common method of producing a spray is to force the fuel under pressure through an orifice after imparting swirl to the emerging fuel jet to increase the spray angle. However, due to the various problems associated with this type of atomizers, such as the need for a special pump to produce a very wide range of fuel flow, and the sensitivity of outlet temperature traverse to any change in fuel flow rate, the idea of using the available energy in the air to atomize the fuel, is very attractive.

Airblast atomization is a simple process in which the fuel is introduced into the high velocity air stream in the form of discrete jets, or as a thin attenuated sheet of uniform thickness which is shattered into drops by the air at the atomizing edge. In some recent designs that fall into the first group the fuel jet is atomized by means of two or three annular and concentric air flows impinging on the jet instead of using only one air stream coaxial with the fuel jet as in the case of Nukiyama and Tanasawa's airblast atomizer (Ref.74). These new designs have given very fine and uniform sprays which again supports the effectiveness of the airblast atomizer as a proper means of fuel injection.

The fuel sheet can be formed in many ways. In Lefebvre and Miller's design (Ref.61) the fuel was supplied from a number of tangential ports to a swirl chamber from which it spilled over a weir to form a thin sheet. In the N.G.T.E. airblast atomizers used in Wigg's tests (Refs. 89 and 90) the liquid was fed along an inner annulus, passed through a double-start square thread into a swirl chamber then flowed outwards on the surface of the inner body as a thin sheet to meet the axial high velocity air stream at right angles to the axis. The spinning cups is another way of producing liquid sheets by the action of centrifugal force which also helps the film to flow outwards at the cup rim to be atomized by the moving-fast air surrounding the cup.

In order to obtain good atomization quality it has been found desirable to subject both sides of the liquid film to high velocity air streams in order to provide maximum physical contact between the air and the fuel, and several atomizers have been designed to meet these requirements. As an example, in Rizkalla-Lefebvre's atomizer (Refs. 78, 79 and 80) the liquid flows through tangential ports into a weir from which it spreads over the prefilming surface. The inner air stream flows through the central circular duct over the liquid film and is then deflected radially outwards by a pintle before striking the inner surface of the film. The other air stream flows through an annular passage surrounding the main body of the atomizer to meet the outer surface of the liquid sheet.

Objective of the Present Work

Due to the importance of the liquid sheet as a factor affecting the quality of atomization it was decided to study the conditions that govern the formation of the sheet, and to what extent its thickness influences the mean drop size of the sprays produced by airblast atomizers. The mechanism of liquid sheet disintegration when subjected to high velocity air streams was also investigated thoroughly to find out the changes which might accompany the different stages of this mechanism under the various conditions of air and liquid properties.

Since combustion systems in gas turbine engines experience a wide range of conditions it was also decided to study the effects of air and liquid properties upon atomization quality. Finally, a general formula for mean drop size was derived which took into account all the forementioned factors over the ranges encountered in practical combustion chambers, to provide a general design basis for airblast atomizers.

CHAPTER 2

LITERATURE REVIEW

CHAPTER 2

LITERATURE REVIEW

Due to the increase of interest in using airblast atomizers for spraying fuel into the combustion chambers of gas turbine engines, much research has been done to reveal its performance and the sort of factors which might be involved in the atomization process. As there is insufficient space here to mention all the informations included in the literature, only the most relevant work will be discussed.

2.1. Nukiyama and Tanasawa (Ref.74)

These early investigations were conducted to show how the performance of the mist-producing apparatus (Fig.1) varied in relation to the relative velocity of air and liquid, the air density and the physical properties of the liquid. It was concluded that the final diameters of the droplets was independent of the size of the water and air nozzles but was determined by the quantity-ratio and relative velocity of the air and water. If the weight of air used was raised to about five times that of the water, it was found that the increase ceased to have any effect.

The authors determined the droplet size by microscopically photographing droplets of high surface tension when sprayed into some kind of oil. Now in order to evaluate the efficiency of atomization it is necessary to average out the droplets of various sizes in the spray in terms of droplets of normalized mean diameter d_o, which could be defined in many different ways. They accepted the definition that the summation of the areas and volumes should be equated as follows :

$$d_o \text{ or } d_{32} = \Sigma nX^3 / \Sigma nX^2 \qquad (1)$$

where n is the number of droplets of diameter X .

Nukiyama and Tanasawa used their experimental data on liquids of different surface tension, viscosity and density to obtain the following expression for the Sauter mean diameter, (d_{32}), in microns :

$$S.M.D. = 585 \frac{\sqrt{\sigma_1}}{V_r \sqrt{\rho_1}} + 597 \left(\frac{\eta_1}{\sqrt{\sigma_1 \rho_1}} \right)^{0.45} \cdot \left(1000 \frac{Q_1}{Q_a} \right)^{1.5} \qquad (2)$$

where V_r is the relative velocity, in m/s, of air and liquid, and Q_1 and Q_a are the volumes of liquid and air flowing.

The experimental ranges were :

ρ_l = liquid density, from 0.8 to 1.2 gr/cm^3

σ_l = liquid surface tension, from 30 to 73 dyne/cm

η_l = liquid viscosity, from 1 to 30 centipoise.

The equation is dimensionally incorrect, however it allows some important conclusions to be drawn. It shows that the effect of liquid viscosity is of little importance at large values of the ratio (Q_a/Q_l) and the droplet size is mainly governed by the relative velocity. At lower values of (Q_a/Q_l) the importance of the first term on the right hand side of equation (2) is reduced, and consequently the influence of the surface tension. The equation does not take into account the effects of air properties, hence its use is limited to the standard atmospheric conditions.

Nukiyama and Tanasawa conducted some tests to find out whether the range of droplet sizes followed some distribution law and they also studied the stages of liquid jet disintegration. These aspects will be discussed later in the relevant chapters.

2.2. Wigg

The effect of scale on fine sprays produced by large airblast atomizers was studied by Wigg (Refs.89 and 90) using various N.G.T.E. systems as illustrated in Fig.2. Three atomizers were made to the same design with values of D of 1.27, 2.54 and 3.59cm. Carbon tetrachloride was added to gear oil until its specific gravity was unity and was used in the bottom of a small beaker to collect the sample. Wigg expressed the variation of mass median diameter (≃ 1.2 S.M.D.) with water/air ratio by the relationship

$$M.M.D. = 4 + (58 + 55\ D^{1.5}) \ / \ (W_a/W_l) \qquad (3)$$

where D = diameter of the inner body. He found that atomizer scale affected the atomization only through its influence on liquid and air flow rates. He also observed no appreciable effect of water pressure (between 20 and 60 psig), and atomizing air temperature (between 290°K to 330°K) on the quality of atomization.

Wigg, in trying to formulate an empirical correlation, stated that when liquid is atomized energy is required to form new surface and to overcome viscous forces, hence considering the loss of kinetic energy and the recombination of water droplets he suggested the following expression :

$$M.M.D. = 2300 \left[\eta_l^{0.5} . W_l^{0.05} . (1+W_l/W_a)^{0.5} / V_{rel} \right] . \left[1+2(W_l/W_a)^{0.7} . W_l^{0.25} \right] \qquad (4)$$

The correlation does not consider the effect of air or liquid density, liquid surface tension and atomizer characteristic dimension on M.M.D.

In a further work, Wigg (Ref.90) used the results from the three atomizers together with those from four other atomizers to derive the following dimensionally consistent formula :

$$M.M.D. \doteq 200 \frac{\nu_l^{0.5} W_l^{0.1} (1 + W_l/W_a)^{0.5} h^{0.1} \sigma_l^{0.2}}{\rho_a^{0.3} V_{rel}} = 200\ N \quad (5)$$

where h = height of air annulus at point of impact, cm. The coalescence of droplets was accommodated by term to the previous equation, as follows:

$$M.M.D. = 200\ N\ (1 + 2.5\ (W_l/W_a)^{0.6}\ W_l^{0.1}) \quad (6)$$

which is now dimensionally incorrect. The range of variable covered was narrow. When the above equations are applied to find the droplet sizes for water and kerosine the predictions seem very close, which does not agree with experimental observations which always give lower values of mean droplet size for kerosine. However, Wigg's work is important for its contribution to a better understanding of the factors involved in the process of airblast atomization.

2.3. Other Important Work on Airblast Atomization

Radcliffe and Clare (Ref.76), used two similar atomizers of different sizes (Fig.3), along with Mothball fuel heated to a temperature such that its viscosity was either 10, 20 or 40 centistokes. They studied the effect of fuel pressure, air pressure, fuel viscosity and fuel gap on atomizer performance. It was stated that the droplet size depended upon the AFR, and that the air pressure and fuel gap only affected droplet size by altering the AFR. They found that for a given AFR, the droplet size was proportional to the square root of the orifice size.

Lefebvre and Miller (Ref.61) used four different types of airblast atomizer to study their effect on atomization quality. They concluded that minimum drop sizes could be achieved by applying high velocity air on both sides of the liquid sheet leaving the atomizing lip. They emphasized the importance of air velocity on fuel atomization and found that varying the AFR at constant air velocity had little effect. They explained the effect of AFR on droplet size by its influence on fuel sheet thickness:- a thicker sheet will tend to increase the thickness of the ligaments and hence the final drop size.

Hrubecky (Ref.51) showed experimentally the importance of injecting the liquid parallel to the air flow to obtain the best degree of atomization. The values of air to fuel volume ratio used in his tests ranged from 1000 to 10,000, which were very high. Air velocity varied from 106 to 316 m/s. Droplet diameters fell in the range from 2 to 250 microns.

Gretzinger and Marshall Jr. (Ref.45) investigated the effect of airblast atomization on droplet size using two types of atomizer, (a) a converging airblast nozzle which was similar to that used by Nukiyama and Tanasawa, and (b) an impingement type. They produced sprays of an aqueous solution of a black dye sampled in mineral oil and found that the smallest drops were formed on the side of the liquid sheet in intimate contact with the gas stream. Large drops were formed on the opposite side of the liquid sheet, thus emphasizing the need for exposing the liquid sheet on both sides to high velocity air to achieve maximum break-up. They suggested the following expressions :

$$\text{M.M.D.} = 2600 \left\{ \left(\frac{W_l}{W_a} \right) \cdot \left(\frac{\eta_a}{V_a L} \right) \right\}^{0.4} \qquad (7)$$

for the converging airblast nozzle, and

$$\text{M.M.D.} = 122 \left(\frac{W_l}{W_a} \right)^{0.6} \cdot \left(\frac{\eta_a}{V_a L} \right)^{0.15} \qquad (8)$$

for the airblast impinging nozzle ,

where L = diameter of wetted periphery between the air and liquid streams.

These correlations are limited to fluids whose physical properties are similar to those used in the tests and are invalid outside the range of M.M.D. from 5 to 30 microns.

The problems of heavy fuel atomization are discussed in Heath and Radcliffe's report (Ref.48). It was not possible to vaporise a residual fuel, and their only alternative was to atomize it using an airblast atomizer, since swirl atomizers could not be expected to work well with fuels of more than 20 centistokes viscosity. They concluded that increasing fuel pressure, viscosity, fuel gap, in which fuel moved radially inwards to the atomizing section, led to higher mean diameter, but the mean diameter would reduce with higher air pressures.

Godbole (Ref.43) studied the effect of ambient pressure on airblast atomizer performance and found that above 30 p.s.i.a. the S.M.D. of sprays reduced according to a power law with an index = -0.6. From 15 to 30 p.s.i.a. there was an increase in S.M.D. with increase in ambient pressure. Above 50 p.s.i.a. there was no significant effect of increasing AFR on mean drop size. The mean value of n in the power law $\text{S.M.D.} \alpha V_a^n$ was (-1.05) where V_a is the air velocity. He found that above AFR of 2.5 there was no significant change in S.M.D. with AFR, but very large changes occurred for AFR's below 1.5.

Fraser, Eisenklam and Dombrowski (Ref.39) recommended twin fluid atomizers for dealing with viscous fluids where the liquid is difficult to disintegrate. They stated that producing small drops at lower working pressures and velocities is possible by designing the nozzle so

that the liquid is spread into a thin sheet.

Jenkins and Booker (Ref.53) determined experimentally the time required for high speed airstreams to disintegrate water drops as :

$$t_s = 20 \; D_o/V_a^{0.72} \qquad (9)$$

where t_s = disintegration time in seconds, D_o = initial drop size in feet and V_a is the air velocity in ft/s.

Miesse (Ref.71), discussing recent advances in spray technology, reported that any two of the three dimensional ratios, Reynolds number (R_e), Weber number (W_e) and Ohnesorge number (Z), are sufficient to provide correlations of the experimental data on atomization, where;

$$R_e = \frac{\rho V t}{\eta}$$

$$W_e = \frac{\rho V^2 t}{\sigma} \qquad (10)$$

and $$Z = \frac{W_e^{\frac{1}{2}}}{R_e} = \frac{\eta}{(\rho t \sigma)^{\frac{1}{2}}}$$

and t is the thickness of liquid stream. The mean diameter (D) of the spary is characterized by the Weber number as follows :

$$\frac{D}{t} = \frac{f(R_e)}{W_e^{1/3}} \qquad (11)$$

where f(R) is a function of Reynolds number which allows for the effects of viscosity. For flat and conical sprays $f(R_e)$ was found to be essentially constant. He also reported the inverse variation of average drop size with the square root of the Weber number. Miesse stated that when a droplet is subjected to a high velocity air stream it will be shattered if the kinetic energy of the air stream exceeds the surface energy of the droplet. Therefore the critical Weber number may be expressed as follows :

$$W_c = 4.25 \times 10^4 \times R_e^{-0.4} \qquad (12)$$

Weiss and Worsham (Ref.88) found that the most important factor controlling the mean droplet size for an airblast liquid spray was the relative air velocity, while the physical properties of the liquid had less effect upon the fineness of the spray. The range of droplet diameters found in a spray depended on the range of excitable wavelengths on the surface of the liquid sheet, the short wavelength limit was due to viscous damping while the long wavelengths were limited due to inertia. Based on these arguments they concluded that :

$$\text{S.M.D.} \quad \alpha \quad V_r^{-4/3}$$

$$\alpha \quad \sigma_l^{1/3}$$

$$\alpha \quad \rho_a^{-2/3} \qquad (13)$$

$$\alpha \quad \eta_l^{2/3}$$

Their experimental results confirmed the dependence predicted for air velocity, but gave slightly different indices for the effects of liquid properties.

2.4. Rizkalla - Lefebvre

Recently, another important contribution to the study of airblast atomization has been made by Rizkalla and Lefebvre (Refs.79 and 80). They investigated the performance of a specially-designed airblast atomizer which was more representative of current practice in gas turbine engines (Fig.4). In this design the liquid flows through six equispaced tangential ports before it is spread into a thin sheet on the prefilmer and then exposed on both sides to high velocity air in a manner calculated to provide maximum physical contact between the air and fuel streams. They devoted the first phase of the work (Ref.79) to studying the influence of liquid physical properties on mean drop size. Measurements of drop size were made using the light scattering technique first suggested by Dobbins et al (Ref.27).

The experimental conditions covered the following ranges :

Liquid surface tension,	- 26 to 73 dyne/cm
Liquid absolute viscosity,	- 1.3 to 124 centipoise
Liquid density,	- 0.8 to 1.8 gr/cm^3
Atomizing air velocity,	- 60 to 125 m/s

The optical apparatus used is described in Ref.78 and shown in Fig.5. Experimental analysis led to the following empirical expression

$$\text{S.M.D.} = 521 \frac{\sigma_l^{0.5} \rho_l^{0.75}}{V_a} (1 + \frac{W_l}{W_a}) + 0.037 \eta_l^{0.85} (\sigma_l \rho_l)^{1.2} (1 + \frac{W_l}{W_a})^2 \qquad (14)$$

This equation was based on results obtained at atmospheric air pressure which raised the question of the effect of higher ambient pressure on droplet size, thus they undertook the second phase of their research programme (Ref.80) using the same atomizer. The two liquids used were kerosine and water and the tests were conducted at constant levels of air velocity and temperature over a range of ambient air pressure from 10^5 to 10^6 N/m^2. By plotting the data obtained as log (SMD) versus log (Air pressure) the slopes of the resulting straight lines gave mean value of 1. Unfortunately, no data were obtained on the effect of high ambient pressure on droplet size for liquids of higher viscosities.

Taking into account the effects of all the variables studied, they were able to derive the following dimensionally consistent formula:

$$S.M.D. = A \frac{(\sigma_l \rho_l t)^{0.5}}{V_a \rho_a} (1 + \frac{W_l}{W_a}) + B \left(\frac{\eta^2}{\sigma_l \rho_a}\right)^{0.425} t^{0.575} (1 + \frac{W_l}{W_a})^2 \qquad (15)$$

where A and B are constants and t is the liquid film thickness at the prefilming lip. Because the liquid film thickness was not measured, the assumption was made that the liquid film thickness was proportional to the diameter of the prefilmer 'D'. They then rewrote the equation in the form :

$$S.M.D. = 0.33 \frac{(\sigma_l \rho_l D)^{0.5}}{V_a \rho_a} (1 + \frac{W_l}{W_a}) + 0.157 \left(\frac{\eta^2}{\sigma_l \rho_a}\right)^{0.425} D^{0.575} (1 + \frac{W_l}{W_a})^2 \qquad (16)$$

This formula covers wide ranges of air velocity and liquid properties and predicts S.M.D.'s within 5% of the experimental values.

2.5. Lorenzetto - Lefebvre

These workers carried out a comparison between "plain-jet" atomization, in which the fuel is injected into a high velocity airstream in the form of a discrete jet, and "film" atomization which is obtained by spreading the fuel into a sheet and then exposing both sides to the airstreams.

Droplet sizes were again measured using the light scattering technique after a number of modifications to improve the accuracy of measurement. As a light source a 5 mW - Helium/Neon Laser was used, which gave a higher intensity and more stable light beam. Details of this technique can be found in Ref.67 and Appendix (C).

In order to separate the AFR effect from those of other parameters, ten air nozzles of different diameter were used. Each of them supplied a different air flow at constant air velocity. It was found that atomizer

performance deteriorates when the AFR decreases to values smaller than 3, while increasing the AFR improved the atomization quality up to a value of 7, above which no further effect of AFR seemed to exist.

It was concluded that in all the tests which were run with the 6.85 mm air nozzle, and with all the plain-jet orifices available namely: 0.397, 0.794, 1.191 and 1.588 mm diameters, the effect of scale for the atomizers tested with water and kerosine was very small. Different conclusions were drawn in the case of high viscosity liquids, which indicated that the larger is the atomizer liquid orifice diameter the larger are the droplet sizes, all other parameters being constant.

The effect of liquid density on droplet size in this work was opposite to that observed by Rizkalla and Lefebvre. The droplet size decreased with increase in liquid density, but at high atomizing velocities and small liquid flow rates, SMD became less sensitive to variation of liquid density. From the results they obtained experimentally, S.M.D. was expressed as :

$$S.M.D. = 0.27 \frac{\sigma_l^{0.32} W_l^{0.135}}{\rho_l^{0.37} V_r} \left(1 + \frac{1}{AFR}\right)^{1.7} + 0.06186 \frac{\eta_l^{0.72} D^{0.53}}{(\sigma_l \rho_l)^{0.5}} \left(1 + \frac{1}{AFR}\right)^{1.8} \quad (17)$$

which is not dimensionally correct.

In order to obtain a dimensionally correct formula dimensional analysis was applied to give in S.I. units, the following formula :

$$S.M.D. = 0.95 \frac{(\sigma_l W_l)^{0.33}}{V_r \rho_l^{0.37} \rho_a^{0.3}} \left(1 + \frac{1}{AFR}\right)^{1.7} + 0.127 \eta_l \left(\frac{D}{\sigma_l \rho_l}\right)^{0.5} \left(1 + \frac{1}{AFR}\right)^{1.8} \quad (18)$$

where S.M.D. is expressed in meters.

The ranges covered in these tests were :

Liquid viscosity	-	1×10^{-3} to 76×10^{-3}	Kg/m.s
Liquid surface tension	-	26×10^{-3} to 73×10^{-3}	N/m
Liquid density	-	794 to 2180	Kg/m^3
Air velocity	-	70 to 180	m/s
Air/Liquid mass ratio	-	1 to 36	

In their discussion of this work it was stated that for real liquids of finite viscosity, the S.M.D. is given as the sum of the first and the second term of the above equation, which means that drop size cannot fall below a certain minimum value no matter how high the atomizing air velocity may be. This minimum size is equal to the second term, and this term is based on fuel properties only.

The results indicate that the "plain-jet" airblast atomizer performs less satisfactorily than the "thin-sheet" airblast atomizer used by Rizkalla and Lefebvre. When S.M.D. values were plotted against Weber number both curves tended to converge at high Weber number i.e. for the high inertia forces obtained at high air velocities but, in general, the "thin-sheet" airblast atomizer gave smaller droplets.

When the results were compared with Nukiyama and Tanasawa's formula (Ref.74) they agreed very closely at lower droplet sizes while there was some deviation at higher S.M.D. values. This was attributed to the way the experiments were conducted in both cases.

To find the fraction of energy applied which is utilized in the creation of new liquid surface, the energy ε required was calculated from ε = (Surface tension) x (Surface area)

$$= \sigma_l \times S \qquad (19) \quad \text{(Ref.42)}$$

while the total power available was calculated assuming adiabatic expansion through the air nozzle. After making some reasonable assumptions they showed how low is the atomization efficiency with this mechanism of atomization.

CHAPTER 3

INTERACTION BETWEEN THE HIGH VELOCITY AIR FLOW AND THE MOVING THIN LIQUID FILM

CHAPTER 3

INTERACTION BETWEEN THE HIGH VELOCITY AIR FLOW AND THE MOVING THIN LIQUID FILM

In spite of the very large amount of work which has been done in the field of two-phase gas-liquid flow, there are no completely satisfactory theoretical models which can help to reveal all the effects of the different variables involved although it is clearly a very important topic. This situation is a consequence of the extreme complexity of two-phase fluid flows where the interface between the phases can have a very complicated form. In the present work consideration is given to gas-liquid interaction due to its controlling effect on liquid film thickness and the mechanism of sheet disintegration.

3.1. Momentum Balance of Gas-Liquid Interface

The pressure gradient in the two-phase flow can be considered to consist of three terms involving friction, acceleration and gravitational head respectively. Hewitt and Hall-Taylor (Ref.49) made the following assumptions to simplify the problem:

a. The liquid phase occupies an area $(1 - \alpha)A$ of the channel and the gas phase occupies an area αA,

b. The density is assumed constant and equal to the density of the respective phase, the velocity and hence the mass flux at any cross section is assumed constant too, although the velocity profile tends to be highly peaked,

c. The shear stress on the channel wall (τ_o) is constant irrespective of peripheral position.

Using the above assumptions, the following equation for pressure gradient is given:

$$-\frac{dP}{dZ} = \frac{S}{A}\,\tau_o + \frac{d}{dZ}\left[\alpha\, G_g u_g + (1-\alpha)\, G_l u_l\right] + g \sin\theta \left[\alpha\, \rho_g + (1-\alpha)\, \rho_l\right] \qquad (20)$$

where S is the periphery of the channel, and G, u and ρ are mass flux, velocity and density of fluid respectively. θ is the angle of inclination of the channel from the horizontal.

In the present work further simplifications can be added by ignoring the last term of the right hand side of equation (20), considering the channel to be in a near horizontal position. Also, the second term of the same side is small compared to the friction term, as in the modern designs of airblast atomizer the gas velocity is required to be constant

near the atomization lip at its maximum value. These assumptions show that the pressure gradient depends only on the friction term as follows :

$$-\frac{dP}{dZ} = \frac{S}{A}\ \tau_o \qquad (21)$$

The shear stress distribution in the thin liquid film is expressed by Calvert and Williams (See Ref.49), using a "flat plate" approximation, and considering the flow in the vertical direction, as :

$$\tau = \tau_i - (\rho_l\ g + \frac{dP}{dZ})\ (t - y) \qquad (22)$$

where τ_i is the interfacial shear stress, t is the film thickness, and y is the distance measured from the solid boundary in the liquid film. Hence, applying equation (22) to find the relation between the wall shear stress and the interfacial shear stress in the horizontal flow gives :

$$\tau_o = \tau_i - \frac{dP}{dZ}\ t \qquad (23)$$

which indicates that for a very thin liquid film the shear stress may be taken as a constant across the liquid film. The pressure drop can be determined either by using one of the known models, such as the homogeneous model and the Lockhart-Martinelli model, or experimentally as described in Ref.(49), using the force balance method.

In the homogeneous model it is assumed that the fluids behave as a homogeneous mixture of density ρ_H which is given by :

$$\frac{1}{\rho_H} = \frac{x}{\rho_g} + \frac{(1-x)}{\rho_l} \qquad (24)$$

where x is defined as the mass flow rate of the gas phase divided by the total mass flow rate of both phases. The pressure gradient is given by :

$$-\frac{dP}{dZ} = \tfrac{1}{2}\ \frac{S}{A}\ \frac{f_{TP}\ G^2}{\rho_H} \qquad (25)$$

where f_{TP} is the two-phase friction factor and is a function of Reynolds number, and in general it is difficult to calculate.

The other model due to Lockhart-Martinelli (Ref.65), is more popular due to its simplicity, and depends on calculating the pressure gradients for the gas and liquid phases flowing alone in single-phase flow within the channel. They defined a new paramater X as :

$$X = \left[\frac{(dP/dZ)l}{(dP/dZ)g}\right]^{\frac{1}{2}} \qquad (26)$$

and then from chart they plotted a parameter ϕ_g or ϕ_l may be determined, where :

$$\phi_{g \text{ or } l} = \left[\frac{(dP/dZ)}{(dP/dZ)_{g \text{ or } l}} \right]^{\frac{1}{2}} \qquad (27)$$

from which the total pressure gradient can be calculated. It is clear that this model could be used in the present work to determine the liquid film thickness in airblast atomizer when it is related to the pressure gradient as will be discussed in a later chapter.

Ellis and Gay (Ref.34) stated that when a gas passes over a liquid stream it exerts a drag on the liquid surface and causes the liquid to flow. The drag will increase with gas flow until the surface becomes unstable and waves will form on the liquid surface. To measure the interfacial shearing stress in the case of parallel flow of two fluid streams analysis of the gas velocity profile must be carried out. They used the observations reported in the literature to confirm the validity of the equations for turbulent velocity profile for flow over a rough wall to be applied to flow over a rippled water surface. Thus, the following equation applies :

$$(u_m - u)/u_* = -3.33 \left[\ln (1 - (1 - y/r)^{\frac{1}{2}}) + (1 - y/r)^{\frac{1}{2}} \right] \qquad (28)$$

where :
- u = point gas velocity, ft/s
- u_m = maximum gas velocity, ft/s
- r = distance of maximum in velocity profile from wall or liquid surface, ft
- y = distance from wall or liquid surface, ft
- u_* = friction velocity $(\tau_o/\rho)^{\frac{1}{2}}$, ft/s
- τ_o = shear stress at a boundary, pdl/ft^2
- ρ = gas density, lb/ft^3

The appropriate values of u_m and r together with pairs of data for u and y can be substituted in the equation to calculate u_* (hence τ_o).

Similar work has been done by Hanratty and Engen (Ref.47) in which they described the liquid volumetric flow in terms of the liquid film thickness, pressure gradient and the drag of the gas at the surface, using Navier-Stokes equation for a two dimensional flow and treating the liquid surface as rough wall.

Kapitsa (Ref.55) stated that, if an experiment is carried out in a tube with a liquid flowing over its internal walls, it is found that the pressure drop in the gas stream along the tube, for equal velocities of gas flow is considerably higher than when the walls are dry.

3.2. Stability of the Interface for Gas-Liquid Flow

The feature of gas-liquid flow is that the interface between the two fluids is not smooth but has a wavy form which is observed to vary very widely in wavelength and in amplitude. Five interfacial conditions have been observed for a horizontal flow: (1) smooth interface, (2) two-dimensional waves, (3) three-dimensional waves, (4) roll waves, and (5) atomization. The condition of the surface depends mainly on the liquid flow rates. For very low gas rates, the liquid surface remains smooth, while the first disturbance on increasing the gas rate is in the form of small ripples which quickly form two-dimensional waves. These waves were found to be more stable the more viscous the solution. An increase in the air velocity past the critical air velocity brings about an increase in the amplitude with slight decrease in wavelength.

These changes continue until there is a transition to a three-dimensional 'pebbled' pattern which occurs at slightly higher gas velocity. These waves have equal wave lengths in the direction of the flow and perpendicular to the direction of flow. At large enough gas flow rates, considering the law of conservation of mass, it can be shown that the crests of long waves move faster than the troughs. This causes the downstream end of the wave to steepen and roll over upon itself. Eventually on further increasing the flow rate, the liquid is torn from the liquid surface and becomes dispersed in the gas phase. As the liquid film becomes thinner, or as the liquid-phase Reynolds number becomes smaller, it is much more difficult to disperse the liquid phase. These patterns were observed experimentally in reports for van Rossum (Ref.84), Hanratty and Woodmansee (Ref.46), and Hanratty and Engen (Ref.47).

Hewitt and Hall-Taylor (Ref.49) in an effort to study the factors affecting the stability of the wave formed at the interface, stated that the gas flowing past the wavy interface generates an increased pressure over the troughs of the waves, and a suction over the crests which protrude into the gas flow, according to the following equation :

$$- \frac{\partial P}{\partial n} = - \rho_g \chi (\bar{u}_g - C)^2 \qquad (29)$$

where $\frac{\partial p}{\partial n}$ is the pressure gradient in the direction normal to the streamline, χ is the curvature of the streamline (reciprocal of radius of curvature), and $(\bar{u}_g - C)$ is the gas velocity relative to the wave.

They derived the condition for neutrally stable waves, i.e. no increase in the amplitude, to be as follows :

$$K_C = (\bar{u}_g - \bar{u}_l)^2 \frac{\rho_g}{\sigma} - \frac{2(\rho_g/\rho_l)}{t_{mean}} \qquad (30)$$

where K_C is the wave number for stable waves and equal to $(2\pi/\lambda)$ and λ is the wavelength. This suggests that the wavelengths of stable waves decreases rapidly with increasing gas flow ratio. In their review to the previous work in horizontal annular flow, they reported that the scale of the small ripples which cover the surface at low liquid flow

rates, varies with gas velocity. For liquid flow rates greater than some critical value disturbances of long wavelength occurred. It was found that the critical value of the dimensionless film thickness $t^+ \left(= \frac{u_* \rho_l t}{\eta_l} \right)$ was constant for any fluid pair, and appeared to increase smoothly with the viscosity ratio η_g/η_l, where u_* is the friction velocity.

3.3. Entrainment of Liquid Droplets in Gas Stream

The sources of droplet entrainment in the gas-liquid flow are the large disturbance waves forming at the interface. The mechanism of droplet entrainment is not completely understood due to the lack of satisfactory experimental techniques, however, two possibilities are suggested in Ref.49. The first mechanism suggests that the gas begins to undercut the wave, and a round, open-ended bubble begins to form and grows leaving a thick filament around its base, which finally, under the effect of the high velocity air, breaks into droplets. The other alternative form of break-up is that a large amplitude wave on the liquid layer tends to steepen at the front and then to form a breaking wave. If the air velocity is very high the wave tips tend to be drawn into thin liquid sheets with subsequent break-up.

It was noticed that for thin liquid films at low liquid Reynolds numbers, the gas velocity for entrainment increases rapidly with decreasing liquid rate and a limiting liquid flow rate may be reached below which no entrainment occurs irrespective of further increases of gas rate. On the other hand, there is likely to be a critical gas velocity below which no entrainment occurs. These arguments suggest that in the case of an airblast atomizer there should be an initial atomization directly from the liquid film before it reaches the atomization lip.

This condition depends mainly on both liquid and air flow rates, and also on the method of spreading the liquid into a sheet which is responsible, to some extent, for creating the wavy flow pattern, and consequently for droplet entrainment from the liquid surface. The critical gas velocity for this entrainment decreases with increasing pressure and decreasing surface tension. van Rossum (Ref.84) defined this velocity as the air velocity below which no droplet entrainment occurs, and reported that for each liquid this velocity is given by V_e (m/s) $\simeq \frac{1}{4}$ σ (dyne/cm), whatever the film thickness.

Calculation of the amount of liquid entrained in the gas flow may be done using graphs illustrated in Ref.49 such as the Paleev and Fillippovich chart, which relates the percentage of liquid flowing in the film and the parameter $Z \left(= \frac{\rho_{gc}}{\rho_l} \left(\frac{\eta_l V_g}{\sigma} \right)^2 \right)$, where ρ_{gc} is the homogeneous gas core density and is calculated by trial and error. The friction factor of the gas-liquid interface is affected by this amount of liquid entrained through its influence upon Reynolds number where the value of the gas flow rate is replaced by the sum of its value and the value of the entrained liquid.

The condition of the liquid-air interface certainly has a big effect on the mechanism of sheet disintegration in airblast atomizers as will be discussed later.

CHAPTER 4

DESIGN OF AIRBLAST ATOMIZER AND EXPERIMENTAL RIGS

CHAPTER 4

DESIGN OF AIRBLAST ATOMIZER AND EXPERIMENTAL RIGS

The process of fuel atomization under the effect of high velocity air needs more investigation to determine the real influence of all the factors which are affecting the formation of the final droplet sizes contained in the spray. The main feature of the well-known airblast atomizer, which is investigated in the present work, is the spreading of the liquid into a thin film on the so-called prefilmer before it is atomized. It is clear that the formation of the liquid film, and the variables which are controlling its thickness is of great importance to the mechanism of disintegration of this film. Thus it was decided to study these aspects in some detail in the proposed programme of tests.

4.1. Airblast Atomizer

Many considerations were involved in designing the two airblast atomizers which were used in all tests. To enable the liquid film to be studied the conventional circular cross-section atomizer design was replaced by a two-dimensional one, so that the issuing film would be flat and consequently easier to measure, control and photograph. The air passages were made aerodynamically smooth, with minimum areas at the atomization edge to obtain maximum air velocities and maintain them during the initial disintegration process. The two air streams which enclosed the liquid sheet were arranged to leave the atomizer in directions parallel to the sheet in order to achieve the best degree of atomization, as reported in the literature. The atomizer was also designed to deal with all the liquids being used in the tests, and embodied a suitable method for introducing the liquid as a thin film.

4.1.1. Atomizer (A)

The design of this atomizer is illustrated in Fig.14. The areas of the air passages at the atomization edge were designed to be nearly equal to those of the atomizer employed in Rizkalla - Lefebvre tests (Refs.79 and 80). It was decided to make the two side plates of the atomizer from perspex to facilitate observation of the formation of the liquid film. The liquid was fed to the central piece (prefilmer) through two side pipes to avoid any disturbance to the air flows. The liquid emerged into the air stream through a plate of sintered metal screwed to, and flush with the prefilmer over its whole width, at a short distance from the atomization edge. Five grades of this sintered metal were tried, and the permeability varied from minimum value of 1.8×10^{-6} for grade A to a maximum of 75×10^{-6} for grade E.

The permeability is defined as :

$$\phi = \frac{V.l.n}{981.A.P.t} \qquad (31)$$

where: V = volume of fluid (in ccs) flowing in t sec

P = pressure drop across filter in gr/cm^2

A = effective area of filter in cm^2

n = absolute viscosity of fluid in centipoises

l = thickness of filter in cm

It was difficult to use grade A due to problems of blockage and the other grades were chosen according to the kind of liquid used. In some cases the liquid did not spread evenly over the prefilmer and it was then essential to change the sintered piece. Two air control parts were fixed at the atomization section to give the two air streams the required directions and maximum velocities. The upper one, which was used to control the air flowing over the liquid film (pintle air), had an inclined hole of a diameter sufficiently large to allow a micrometer rod to move and reach the liquid film at right angles to the prefilmer surface as shown in Fig.14. This micrometer was used to measure film thickness in some tests.

It was also possible to slide both the air control parts inside the atomizer to be at the same cross section with the prefilmer edge for photographic purposes.

4.1.2. Atomizer (B)

The main difference in the design of this atomizer and the previous one is the method of injecting the liquid. In order to study the influence of liquid sheet thickness on mean drop size it was essential to be able to control its initial value by some mechanical means. As shown in Fig.15, the liquid was injected through a variable-width gap, which could be adjusted by a screw having a special thread to control the sheet thickness quite accurately. This design required the prefilmer to be made in two parts to form the exit slot. The gap width between these parts was easily read from a dial indicator, which was divided into 0.0001 in (about 2.5 microns) increments, and touched the upper part of the prefilmer as near as possible to the atomizing edge. The gap was frequently checked using accurate feeler gauges. The two air control pieces were identical and were designed to impart an air stream direction nearly parallel to the issuing film. The two perspex side walls used with design (A) were replaced by metal ones, but the method of feeding the liquid through the side walls into the central piece (prefilmer) was kept the same. The width of the atomizer was made shorter (5 cm) to control the gap width more accurately. The atomizer is shown in Plate 1.

Atomizer (A) was designed primarily to study the droplet distributions of the sprays and also the mechanism of disintegration of liquid sheets, using the photographic technique. The second atomizer, (B), was intended to establish the relationship between the liquid film thickness and Sauter mean diameter of the sprays, taking into consideration all other factors, although it was also used in some tests to study the disintegration of the liquid sheets. The high pressure tests were conducted using atomizer (B), in addition to another much larger airblast atomizer of conventional design as will be discussed later.

4.2. Atmospheric Test Rig

4.2.1. Air System

As the air flow rates required in these tests were relatively low a small rotary fan was adequate to supply flow rates up to 20×10^3 N/m^2 (~ 3 psig). The air flow was divided into two separate paths leading to the atomizer. Special air ducts were used to connect the air supply pipes to the rectangular cross-section channels of the atomizers with minimum possible disturbance to the flows. The two air streams were regulated using isolation valves, and also by bleeding off air at the outlet of the fan. Mass flow rates were measured using orifice plates fitted with D and D/2 pressure tappings, according to B.S.1042. The air temperature was measured also by means of thermocouples, with the reference junction at 0^{o}C, while the air velocity of both streams were measured on a rake of four pitot tubes to determine the average value.

4.2.2. Liquid System

The method of supplying the liquid to the atomizers varied according to the liquid being used. Water was delivered directly from the test house water supply, although in some instances a water pump was needed to give the required flow rate. Kerosine was fed to the system from a nitrogen pressurized drum, while all the special liquids were fed by the same method from a smaller container. Liquid flow rates were measured on Fisher and Porter flow-meters, which were calibrated for all liquids. The sprays were discharged into a long duct and the liquid was collected in a container outside the test house. The atmospheric test rig is shown in Plates 2 and 3.

4.3. High Pressure Test Rig

High pressure air from the compressor house, which was able to deliver air up to 1720×10^3 N/m^2 (250 psig) and 3.18 Kg/s (7 lb/s), was fed into a large cylindrical chamber which housed the atomizer. The air mass flow rate was measured using an orifice plate made to B.S.1042 standards. The air and liquid issuing from the atomizer flowed into a cylindrical collector provided with a butterfly valve to control its pressure and another valve to drain the accumulated liquid. A pressure tapping was fitted to the collector to adjust the pressure drop across the atomizer. Two toughened plate glass windows were mounted at the outer ends of two short horizontal pipes, which were connected to the collector as shown in Fig.16.

To avoid the expected problem of liquid deposition on the windows, a circular plate having a small central hole was fitted close to each window, and the intervening space was supplied with high pressure air from a separate source. The ensuing flow of air through each small hole successfully avoided the penetration of liquid drops onto the window.

Special liquid pumps were employed to deal with the large quantity of water and kerosine required for the big airblast atomizer of the conventional design, while for atomizer (B) the pressurized liquid drum was again used. The high pressure test rig is shown schematically in Fig.16.

4.4. Special Liquids

In order to study the effects of physical properties of liquids on atomization quality, it is essential to separate the influence of the property under investigation from the influences of the other properties. From a large number of trial solutions, Rizkalla and Lefebvre (Refs.79 and 80) chose appropriate liquid solutions to obtain the wide variations of each physical property while keeping the others nearly constant. For measuring experimentally the main liquid properties namely viscosity, surface tension and density, Rizkalla(Ref.78) has summarized the methods used in each case. The liquids and solutions used in the present investigation are presented in Tables 1, 2 and 3, and cover the following ranges :

Viscosity	-	0.998×10^{-3} to 123.921×10^{-3}	kg/m.s
Surface tension	-	26.77×10^{-3} to 73.45×10^{-3}	N/m
Density	-	0.784×10^{3} to 1.830×10^{3}	kg/m^3

4.5. Air/Liquid Flow Characteristics of Atomizers

The mean values of mass flow rate for shroud air and pintle air are given in Fig.17 together with the total atomizing air flow at equal velocities for both air streams, for atomizer (A). Also Fig.18 shows a chart of air to liquid mass ratios plotted against air velocity for different liquid flow rates, for the same atomizer.

For atomizer (B), the air flow rates of both air streams at constant air velocities, and the total atomizing air are given in Fig.19, while air/liquid ratios for various air velocities and liquid flow rates are given in Fig.20.

The ranges covered with the two atomizers are :

Air velocity	-	54 to 122 m/s
Liquid flow rate	-	4.5 to 27.2 gr/s
Air/liquid ratio	-	0.8 to 11.3

CHAPTER 5

MECHANISM OF DISINTEGRATION OF LIQUID SHEETS

CHAPTER 5

MECHANISM OF DISINTEGRATION OF LIQUID SHEETS

The stability of the liquid film flowing over the prefilmer under the effect of high velocity air, and the possibility of having early atomization directly from the film surface upstream of the atomizing edge were discussed in Chapter 3. In this chapter, the complete mechanism of disintegration of a liquid sheet will be discussed, from the moment it leaves the prefilmer until a uniform spray is formed. A review of the different mechanisms presented in the literature will be given first, then the technique used in the present work, and finally the discussion and conclusions which may be drawn from the results obtained in this group of tests.

5.1. Review

York, Stubbs and Tek (Ref.93) described the force balance between the interfacial tension forces and aerodynamic forces as the basic concept for liquid film instability and wave formation, which are considered the major factors in the break up of the film. The velocity difference between the air stream and liquid film moving along a continuous interface speeds up the growth of waves until eventually the liquid film may disintegrate and be swept away in the air flow. It was stated that the forces arising from interfacial tension oppose any movement of the interface from the plane and attempt to reinstate the original equilibrium, while the aerodynamic forces increase any deviation of the interface from the plane and attempt to make the equilibrium unstable.

Photographic techniques were used by Fraser, Dombrowski and Routley (Ref.37) to explain the mechanism of disintegration of a liquid sheet. They found that the sheet breaks down into drops through the formation of unstable ligaments of a diameter depending mainly upon the sheet thickness, and the wavelength of the waves initiated on the liquid surface. It was stated that, using Rayleigh's analysis, the collapse of a ligament of an inviscid liquid produces drops of diameter = 1.89 x diameter of the ligament. From this discussion it can be seen that the film thickness has a major effect on ligament diameter, which in turn controls the drop size. This highlights the importance of producing thin liquid sheets to improve the quality of atomization.

Fraser, Eisenklam and Dombrowski (Ref.39) found that in airblast atomizers thin threads are torn off the slower-moving liquid by the effect of the surrounding high velocity air stream. With a non-viscous liquid threads are formed which have their greatest instability when the length is 4.5 x diameter.

Castleman, jr (Ref.14) came to the same conclusion that ligament formation is a necessary step between the large mass of liquid and the discrete droplets. He found that with increase in air speed the ligaments appear both finer and shorter, while at air speeds above 100 m/s the ligaments have largely vanished and the small drops appear

to be torn directly from the main mass. From some simple calculations, taking into account the amplitude of surface disturbance of a ligament, Castleman found the upper limit to the collapse time to be 1.5×10^{-5} sec, which appears to be brief enough to account for the phenomena of disappearance of the ligaments from photographs taken at high air speeds. When alcohol was used instead of water, due to its lower surface tension, the ligaments were formed more readily and atomized at a much lower air velocity. To describe why the drop size ceases to decrease any more at high air velocities, Castleman reported that at certain point the ligaments collapse practically as soon as they are formed. It is interesting to note that his curves of droplet size against air velocity flattened at about 100 to 120 m/s, as found in many reports.

Dombrowski and Fraser in another study on the disintegration of liquid sheets (Ref.29) designed a special flash for their photographic investigations to combine a high intensity of light with very short duration. A large variety of liquids was chosen to study the separate effect of each liquid property. It is noticed from the pictures provided, that with an increase of viscosity from 1×10^{-3} to 5.3×10^{-3} Kg/m.s, the position of disintegration has moved much farther away from the atomizer, and the sheet area before disintegration is much larger. The effect of liquid density on sheet disintegration was reported to be insignificant. The combined effect of increase in density and surface tension at a constant viscosity as with mercury, for example, gives a sheet that is highly resistance to turbulence by air friction. The liquid sheet with the highest viscosity and surface tension is the most resistance to disruption as shown in their pictures.

5.2. Photographic Technique

Many techniques were tried during the present work. It was felt that, to get a very clear idea about what was occurring at the atomization edge, it was necessary to concentrate on a small area of the liquid leaving the edge, and to use a transmitted light to form a shadow of the spray. After trying many types of flash, of duration time varying from 2 to 5 microseconds, it was found that they were not fast enough to stop the motion of the spray, especially at high air velocities. To avoid this drawback and also for safety reasons, a flash unit, which worked by means of an Argon bottle (Lunartron made), was used to give very fast sparks of 0.2 microsecond. The big advantage of this unit was that, it had an ordinary lamp for adjusting purposes, which enabled the operator to line up the apparatus, and also to choose the required area precisely. The flash from the unit was collimated by a convex lens, then reflected upwards by a mirror to pass through the spray as a circular beam. Finally, the light beam was focussed by the camera lens on an Ilford film. The camera was placed about 10 cm above the level of the atomizing edge which covered half of the circular light beam, hence only the other half, which showed the spray at the moment it left the edge, was photographed. The photographic technique is illustrated in Plate 4.

Some photographs were taken for the whole spray using direct incident light. These helped to give a good general idea about the spray, but they did not show any details of sheet disintegration.

5.3. Factors Influencing Sheet Disintegration

5.3.1. Effect of Air Velocity

The most important conclusion which may be drawn from all the photographs obtained is that the formation of ligaments is an essential stage in the disintegration mechanism between the continuous liquid film and the separate droplets at all levels of air velocity. To study the effect of air velocity on the mechanism for constant liquid flow rate, the velocity was increased from 54.9 to 122 m/s, at 22.7 gr/s water flow rate. The two conditions are shown in Figs.77 and 78 respectively, and it is obvious that the ligaments have very thick stems and are much longer at low air velocity, before they disintegrate into big drops, while at high air velocity the threads formed at the edge are thinner and shorter and disintegrate into smaller drops. In general, at higher air velocity the whole mechanism of atomization occurs nearer to the atomizing edge.

Figs. 79, 80 and 81 show that, when the air velocity takes the values of 54.9, 91.5 and 122 m/s at a constant water flow rate of 9 gr/s the number of threads drawn from the film increases with velocity increase, and again they are thinner and shorter at a higher velocity. It can be seen also that some of the ligaments do not disintegrate directly to drops but into smaller parts which flow further downstream where they are shattered into drops (Figs. 77, 78, 79 and 80). Figs. 82 and 83 confirm the above remarks at two air velocity levels.

The same mechanism is apparent in the case of kerosine, as shown in Figs. 84 and 85, where the velocity increases from 54.5 to 122 m/s at 4.5 gr/s flow rate. It is also clear that the threads are shorter and thinner than for water due to the lower surface tension of kerosine.

5.3.2. Effect of Liquid Flow Rate

The formation of the ligaments at higher liquid flow rate does not start at the atomizing edge but at some short distance downstream, and they are obviously thicker. Figs. 79, 82 and 77 show the above for water flow rates of 9, 13.6 and 22.7 gr/s respectively, and at a constant air velocity of 54.9 m/s.

The same comments apply to kerosine as shown in Figs.85 and 86 where the flow rates are 4.5 and 13.6 gr/s respectively. It is clear that the thicker ligaments break into bigger drops which then need a longer distance to disintegrate further into smaller drops. When final disintegration occurs it does so at a relatively low air velocity.

5.3.3. Effect of Surface Tension

It is well known that liquids of high surface tension are more difficult to disintegrate by aerodynamic forces, and the resulting threads should therefore be thick and long compared to those obtained with low surface tension liquids. Figs. 87 and 88, for two different liquid solutions of 51.9×10^{-3} and 26.8×10^{-3} N/m surface tension,

show that the threads look sharp and of nearly uniform diameters for low surface tension, while at high surface tension most of the threads have thick stems and thin ends, similar to the picture obtained with water.

In some other tests the surface tension was kept constant at 26.8×10^{-3} N/m, while the liquid flow rates varied from 4.5, 7.5 to 12.5 gr/s. The results obtained are shown in Figs. 89, 88 and 90 respectively. At the lowest flow rate, the liquid threads are very thin and tend to take curved shapes, whereas at high liquid flow rate the threads form a complex pattern of thicker ligaments. Parts of these threads separate and flow downstream where they are eventually atomized to drops as is shown clearly in Fig.90.

5.3.4. Effect of Liquid Density

The mechanism of liquid sheet disintegration should be affected to some extent by a change in liquid density. For liquids of high density one would expect more resistance to disintegration with a resulting effect on the shape of the ligaments formed at the atomizing edge. Two levels of densities were employed in these experiments namely 1.213×10^3 and 1.83×10^3 Kg/m^3, and the air velocity was kept constant at 91.5 m/s.

For the minimum liquid flow rate of 4.5 gr/s, Figs.91 and 92 illustrate respectively the effects of low and high density. In Fig.91 the threads appear to form directly from the liquid sheet, and they are thin and of uniform diameter. With the higher density liquid the film does not directly produce threads, but they are drawn from liquid patches formed from the sheet at the atomizing edge as shown in Fig.92.

At a higher liquid flow rate of 6.8 gr/s the ligaments become thicker, and each ligament soon breaks into many thin threads giving a tree-like form, but still the stems of these trees are thicker at high liquid density, as shown in Figs.93 and 94. At the maximum flow rate of 12.5 gr/s, by direct comparison between Figs. 95 and 96 one can conclude that the whole disintegration mechanism is completed within a shorter distance from the edge for a low density liquid, while some of the thick ligaments of high density liquids tend to join each other to form another atomizing lip which soon break into a shower of shorter threads and drops under the influence of high air velocity.

5.3.5. Effect of Liquid Viscosity

The shear force needed to disintegrate a liquid sheet is certainly higher for high viscosity liquids according to the relation between both factors, therefore it is expected to find very long threads and separated parts of the film leaving the atomizing edge as a first stage in the disintegration mechanism, and the droplets will take their final form at a relatively far distance from the edge.

Two levels of viscosity of 2.87×10^{-3} and 17×10^{-3} Kg/m.s were examined in the tests conducted on atomizer (A) for a constant air velocity of 91.5 m/s. Starting with the liquid of lower viscosity, it

is shown in Fig.97 that at a low liquid flow rate of 4.5 gr/s, the liquid film breaks under the action of air velocity into many relatively long threads. When the flow rate increases to 6.8 gr/s the liquid starts to leave the prefilmer in big patches which break in the usual way into thick ligaments and finally to thin threads. These disintegrate further into various drop sizes as shown in Fig.98.

The mechanism of disintegration of high viscosity liquids may be studied in the light of Figs.99 to 102. The effect of high viscosity dominates over the small change in liquid flow rate from 4.5 gr/s in the first two figures, to 6.8 gr/s in the other two, since the mechanism in general looks similar in all four figures. As predicted before, there is no doubt that the threads are very long, and in some parts they are at least five times longer than the ones formed with low viscosity liquids. In all figures the big patches are evident and some of them are in the stage of separation from the liquid film as shown particularly in Fig.100. Some others still keep their bulky shape for a distance downstream of the edge before breaking into smaller patches and thick ligaments. At the top of Figs.100 and 101 it can be seen that the ligaments managed to keep attached to the liquid film for a long distance before being torn out.

Considering the scale of these figures (10.5 magnification), it is easy to measure the diameter of some drops which have travelled the whole distance from the atomizer to the edge of the picture. Most of these drops have diameters above 400 microns. Fig.103 shows the disintegration process of a liquid film produced by atomizer (B) at an air velocity of 91.5 m/s, a low liquid flow rate of 3 gr/s and a very high viscosity (44×10^{-3} Kg/m.s). It is apparent that the film break into very few and long threads of nearly straight shape. The photograph also shows some liquid patches protruding from the atomizing edge and ready to form other threads. This picture gives a clear idea of the mean drop size and the uniformity of the spray produced under these conditions.

5.3.6. Effect of Liquid Film Thickness

Atomizer (B) was used to conduct a set of tests at two thickness levels of 0.0178 and 0.0356 cm and at a constant air velocity and water flow rate of 91.5 m/s and 16.4 gr/s respectively. Figs.104 and 105 show the two cases, and in general it can be concluded that the thicker film breaks into ligaments and patches of bulky and non-uniform shapes, while for the thinner film, individual ligaments of relatively thin diameter are drawn from the film, as shown on the right side of Fig.104. Both levels of film thickness employed here are higher than the thickness expected for atomizer (A) running at the same conditions of air velocity and liquid flow rate.

From the figures studied in this section and the previous figures included in this chapter it is seen that the mechanism of film disintegration is similar in both atomizers from the viewpoint of forming ligaments as an essential stage in the conversion of a liquid film into separate drops in spite of the differences in the manner in which the film is produced in the two atomizers.

CHAPTER 6

DROPLET SIZE DISTRIBUTION IN SPRAYS

CHAPTER 6

DROPLET SIZE DISTRIBUTION IN SPRAYS

6.1. Introduction

One of the most important properties of liquid sprays is the frequency of occurrence of the various sizes of droplets, or the size distribution in the spray. The interest in the drop size distributions of sprays from gas turbine fuel atomizer has increased recently, and that stems from the need to control exhaust emissions, which depend to a great extent upon the quality of atomization. In general, the existence of very small droplets in a spray helps to start the combustion process in combustion chambers, while the big drops do not burn completely and increase the level of pollutant emissions, although they play a significant part in widening the flame stability limits due to the creation of regions of rich mixture.

In studying the evaporation rates of sprays, the mean droplet size cannot adequately give enough information and the whole distribution of drop sizes must be taken into account. Dickinson and Marshal, jr. (Ref.26) concluded that sprays with less uniform drop size distributions evaporate more rapidly in the initial interval of time than more uniform sprays with the same mean diameter because of the presence of many smaller drops. However they take much longer time for complete evaporation because of the very large drops they contain. Also it was reported that the size distribution of drops changes during evaporation in such a way that the average diameter of the remaining drops increases in the moderately or highly non-uniform sprays, and decrease in the more uniform sprays. This is again due to the existence of more smaller drops in the former case.

In this chapter, the drop size distribution under different conditions and the factors affecting it will be discussed.

6.2. Methods of Expressing Size Distributions

There are two forms of plotting drop distributions according to the different applications. One of them is the cumulative form, in which the distribution is expressed as the fraction by weight or volume of the total drops having a diameter larger than a given diameter. This gives a curve falling from 1 to 0 as the drop size increases from minimum to maximum. The second is the differential form and expresses the relative frequency of drops of any given size, hence the minimum frequency occurs at both minimum and maximum drop sizes, while the peak frequency coincides with the most probable drop diameter. The first form gives an idea about the percentage of mass or volume of spray left above a certain drop diameter, while the second form gives a general picture of the spray as a whole.

6.3. Mathematical Distribution Equations

It is of great help to derive either theoretically or experimentally a certain formula which can represent the actual distribution of sizes in a spray. Many expressions have been derived and some of them proved to follow the real curves closely. Such expressions can be used to calculate the mean drop size, which obviously will be different from the one calculated directly from the data since these expressions can never give the exact shape of the actual distribution. However, it is quite reasonable to accept the values calculated from the equations, because it is known that, the sample used to plot the actual curve can differ from one moment to another, and a few large drops in any given sample may shift the mean size to a much higher value, while they may not exist at all in another sample.

6.3.1. Nukiyama-Tanasawa Equation (Ref.74)

This is a completely empirical equation and appears in the following form :

$$dn = 0.5\, n\, b^3\, X^2 \exp(-bX)\, dX \qquad (32)$$

where, n = total number of droplets

X = mean diameter of a number of droplets 'dn' of diameters lying in the interval $(X - \Delta X/2)$ and $(X + \Delta X/2)$, and

b = size parameter

The quantity b varies mainly with the density and surface tension of the liquid, the density of the air and the relative velocity between air and liquid. The equation in this form does not give information about the spread of drop sizes, and in many cases gives values of S.M.D. larger than any experimentally observed drop diameter, as observed by Mugele and Evans (Ref.72).

6.3.2. Rosin-Rammler Equation

This equation was derived first for the investigation of size distribution in powdered coal (Ref.83), but it could be applied with success to liquid drops. This distribution function is generally given in the 'cumulative volume' form :

$$1 - v = \exp - (X/\bar{X})^q \qquad (33)$$

where, $1 - v$ = volume fraction of drop material occurring in drops of diameter greater than X

$\bar{X}$ = size parameter, and

q = distribution parameter.

From Equation (33), the 'volume distribution' equation is :

$$\frac{dv}{dX} = \frac{qX^{q-1}}{\bar{X}^{q}} \exp - (X/\bar{X})^{q} \qquad (34)$$

A high value of q implies a more uniform spray, or in other words means a small fractional variation of drop size on either side of the mean is sufficient to embrace a large fraction of the total sample.

The Sauter mean diameter is given by :

$$S.M.D. = \bar{X} / \underline{\Gamma} (1 - \frac{1}{q}) \qquad (35)$$

where tables of gamma function can be used.

Although this equation assumes an infinite range of X values, it has the advantage of simplicity, and as described by Rosin and Rammler, it permits the curves to be extrapolated into the range of finest droplets where measurements are difficult and take a very long time.

6.3.3. Upper Limit Distribution Function

This is a modified form of the log-probability equation which is based on the normal distribution function. The volume distribution equation is given by :

$$\frac{dv}{dy} = \frac{\delta}{\sqrt{\pi}} \exp (- \delta^2 y^2) \qquad (36)$$

where $y = \underline{\ln} \frac{aX}{X_m - X}$, and as y goes from $-\infty$ to $+\infty$, X goes from X_o (minimum size in distribution) to X_m (maximum drop size), and δ is related to the standard deviation of y, and hence of X. "a" is a dimensionless constant. The Sauter mean diameter is given by :

$$S.M.D. = X_m / (1 + a.\exp (1/4\delta^2)) \qquad (37)$$

It follows that a reduction in $\underline{\delta}$ implies a more uniform distribution. This equation assumes more realistic spray of maximum and minimum drop sizes, but it involves difficult integration, which necessitates the use of log-probability paper. The value of X_m must be assumed, and usually it takes many trials to find the most suitable value (Ref.72).

20

6.4. Measurement and Counting of Drop Sizes

The photographic technique used in studying the mechanism of sheet disintegration was employed again here to measure drop sizes. Direct pictures were taken of the sprays, using a very fast flash of 0.2 μs duration time, and by projecting the slides onto a screen divided

into 9 sections the drops appeared magnified 65 times, which allows accurate measurement of each drop. The drops that were in focus appeared very clearly, while the others were less clear. At high air velocity conditions the drop images tended to have elongated shape in the direction of flow; therefore the measurements were taken perpendicular to the flow direction. Between 1200 and 1500 drops were measured and counted in each sample, then the drops were arranged in groups according to their different diameters. Figure 21 shows an example of plotting the results as a step diagram to give drop size distribution.

The Sauter mean diameter of the spray can be found directly from the results, and an example of the calculation is given in Appendix (A).

This technique has many advantages, such as it does not disturb the flow by any means, and also it takes a very short time to get the required photograph of the spray (Plate 4).

6.5. Discussion of Results

6.5.1. Effects of Air Velocity and Liquid Flow Rate

Figures 22, 23 and 24 show the two different methods of plotting the distribution, which are mentioned in section 6.2. The first figure represents the number fraction against drop diameter, while the second one shows instead the volume fraction against drop diameter, and it is clear that the curves are skewed to the right in the second case because each group is now weighted in proportion to X^3. The beneficial effect of increasing air velocity from 54.86 to 91.44, then to 121.92 m/s at a constant water flow rate, is very obvious. Not only does the mean diameter decrease but the spray becomes more uniform. The distribution parameter (q), which gives an indication of the uniformity, increases from 3.35 to 3.6. The number of large drops existing in the spray falls down rapidly with increase of air velocity. As an example of the value of plotting volume fraction of spray occurring above a certain diameter against that diameter, as in Fig.24, it can be seen that for an air velocity of 54.86 m/s, 10 percent of the spray volume occurs in drops of diameter greater than 172 microns. At an air velocity of 121.92 m/s the same percentage occurs above 93 microns, which helps to show the effect of air velocity.

Figures 25 and 26 confirm the influence of air velocity on drop distribution for kerosine, and also show that the distributions are shifted to lower values of drop diameter.

The effect of liquid flow rate on drop distribution is shown in Fig.27. There is a relatively small improvement in the uniformity of the spray when the liquid flow rate falls from 22.7 to 9 gr/s at an air velocity of 121.92 m/s. The corresponding values of distribution parameter (q) are 3.565 and 3.74 respectively. More large drops appear at higher liquid flow rates as shown in the figure.

6.5.2. Effect of Liquid Properties

1. Viscosity

In general, high viscosity liquids tend to give a less uniform spray. In Fig.28, two distributions are plotted corresponding to viscosities of 17.1×10^{-3} and 2.87×10^{-3} Kg/m.s. The improvement in uniformity due to reduction in viscosity is clear in both Fig.28 and 29, which appears also in the values of (q) which increases from 2.826 to 3.23. This result agrees with the fact that viscosity forces tend to impair atomization quality.

2. Surface Tension

Figure 30 gives a good idea of the effect of surface tension on drop size distribution. The liquid of low surface tension (26.77×10^{-3} N/m) gives size distribution which are considered quite uniform. The values of (q) for both distributions are higher than the case of water sprays, and that is expected because of the higher surface tension of water.

3. Density

The influence of liquid density on drop size distribution is not significant as shown in Fig.31. Changing the density from 1.213×10^3 to 1.83×10^3 Kg/m^3, at constant air velocity and liquid flow rate, seems to give similar distributions in the whole range of drop sizes. However, there is small shift towards lower drop sizes in the case of lower density, which suggests a lower mean drop diameter.

6.6. Evaluation of the Mathematical Expressions

It is of great interest to apply the proposed mathematical equations to the results obtained in the present work, to see how close they are to the actual distributions. It is also important to know the relative merits of each expression when applied to different situations. Rosin-Rammler and the upper limit distribution function (ULDF) will be considered here. Appendix (A) shows a complete example of the calculations involved.

To plot these mathematical expressions, it is necessary to calculate the constants for the equations. Figure 32 illustrates how the constants are obtained for the Rosin-Rammler equation. By plotting $\log\left(\frac{1}{1-v}\right)$ against X on log-log paper, the distribution parameter (q), which appeared in the previous section as the criteria of spray uniformity, can be found from the slope of the straight line, and $\bar{X}$, which is the size parameter is the value of X for which $1 - v = e^{-1}$, where $1 - v$ is the volume fraction of the spray occurring in drops greater than X.

To obtain the constants of the upper limit distribution function, the cumulative volume fraction 100 v is plotted against $X/(X_m - X)$ on probability-log paper, after assuming a value for the maximum drop size X_m to give the best straight line. The parameter δ, which is related to the standard deviation of the drop size, is found from the slope of the line, as shown in Fig.33.

For water, Figs.34 and 35 show that both expressions give quite good agreement with the actual distributions. While the upper limit equation follows very closely the experimental curve in Fig.34, Rosin-Rammler gives better agreement in Fig.35.

It is very obvious from the examples given in Figs.36, 37 and 38, which were chosen from the results on the effect of liquid properties, that the Rosin-Rammler equation gives curves which agree closely with the experimental data, while the ULDF curves are quite acceptable in regard to their general shape. Another conclusion that can be drawn from this comparison is that the distribution calculated from the upper limit equation always have a lower maximum frequency of occurrence (apex of the distribution) than the Rosin-Rammler distributions, and it occurs at slightly smaller drop size.

In some figures the values of S.M.D. calculated from the two mathematical expressions are compared with the corresponding S.M.D. values as measured by the photographic and optical techniques. It is interesting to see that the two expressions give values very close to the S.M.D. measured optically, which means these equations predict the values of Sauter mean diameter accurately. The photographic method always give higher values for S.M.D., and this can be attributed to the fact that, most of the small droplets are too difficult to see and measure, hence the mean droplet size shifts to a higher value.

6.7. Comparison Between Present Results and Simmons' Correlation

The process of measuring and counting the individual drops in a sample to obtain the drop size distribution is a very tedious and time consuming job, and usually there are many errors involved in the sampling technique and counting method. Thus, it was very helpful step on Simmons' part (Ref.85), to obtain a correlation from which the drop size distribution can be found knowing only the mass median diameter or the Sauter mean diameter. A vast amount of data was obtained for sprays produced by both airblast and pressure atomizers, under various conditions. He plotted the drop size/cumulative volume distribution for the atomizers in "root/normal" way, using a square root scale for drop diameter, and a probability scale for the cumulative volume less than a stated value of drop diameter, in order to linearize the data. When the results were normalized in terms of mass median diameter, Simmons found that, a straight line through the mass median point exhibited a good fit to the data, with a possible error of not more than 5% and a standard deviation of 0.238.

There are two important uses of the drop size/volume fraction correlation. The whole distribution of a given spray can be found directly from the correlation, knowing the value of S.M.D., which can be measured optically, for example. The other use is to estimate the volume fraction greater or less than a particular drop size, and that is important for ignition. For example, if to ease ignition 5% of the fuel spray volume is required in the form of drops less than 50 microns diameter, then from the charts provided in his report, or from the main correlation, it is found that the S.M.D. of the spray should not exceed 110 microns.

To compare the present results with Simmons' correlation all the experimental points were plotted together with his straight line. As shown in Fig.39, the line which fits the data best is slightly different with a standard deviation of 0.2. The predicted distributions, as found from Simmons' correlation, were plotted for two different S.M.D.'s, 81 and 45.5 microns, with the actual distributions, as a different way of comparison, and again the actual lines slightly depart from the predicted ones as shown in Fig.40.

CHAPTER 7

LIQUID FILM THICKNESS

CHAPTER 7

LIQUID FILM THICKNESS

Since the liquid films involved in airblast atomization are very thin and inaccessible due to the complications in the design, accurate measurement of their thickness is not an easy job. In this chapter, a brief review of the possible methods, and the techniques used in the experiments will be given. It would be clearly of great help if an expression for the film thickness could be derived, which took into consideration all the factors that might affect the thickness.

7.1. Experimental Methods for Thickness Measurement

The details of the different methods are given in Appendix (B), and some of these methods which have been described in the literature will be mentioned here.

If two metallic plates are placed on opposite sides of a duct in which air and liquid streams are flowing separately, the capacitance between the two plates depends on the dielectric constants of air and liquid, and also on the thickness of each phase. This technique involves the problem of measuring the capacitance precisely.

van Rossum (Ref.84) used rectangular electrodes, which were made flush with the surface over which the film was flowing. He measured the electrical resistance of the liquid film between the two electrodes, which could be related directly to the liquid film thickness above the electrodes. The method has the advantage of giving information about the instantaneous variation of film thickness with time.

Charvonia (Ref.15) measured film thickness by means of a photometric technique which was based upon Lambert's law. The light transmitted by a layer of light-absorbing medium is related to the thickness of that layer (t), in terms of the intensity of the light beam and the absorption coefficient, which can be increased by adding dye to the liquid. The method suffers from the drawback that the light can be scattered and refracted away from the detector.

An optical interference method has been used for the measurement of extremely thin liquid films. The method consists of photographing and measuring the interference fringes produced in the film by a broad monochromatic light source. The method requires the free film surface and the solid wall to be specular reflectors.

Polarized light when reflected from a clean metallic surface is elliptically polarized, but the presence of a thin transparent film on the surface will cause a change in this ellipticity to an extent depending upon the film thickness. Hence it can be measured.

A laser anemometer can be used to measure the velocity of the liquid stream by adding some particles, which tend to scatter the laser beam. The scattered light is detected by some sort of photomultiplier, and from the liquid flow rate and geometry of the duct the film thickness may be calculated.

7.2. Method of Measurement Used in the Present Experiments

The simplest method of measuring the film thickness in the present situation of a two-dimensional atomizer, was to use a needle contact device. A special type micrometer of large barrel was part of a D.C. electric circuit, which consisted of a number of transistors. The amplified current from the transistors was used to light a lamp when the circuit was closed by the first contact between the needle and the liquid surface. This micrometer was able to measure liquid thickness of the order of 2.5 microns (~ 0.0001 in). The point of contact was also observed optically by means of light reflected on the liquid surface and magnified by a lens the other side. Atomizer (A), which had perspex side walls, was used in these tests, and a number of readings were taken at each condition to obtain the average thickness accurately. For kerosine, which was not electrically conductive, the point of contact was observed optically.

7.3. Results

The effect of air velocity on water film thickness is shown in Fig.41. It is seen that, as the air velocity increases the consequent result is a reduction in the film thickness, and this is expected since the shear stress exerted by the air on the liquid surface will be greater. Obviously, raising the liquid flow rate gives much thicker films as shown in the figure.

The results for kerosine show similar trends regarding the effects of air velocity and liquid flow rate on the film thickness, as shown in Fig.42. The only difference which can be noticed between both figures is that kerosine always gives thicker liquid films under the same conditions than water, and this is attributed to the higher viscosity of the kerosine, which is 1.293×10^{-3} Kg/m.s compared to 0.998×10^{-3} Kg/m.s for water.

For high viscosity liquids the flow through the sintered metal of atomizer (A) gave non-uniform films, therefore the effect of the viscosity will be discussed in the next section.

7.4. Derivation of Film Thickness Expressions

7.4.1. Lockhart-Martinelli

In Chapter 3, Lockhart-Martinelli's model, mentioned in Ref.(49), was referred to as an example of measuring the pressure drop in duct containing two fluids flowing separately. The model will be adopted

here to find the liquid film thickness on the prefilmer at the part where air velocity is a maximum, after making some reasonable assumptions.

The equivalent diameter of the pintle air passage must be calculated and used in the model, which is based on the annular cross-section ducts; this diameter will be assumed here as follows :

$$d_e = 4 \times \frac{A}{l} \qquad (38)$$

where A = cross-sectional area of pintle air duct at point of maximum velocity, and measured perpendicular to air flow direction

l = prefilmer perimeter

The Reynolds number of each fluid, assuming it is flowing alone in the equivalent pipe and occupying the whole area, is found from :

$$R_e = \frac{W\, d_e}{A_e\, \eta} \qquad (39)$$

where A_e = area based on d_e.

The friction factor (f) is calculated using the standard formulae for pipes from :

$$f = 0.079/R_e^{0.25} \quad \text{(for turbulent flow)}$$
$$\text{or} \quad f = 16/R_e \quad \text{(for laminar flow)} \qquad (40)$$

Thus, the pressure drop for each fluid can be found from the usual Fanning equation :

$$\left(\frac{dP}{dZ}\right)_{l,g} = \frac{4f}{d_e} \left(\tfrac{1}{2}\rho V^2\right) \qquad (41)$$

where V = velocity based on equivalent diameter. The parameter X, which is given by equation (26), is directly determined ($X = ((dP/dZ)_l / (dP/dZ)_g)^{\frac{1}{2}}$). From Lockhart-Martinelli's chart, according to the condition of each flow, the parameter ϕ_l, which is given by equation (27), could be found ($\phi_l = ((dP/dZ)_{Total} / (dP/dZ)_l^{\frac{1}{2}})$.

Armand, Turner and Wallis, as stated in Ref.49, found experimentally that :

$$\phi_l^2 \; \alpha \left(1 / (1 - \alpha)^2\right) \qquad (42)$$

where $1 - \alpha$ = percentage of pipe area occupied by liquid flow.

The value of the proportionality constant was proved to be unity, therefore from the value of $(1 - \alpha)$ the film thickness may be calculated.

The graphs of liquid film thickness plotted against the liquid properties cover the following ranges :

Viscosity - 1×10^{-3} to 124×10^{-3} Kg/m.s

Density - 0.812×10^{3} to 2.18×10^{3} Kg/m^3

Figures 43 and 44 show the effect of air flow rate on film thickness at different liquid flow rates for water and kerosine respectively. They exhibit the same trend, as found experimentally, and show a reduction of film thickness with increase of air flow. The experimental curves show slightly higher values of film thickness at low air flow rate and high liquid flow rate, and lower values at high air flow rate and high liquid flow rate than the values predicted from the model.

The effect of liquid viscosity on film thickness is illustrated in Fig.45 for a constant air flow rate, and various liquid flow rates. The values of thickness rise rapidly as the viscosity increases, which could explain the presence of the very long ligaments which are associated with the atomization of high viscosity liquids as described earlier. It is clearly a very difficult task for the air to atomize such a thick film properly, and the final drop sizes are inevitably large.

Figure 46 shows the effect of liquid density on film thickness. As density increases the film becomes thinner, but at high density levels the reduction in film thickness becomes less significant.

7.4.2. Calculation of Film Thickness From the Shear Stress Equation

It is important to evaluate the ability of the above method to predict the liquid film thickness accurately, therefore a simple treatment will be employed here to derive an expression, which can be used to give a clear idea about the factors affecting the thickness, and also to calculate it if required.

The shear stress in the thin liquid film will be assumed constant and equal to the wall shear stress, therefore :

$$\tau_i = \eta_l \frac{V_l}{t} = \eta_l \frac{2u_l}{t} \qquad (43)$$

where V_l = interfacial liquid velocity

t = liquid film thickness

u_l = mean velocity of liquid film.

Equation (43) may be written in the following form :

$$\tau_i = \eta_1 \times \frac{2 W_1}{t \times \rho_1 \times A_1} = \eta_1 \times \frac{2 W_1}{t^2 \times \rho_1 \times \pi d_e} \qquad (44)$$

where d_e = equivalent diameter of pipe

A_1 = cross-section area of liquid film

The interfacial friction factor is given by :

$$f_i = \frac{\tau_i}{\frac{1}{2} \rho_g u_g^2} \qquad (45)$$

where u_g = gas velocity based on equivalent pipe area.

Substituting τ_i from Equation (44) into Equation (45) gives:

$$f_i = \frac{2 \eta_1 W_1}{(\frac{1}{2}\rho_g u_g^2)(\pi t^2 d_e \rho_1)} \qquad (46)$$

To find the film thickness, it is essential to determine the value of the friction factor either experimentally or from some empirical expressions. As stated in Ref.49, the friction factor can be expressed for annular flow by :

$$f_i = f_g (1 + 300 (t/d_e)) \qquad (47)$$

where f_g = friction factor of gas flowing in the absence of the liquid film in a smooth tube and equal to $0.079/(R_{eg})^{0.25}$ in the case of turbulent flow (Blasius equation).

From Equations (46) and (47), an expression for the film thickness can be written as :

$$\frac{0.079\ t^2}{\left(\frac{W_g\ d_e}{A_e\ \eta_g}\right)^{0.25}} (1 + 300 (t/d_e)) = \frac{4 \eta_1 W_1}{\pi \rho_g \rho_1 d_e u_g^2} \qquad (48)$$

The value of film thickness (t) may be found by iteration. This was tried successfully in the present work, and the values calculated from this equation reasonably agreed with the previous method, although it always gave lower values. This result helps to

prove the validity of both methods in their application to liquid films in airblast atomizers. If there is any swirl in the liquid motion due to the method of injection the overriding effect of the shear stress exerted by the air flow on the liquid film will tend to cause the film to flow in a near axial direction. Thus, the liquid velocity (u_l) could be considered as the axial component of film velocity.

Equation (48) shows clearly the effect of liquid properties on film thickness, and also it emphasizes the influence of liquid flow rate and air velocity. It seems that liquid surface tension does not affect the thickness of the film nor the interfacial friction factor. However, it has a significant effect on the entrainment of droplets from the liquid surface into the air stream. The reduction of surface tension will decrease the critical air velocity for entrainment and also increase the quantity of the entrained liquid.

7.4.3. The Proposed Expression for Film Thickness

Any proposed expression should take into account all the factors which may affect the film thickness, and could be written in the form :

$$t = f\ (W_l^{\,a},\ \eta_l^{\,b},\ \rho_l^{\,c},\ u_a^{\,d},\ \rho_a^{\,e},\ d_e^{\,f}) \qquad (49)$$

The exponents of these variables were determined from the available graphs of the different factors, and the following expression is suggested after calculating the constant of the equation:

$$t = \frac{0.01075}{d_e^{\,0.55}} \left(\frac{\eta_l^{\,0.35}}{u_a^{\,0.9}} \right) \left[\frac{W_l^{\,0.55}}{(\rho_a\ \rho_l)^{0.45}} \right] \qquad (50)$$

where t and d_e in cm

W_l in gr/s

u_a in m/s

ρ in gr/cm^3

η_l in centipoise

The ranges covered by this equation are as follows :

Liquid viscosity	-	1 to 124 centipoise
Liquid density	-	0.812 to 2.18 gr/cm^3
Air velocity	-	54 to 122 m/s
Liquid flow rate	-	4.5 to 27.2 gr/s

In strict S.I. units Equation (50) becomes :

$$t = \frac{2.15}{d_e^{0.55}} \left(\frac{\eta_l^{0.35}}{u_a^{0.9}} \right) \left[\frac{W_l^{0.55}}{(\rho_a \rho_l)^{0.45}} \right] \qquad (51)$$

where t is expressed in metres.

Equation (51) could be of value in the design of airblast atomizers in predicting the thickness of the liquid sheet flowing over the prefilmer, especially as the thickness of the liquid film at the atomizing edge affects to a great extent, the disintegration of that sheet, and also the final drop sizes. This equation also helps in making comparisons between the expressions which predict the Sauter mean diameter and the equation derived in the present work, as will be discussed in the following chapters.

CHAPTER 8

RESULTS OF DROPLET SIZES

CHAPTER 8

RESULTS OF DROPLET SIZES

8.1. Drop Size Measurement

The performance of any atomizer is usually expressed in terms of the mean drop size it produces under various operating conditions. Different definitions of mean drop size are used in the field of fuel atomization, however, the Sauter mean diameter is generally considered the most suitable one, because it is most relevant to the rates of evaporation and combustion.

The Sauter mean diameter of a spray may be measured either by one of the methods which employ drop collection, e.g. coated slides and the liquid nitrogen technique, or by photographic or optical methods. The main drawback of the first group is the need to introduce some sort of collecting device into the spray. The photographic technique was used successfully in this work to find the drop distribution and Sauter mean diameter of many sprays, but it is not the best method if a large number of readings is required. However optical techniques can fullfil these requirements and eliminate the forementioned drawbacks.

8.2. The Scattering of Light

The optical properties of a medium are characterized by its refractive index and, as long as this is uniform, light will pass through the medium undeflected. Whenever there are discrete variations in the refractive index due to the presence of particles, part of the radiation will be scattered in all directions, while the other part is transmitted unperturbed. In droplet size analysis the number of drops under observation should be large enough to ensure that a representative sample is obtained automatically. The cumulative effect is obtained by adding the intensity scattered by each drop as if it were present alone.

Dobbins et al (Ref.27) studied the forward scattering of a parallel beam of monochromatic light passing through a spray and found that for sprays described by the upper limit distribution function, as defined before, having characteristic parameters of spread and skewness within specified limits, the scattered light intensity profiles were coincident and the S.M.D. could be obtained from the distance traversed by the beam to have 1/10th of the intensity at the optical axis. The 1/10th intensity is chosen to find the S.M.D. because it gives the least deviation, as described by Roberts and Webb (Refs.81 and 82) who also widened the spread and skewness in the ULDF making it possible to apply the method to sprays produced by airblast atomizers. The mean theoretical illumination profiles are given in Fig. 6.

8.3. Optical Apparatus (Fig.7)

In order to obtain a highly collimated monochromatic beam of light a 5 mW - Helium/Neon Laser (by Spectra Physics) working at 6328 Å wavelength was used. The laser beam is spatially filtered and collimated by an optical assembly (Fig.8) screwed to the laser head. The spatial filter employs an aperture placed at the focus of an expanding lens to pass only the fundamental laser mode. The optical unit connected to the filter unit is a beam expanding telescope to produce a highly collimated beam. The light beam is then chopped by a rotating perforated disc to reduce the stray light and increase the sensitivity of the system.

The parallel beam is diffracted through the spray under investigation and focussed by a 60 cm focal length receiver onto a 22 microns aperture. Eventually the light travels the distance to the photomultiplier cathode through the eyepiece mounting and the shutter assembly shielding the photomultiplier tube (Fig.10). The 44 mm diameter cathode provides very high quantum efficiency in the red (Fig.11), and the end window is internally corrugated to enhance the red sensitivity due to multiple reflection of the incident light. An interchangeable neutral density filter is located in front of the photo-tube, and a constant 750 V voltage supply to the photomultiplier is maintained to keep the mean anode current under 10 μA for highest stability.

The electrical signal from the photomultiplier is passed into the Synchronous Demodulator (Fig.9 and Plate 5) to reach an X - Y plotter, where it is amplified by a logarithmic amplifier module. The X-axis displacement of the plotter is electrically connected to a linear displacement transducer which is mechanically linked to the photomultiplier trolley (Plate 6). The combination of the X - Y displacements allow the light intensity profile to be plotted, hence the maximum intensity can be found by extrapolating the curve towards the centre line to eliminate the unscattered beam profile. The traverse distance "r" at 1/10th of the maximum intensity is determined, then from the curve shown in Fig.12, which has been calculated for conditions of $\lambda = 6328$ Å and $f_c = 60$ cm (focal length of condensing lens) from the curve of Fig.6, the SMD of the spray tested is obtained.

In practice all readouts were monitored with a D.V.M. and an oscilloscope to observe the scattered light intensity. Typical plots of light intensity profile are shown in Fig.13.

All tests were carried out at a light beam position 14 cm from the atomizer face, and some readings were taken at 24 cm and 30 cm distance also to check whether the measured S.M.D. values would be different at these distances. It was found that variation in S.M.D. was negligible over this range.

8.4. Experimental Programme

The atomization process is governed by many variables, and the mean drop size of a spray is determined by the combined effect of these variables, therefore it is essential to study the effect of each

parameter separately. The design of atomizer(B),which was used in these tests, enabled one parameter, namely film thickness to be fixed during each set of tests. As mentioned previously, the value of the thickness could be adjusted accurately by controlling the liquid gap. The effects of relative air velocity and air/liquid ratio on mean drop size were examined in the first part of the tests, at each sheet thickness, mainly for water and kerosine, hence the effect of film thickness could be determined directly.

The second phase of tests was confined to the separate effects of liquid viscosity, surface tension and density using the special liquids described in Tables 1, 2 and 3. These tests were repeated to obtain sufficient information on the influence of the liquid properties on the S.M.D. at different liquid thicknesses.

Additionally a special series of tests was carried out to determine the effect of air pressure on mean droplet size for both low and high viscosity liquids.

The main purpose of conducting these tests was to establish an expression for S.M.D. as a function of all the variables mentioned above, which could be of practical importance.

8.5. Effect of Atomizing Air Velocity

The resulting drop size is determined from the balance between the external force represented by the momentum of the air stream, which is a function of air velocity, and the internal forces due to the surface tension and viscosity of the liquid drops. Thus one would expect to have smaller drops at higher levels of air velocity. Also, it was noted in the previous chapter that the liquid ligaments formed at the atomizing edge are thinner and shorter at higher air velocities. Also they disintegrate further to smaller drops near the atomizing edge where the air velocity is still high, and this obviously leads to better atomization.

Figure 47 shows the drop in S.M.D. with increase of air velocity for various water flow rates and a film thickness of 0.0089 cm, while Fig.48 gives the same result but at different ALR's. It is clear that the largest drop size is obtained when the air velocity is minimum and liquid flow rate is maximum.

For kerosine, Figs.53 and 54 show the same trend but with lower values of S.M.D. at all conditions. In all these tests the velocities of both air stream were kept equal.

8.6. Air/Liquid Ratio Effect

When the liquid flow rate increases at a constant air flow rate the drop size is expected to be large due to insufficient energy being available in the air to atomize the thicker liquid ligaments formed from the sheet edge.

Figures 49 and 55 show the effect of A.L.R. on mean drop size for water and kerosine respectively. When the values of A.L.R. falls below about 3.5 the S.M.D. starts to increase, and at values of A.L.R. less than two the atomization quality deteriorates rapidly. The beneficial effect of high A.L.R. diminishes very quickly when its value exceeds about 5.5, and above this value it is clear, from the figures, that the curves of the Sauter mean diameter against A.L.R. become nearly flat, which means no more improvement in atomization quality can be gained from further increase in air flow rate.

For high viscosity liquids, when S.M.D. is plotted against $(1 + W_l/W_a)$, it can be observed in Fig.61, which is reproduced from Fig.59, that as the value of A.L.R. increases the quality of atomization is improved.

8.7. The Influence of Liquid Film Thickness

A thick film is more difficult to atomize than a thin film due to the fact that, for any given quantity of liquid the area of the liquid sheet which is exposed to the air stream should be as large as possible. With thick films the air stream is able to atomize the layers near the surface of the sheet to produce fine drops, but its effect on the inner layers is less depending on how thick is the sheet, and the mean droplet size of the resulting spray is therefore large.

The liquid film thickness was varied from 0.0089 cm to 0.0385 cm for water, and from 0.0089 cm to 0.0435 cm for kerosine. The range of air velocity was from 54.9 to 122 m/s. Figures 50, 51 and 52 show how the S.M.D. of water sprays increases with increase in liquid film thickness for various air velocities, liquid flow rates, and air/liquid ratios respectively. Figures 56, 57 and 58 show the corresponding results for kerosine.

The effect of film thickness on S.M.D. for high viscosity liquids is shown in Fig.60, and it is again clear that thicker films results in larger mean drop sizes. The film thicknesses used are fairly high (from 0.0254 to 0.1016 cm) to simulate the conditions of high viscosity liquids.

For liquids of different surface tension the influence of film thickness is similar and always the mean droplet size is larger for thicker films (Fig.63), and the same conclusion can be drawn for liquids of different densities, as shown in Fig.65.

8.8. Effect of Liquid Properties

8.8.1. Viscosity

It was observed in a previous chapter that high viscosity liquids, when atomized by the effect of air flow, give very long ligaments as a first step in the disintegration mechanism, and that is because the viscous forces tend to suppress the formation of the surface waves, which are responsible for the atomization, and also resist the further disintegration of the ligaments to drops and then to droplets. This last

stage of the disintegration process occurs at a region of relatively low air velocity, hence one expects high viscosity liquids to produce relatively large drops.

Viscosity was varied from 1.29×10^{-3} to 76.5×10^{-3} Kg/m.s, and in the first group of tests the liquid flow rate and film thickness were kept constant at 4.5 gr/s and 0.0508 cm respectively.

It was found that S.M.D. increased rapidly with increase in absolute viscosity for various air velocities. It is worth mentioning here again the beneficial effect of increasing the air velocity on the resulting mean drop size, as shown in Fig.59. When the air velocity was kept constant at 91.5 m/s, and the film thickness varied from 0.0254 to 0.1016 cm, S.M.D. increased with increase in absolute viscosity and/or the increase in film thickness as shown in Fig.60.

8.8.2. Surface Tension

The surface tension of a liquid tends to give the drops more resistance against the shattering effect of air streams. Also, the ligaments drawn from a film of high surface tension liquid are usually thicker and longer and tend to have wider bases at the atomization edge. Both effects lead to higher values of S.M.D. at high surface tension.

The variation of S.M.D. with surface tension is given in both Figs.62 and 63 for various air velocities and various film thicknesses respectively, at constant liquid flow rate of 9.1 gr/s. In these experiments the range of surface tension was from 26.8×10^{-3} to 73.5×10^{-3} N/m. Increase in S.M.D. with increase in surface tension is observed in both figures.

8.8.3. Density

In discussing the effect of liquid density on the disintegration of liquid films in a previous chapter, it was observed that for low density liquids the threads were rather thin and seemed to form directly from the film. At higher liquid densities the formation of threads was delayed, and the liquid film continued to travel from many parts of the atomizing edge for some distance downstream before breaking into threads and subsequently into drops. Atomization thus occurred at relatively low air velocity leading to higher values of S.M.D.

The range of liquid density studied was from 0.933×10^{3} to 1.83×10^{3} Kg/m^3 which was rather narrow. Figure 64 shows the observed increase in S.M.D. with increase in density for various air velocities. It is clear that the rate of increase of S.M.D. is generally quite small and only very slight increase occurs at densities above 1.6×10^{3} Kg/m^3, especially at the higher air velocities.

The same comments apply to Figure 65, in which the air velocity is kept constant, while film thickness is varied.

8.9. Effect of Air Pressure

The first set of tests was carried out using a large conventional airblast atomizer to study the effect of high pressure air on the mean drop size of the spray.

The air pressure was raised up to 1.0133×10^6 N/m^2 (10 standard atmospheres), and the liquids used were water and kerosine. The beneficial effect of air pressure upon the quality of atomization (i.e. upon S.M.D.) is shown in Fig.66. Three values of liquid flow rate were chosen at each air pressure level to obtain three constant values for A.L.R. over the whole range of air pressures.

In all readings the pressure drop across the atomizer was maintained at 3.5 percent of the upstream pressure in order to maintain a constant air velocity.

Atomizer (B) was also used in the high pressure rig to conduct both the second and the third group of tests, due to its capability of producing liquid sheets of known thickness. Figure 67 shows the results of high pressure tests on water, and it is clear that S.M.D. decreases rapidly when the air pressure is increased from atmospheric to about 7.5×10^5 N/m^2 at constant air velocity and temperature. The air/liquid ratio varied from 2 to 5 which is the important range for mean drop size as noted before (Figs.49 and 55).

The objective of the third set of tests was to determine the effect of air pressure on liquids of high viscosity, hence two levels of viscosity of 6×10^{-3} and 17×10^{-3} Kg/m.s were chosen for these experiments while the pressure changed from 1×10^5 to 5.5×10^5 N/m^2.

For constant air velocity the mean drop size decreased with increase in air pressure, as given in Table 4, which confirms previous conclusions of the beneficial effect of increase in ambient pressure on atomization quality which can be attributed to the larger aerodynamic forces acting on the liquid sheet at higher values of air density.

CHAPTER 9

ANALYSIS OF EXPERIMENTAL RESULTS

CHAPTER 9

ANALYSIS OF EXPERIMENTAL RESULTS

The effects of the variables involved in the process of fuel atomization were carefully studied in the foregoing chapters, and all the experimental results were presented in figures, in such a way as to give a clear picture of the separate influence of each variable. It is of great importance to arrange these variables into an expression which takes into consideration their relative effects, to enable the Sauter mean diameter of a given spray to be predicted at any specified condition. Also, it is essential for the proposed equation to be valid over a wide range of air and liquid properties so that it may be applied to many different types of airblast atomizer.

The experimental results showed that liquid viscosity has a separate effect from air velocity and density, which both have a dominant effect on the S.M.D. of sprays of low viscosity liquids, which suggests an equation for S.M.D. consisting of two terms. For low viscosity liquids, the term which is dominated by viscosity will be negligibly small, and the value of S.M.D. will depend mainly on the other term, while both terms will determine the S.M.D. for high viscosity liquids.

The surface tension and density of liquids should be included in the equation due to their effects on the mean drop size, increase in either property will result in a larger S.M.D. It has been shown before that, thinner liquid sheets should give finer sprays, and this result was observed for both low and high viscosity liquids. The last parameter which must appear in the equation is the air to liquid ratio, which proved to have a beneficial effect upon the quality of atomization.

9.1. Dimensional Analysis

From all the results obtained from the experiments, and considering the relative importance of each factor the following expression was derived :

$$S.M.D. = 19.95\left(\frac{\sigma_l^{0.6}\ \rho_l^{0.25}}{\rho_a^{0.85}\ V_r^{1.2}}\right)(t)^{0.4}\left(1+\frac{W_l}{W_a}\right)^{0.85} + 16.9\left(\frac{\eta^2}{\sigma_l\ \rho_l}\right)^{0.45}(t)^{0.55}\left(1+\frac{W_l}{W_a}\right) \qquad (52)$$

where

σ_l	=	liquid surface tension	dyne/cm
ρ_l	=	liquid density	gr/cm^3
η_l	=	liquid viscosity	centipoise
V_r	=	atomizing air velocity	m/s
ρ_a	=	air density	gr/cm^3

t	=	liquid film thickness	cm
W_l	=	liquid flow rate	gr/s
W_a	=	air flow rate	gr/s
S.M.D.	=	Sauter mean diameter	microns

The equation is dimensionally correct, and when S.I. units are used equation (52) becomes :

$$S.M.D. = 0.50\left(\frac{\sigma_l^{0.6}\ \rho_l^{0.25}}{\rho_a^{0.85}\ V_r^{1.2}}\right)(t)^{0.4}\left(1+\frac{W_l}{W_a}\right)^{0.85} + 0.107\left(\frac{\eta_l^{2}}{\sigma_l\ \rho_l}\right)^{0.45}(t)^{0.55}\left(1+\frac{W_l}{W_a}\right) \qquad (53)$$

where S.M.D. is in metres and all units are in N, Kg, m, and s.

9.2. Comparison Between Experimental Results and Derived Equation

The values of S.M.D. calculated from Equation (52) were plotted against the experimental values in Figs.68 to 71 to show the ability of this equation to predict the S.M.D. of sprays produced by airblast atomizers over a wide range of air and liquid properties.

The agreement is very good in the case of high viscosity liquids, as shown in Fig.68, in the range of 1.29×10^{-3} to 44×10^{-3} Kg/m.s, but the agreement is less satisfactory when the air velocity is low. Figure 69 shows the density data, and in general, within the range of liquid density from 0.933×10^{3} and 1.83×10^{3} Kg/m^3, the correlation is satisfactory.

The surface tension of the liquids studied varied from 26×10^{-3} to 73.5×10^{-3} N/m (26 to 73.5 dyne/cm) and the ability of equation (52) to predict values of S.M.D. close to the experimental values can be observed in Fig.70.

Water and kerosine were usedas low viscosity liquids to establish the relationship between S.M.D. and air velocity, and when the equation was applied in this case it was found that the agreement was good in the range of air velocity between 70 and 122 m/s and of air to liquid mass ratio between 1.6 and 7.0. The main feature of Fig.71 is that the scatter increases at higher values of S.M.D., while the agreement is quite close at low values of S.M.D.

From the forementioned discussion it can be concluded that equation (52) gives very good correlation with the experimental results and covers wide ranges of all the variables influencing the process of atomization.

9.3. Comparison Between Equation (52) and Rizkalla-Lefebvre's Equation and Results

It is worthwhile to apply the present equation to Rizkalla-Lefebvre's work to check whether the predicted values of S.M.D. will agree with the values calculated from their equation and to see how close they are to the experimental results obtained on their aromizer.

The main difference between both equations is the appearance of the film thickness in the present equation, which can take different values under the different conditions of air and liquid properties, instead of the prefilmer diameter in Rizkalla-Lefebvre's equation, which is constant. Thus the first step that must be taken before making the comparison is to calculate the film thickness for each condition, taking into consideration the dimensions of the atomizer, from Equation (50).

Figure 72 shows a direct comparison between the present equation and the Rizkalla-Lefebvre's equation. The experimental points they obtained are also plotted in this figure. The range of air velocity was from 54 to 122 m/s, and the water flow rate was 9.1 gr/s. It is quite impressive to note the close agreement between the present equation and both their experimental results and the equation they derived, especially at air velocities above 80 m/s, bearing in mind that the calculations went through two equations, (50) and (52), which increased the possibility of a large deviation from their equation. At low air velocity Equation (52) predicts higher values of S.M.D.

The comparison for kerosine is shown in Fig.73, and the agreement at air velocities above 80 m/s is clear. Over a considerable length of their experimental curve Equation (52) gives a nearly coincident plot. For liquids of high viscosity the equation derived in this work follows closely the experimental curve of Rizkalla and Lefebvre in the range from 2.8×10^{-3} to 50×10^{-3} Kg/m.s., as given in Fig.74, and that indicates the capability of Equation (52) to predict values of S.M.D. which are in reasonable agreement with their work for both low and high viscosity liquids. This conclusion is shown in Figs.75 and 76 where the mean drop diameter calculated from Equation (52) are plotted against the values they measured.

It is important to notice that for viscous liquids Rizkalla-Lefebvre's equation assumes that the air density has a significant effect on both terms, but in the present study the experiments show that the dependence of S.M.D. on air density is only through the first term. The second term of Equation (52) takes an approximately constant value when the air/liquid ratios are considered for all levels of air pressure (Table 4).

9.4. Comparison Between Equation (52) and Wigg's Work

It is quite difficult to compare the present equation directly with Wigg's equations due to differences in the method of forming the liquid sheets and exposing them to the air streams. In the N.G.T.E. atomizers he used, the liquid passes through the inner annulus and flows outwards as a thin sheet at right angles to the axial air stream.

Thus the film thickness cannot be predicted from Equation (50). However, the comparison may be done by applying both equations to Rizkalla and Lefebvre's results.

Figure 72 shows that Wigg's equation predicts lower values of S.M.D. than the experimental results for water, while it gives higher values but better agreement for kerosine in Fig.73. In general his equation takes a nearly parallel form to the experimental curves over the whole range of air velocity, although in some cases the difference between both curves is large.

For high viscosity liquids, Wigg's equation predicts very high S.M.D.'s compared to the results obtained by Rizkalla and Lefebvre, and also to the equation derived in this work when applied to their atomizer, as shown in Fig.74.

CHAPTER 10

CONCLUSIONS

CHAPTER 10

CONCLUSIONS

Due to the increasing application of airblast atomizers in modern gas turbine engines, all the variables which may have some effect on the process of atomization should be investigated. So far very little has been done concerning the effect of the liquid film thickness on the mean drop size of sprays produced by this type of atomizer, and the mechanism of disintegration of this film.

To facilitate the study of factors, two specially designed airblast atomizers of two-dimensional cross section, producing flat liquid sheets, were used. The conclusions drawn from this work may be stated as follows :

(A) Disintegration of Liquid Sheet

(1) In the process of sheet disintegration the formation of liquid ligaments is an essential stage between the continuous liquid film and the separate droplets, and these ligaments exist under all air and liquid conditions.

(2) With increase in air velocity the ligaments become shorter and thinner, and take a more uniform and straight shape. All the disintegration processes occur closer to the atomizing edge with increase in air velocity.

(3) Liquids of low surface tension are easy to disintegrate by the action of air flow and the resulting ligaments or threads are shorter in length, while sheets of high viscosity liquids break into long thick threads which may assume complex shapes.

(4) With high density liquids the disintegration of the sheet starts at a short distance downstream of the atomizing edge where the threads appear to be drawn from the disrupted film, which suggests that more resistance to air effects should be expected from high density films.

(5) Longer threads break up into larger drops due to the fact that the atomization process is completed far from the atomizing edge in regions of relatively low air velocity.

(6) Thicker liquid sheets result in thicker ligaments, which in turn disintegrate to larger drops. This highlights the importance of spreading the liquid into a thin sheet for good atomization quality.

(B) Drop Size Distribution in Sprays

(1) The distribution of drop sizes in a spray gives useful information on the uniformity of that spray. The presence of some very small droplets is important for initiating combustion, while the bigger drops are responsible for soot formation and hydrocarbon emissions.

(2) The mathematical expressions of Rosin-Rammler and the upper limit distribution function follow the experimentally observed distributions quite closely for both low and high viscosity liquid sprays, and at all air velocity levels, which makes it possible to use the distribution parameter defined in these expressions to compare the uniformity of various sprays, and also in calculating their mean drop sizes.

(3) High air velocity has a beneficial effect on producing a more uniform spray containing fewer large drops, while increase in liquid flow rate will slightly reduce the uniformity of the spray.

(4) The influence of liquid surface tension and viscosity are similar, that increase in either will tend to shift the distribution curve towards higher drop levels, and the sprays produced are less uniform. Liquid density has an insignificant effect on drop size distribution, although there is a slight displacement to lower drop sizes at lower densities.

(5) S.M.D.'s calculated from the mathematical expression agree very closely with the values obtained by the optical technique, while S.M.D.'s determined by measuring and counting all the drops present in a sample obtained by a photographic technique always have a higher value. This is attributed to the absence of the smallest droplets which do not appear on the photographic slides.

(6) The experimental points fit reasonably well with Simmons' correlation of a drop size distribution when plotted in a 'square root/normal probability' way, although in general the mean line of these points is slightly different, with a lower standard deviation.

(C) Liquid Film Thickness

(1) The thickness of the liquid sheet depends on both air and liquid properties and also on the dimensions of the airblast atomizer. High values of liquid viscosity and flow rate result in thicker films, while high air velocity and high density produce opposite effects. A thinner film may also be obtained by using a larger prefilmer diameter.

(2) The above conclusions are supported by the experimental data, the available models, and the theoretical derivations.

(3) Liquid surface tension appears to have no effect on film thickness. However, it does have a significant influence on the entrainment of droplets from the liquid surface into the air stream upstream of the prefilmer edge. Thus low surface tension decreases the critical air velocity for entrainment, and also increases the quantity of entrained liquid.

(4) An expression is proposed to predict the film thickness as follows :

$$t = \frac{2.15}{d_e^{0.55}} \left(\frac{\eta_l^{0.35}}{u_a^{0.9}} \right) \cdot \left[\frac{W_l^{0.55}}{(\rho_a \rho_l)^{0.45}} \right]$$, which takes

into account the effects of air and liquid properties and also the characteristic dimension of the atomizer.

(D) Mean Drop Size

(1) The values of the S.M.D. were determined experimentally by the scattering light technique which employed an He-Ne Laser as a light source. This method proved to be accurate over the range of drop sizes normally encountered in airblast atomizers.

(2) The special liquid solutions used in the tests enabled the separate effects of viscosity, surface tension and density on atomization quality to be evaluated while the design of the variable liquid gap helped to vary and control the initial film thickness.

(3) For liquids of low viscosity such as water and kerosine the mean drop size decreases rapidly with increase in air velocity while high surface tension impairs atomization quality. The effect of liquid density on drop size is similar to that of the surface tension but to a lesser degree, especially at high levels of density.

(4) For good atomization the air/liquid ratio should ideally exceed a value of 1.6. As this ratio is increased the quality of atomization will gradually improve. However, no further improvement is gained by increasing the air/liquid ratio above a value of about 7.

(5) Thicker liquid films result in coarser sprays. This can be observed from the continuous increase in mean drop size with increase in film thickness.

(6) Liquid viscosity has an effect on S.M.D. that is quite separate and distinct from that of air velocity, and it is obvious that atomizers dealing with heavy liquids will produce sprays of large mean drop sizes no matter how high the air velocity. This suggests heating up the liquid to lower its viscosity to an acceptable level before feeding it into the atomizer.

(7) Increasing the ambient pressure has a beneficial influence on atomization quality, especially for low viscosity liquids.

(8) Based on consideration of all the effects mentioned above the mean drop diameter may be predicted by the following dimensionally correct equation :

$$\text{S.M.D.(in m)} = 0.50 \left(\frac{\sigma_l^{0.6} \rho_l^{0.25}}{\rho_a^{0.85} V_r^{1.2}} \right) (t)^{0.4} \left(1 + \frac{W_l}{W_a}\right)^{0.85} + 0.107 \left(\frac{\eta_l^2}{\sigma_l \rho_l} \right)^{0.45} (t)^{0.55} \left(1 + \frac{W_l}{W_a}\right)$$

which covers the following ranges :

Air velocity	70 to 122 m/s
Air/liquid ratio	1.6 to 7
Air pressure	1.0133×10^5 to 10.133×10^5 N/m^2
Liquid viscosity	1×10^{-3} to 44×10^{-3} Kg/m.s.
Liquid surface tension	26×10^{-3} to 73.5×10^{-3} N/m
Liquid density	0.78×10^3 to 1.83×10^3 Kg/m^3

and liquid film thickness is in m, and air density is in Kg/m^3.

(9) It is obvious from the equation that air density affects S.M.D. through the first term, while the second term is dominated by the viscosity.

(10) The equation was applied to Rizkalla and Lefebvre's atomizer (Refs.79 and 80) and showed reasonable agreement with their equation and experimental results for both low and high viscosity liquids, although the present equation predicted higher mean drop sizes at low air velocities.

(11) The comparison with Wigg's equation (Ref.90) was carried out by applying both equations to Rizkalla and Lefebvre's atomizer. There is some agreement in the case of kerosine, but Wigg's equation predicts lower values of S.M.D. than both the present equation and Rizkalla-Lefebvre's equation when applied to water. There is no agreement for liquids of high viscosity.

10.1. Suggestions for Future Work

1. Due to the fact that the use of heavy and residual fuels in gas turbine engines is inevitable, the problems which accompany the atomization and combustion of these fuels should be studied carefully. Certainly, a good way to produce reasonable fine sprays is by means of an airblast atomizer. Thus it is of great importance to investigate the capability of this atomizer to deal with heavy fuels, and to ascertain the best operating conditions to achieve the best possible results.

2. To avoid the tedious procedure of counting and sizing of drops some modifications should be made to the light scattering method to enable both mean drop size and drop size distribution to be determined directly.

3. The effect of atomizer linear dimension needs more work to establish its precise influence on the mean drop size, and its relation to other variables involved in the atomization process.

REFERENCES

REFERENCES

1. ANSON, D. — "Influence of the Quality of Atomization on the Stability of Combustion of Liquid Fuel Sprays" Fuel, Quarterly Journal of Fuel Science, Vol.32, 1953, p.p.39-51.

2. BATER, K.M. and POULTON, W.R. — "The Performance of an Airspray Atomizer in the Primary Zone of a Gas Turbine Combustion Chamber" N.G.T.E. C.P.C.Note No.23, June 1966.

3. BENNETT, P.G. — "Airblast Atomization" Cranfield Thesis, Department of Aircraft Propulsion, June 1962.

4. PB.CHEMICALS INTERNATIONAL LTD. — "Hyvis Polybutenes" Technical Booklet No. HB 102/2.

5. BERBENTE, C.P. and RUCKENSTEIN, E. — "Hydrodynamics of Wave Flow" A.I.Ch.E. Journal, Sept.68, 772.

6. BEVANS, R.S. — "Mathematical Expressions for Drop Size Distribution in Sprays" Conference on Fuel Sprays, University of Michigan, Ann Arbor, Michigan, March 30-31 - 1949.

7. BLOCK, A.G. BAZAROV, S.M. and NAKHMAN, Yu.V. — "Some General Laws Governing Droplet Size Distribution on Atomization of Liquid" Thermal Energy 14, 7, pp 45 - 1967.

8. BORDNER, G.L. NAYFEH, A.H. and SARIC, W.S. — "Stability of Liquid Films Adjacent to Compressible Streams" College of Engineering, Virginia Polytechnic Institute and State University, VPI-E-73-3 - Jan.1973.

9. BRIFFA, F.E.J. and DOMBROWSKI, N. — "Entrainment of Air Into a Liquid Spray" A.I.Ch.E.Journal, Vol.12, No.4, July 1966, pp. 708 - 717.

10. BROWNING, J.A. and KRALL, W.G. — "Effect of Fuel Droplets on Flame Stability, Flame Velocity and Inflammability Limits" 5th Symposium on Combustion (International) 1955, pp.159-163.

11. BRYAN, R.H. — "An Experimental Study of an Airblast Atomizer" Cranfield M.Sc.Thesis, Department of Aircraft Propulsion, Oct.1967.

12. BRYAN, R.H. GODBOLE, P.S. and NORSTER, E.R. "Some Observations of the Atomizing Characteristics of Airblast Atomizers" Cranfield International Symposium Series, Vol.11, Edited by E.R.Norster, Pergamon Press, 1971.

13. BUEVICH, Yu.A. and GUPALO, Yu.P. "Stability of a Laminar Film Flow" Mekhanika Zhidkosti, Gaza, Vol.1, No.1, pp 105, 1966.

14. CASTLEMAN, R.A. "The Mechanism of Atomization of Liquids" National Bureau of Standards Journal of Research (U.S.Dept.of Commerce), Vol.6, No.281, 1931, p.369.

15. CHARVONIA, D.A. "An Experimental Investigation of the Mean Liquid Film Thickness and the Characteristics of the Interfacial Surface in Annular, Two-Phase Flow" Paper Presented at Winter Ann.Meeting of A.S.M.E. N.Y. Nov.26th - Dec.1st. 61-WA-243.

16. CHIN, J. and KEVORKIAN, V. "Mass Production of 300-Micron Water Droplets by Air-Water, Two-Phase Nozzles" Industrial and Engineering Chemistry, Process Design and Development, Vol.7, No.4, Oct. 68, pp.586.

17. CLARE, H. and ASHWOOD, P.F. "Measurement of the Thickness of a Liquid Film on the Surface of a Rapidly Rotating Disc" Instrument Practice, Vol.16, 1, Jan.62, pp.70.

18. CLARE, H. GARDINER, J.A. and NEALE, M.C. "Study of Fuel Injection in Air Breathing Combustion Chambers" Advisory GP for Aero Res.& Dev.(AGARD) NASA Sci & Tech. Aero Repts. 1964.

19. CLARE, H. and RADCLIFFE, A. "An Airblast Atomizer for Use with Viscous Fuels" Journal of Institute of Fuels, Vol.27, Oct.1954, p.510.

20. CLARK, C.J. and DOMBROWSKI, N. "On the Photographic Analysis of Sprays" Aerosol Science, 1973, Vol.4, pp. 27, Pergamon Press.

X 21. COHEN, L.S. and HANRATTY, T.J. "Height of a Liquid Film in a Horizontal Concurrent Gas-Liquid Flow". A.I.Ch.E. Jnl. March 66, Vol.12, No.2, 290.

22. COHEN, N. and WEBB, M.J. "Evaluation of Swirl Atomizer Spray Characteristics by a Light Scattering Technique" Princeton University Aeronautical Engineering Laboratory Rept. No.597, Feb.1962.

23. COLLIER, J.G. and HEWITT, G.F. "Film Thickness Measurement in Two-Phase Flow" British Chemical Engineering May 1967, pp.709.

24. CRAPPER, G.D. DOMBROWSKI, N. JEPSON, W.P. and PYOTT, G.A.D. "A Note on the Growth of Kelvin-Helmholtz Waves on Thin Liquid Sheets" Jnl.of Fluid Mech. 1973, Vol.57, Part 4, pp.671.

25. DEISS, W.E. "The Optical Determination of Particle Sizes Obeying the Upper Limit Distribution Function" Princeton University Thesis, Dept. of Aeronautical Engineering, May 1960.

26. DICKINSON, D.R. and MARSHALL,Jr. W.R. "The Rates of Evaporation of Sprays" A.I.Ch.E. Jnl. Vol.14, No.4, July 68, pp.541.

27. DOBBINS, R.A. CROCCO, L. and GLASSMAN, J. "Measurement of Mean Particle Sizes of Spray from Diffractively Scattered Light" A.I.A.A.Jnl. Vol.1, No.8, Aug.63, pp.1882.

28. DOMBROWSKI, N. "A Method of Identifying Double-Flash Exposures" British Jnl.of Applied Physics, Vol.6,No.1, Jan.55, pp.17.

29. DOMBROWSKI, N. and FRASER, R.P. "A Photographic Investigation into the Disintegration of Liquid Sheets" Philosophical Trans. of the R.Society of London, Series A. Mathematical and Physical Sciences, No.924, Vol.247, pp.101, Sept.54.

30. DOMBROWSKI, N. FRASER, R.P. and PECK, G.T. "A Short Duration, Double-Flash System for Simultaneous or Delayed Operation" Jnl.of Sci.Instruments, Vol.32, No.9, Sept.55, pp.329.

31. DOMBROWSKI, N. and JOHNS, W.R. "The Aerodynamic Instability and Disintegration of Viscous Liquid Sheets" Chem.Eng. Sci. 1963, Vol.18, pp.203.

32. DORMAN, R.G. "The Atomization of a Liquid in a Flat Spray" British Jnl.of Appl.Physics, Vol.3, June 52, pp.189.

33. DURST, F. and WHITELAW, J.H. "Local Velocity Measurements in Atomized Sprays" Imperial College of Science and Technology, Dept. of Mech.Eng. Oct.71 (ET/TN/A112).

34. ELLIS, S.R.M. and GAY, B. "The Parallel Flow of Two Fluid Streams: Interfacial Shear and Fluid-Fluid Interaction" Trans.of the Inst.of Ch.Engs. Vol.37, No.4, 1959, pp.206.

35. FRASER, R.P. "Liquid Fuel Atomization" 6th Symposium on Combustion (International), 1957.

36. FRASER, R.P. and DOMBROWSKI, N. "The Dependence of Interpretation on Photographic Technique in Fluid Kinetics Research" Proc.of the Third International Congress on High-Speed Photography, London 10th-15th Sept. 1956.

37. FRASER, R.P. DOMBROWSKI, N. and ROUTLEY "The Mechanism of Disintegration of Liquid Sheets in Cross-Current Air Streams" Appl.Sci.Research, Volumes A11-A12, 1962-63.

38. FRASER, R.P. DOMBROWSKI, N. and ROUTLEY, J.H. "The Atomization of a Liquid Sheet by an Impinging Air Stream" Chem.Eng. Sci. Vol.18, No.6, June 1963, pp.339.

39. FRASER, R.P. EISENKLAM, P. and DOMBROWSKI, N. "Liquid Atomization in Chemical Engineering" British Chem.Eng. Vol.2, pp 414, 496, 536 and 610, 1957.

40. FRIEDMAN, S.J. and MILLER, C.O. "Liquid Films in the Viscous Flow Region" Ind.and Eng.Chem., July 1941, Vol.33, No.7, pp.885.

41. GIFFEN, E. "Atomization of Fuel Sprays" Engineering, Vol.174, July 1952, pp.6.

42. GIFFEN, E. and MURASZEW, A. "The Atomization of Liquid Fuels" Chapman and Hall Ltd. 1953.

43. GODBOLE, P.S. "The Effect of Ambient Pressure on Airblast Atomizer Performance" Cranfield Thesis, Dept.of Aircraft Propulsion, Sept.68.

44. GODFREY, D. "An Assessment of a Light Scattering Technique for Drop Size Measurement" Cranfield Thesis, Dept. of Aircraft Propulsion, Sept. 1969.

45. GRETZINGER, J. and MARSHALL, Jr.W.R. "Characteristics of Pneumatic Atomization" Jnl.of the American Institute of Chem. Eng. Vol.7, No.2, June 61, pp.312.

46. HANRATTY, T.J. and WOODMANSEE, D.E. "Stability of the Interface for a Horizontal Air-Liquid Flow" Symposium on Two-Phase Flow, Exeter 21-23 June 1965, Vol.1, pp. A101.

47. HANRATTY, T.J. and ENGEN, J.M. "Interaction Between a Turbulent Air Stream and a Moving Water Surface" A.I.Ch.E. Jnl. Vol.3, No.3, pp.299,Sept.57.

48. HEATH, H. and RADCLIFFE, A. "The Performance of an Airblast Atomizer" N.G.T.E. Rept.No.71, June 1950.

49. HEWITT, G.F. and HILL-TAYLOR, N.S. "Annular Two-Phase Flow" Pergamon Press 1970.

50. HEWITT, G.F. KING, R.D. and LOVEGROVE, P.C. "Techniques for Liauid Film and Pressure Drop Studies in Annular Two-Phase Flow" Chem.Eng. Division, Atomic Energy Research Establishment, Harwell, Berkshire, 1962.

51. HRUBECKY, H.F. "Experiments in Liquid Fuel Atomization" Jnl.of Appl.Physics, Vol.29, 1958.

52. JACKSON, M.L. "Liquid Films in Viscous Flow" A.I.Ch.E. Jnl. Vol.1, No.2, pp.231, June 55.

53. JENKINS, D.C. and BOOKER, J.D. "The Time Required for High Speed Air Streams to Disintegrate Water Drops" Ministry of Aviation, Aeronautical Research Council C.P. No.827, 1965.

54. JOYCE, J.R. "Fuel Atomizers for the Gas Turbine" Shell Thornton Research Centre, Miscellaneous 396, 1948.

55. KAPITSA, P.L. "Wave Flow in Thin Films of Viscous Liquids" Zhurnal Eksper.Teor.Fiz. Vol.18, No.1, pp.19, 1948.

56. KERKER, M. "The Scattering of Light" Academic Press, 1969.

57. KUYPERS, J.F.D. "Effect of Fuel Injection Method on Exhaust Smoke and Weak Extinction Performance of an Industrial Gas Turbine Combustor" C.I.T. Thesis Sept.1972.

58. LEE, D.W. "The Effect of Nozzle Design and Operating Conditions on the Atomization and Distribution of Fuel Sprays" National Advisory Committee for Aeronautics, 18th Annual Rept.1932, No.425, pp.505.

59. LEFEBVRE, A.H. "Progress and Problems in Gas Turbine Combustion"
10th Symposium on Combustion, 1965, pp.1129.

60. LEFEBVRE, A.H. "Design Considerations in Advanced Gas Turbine Combustion Chambers"
Cranfield International Symposium Series, Vol.10, Edited by E.I.Smith, Pergamon Press, 1968, pp. 3-19.

61. LEFEBVRE, A.H. and MILLER, D. "The Development of an Airblast Atomizer for Gas Turbine Application"
Cranfield College of Aeronautics, Rept. Aero No.193, June 1966.

62. LEFEBVRE, A.H. and NORSTER, E.R. "A Proposed 'Double Swirler' Atomizer for Gas Turbine Fuel Injection"
Cranfield S.M.E. Report No.1, June 1972.

63. LEWIS, H.C. EDWARDS, D.G. GOGLIA, M.J. RICE, R.I. and SMITH, L.W. "Atomization of Liquids in High Velocity Gas Streams"
Industrial and Eng.Chemistry, Vol.40, No.1, Jan.48, pp.67.

64. LILLELEHT, L.U.and HANRATTY, T.J. "Relation of Interfacial Shear Stress to the Wave Height for Concurrent Air-Water Flow"
A.I.Ch.E. Jnl. Dec.1961, 548.

65. LOCKHART, R.W. and MARTINELLI, R.C. "Proposed Correlation of Data for Iso-Thermal Two-Phase, Two Component Flow in Pipes"
Chem. Eng.Progress, Vol.45, No.1, Jan 49, 39.

66. LONGWELL, J.P. and WEISS, M.A. "Mixing and Distribution of Liquids in High-Velocity Air Streams"
Industrial and Engng. Chemistry, Vol.45, No.3, March 53, 667.

67. LORENZETTO, G.E. "Influence of Liquid Properties on Plain Jet Air-Blast Atomization"
Cranfield Ph.D.Thesis, April 1976.

68. LUCAS, J. "The Jet-Engine Fuel System", Flight, Vol.49, Jan.1946, p.41.

69. MACEY, W.R. "A Study of the Factors Influencing Fuel Prefilming and Spray Angle in Airblast Atomizers"
Cranfield S.M.E. Thesis, Sept.1971.

70. MAYER, E. "Theory of Liquid Atomization in High Velocity Gas Streams"
A.R.S. Jnl., Vol.31, 1961, pp.1783.

71. MIESSE, C.C. "Recent Advances in Spray Technology" Appl.Mechanics Reviews, Vol.9, No.8, August 56, pp.321.

72. MUGELE, R.A. and EVANS, H.D. "Droplet Size Distribution in Sprays" Jnl.of Industrial and Engng.Chemistry, Vol.43, No.6, pp.1317, June 1951.

73. NORSTER, E.R. and LEFEBVRE, A.H. "Effects of Fuel Injection Methods on Gas Turbine Combustor Emissions" Symposium on Emissions from Continuous Combustion Systems. General Motors Research Laboratories, Michigan, U.S.A. 1971.

74. NUKIYAMA, S. and TANASAWA, Y. "Experiments on the Atomization of Liquid by Means of an Air Stream" Trans.of the Society of Mechanical Engs. (Japan), Repts. 1-6, Vols.4-6, 1938-1940.

75. POPOV, M. "Model Experiments on Atomization of Liquids" N.A.S.A. T.T. F.65, July 1961.

76. RADCLIFFE, A. and CLARE, H. "A Correlation of the Performance of Two Airblast Atomizers with Mixing Sections of Different Size" N.G.T.E. Rept.No. 144, Oct.1953.

77. RANGER, A.A. and NICHOLLS, J.A. "Aerodynamic Shattering of Liquid Drops" A.I.A.A. Jnl. Vol.7, No.2, Feb.1969, pp.285.

78. RIZKALLA, A.A. "The Influence of Air and Liquid Properties on Airblast Atomization" Cranfield Ph.D. Thesis, Sept. 1974.

79. RIZKALLA, A.A. and LEFEBVRE, A.H. "Influence of Liquid Properties on Airblast Atomizer Spray Characteristics" A.S.M.E. Gas Turbine Conference, Zurich, April 1974, to be published in A.S.M.E. Trans. Jnl.of Engng.for Power.

80. RIZKALLA, A.A. and LEFEBVRE, A.H. "The Influence of Air and Liquid Properties on Airblast Atomization" A.S.M.E. Symposium on Fluid Mechanics of Combustion, Montreal Conference, May 74, to be published in A.S.M.E. Trans.Jnl.of Fluids Engng.

81. ROBERTS, J.H. and WEBB, M.J. "Measurement of Droplet Size for Wide Range Particle Distributions" A.I.A.A. Jnl.Vol.2, No.3, March 64, pp.583.

82. ROBERTS, J.H. and WEBB, M.J. "The Use of the Upper Limit Distribution Function in Light Scattering Theory as Applied to Droplet Diameter Measurement" Princeton University Aeronautical Eng.Lab. Rept.No.650, 1963.

83. ROSIN, P. and RAMMLER, E. "The Laws Governing the Fineness of Powdered Coal" The Institute of Fuel, Oct.33, pp.29, Vol.7.

84. ROSSUM, J.J. van "Experimental Investigation of Horizontal Liquid Film Wave Formation, Atomization, Film Thickness" Chemical Engng. Science 1959, Vol.11,pp.35.

85. SIMMONS, H.C. "The Correlation of Drop Size/Volume-Fraction Distributions in Fuel Nozzle Sprays" Paper Submitted for ASME Winter Ann.Meeting, Dec.5-10, 1976.

86. TAILBY, S.R. and PORTALSKI, S. "Wave Inception on a Liquid Film Flowing Down a Hydrodynamically Smooth Plate" Chem.Engng.Sci.1962, Vol.17, pp.283.

87. TIPLER, W. "The Measurement and Significance of Fuel Spray Momentum" London Shell International Petroleum Co.Ltd. Oil Products Development Division O.P.D. Rept.No.202/62M.

88. WEISS, M.A. and WORSHAM, C.H. "Atomization in High Velocity Air Streams" Appl.Sci.Research, Vol.29, No.4, April 59.

89. WIGG, L.D. "The Effect of Scale on Fine Sprays Produced by Large Airblast Atomizers" N.G.T.E.Rept.No.236, July 1959.

90. WIGG, L.D. "Drop-Size Prediction for Twin-Fluid Atomizers" Jnl.of the Institute of Fuel, Vol.27,No.286, Nov.64, pp.500.

91. WOODMANSEE, D.E. HANRATTY, T.J. "Mechanism for the Removal of Droplets from a Liquid Surface by a Parallel Air Flow" Chemical Engng Sci. 1969, Vol.24, pp.299.

92. YORK, J.L. and STUBBS, H.E. "Photographic Analysis of Sprays" Trans.of A.S.M.E. Oct.1952, pp.1157.

93. YORK, J.L. STUBBS, H.E. and TEK, M.R. "The Mechanism of Disintegration of Liquid Sheets" A.S.M.E.Paper No.53-S-40, 1953.

APPENDICES

APPENDIX A

AN EXAMPLE OF THE CALCULATION AND REPRESENTATION OF DROP SIZE DISTRIBUTION

An example of all the necessary calculations involved in finding the drop size distribution and the relevant mathematical expressions is given here for a spray produced from an airblast atomizer under the conditions of air velocity and water flow rate of 91.44 m/s and 13.6 gr/s respectively. The drops, which were measured and counted by means of the photographic technique described in Chapter 6, are arranged in groups each of diameter (X) and number of drops (n). It is required to:

1. Calculate the S.M.D. directly from the data.

2. Plot the volume fraction ($\Delta v/V$) and number fraction ($\Delta n/N$) of each group against the corresponding drop diameter (X).

3. Plot the drop distribution in the cumulative volume of drops having diameters larger than a given diameter ((1 - v) against X).

4. Compare the distributions due to the mathematical expressions and the experimental one.

5. Calculate the S.M.D. of the spray from these expressions.

Procedure of Calculation

1. It is clear from Table (A.1) that the value of S.M.D. may be calculated directly from : $\Sigma nX^3/\Sigma nX^2$ which is 91 microns in the present example.

2. The plots of $\Delta v/V$ and $\Delta n/N$ against X are shown respectively in Figs.23 and 22.

3. From Table (A.1) the drop distribution, (1-v) against X, may be plotted, and Fig.24 shows similar plots for other sprays to give a good idea of the shape of the distributions, and the information which may be obtained from this type of representation.

4. To find the size parameter ($\bar{X}$) and the distribution parameter (q) of the Rosin-Rammler equation, Table (A.2) is used to plot $\ln\left(\frac{1}{1-v}\right)$ vs X on log-log paper in a manner similar to Fig.32. Then the value of X for which $1 - v = e^{-1}$, and the slope of the straight line represent the two parameters. The values in the present example are $\bar{X} = 106$ and $q = 3.46$.

The parameters of the U.L.D.F. are determined by plotting $u \left(= \frac{X}{X_m - X}\right)$ against 100 v on log-probability paper, where X_m

is the maximum size drop which is found by trial and error to give the best alignment of data points. The inclination of the line gives directly the parameter (δ), while the value of a is determined from $a = 1/u_{50}$ where u_{50} is the value of u at 100 v = 50 as shown in Fig.33. In this case X_m = 235 microns, δ = 1.05, and a = 1.515.

From the equations given in Chapter 6 both expressions may be plotted with the experimental distribution, as shown in Fig.35.

5. The values of S.M.D. are obtained from both expressions according to the equations given in Chapter 6. The values are:

S.M.D. = 83 microns (Rosin-Rammler)

and S.M.D. = 82 microns (U.L.D.F.)

which illustrates how close are the values of S.M.D. when predicted by both expressions.

X(microns)	n	$nX^2 \times 10^{-3}$	$nX^3 \times 10^{-6}$	$\Delta v/V \times 100$	1 - v	$\Delta n/N \times 100$
17.65	72	22.50	0.3975	0.0723	0.9993	5.8
35.30	330	411.00	14.508	2.638	0.9730	26.59
52.95	288	807.19	42.734	7.770	0.8952	23.21
70.60	238	1185.87	83.709	15.221	0.7430	19.18
88.25	130	1012.10	89.303	16.238	0.5810	10.48
105.90	98	1098.68	116.330	21.152	0.3691	7.90
123.55	56	854.53	105.559	19.120	0.1771	4.51
141.20	21	418.54	59.088	10.744	0.0697	1.69
158.85	5	126.12	20.031	3.642	0.0332	0.40
176.50	2	62.28	10.991	1.999	0.01325	0.16
194,15	1	37.68	7.315	1.33	0	0.08
SUM TOTAL	1241	6036.57	549.9654	100	-	100

TABLE A.1.

X (microns)	1 - v	$\ln \frac{1}{1-v}$	100 v	$u = \frac{X}{X_m - X}$	dv/dX x 100		
					U.L.D.F.	R.R.	Experimental
17.65	0.9993	0.00072	0.0723	0.082	0.0287	0.0397	0.004
35.30	0.9730	0.0275	2.71	0.177	0.291	0.213	0.149
52.95	0.8952	0.1107	10.48	0.290	0.689	0.540	0.440
70.60	0.7430	0.2971	25.70	0.430	0.978	0.940	0.863
88.25	0.5810	0.5436	41.94	0.600	1.065	1.223	0.920
105.90	0.3691	0.9967	63.09	0.820	0.967	1.202	1.199
123.55	0.1771	1.7311	82.29	1.110	0.752	0.870	1.088
141.20	0.0697	2.6642	93.04	1.501	0.497	0.446	0.609
158.85	0.0332	3.4043	96.68	2.080	0.268	0.154	0.206
176.50	0.01325	4.3241	98.68	3.030	0.106	0.033	0.113
194.15	0	-	100	4.750	0.024	0.0043	0.075

TABLE A.2.

APPENDIX B

METHODS OF MEASURING LIQUID FILM THICKNESS

(1) Photometric Method

The principle of this technique is to pass a beam of light of constant intensity perpendicularly through the liquid film and to detect the intensity on the other side by means of photomultiplier. The light transmitted by a layer of light-absorbing medium (T) is related to the thickness of that layer (t) by Lambert's law :

$$T = I/I_o = \exp(-Kt) \qquad (a)$$

where I_o = intensity of the light source

I = intensity of light beam after passing through the film

K = the absorption coefficient

The output of the photomultiplier tube is fed through a d.c. microameter to enable the thickness to be measured and, if required, to an oscilloscope for making photographic records of the liquid surface shape. To increase the sensitivity of the apparatus it is necessary to increase the value of k by adding small quantities of a suitable dye. This method was reported to be accurate by Charvonia (Ref.15) although many criticisms could be made against this technique. For example the intensity of light detected may be reduced by means other than absorption. The light may be scattered and reflected away from the detector in case of wavy liquid surface. To apply this method to measure liquid film thickness in an airblast atomizer the light beam must find a clear path to penetrate perpendicularly through the film.

(2) Some Electrical Methods

The electrical resistance (R) of a liquid film contained between two thin electrodes that are flush with the surface over which the film is flowing is related to the film thickness through a simple expression of the form :

$$t = \text{constant} \times r/R \qquad (b)$$

where r is a reference resistance of the liquid, and the constant can be found from calibration of the apparatus as given in Ref.84.

For thin films the dependence of conductance upon film thickness is linear and independent of probe size when made flush with the surface, as in the above method. The following relationship is reported in Ref.49:

$$C = 2.918\ Kt \qquad (c)$$

where C is conductance in millimho between the probes for a thickness of t in thousandths of an inch, with a liquid of specific conductivity K ($ohm^{-1}.cm^{-1}$).

If there are two different media existing between two parallel metallic plates, then the system is considered equivalent to two condensers connected in series. Thus, in the case of an air stream flowing over a liquid film, with thickness t_2 and t_1 respectively, the total capacitance is equal to :

$$C = \frac{A\ \varepsilon_o\ \varepsilon_1\ \varepsilon_2}{t_2\varepsilon_1 + t_1\ \varepsilon_2} \qquad (d)$$

where A = area of metallic plate

ε_1 & ε_2 = dielectric constants of air and liquid respectively

ε_o = dielectric constant of free space = 8.85×10^{-12} Farad/m

The value of film thickness (t_1) calculated from equation (d) depends mainly on the accuracy of the circuits which are used to determine the capacitance. In general a small error in measuring the capacitance may result in a significant deviation from the actual film thickness.

(3) Hot Wire Anemometry

This technique depends on the convective heat loss from an electrically heated sensing element to the surrounding fluid. This loss is a function of the temperature and geometry of the sensor and the velocity of the fluid and its temperature. The heat loss is equal to the electrical power delivered to the sensor and, assuming no change in the temperature of the fluid, the velocity of that fluid can be calculated from the reading of an electrical bridge.

By this means the film thickness can be determined when the liquid flow rate is given. The size of the sensor must be extremely small to avoid any disturbance to the liquid film and its position should be chosen carefully to obtain accurate and representative values of film thickness.

(4) Fluorescence Spectrometer Method

If a fluorescent dyestuff is added to the liquid, and a beam of light of a given wavelength is passed into the liquid film, then the incident light will excite a fluorescence of a different wavelength. The amount of fluorescent light emitted increases with increasing film thickness and this amount may be metered by separating the fluorescent light from the reflected components of the incident light by means of a spectrometer and then measuring the resultant intensity with a photomultiplier.

An apparatus employing this technique is described by Hewitt et al (Ref.50) and is reported to be quite accurate and does not interrupt the liquid film. This method is most suitable when the liquid is recirculating but with airblast atomizers, there is a continuous discharge of liquid

which cannot be recirculated. This requires the continual addition of small amounts of dyestuff which may cause problems.

Some other methods of measuring the liquid film thickness are contained in chapter 7 to cover most of the available techniques in this field.

APPENDIX C

DESCRIPTION AND SPECIFICATION OF OPTICAL BENCH

The optical apparatus, which is shown diagrammatically in Fig.7 and Plates 3, 5 and 6 was used to measure the Sauter mean diameter of the sprays under investigation with more accuracy than in previous studies due to the inclusion of more advanced optical and electronic units. The 5 mW-Helium/Neon Laser by Specta Physics (Model 120) has the following characteristics :

Beam Diameter :	0.65mm at $1/e^2$ points
Beam Divergence :	1.7 milliradians at $1/e^2$ points
Wave length :	632.8 nm (6328 Å)
Beam Amplitude Noise (1 to 100 KHz):	< 0.5% r.m.s.
Beam Amplitude Ripple (120 Hz) :	< 0.2% r.m.s.
Beam Polarization :	Linear to better than 1 part per thousand
Plane of Polarization :	Vertical

The "spatial filter" (Model 332) has an aperture of 22 microns placed at the focus of the expanding lens of 12.8mm focal length, and the aperture assembly position in the optical unit may be adjusted in the X and Y position by two adjustment knobs and in the Z position (axial alignment) by a rotational lock ring.

"Beam Expanding Telescope" unit (Model 333) is screwed to Model 332 to produce a highly collimated beam of a diameter determined by the initial beam diameter (0.65 mm) and by the multiplication factor i.e. the ratio of focal lengths of the collimating and expanding lenses: 85/128 = 6.64. A beam diameter of 4.32mm is then obtained at $1/e^2$ points, and this enlargement of the beam is to reduce the beam divergence or spread.

Both the collimated light beam and the light from a small lamp are chopped in a synchronous way by a rotating perforated disc, and the electrical signals produced by the photomultiplier tube and the photo-cell transducer which is detecting the lamp light are passed into the Gate circuit (Fig.9), thus the unwanted output of the phototube due to stray light in the system is reduced and sensitivity is increased.

The receiving side consists of 60 cm focal length lens focussing the monochromatic beam onto a 22 microns aperture which is part of Spectra-physics Model 332 stripped of its condensing lens, and finally the beam travels the distance to the photomultiplier tube through an interchangeable neutral density filter. The tube (located in a PR-1400 RF photomultiplier housing by "Products for Research,Inc.") is of the type 9658R, manufactured by E.M.I. and has 11 venetian blind dynodes having highly stable CsSb secondary emitting surfaces. With this tube at λ = 6328 Å a Quantum Efficiency of 11.4% and a responsivity of 57 mA/w is achieved.

The electrical signal from the photomultiplier is passed into the Synchronous Demodulator, (Fig.9) and (Plate 5), to reach the X - Y plotter (type Bryans 26001, main frame A4, single pen) where it is amplified by a logarithmic amplifier module(type Bryans 26236). The X-axis displacement of the plotter is electrically connected to a Hewlett-Packard 7 DCDT-1000 linear displacement transducer which is mechanically linked to the photomultiplier trolley (Plate 6).

This arrangement allows to plot the scattered light profile which can be used to find 1/10th of the maximum intensity and the corresponding traverse distance and hence the Sauter mean diameter. The main feature of these plots is that the interpolation of the curves to eliminate the unscattered parts takes place over a shorter distance from the optical axis, which certainly improves the accuracy of determining the S.M.D.

TABLES

TABLE (1)

Solutions of the synthetic hydrocarbon polymer, Hyvis Polybutene No. 05 in kerosine to obtain a wide range of viscosity :

Solution	η_1	σ_1	ρ_1
Pure kerosine	1.293	27.67	0.784
30% Hyvis 05	2.868	28.67	0.800
40% Hyvis 05	4.286	28.78	0.809
50% Hyvis 05	6.042	28.87	0.812
60% Hyvis 05	9.789	29.17	0.819
70% Hyvis 05	17.014	30.08	0.823
80% Hyvis 05	33.802	30.16	0.828
85% Hyvis 05	44.104	30.27	0.830
90% Hyvis 05	76.541	30.46	0.833
95% Hyvis 05	123.921	30.70	0.838
Pure Hyvis 05	218.562	30.96	0.840

TABLE (2)

Mixtures of sec-Butyl Alcohol (Butan - 2 ol) with water to obtain different values of surface tension :

Solution	η_1	σ_1	ρ_1
Pure Water	0.998	73.45	0.998
1.48 % Butan-2-ol	1.127	55.94	0.990
2.44 % Butan-2-ol	1.131	51.89	0.988
3.85 % Butan-2-ol	1.150	46.45	0.986
6.98 % Butan-2-ol	1.274	39.45	0.983
11.11 % Butan-2-ol	1.404	33.96	0.980
16.67 % Butan-2-ol	1.712	29.07	0.978
25.93 % Butan-2-ol	2.342	26.77	0.968
Pure Butan-2-ol	3.468	24.16	0.807

TABLE (3)

Dibromo-ethane (ethylene dibromide) diluted with methylated spirit to obtain a wide range of density :

Solution	η_1	σ_1	ρ_1
Pure methylated spirit	1.530	26.17	0.812
9.09 % Dibromo-ethane	1.537	29.86	0.933
13.04 % Dibromo-ethane	1.545	30.29	0.978
16.67 % Dibromo-ethane	1.552	30.71	1.031
23.08 % Dibromo-ethane	1.559	31.14	1.123
28.47 % Dibromo-ethane	1.566	31.56	1.213
37.50 % Dibromo-ethane	1.574	31.99	1.315
44.44 % Dibromo-ethane	1.581	32.42	1.430
50.00 % Dibromo-ethane	1.588	32.84	1.503
54.00 % Dibromo-ethane	1.597	33.27	1.634
60.00 % Dibromo-ethane	1.603	33.70	1.830
Pure Dibromo-ethane	1.727	42.05	2.180

what 't'=?

TABLE (4)

Variation of S.M.D. with ambient air pressure for high viscosity liquids.

Liquid properties	Test No.	Air Press. $N/m^2 \times 10^{-5}$	Air Density Kg/m^3	W_l/W_a	S.M.D. microns
Viscosity = 17.014×10^{-3} Kg/m.s. Surface Tension = 30.08×10^{-3} N/m Density = 0.823×10^{3} Kg/m^3	1	1.73	2.06	0.0524	87
	2	2.42	2.88	0.054	69
	3	3.10	3.72	0.0477	61
	4	3.80	4.55	0.05	57
	5	4.50	5.40	0.05	54
	6	5.20	6.20	0.05	51
Viscosity = 6.042×10^{-3} Kg/m.s. Surface Tension = 28.87×10^{-3} N/m Density = 0.812×10^{3} Kg/m^3	7	2.42	2.88	0.16	63
	8	3.10	3.72	0.16	53
	9	3.80	4.55	0.173	49
	10	4.50	5.40	0.16	45
	11	5.20	6.20	0.18	43

Pressure Drop $\frac{\Delta P}{P} = 2.6\%$

FIGURES

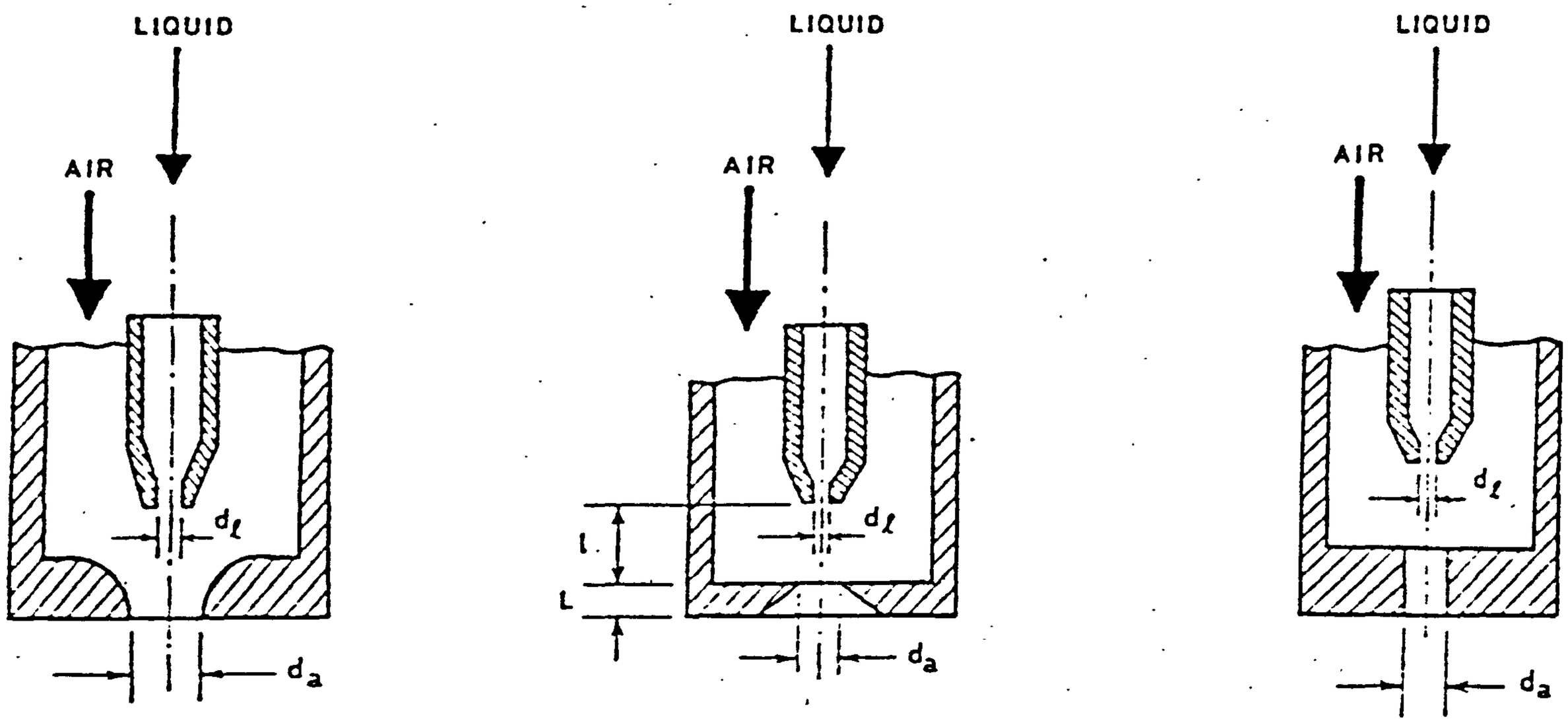

(a) Convergent Air Nozzle (b) 120° Sharp-Edged Orifice (c) Cylindrical Air Nozzle

NUKIYAMA AND TANASAWA ATOMIZERS

FIG.1

FIG. 2

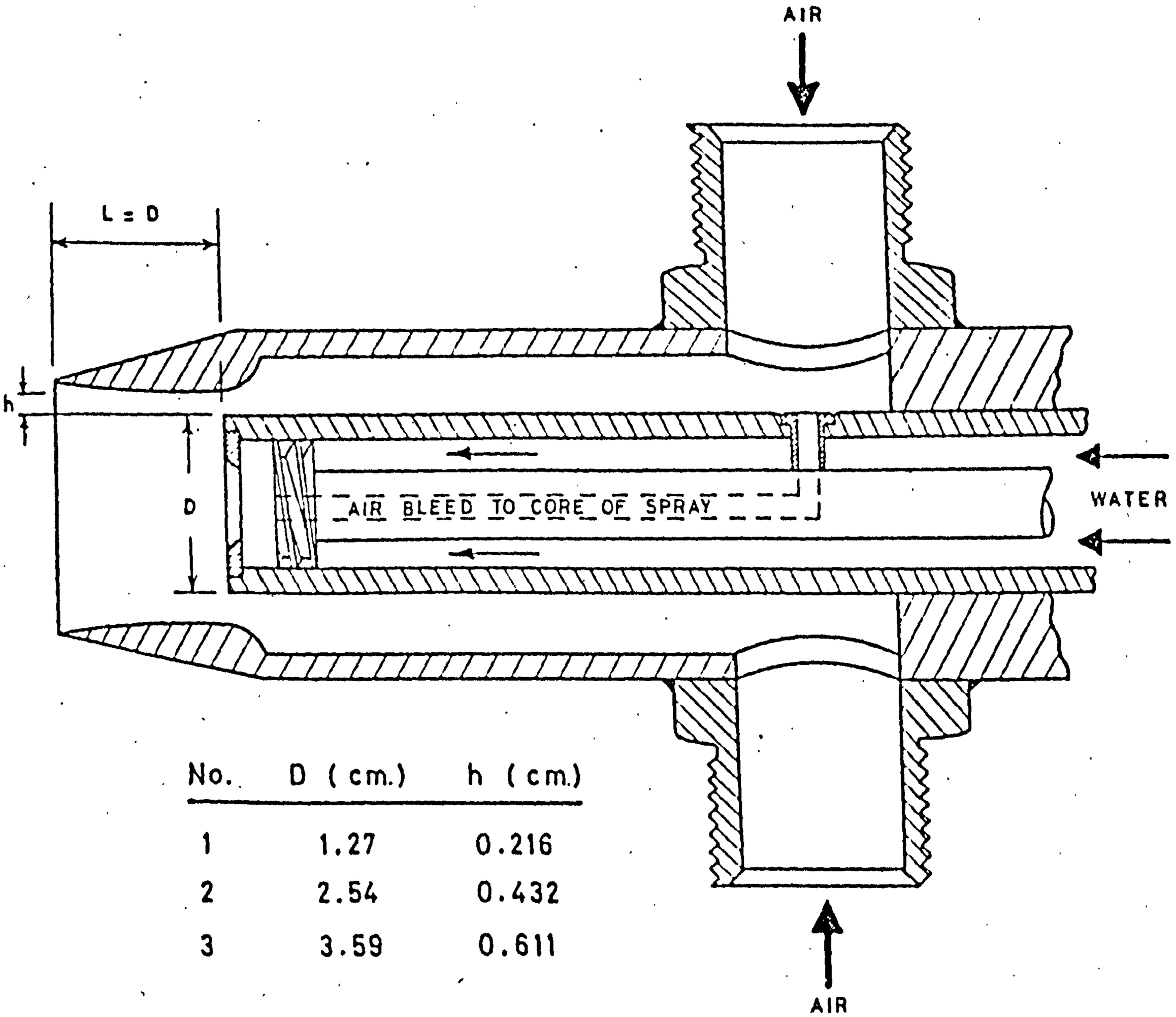

No.	D (cm.)	h (cm.)
1	1.27	0.216
2	2.54	0.432
3	3.59	0.611

N.G.T.E. AIRBLAST ATOMIZER

FIG. 3

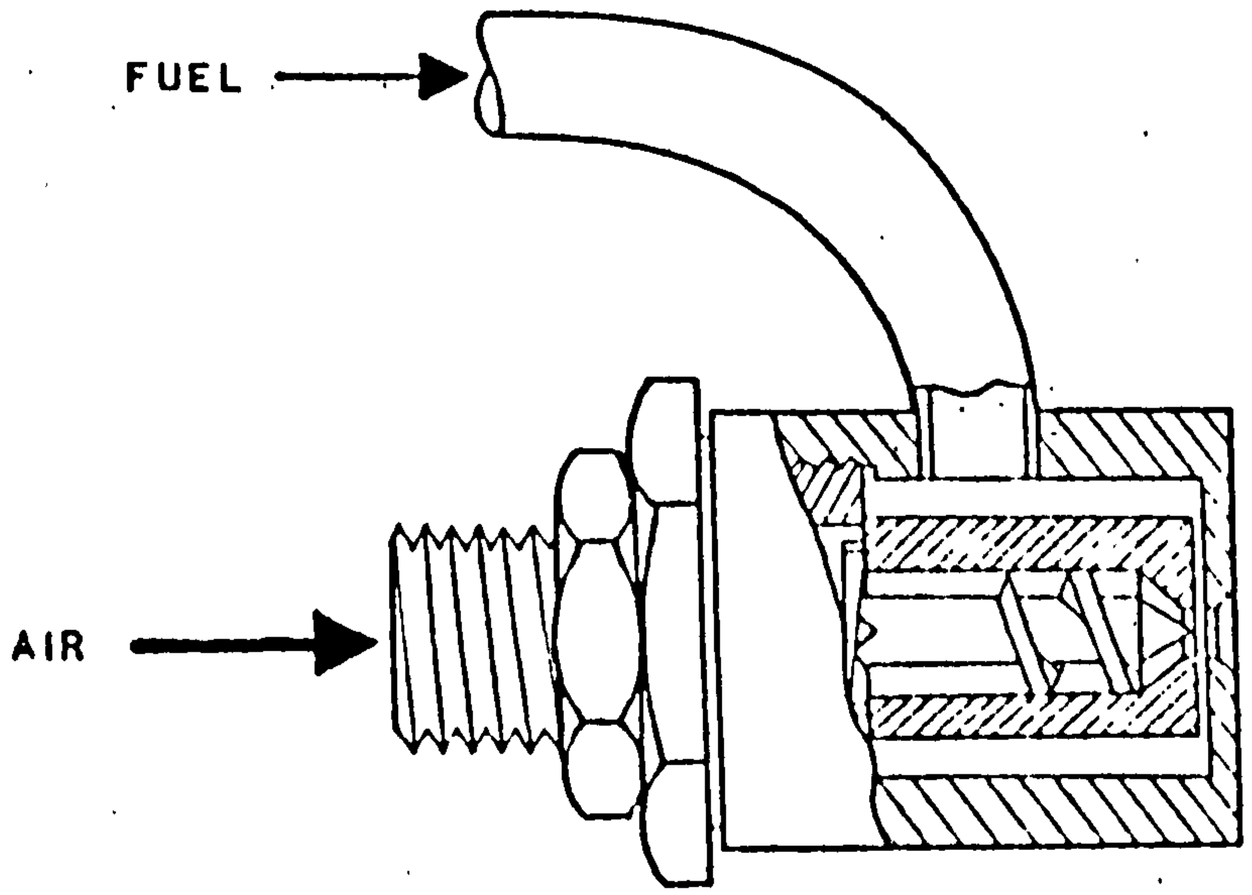

(a) 1/8-Inch Orifice

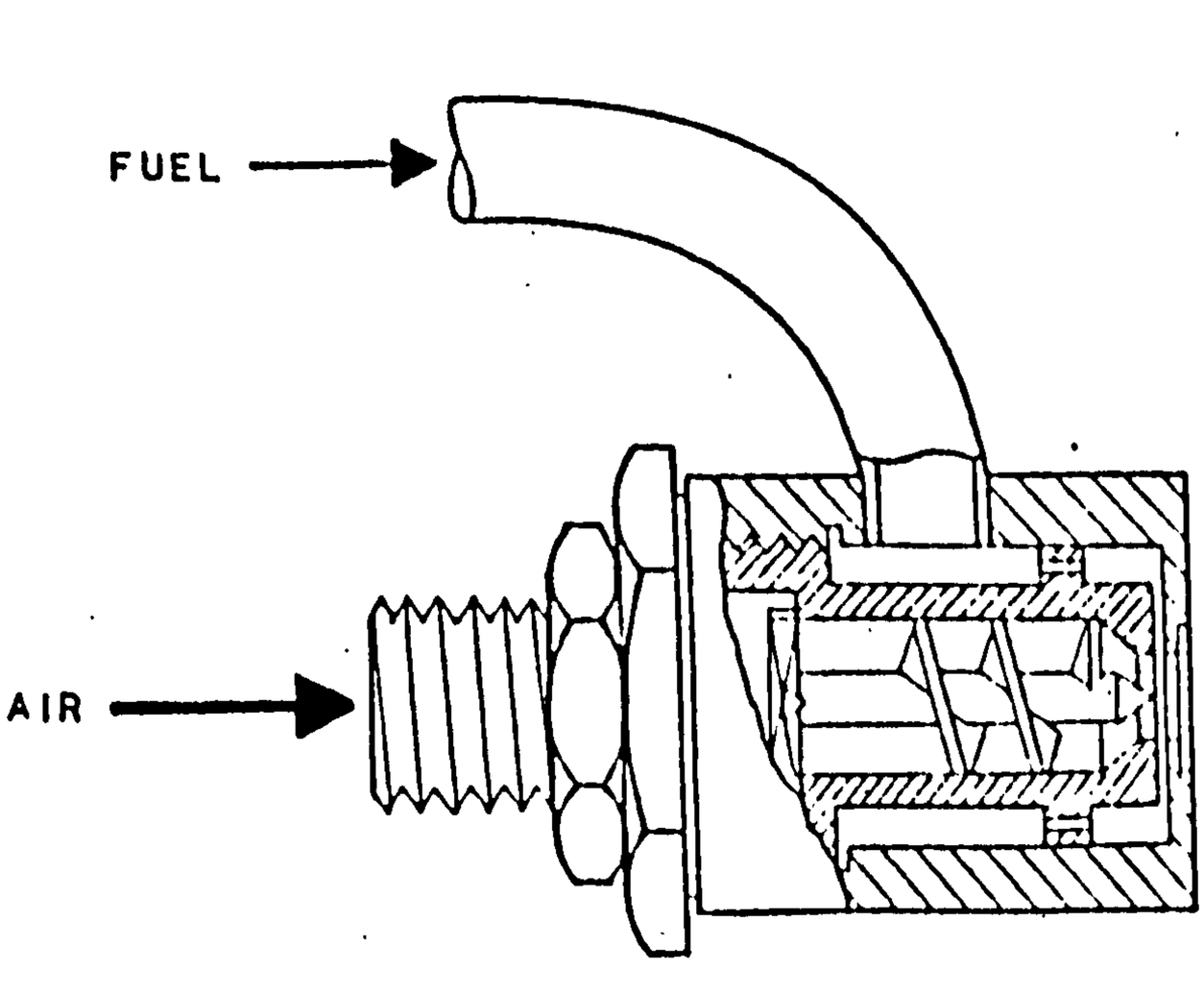

(b) 1/4-Inch Orifice

EARLY N.G.T.E. HIGH PRESSURE AIR ATOMIZERS

FIG. 4

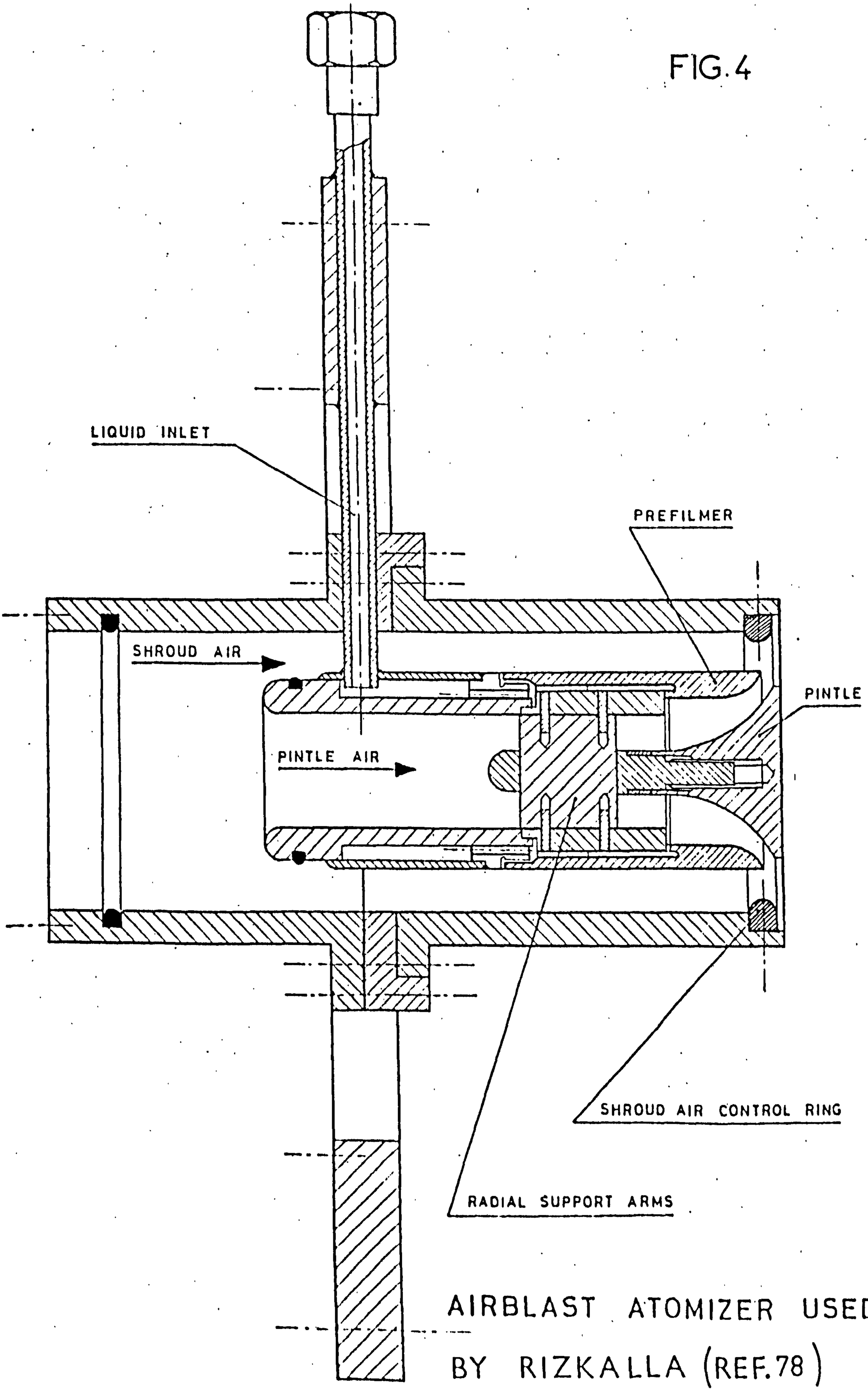

AIRBLAST ATOMIZER USED BY RIZKALLA (REF. 78)

FIG.5

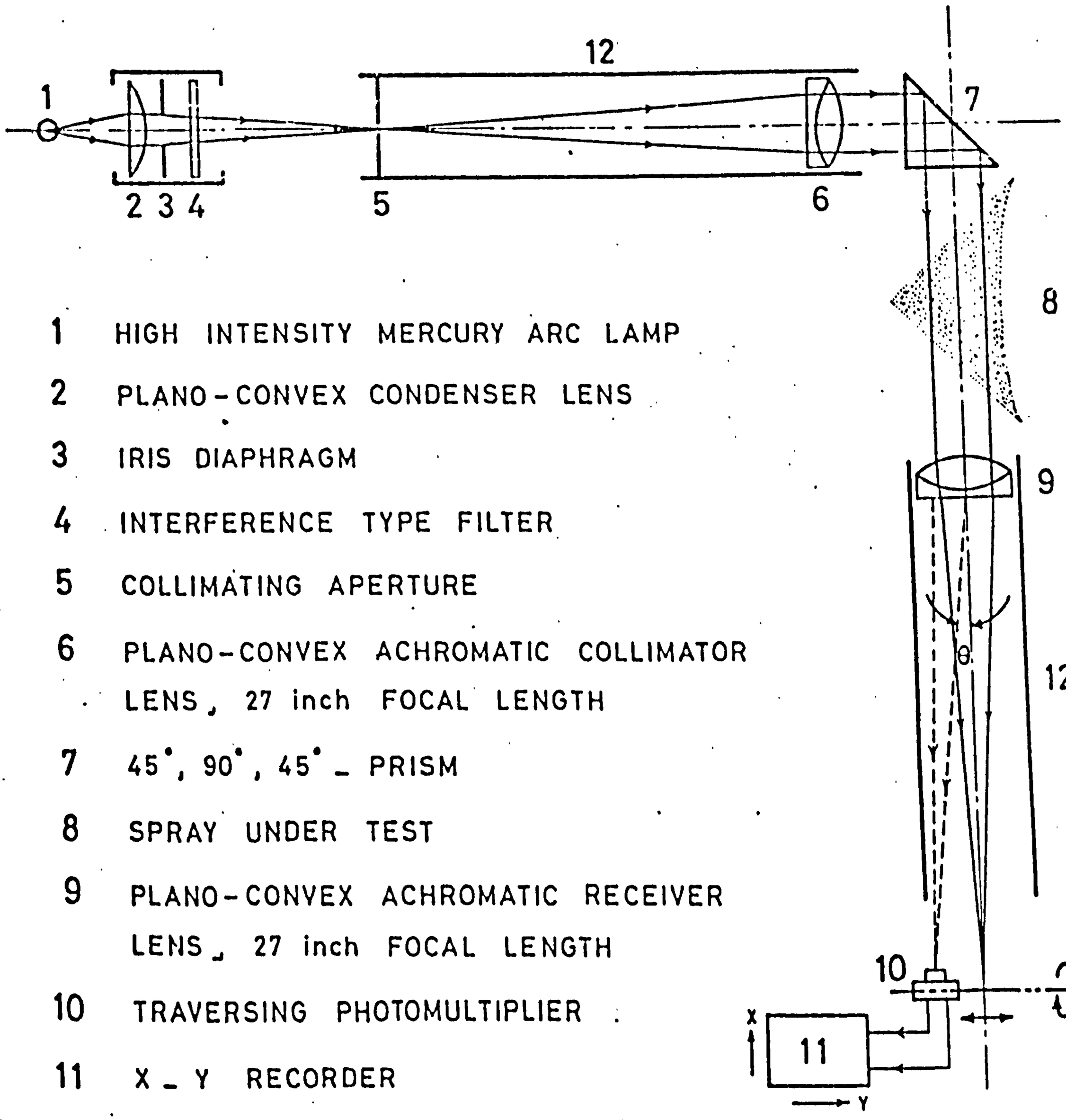

1 HIGH INTENSITY MERCURY ARC LAMP

2 PLANO-CONVEX CONDENSER LENS

3 IRIS DIAPHRAGM

4 INTERFERENCE TYPE FILTER

5 COLLIMATING APERTURE

6 PLANO-CONVEX ACHROMATIC COLLIMATOR LENS, 27 inch FOCAL LENGTH

7 45°, 90°, 45° - PRISM

8 SPRAY UNDER TEST

9 PLANO-CONVEX ACHROMATIC RECEIVER LENS, 27 inch FOCAL LENGTH

10 TRAVERSING PHOTOMULTIPLIER

11 X - Y RECORDER

12 STRAY LIGHT SHIELD

THE OPTICAL BENCH IN DIAGRAMMATIC FORM - RIZKALLA (REF.78)-

FIG. 6

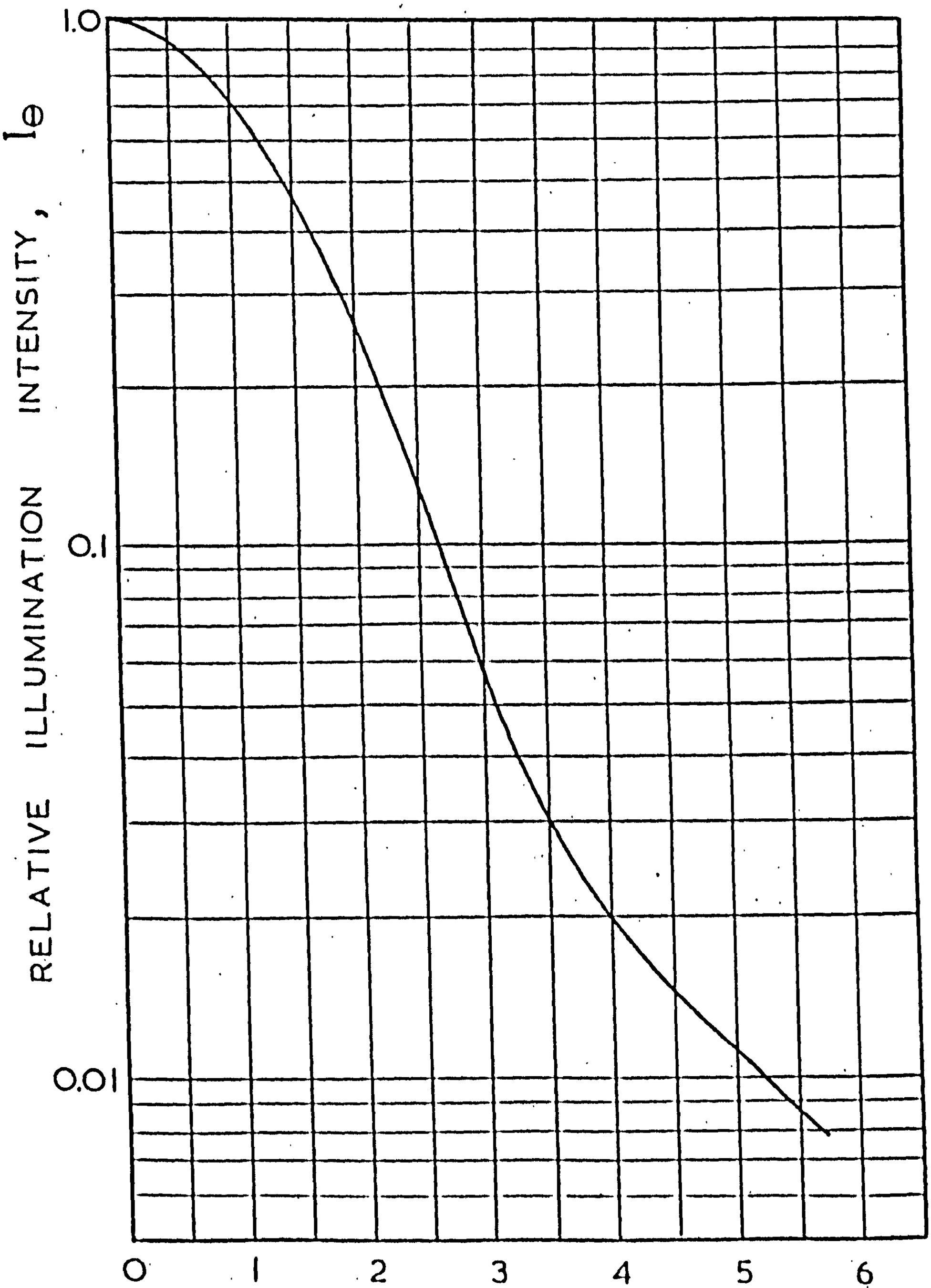

MEAN THEORETICAL ILLUMINATION PROFILE

(Roberts and Webb)

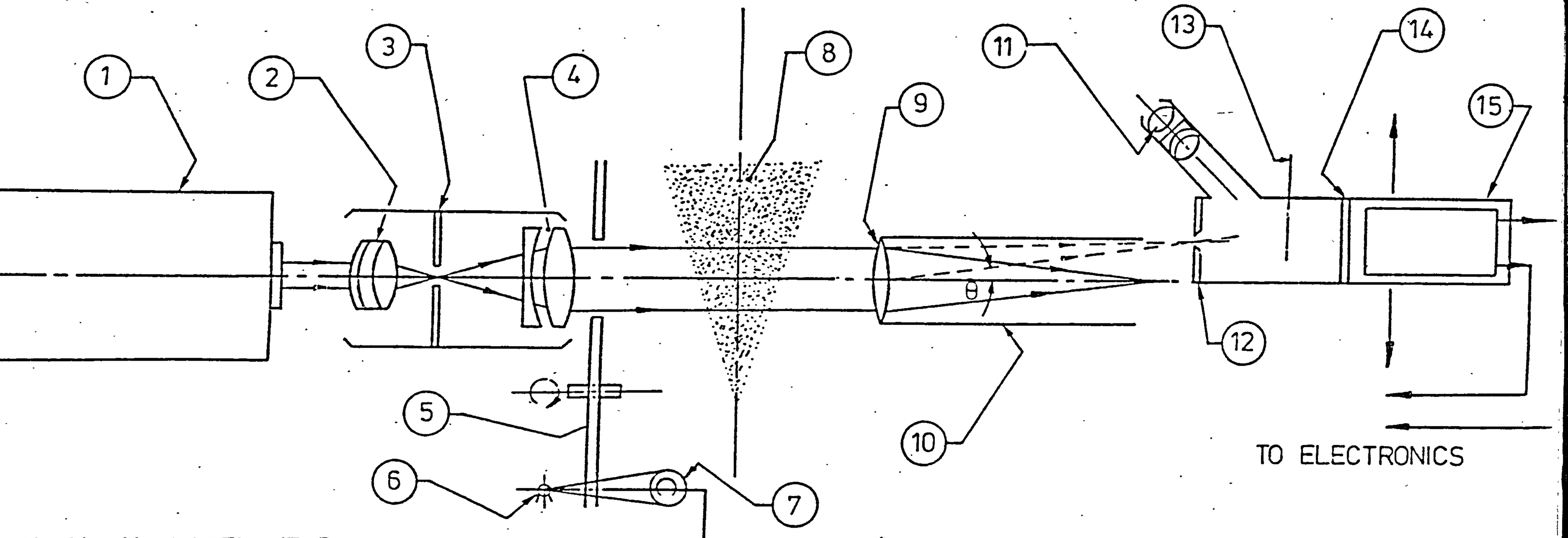

1) He-Ne LASER HEAD
2) CONDENSING LENS
3) SPATIAL FILTER (APERTURE)
4) TELESCOPE-COLLIMATING LENS
5) ROTATING DISC (CHOPPER)
6) SMALL LAMP
7) PHOTO CELL

TO ELECTRONICS

8) SPRAY UNDER TEST
9) RECIEVER LENS (60cm FOCAL LENGTH)
10) STRAY LIGHT SHIELD
11) EYEPIECE
12) PIN-HOLE APERTURE
13) SHUTTER
14) NEUTRAL DENSITY FILTER
15) TRAVERSING PHOTOMULTIPLIER

FIG.7

THE OPTICAL BENCH IN DIAGRAMATIC FORM

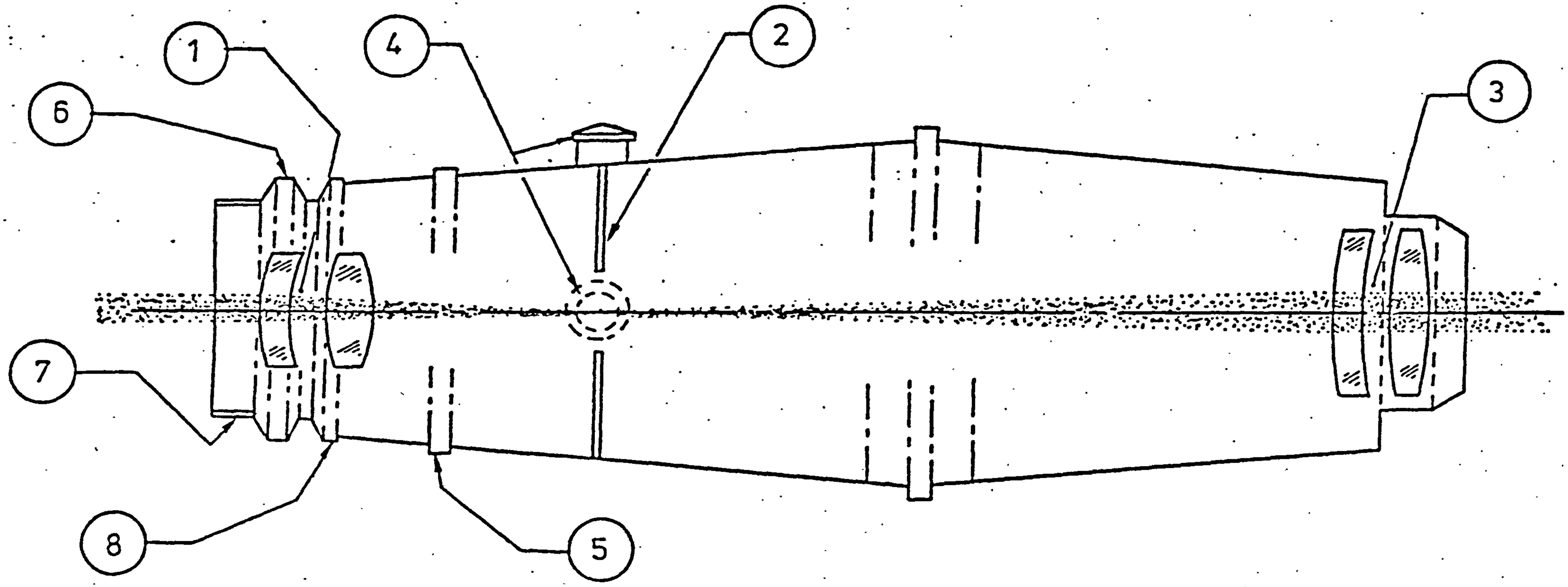

1) EXPANDING LENS :- EQUIVALENT FOCAL LENGTH: 12.8mm
2) SPATIAL FILTER :- PRECISION PIN HOLE:. 22μ
3) TELESCOPE COLLIMATING LENS :- EQUIVALENT FOCAL LENGTH 85mm
4) APERTURE X & Y MOTION ADJUSTING KNOBS :-
5) APERTURE Z MOTION ADJUST RING :-
6) ROTATIONAL LOCK RING :-
7) 1"-32 MOUNTING THREAD :-
8) AXIAL ALIGNMENT LOCK RING :-

FIG. 8

BEAM EXPANDING AND COLLIMATING TELESCOPE

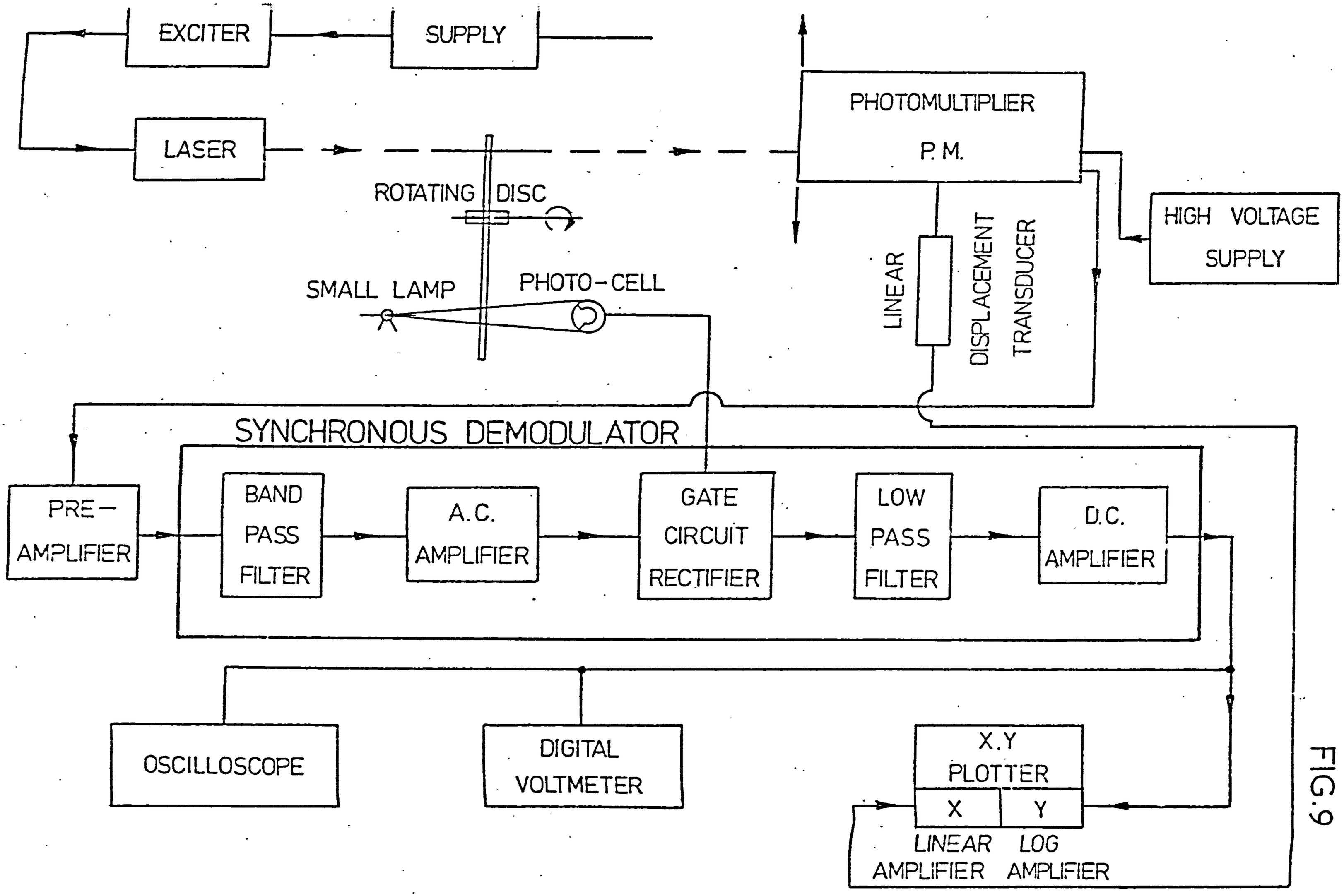

FIG. 9

BLOCK DIAGRAM OF LIGHT SCATTERING INSTRUMENTATION

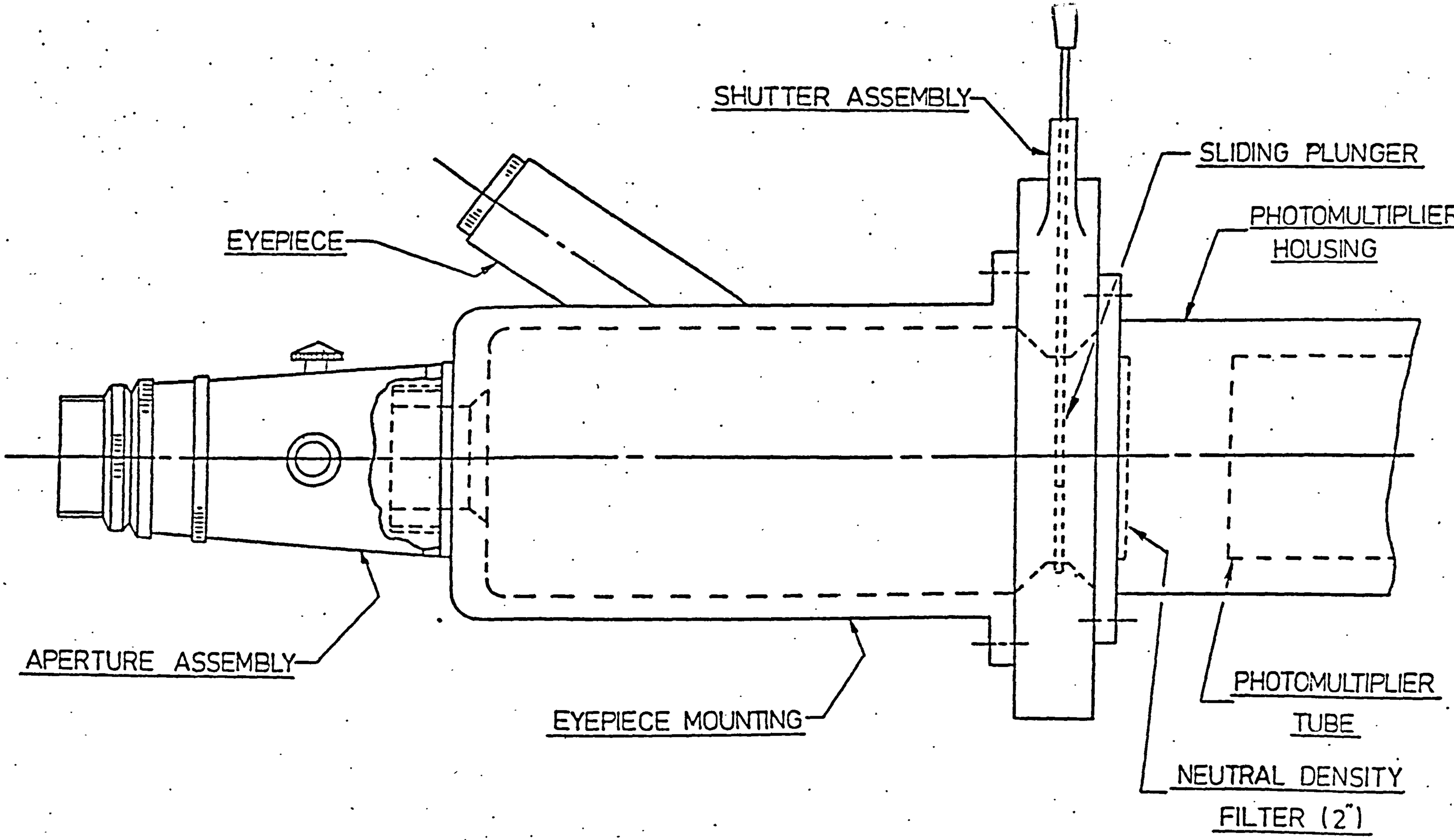

OPTICAL RECEIVING SYSTEM

FIG.10

FIG. 11

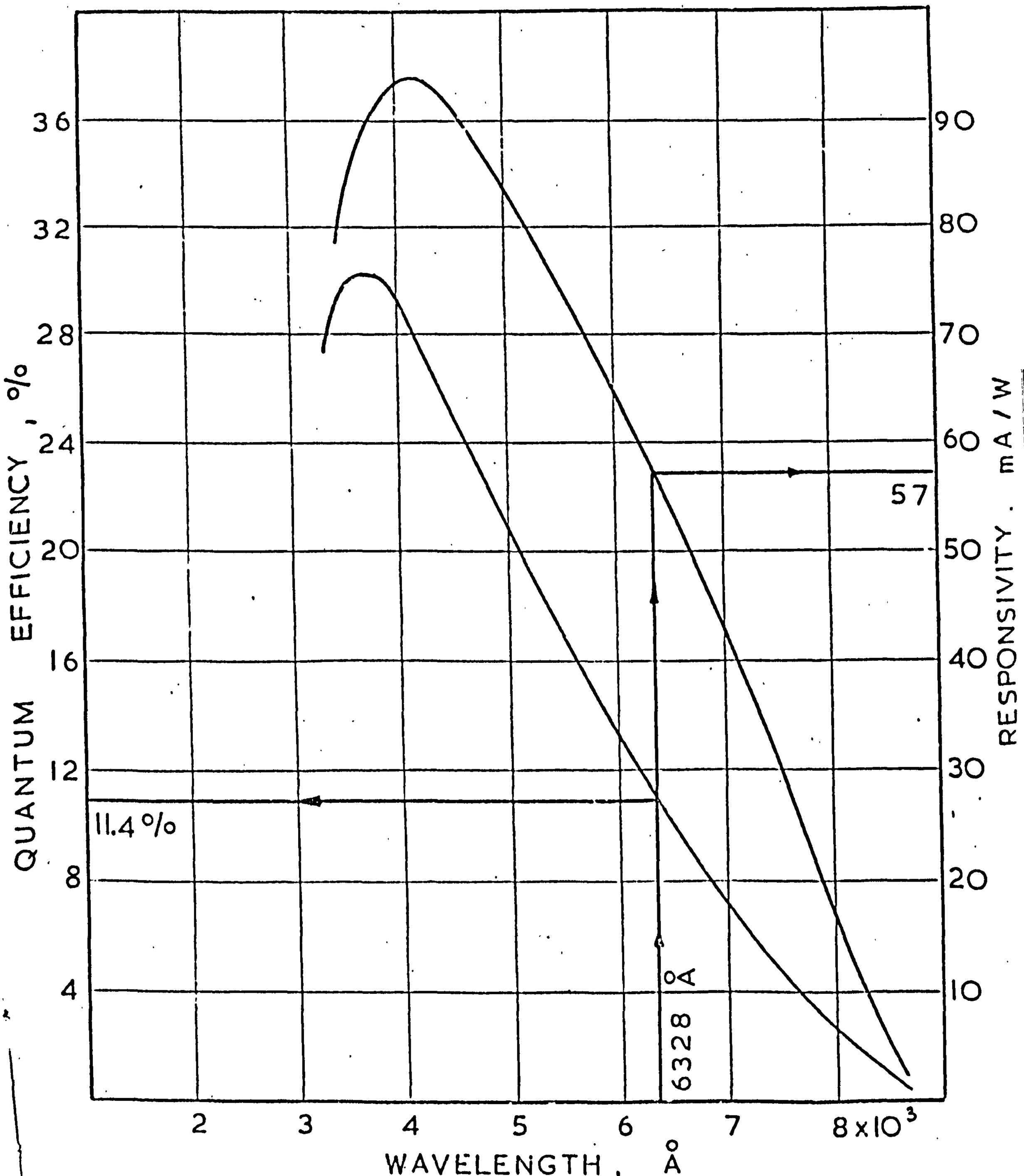

E.M.I. - 9658 MR PHOTOMULTIPLIER

SPECTRAL RESPONSE

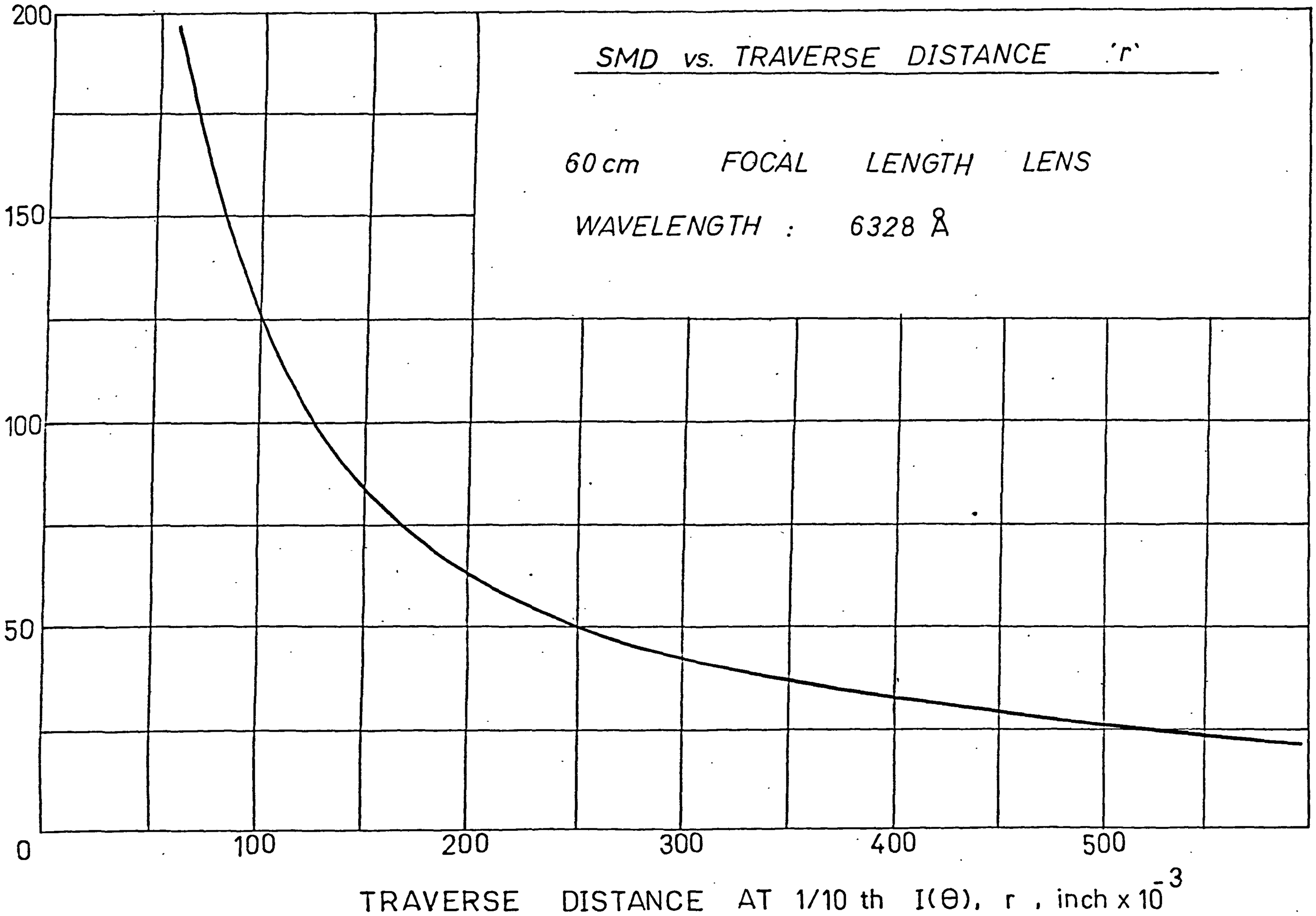
SMD vs. TRAVERSE DISTANCE 'r'
60 cm FOCAL LENGTH LENS
WAVELENGTH : 6328 Å
SMD, microns
200
150
100
50
0
100
200
300
400
500
TRAVERSE DISTANCE AT 1/10 th I(θ), r , inch x 10⁻³

FIG. 12

FIG. 13

TYPICAL X-Y RECORDER PLOT

Liquid Surface Tension = 46.5×10^{-3} N/m

Film Thickness = 0.01525 cm

Liquid Flow Rate = 9.1 gr/s

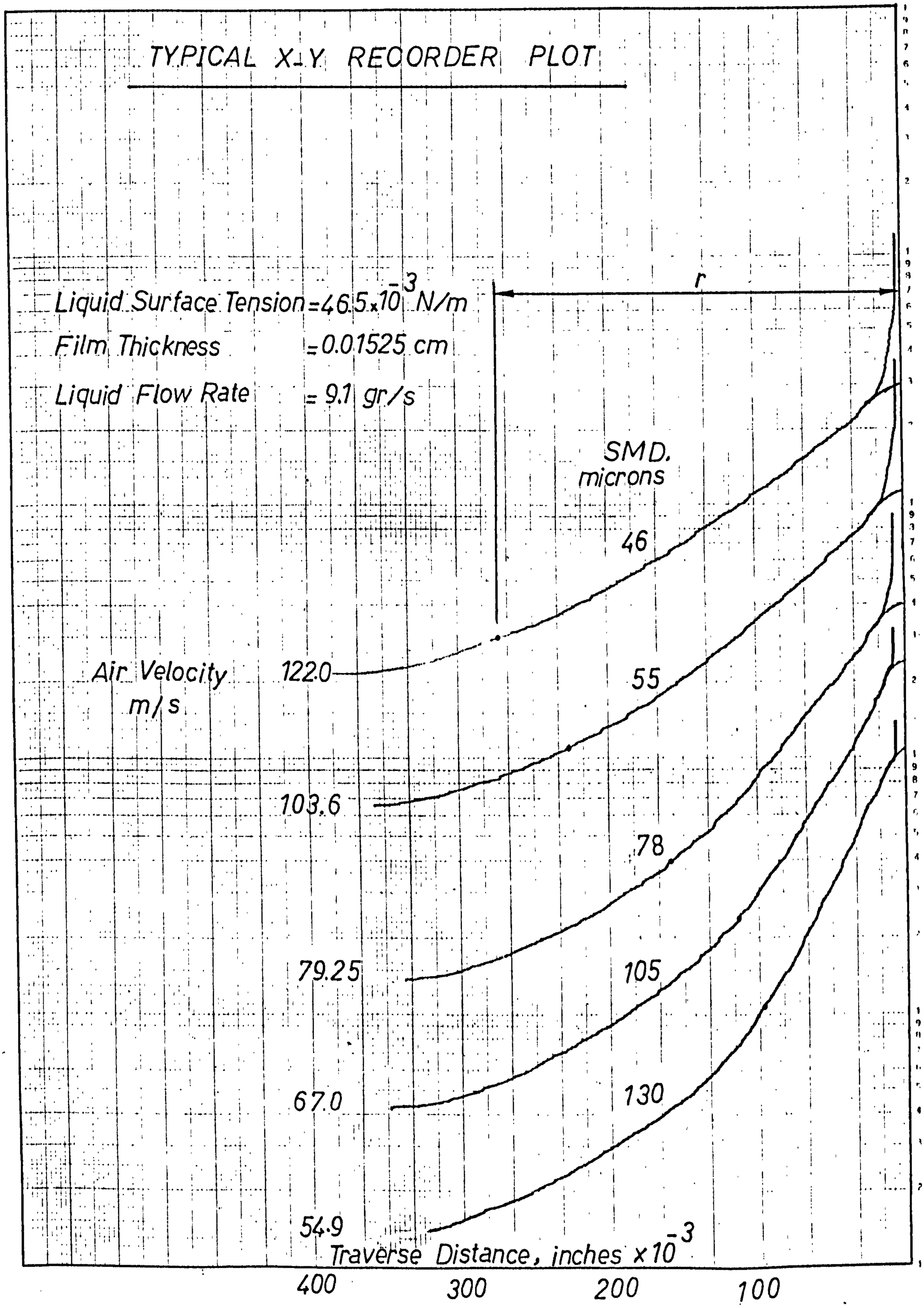

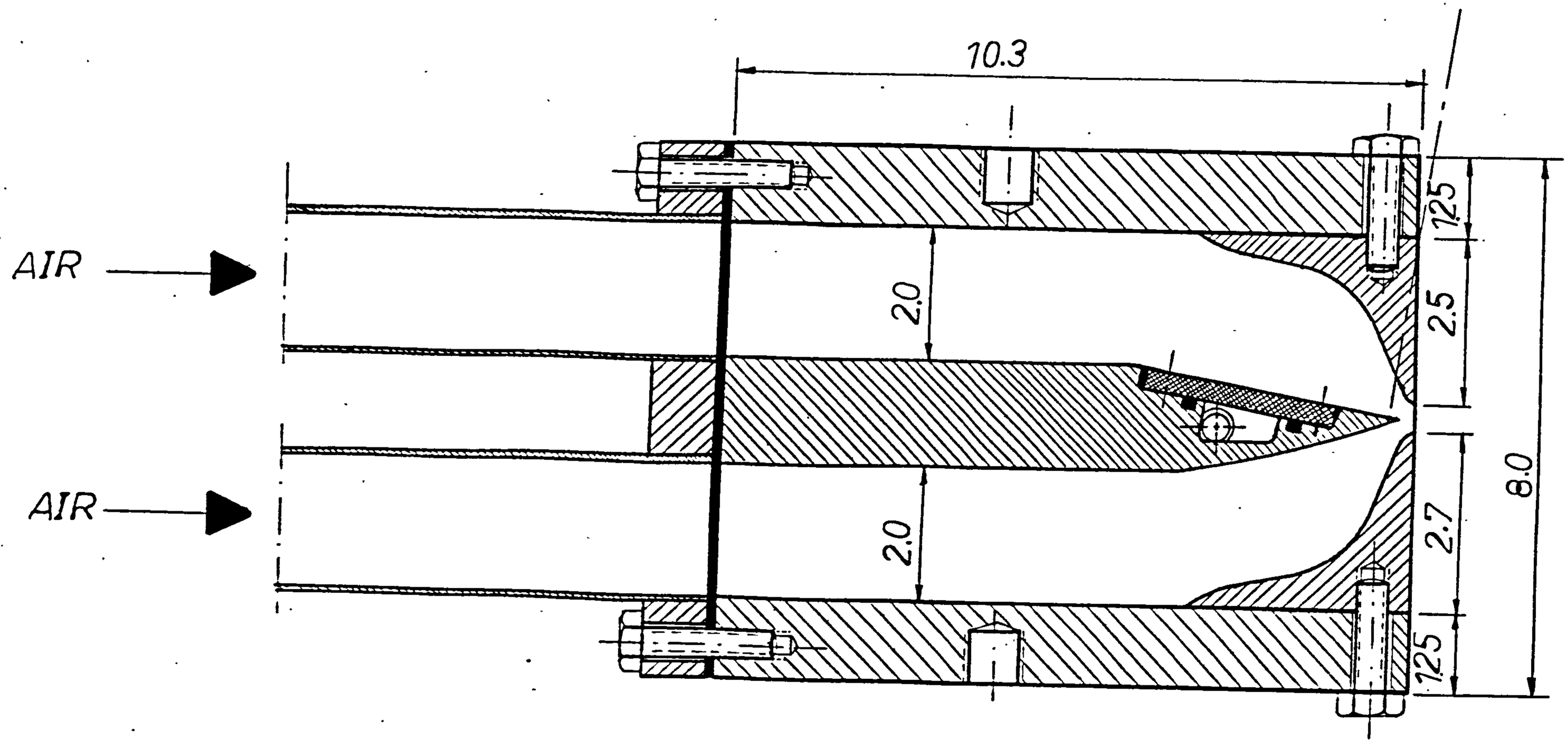

Sec. Elevation

ATOMIZER (A) Scale 1:1

In cm

FIG.14

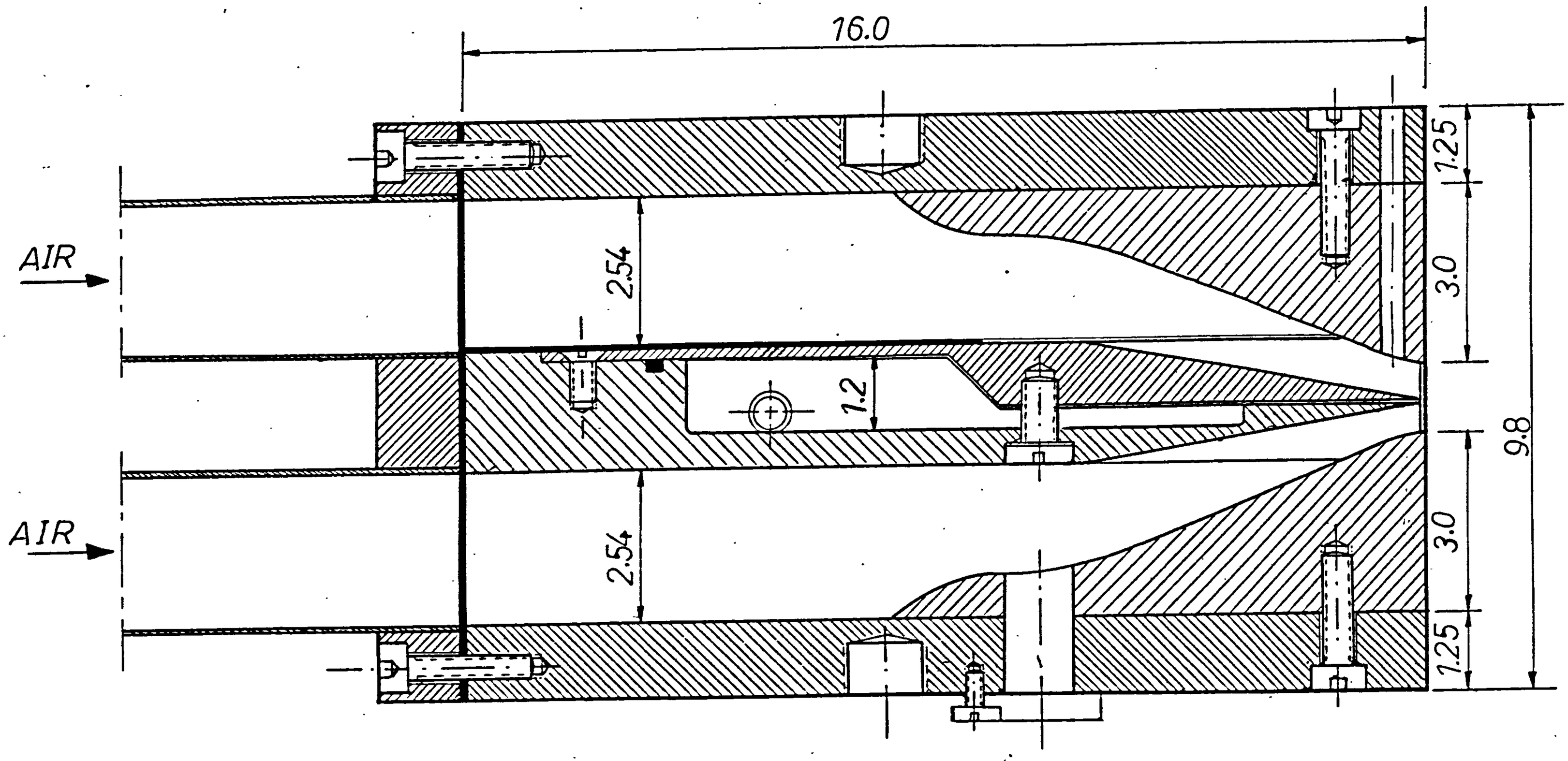

Sec. Elevation

ATOMIZER (B) Scale 1:1

In cm.

FIG.15

FIG.16

SCHEMATIC G.A. of the HIGH PRESSURE TEST RIG

1 Inlet Air Duct

2 Orifice Plate

3 Isolation Valve

4 Air Chamber

5 Atomizer

6 Observation Section

7 Collecting Pipe

8 Pressurizing Valve

9 Exhust Duct

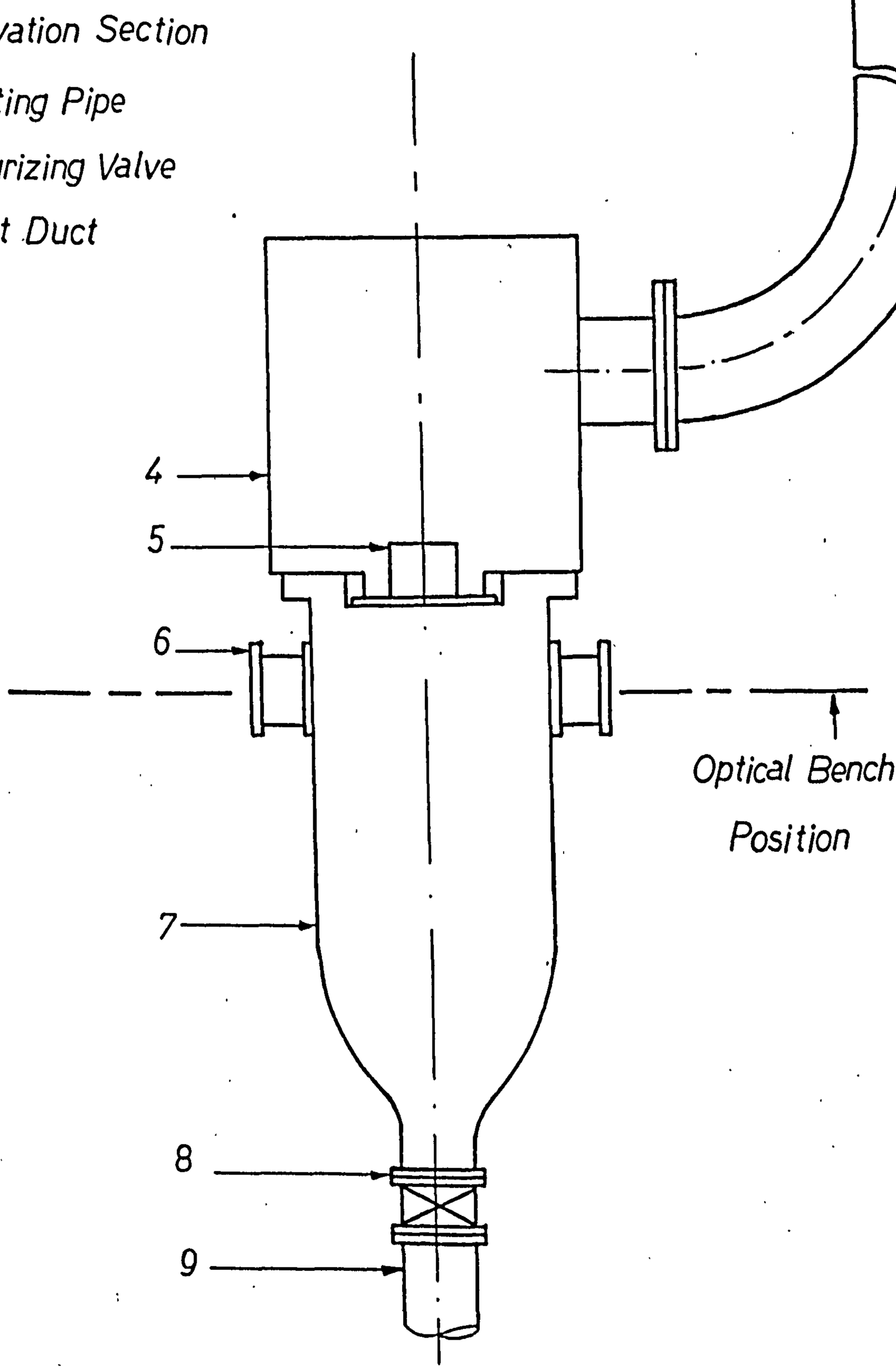

FIG.17

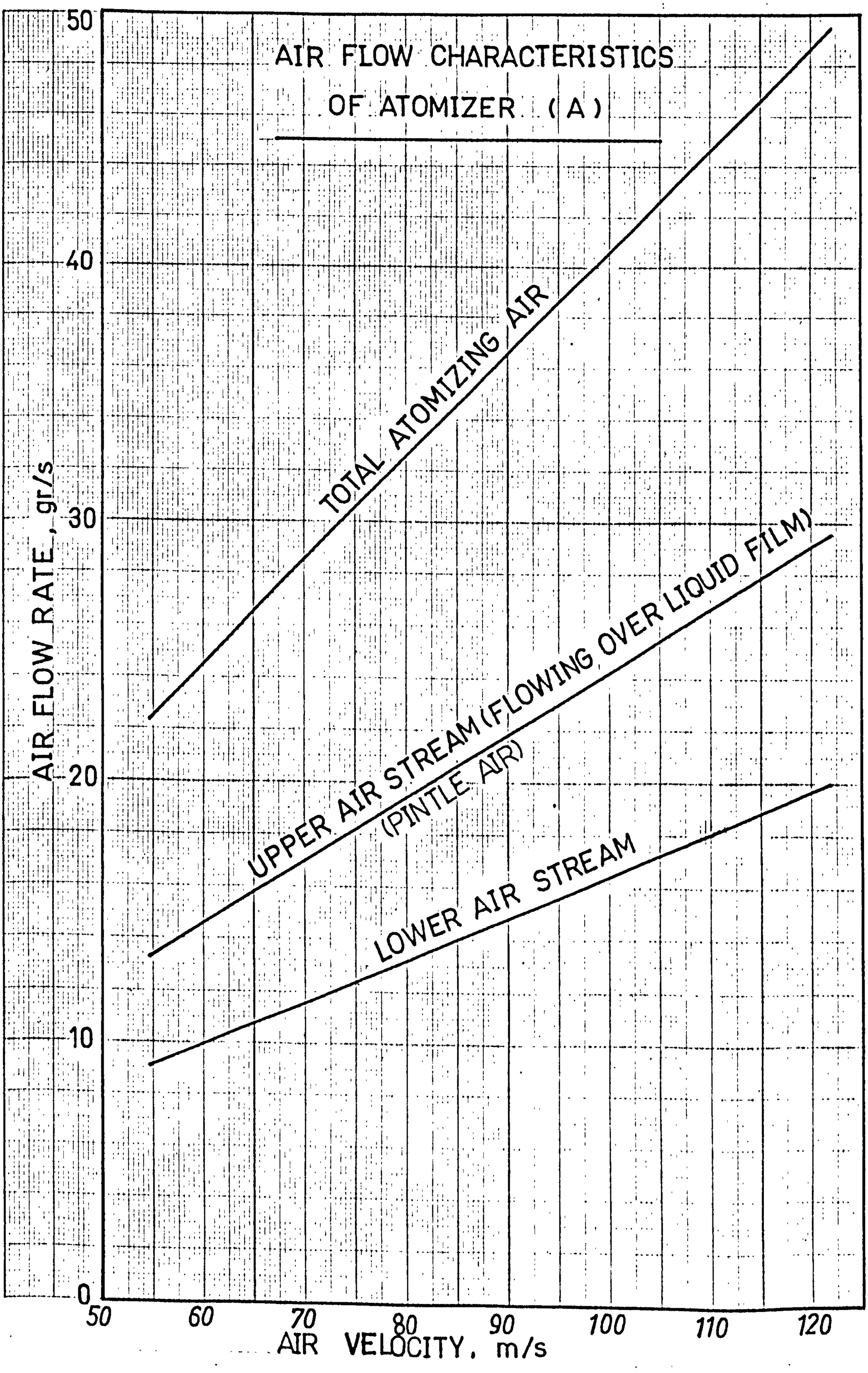
AIR FLOW CHARACTERISTICS
OF ATOMIZER (A)
TOTAL ATOMIZING AIR
UPPER AIR STREAM (FLOWING OVER LIQUID FILM)
(PINTLE AIR)
LOWER AIR STREAM
AIR FLOW RATE, gr/s
AIR VELOCITY, m/s
0
10
20
30
40
50
60
70
80
90
100
110
120

FIG. 18

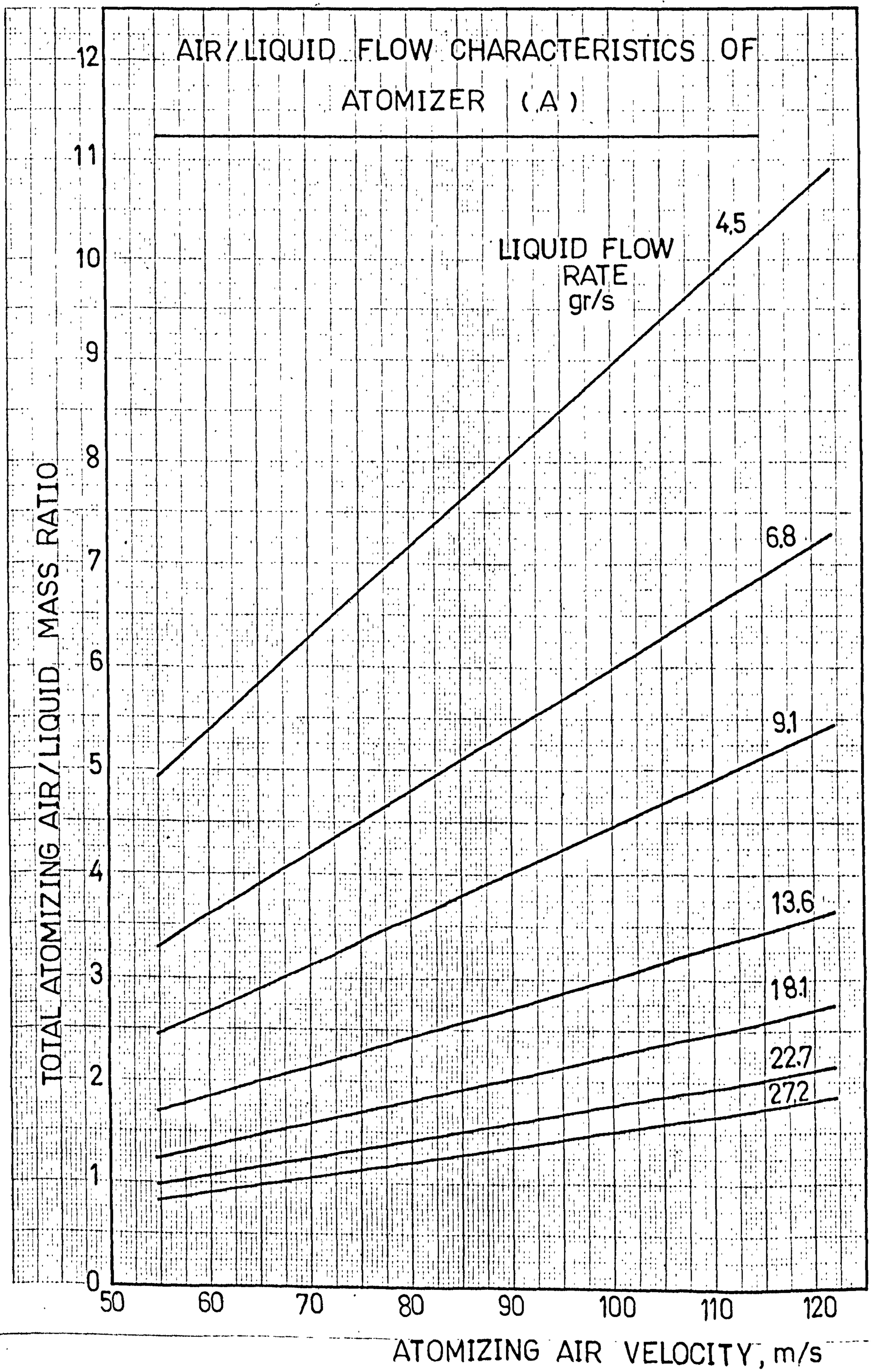
AIR/LIQUID FLOW CHARACTERISTICS OF ATOMIZER (A)
TOTAL ATOMIZING AIR/LIQUID MASS RATIO
0
1
2
3
4
5
6
7
8
9
10
11
12
50
60
70
80
90
100
110
120
ATOMIZING AIR VELOCITY, m/s
LIQUID FLOW RATE gr/s
4.5
6.8
9.1
13.6
18.1
22.7
27.2

FIG.19

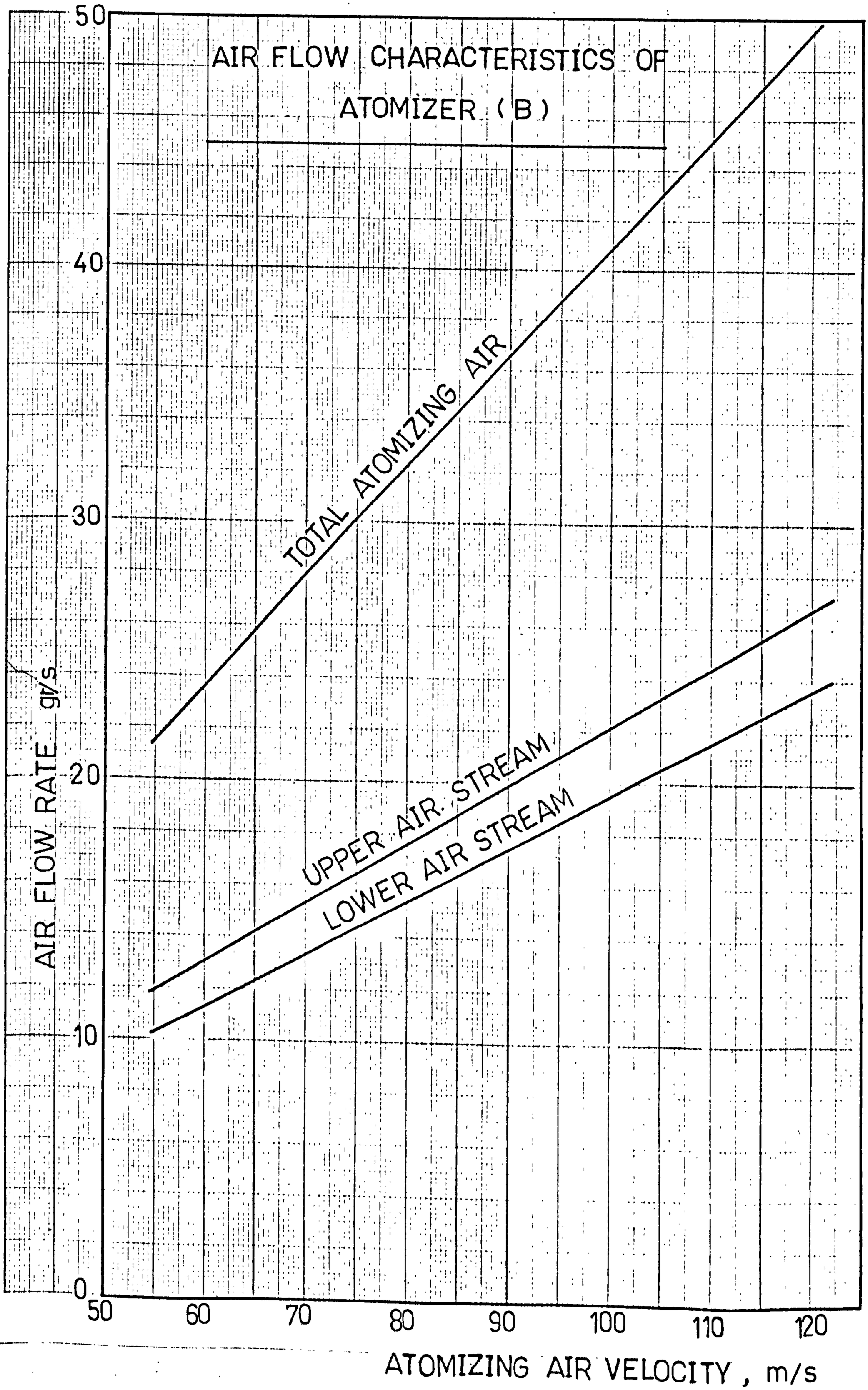
AIR FLOW CHARACTERISTICS OF ATOMIZER (B)
TOTAL ATOMIZING AIR
UPPER AIR STREAM
LOWER AIR STREAM
AIR FLOW RATE gr/s
50
40
30
20
10
0
50
60
70
80
90
100
110
120
ATOMIZING AIR VELOCITY , m/s

FIG. 20

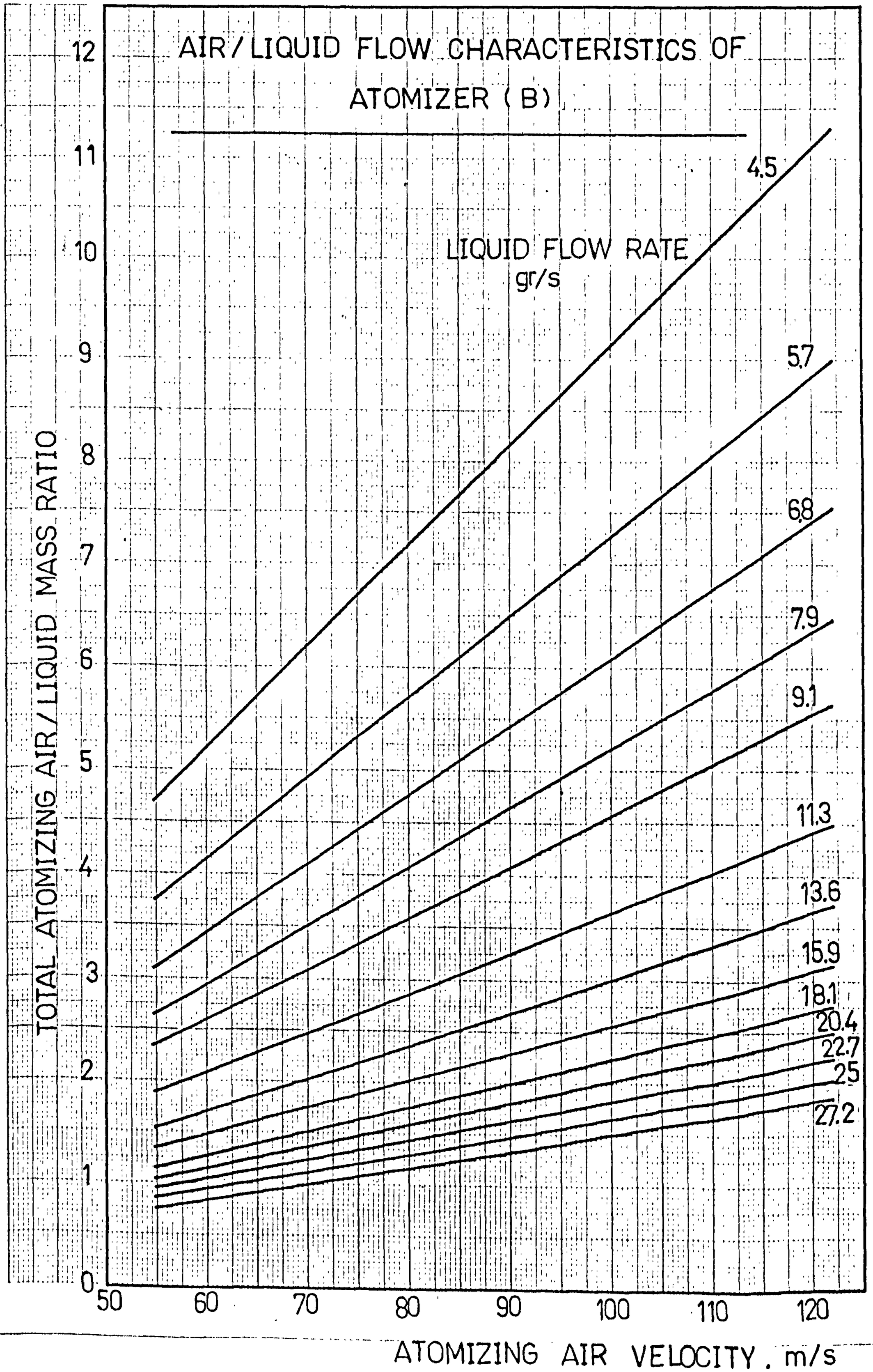
AIR/LIQUID FLOW CHARACTERISTICS OF ATOMIZER (B)
LIQUID FLOW RATE gr/s
4.5
5.7
6.8
7.9
9.1
11.3
13.6
15.9
18.1
20.4
22.7
25
27.2
TOTAL AIR/LIQUID MASS RATIO
0
1
2
3
4
5
6
7
8
9
10
11
12
50
60
70
80
90
100
110
120
ATOMIZING AIR VELOCITY, m/s

FIG. 21

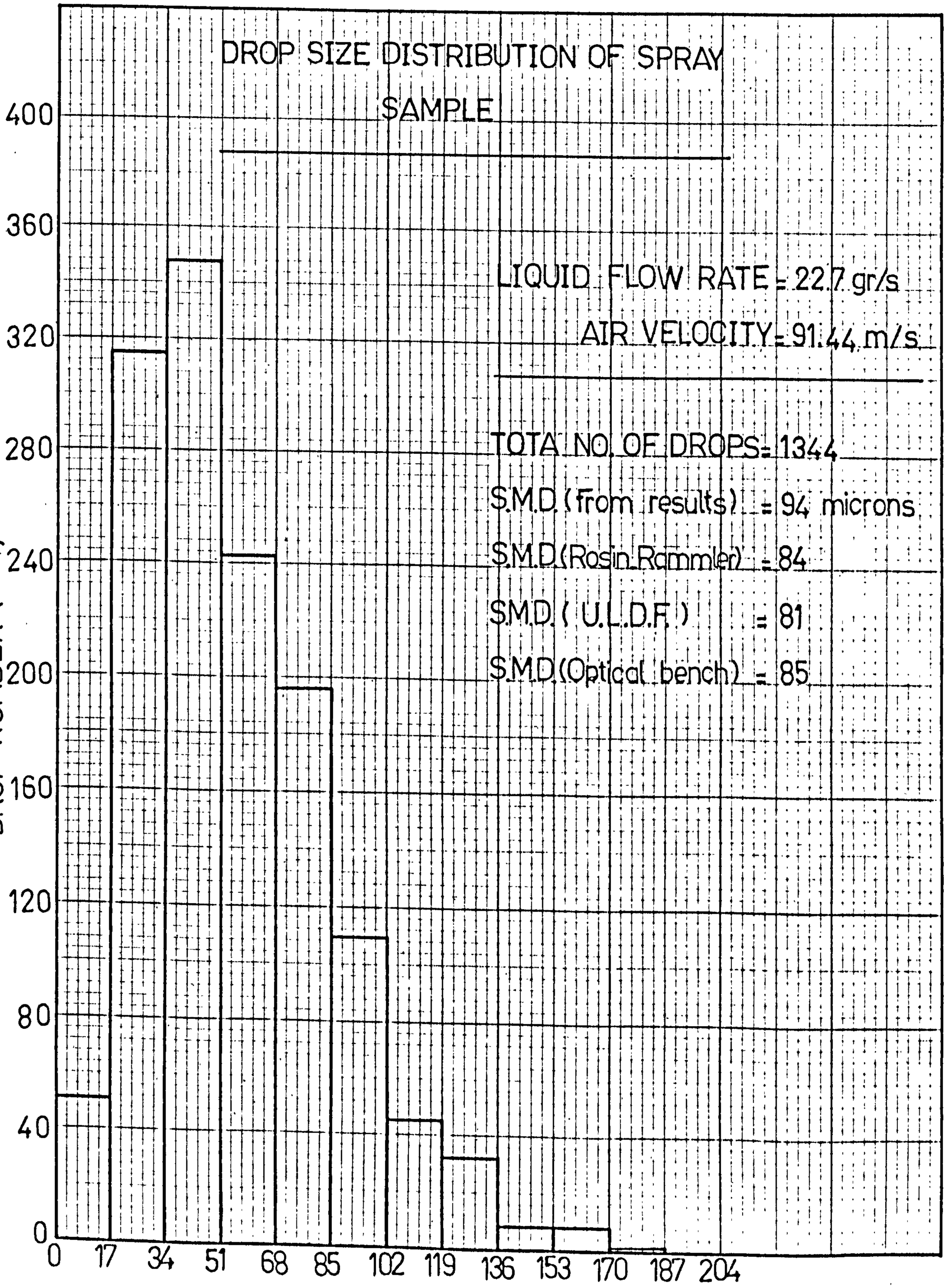
DROP SIZE DISTRIBUTION OF SPRAY SAMPLE
LIQUID FLOW RATE = 22.7 gr/s
AIR VELOCITY = 91.44 m/s
TOTA NO. OF DROPS = 1344
S.M.D. (from results) = 94 microns
S.M.D (Rosin Rammler) = 84
S.M.D. (U.L.D.F.) = 81
S.M.D (Optical bench) = 85
DROP NUMBER (n)
0
40
80
120
160
200
240
280
320
360
400
0 17 34 51 68 85 102 119 136 153 170 187 204
DROP DIAMETER, microns

FIG. 22

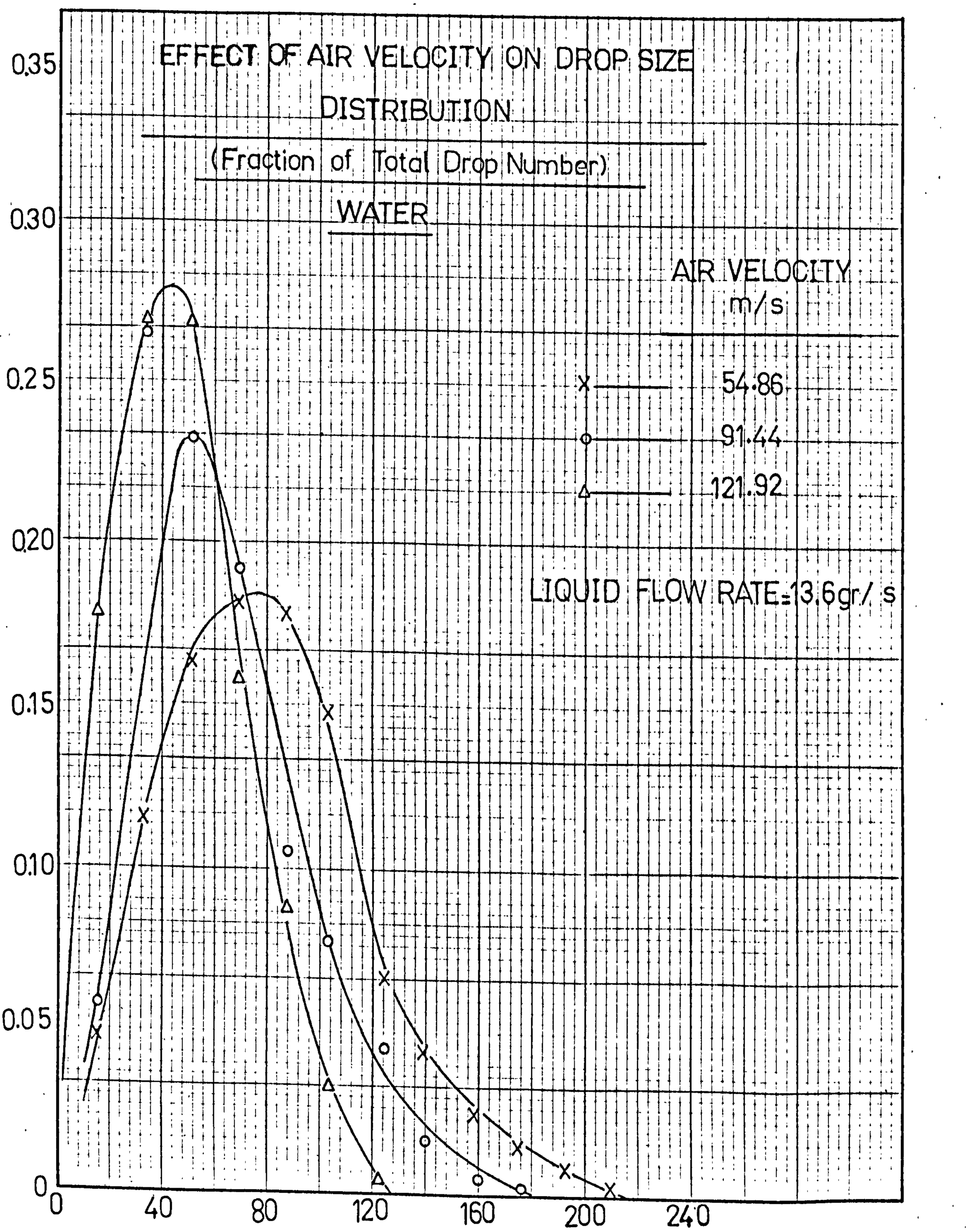
EFFECT OF AIR VELOCITY ON DROP SIZE DISTRIBUTION
(Fraction of Total Drop Number)
WATER
AIR VELOCITY m/s
X 54.86
91.44
121.92
LIQUID FLOW RATE=13.6gr/s
FRACTION OF TOTAL NUMBER
0.35
0.30
0.25
0.20
0.15
0.10
0.05
0
0
40
80
120
160
200
240
DROP DIAMETER, microns

FIG. 23

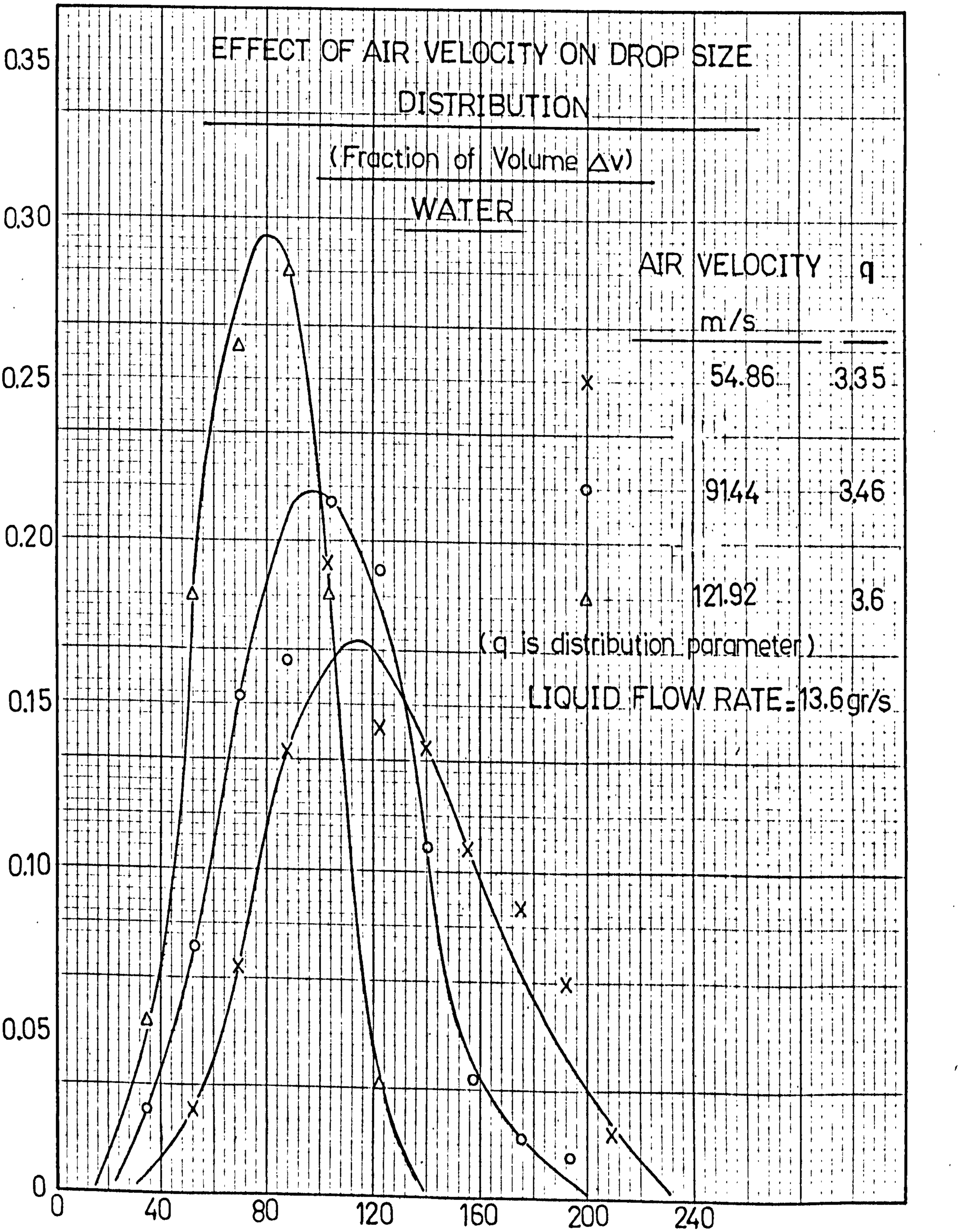
EFFECT OF AIR VELOCITY ON DROP SIZE DISTRIBUTION
(Fraction of Volume Δv)
WATER
AIR VELOCITY q
m/s
54.86 3.35
91.44 3.46
121.92 3.6
(q is distribution parameter)
LIQUID FLOW RATE = 13.6 gr/s
FRACTION OF VOLUME (Δv)
0.35
0.30
0.25
0.20
0.15
0.10
0.05
0
0
40
80
120
160
200
240
DROP DIAMETER, microns

FIG. 24

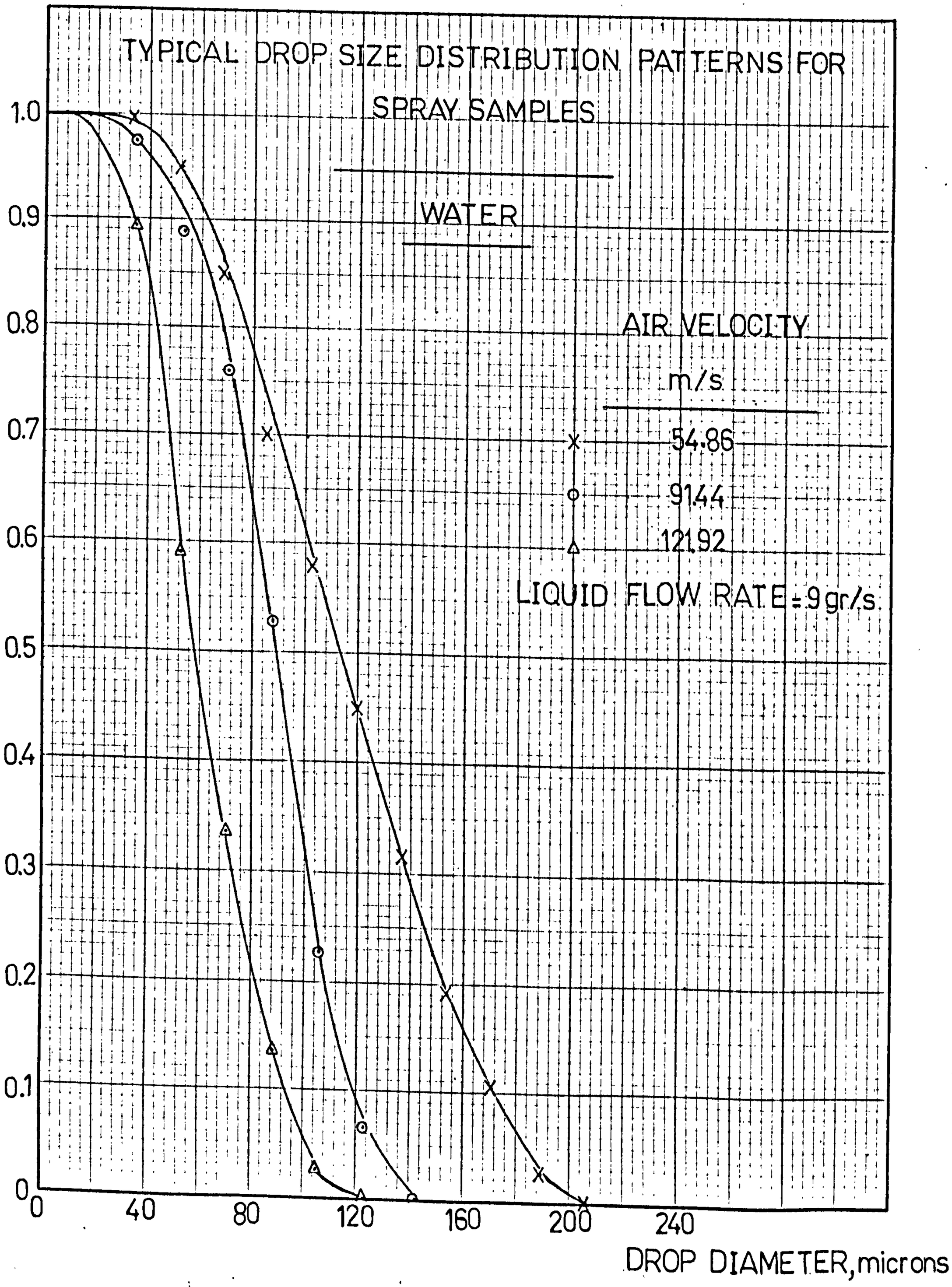
TYPICAL DROP SIZE DISTRIBUTION PATTERNS FOR SPRAY SAMPLES
WATER
AIR VELOCITY m/s
54.86
91.44
121.92
LIQUID FLOW RATE = 9 gr/s
FRACTION VOLUME OF SPRAY (1 - v)
1.0
0.9
0.8
0.7
0.6
0.5
0.4
0.3
0.2
0.1
0
0
40
80
120
160
200
240
DROP DIAMETER, microns

FIG.25

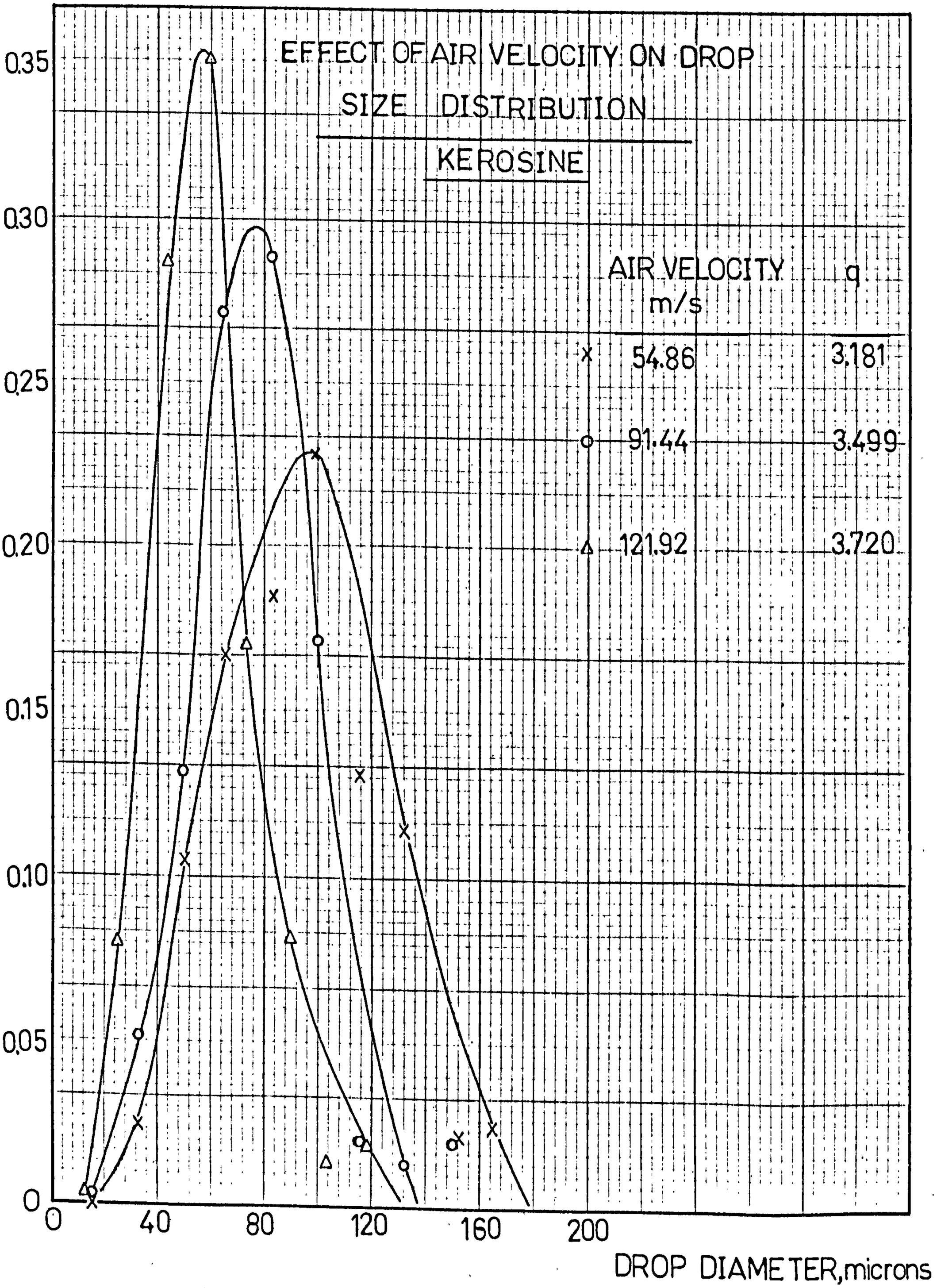
EFFECT OF AIR VELOCITY ON DROP SIZE DISTRIBUTION
KEROSINE
AIR VELOCITY m/s
q
x 54.86 3.181
o 91.44 3.499
Δ 121.92 3.720
FRACTION OF VOLUME(ΔV)
0.35
0.30
0.25
0.20
0.15
0.10
0.05
0
0
40
80
120
160
200
DROP DIAMETER, microns

FIG. 26

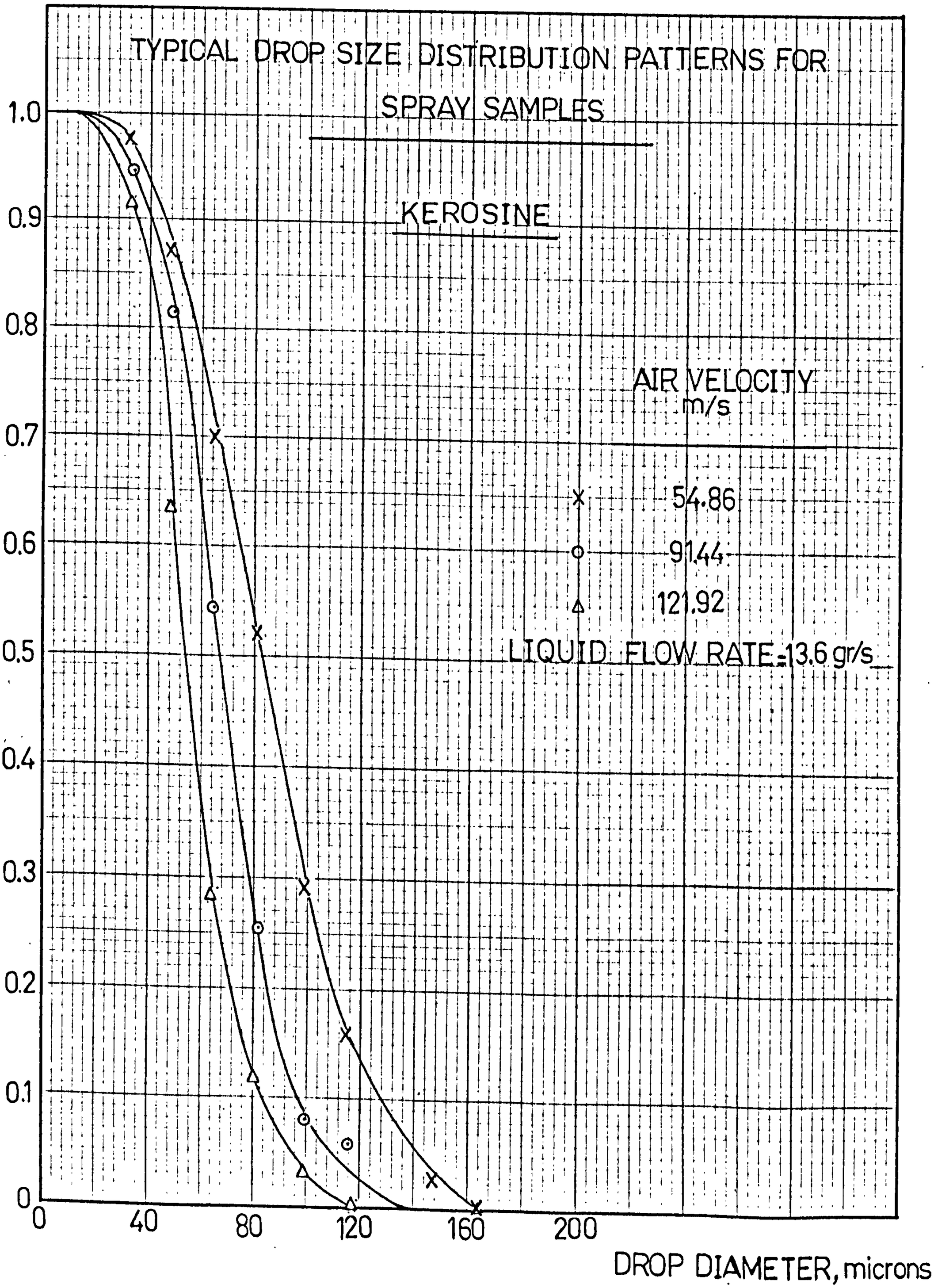
TYPICAL DROP SIZE DISTRIBUTION PATTERNS FOR SPRAY SAMPLES
KEROSINE
AIR VELOCITY m/s
54.86
91.44
121.92
LIQUID FLOW RATE - 13.6 gr/s
FRACTION VOLUME OF SPRAY (1-v)
1.0
0.9
0.8
0.7
0.6
0.5
0.4
0.3
0.2
0.1
0
0
40
80
120
160
200
DROP DIAMETER, microns

FIG. 27

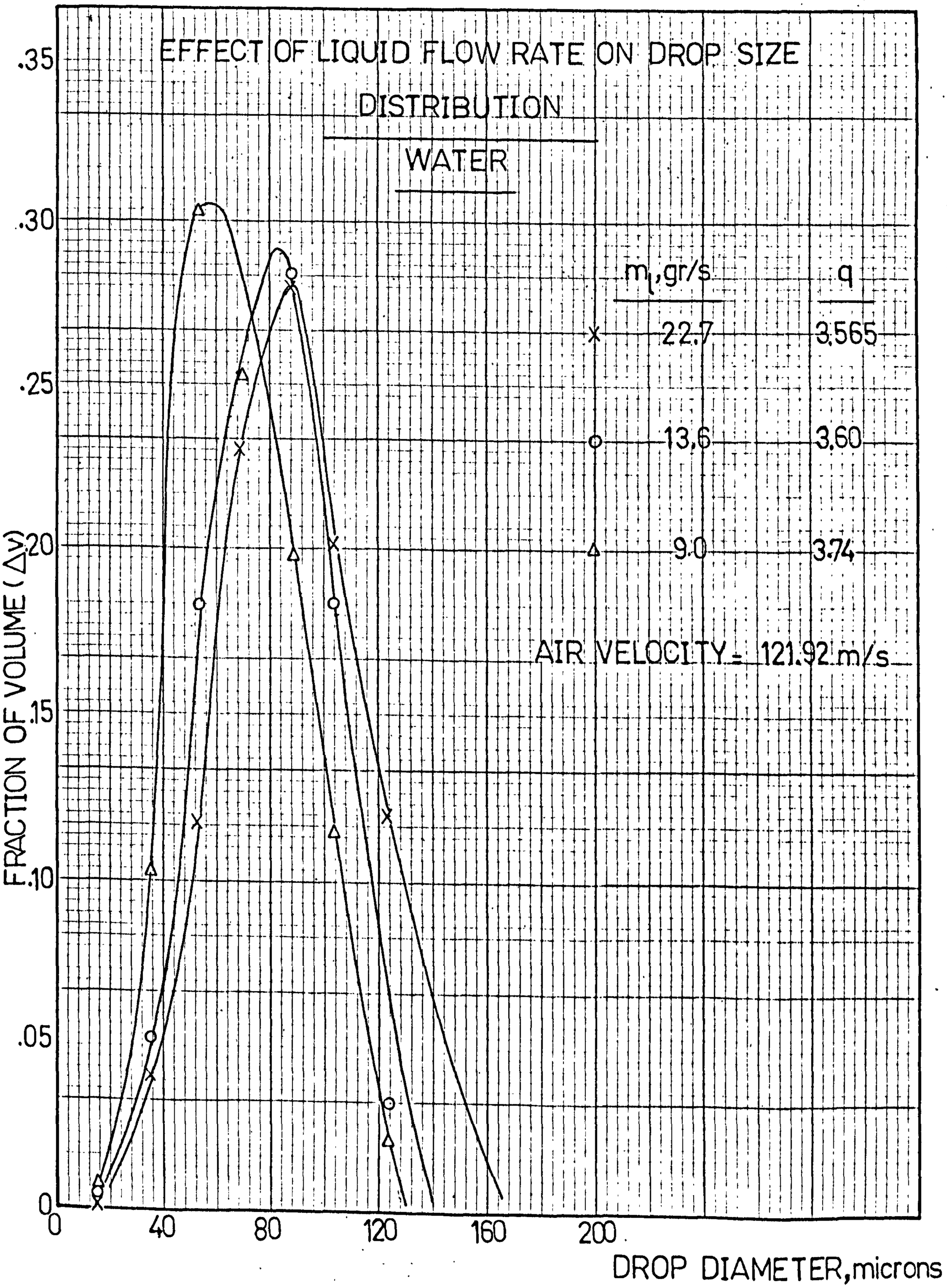
EFFECT OF LIQUID FLOW RATE ON DROP SIZE DISTRIBUTION
WATER
m_l, gr/s
q
22.7
3.565
13.6
3.60
9.0
3.74
AIR VELOCITY = 121.92 m/s
FRACTION OF VOLUME (ΔV)
.35
.30
.25
.20
.15
.10
.05
0
0
40
80
120
160
200
DROP DIAMETER, microns

FIG. 28

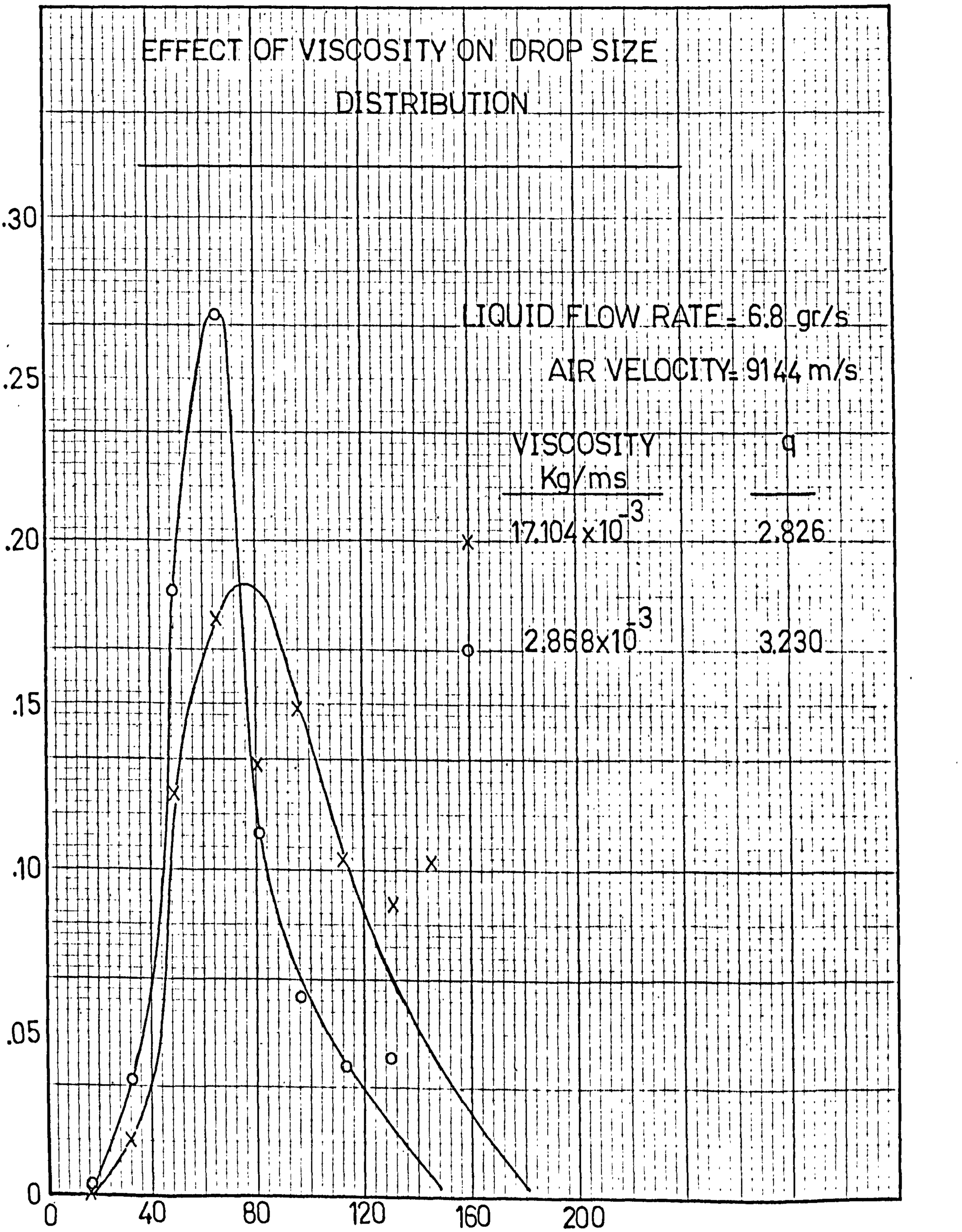
EFFECT OF VISCOSITY ON DROP SIZE DISTRIBUTION
LIQUID FLOW RATE = 6.8 gr/s
AIR VELOCITY = 9144 m/s
VISCOSITY Kg/ms
q
17.104 x 10⁻³
2.826
2.868x10⁻³
3.230
FRACTION OF VOLUME(ΔV)
.30
.25
.20
.15
.10
.05
0
0
40
80
120
160
200
DROP DIAMETER, microns

FIG. 29

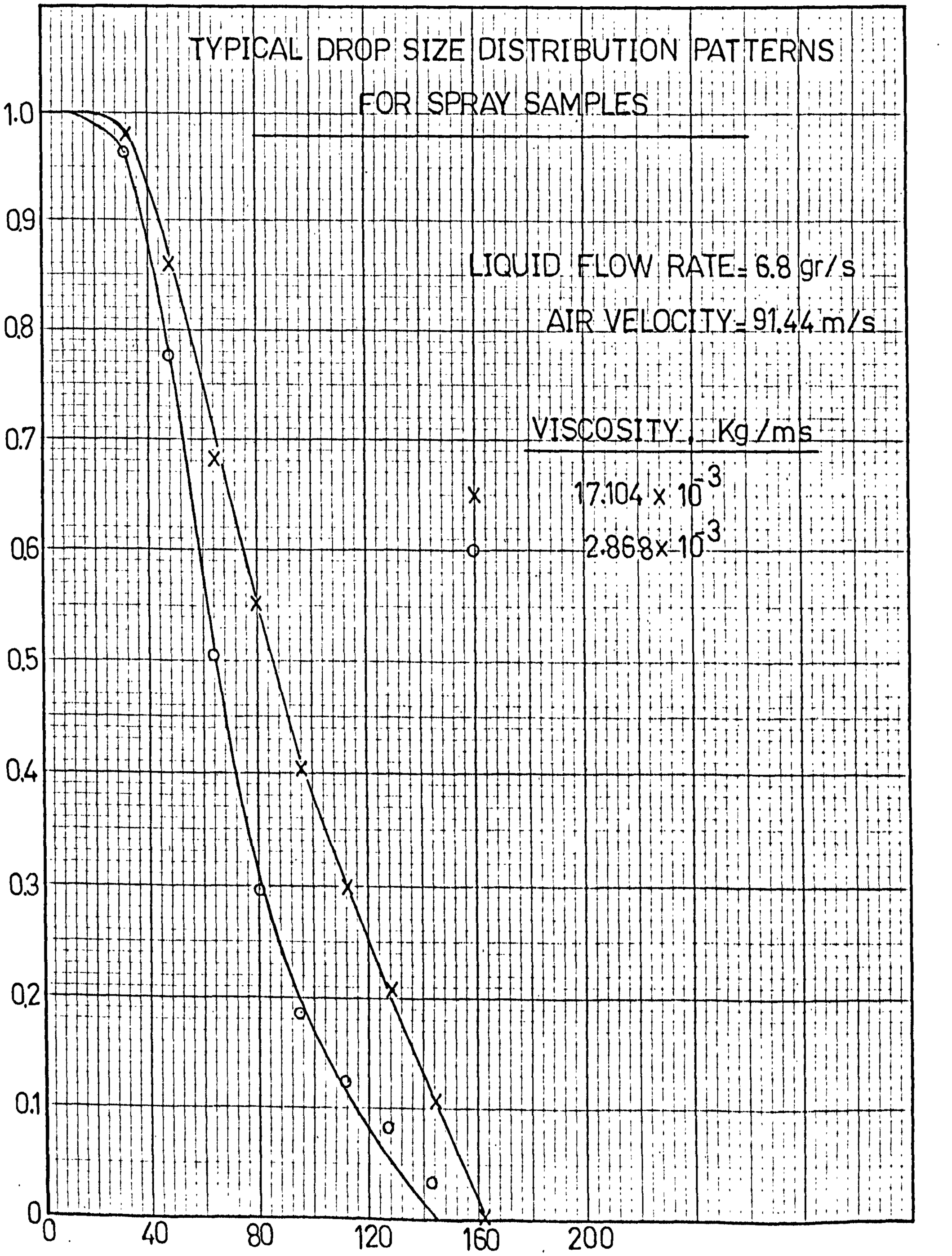
TYPICAL DROP SIZE DISTRIBUTION PATTERNS
FOR SPRAY SAMPLES
LIQUID FLOW RATE= 6.8 gr/s
AIR VELOCITY= 91.44 m/s
VISCOSITY, Kg/ms
x 17.104 x 10-3
o 2.868x10-3
FRACTION VOLUME OF SPRAY (1-v)
1.0
0.9
0.8
0.7
0.6
0.5
0.4
0.3
0.2
0.1
0
0
40
80
120
160
200
DROP DIAMETER, microns

FIG.30

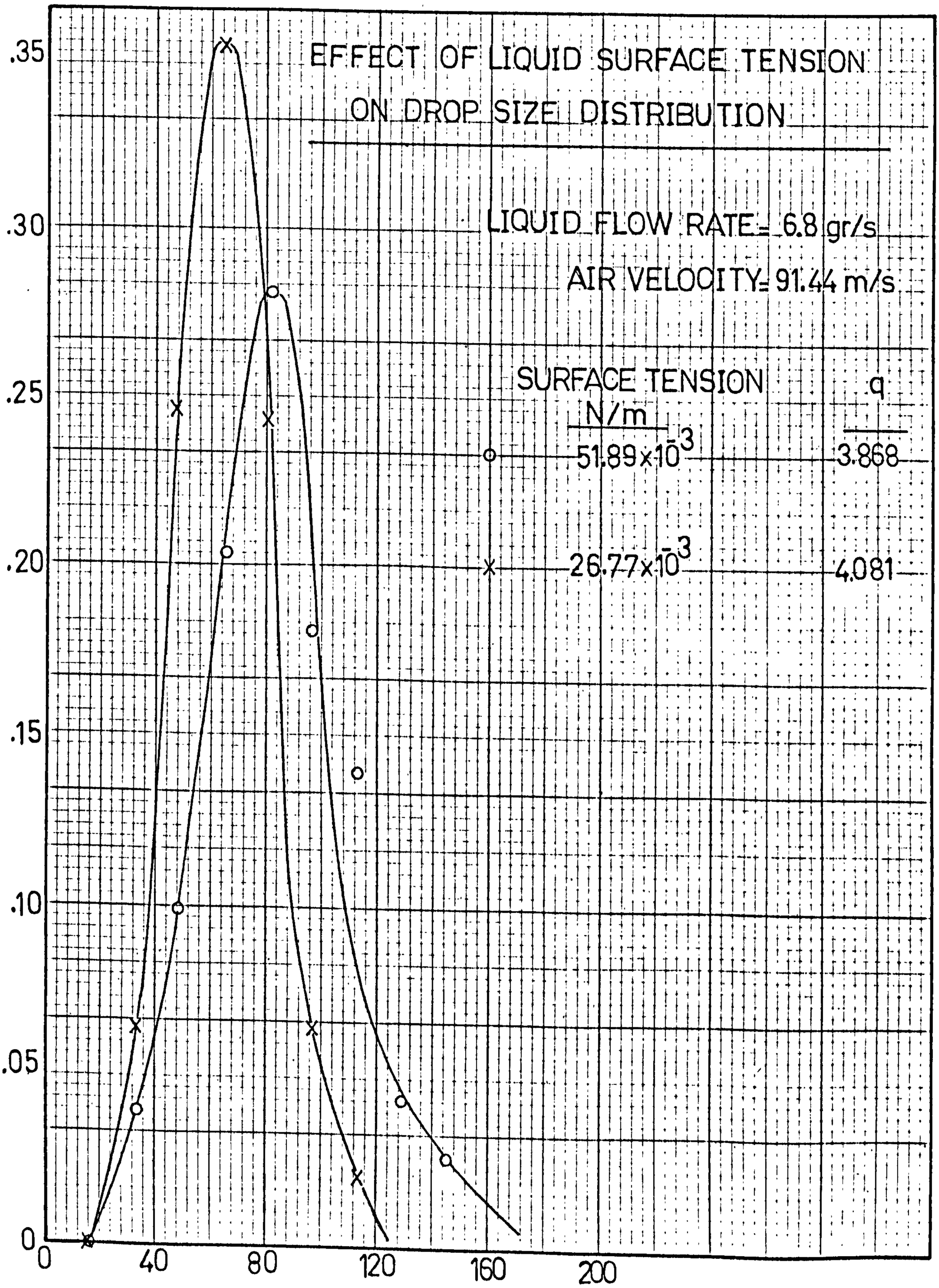
EFFECT OF LIQUID SURFACE TENSION
ON DROP SIZE DISTRIBUTION
LIQUID FLOW RATE = 6.8 gr/s
AIR VELOCITY = 91.44 m/s
SURFACE TENSION N/m
q
51.89×10⁻³
3.868
26.77×10⁻³
4.081
FRACTION OF VOLUME(Δv)
.35
.30
.25
.20
.15
.10
.05
0
0
40
80
120
160
200
DROP DIAMETER, microns

FIG. 31

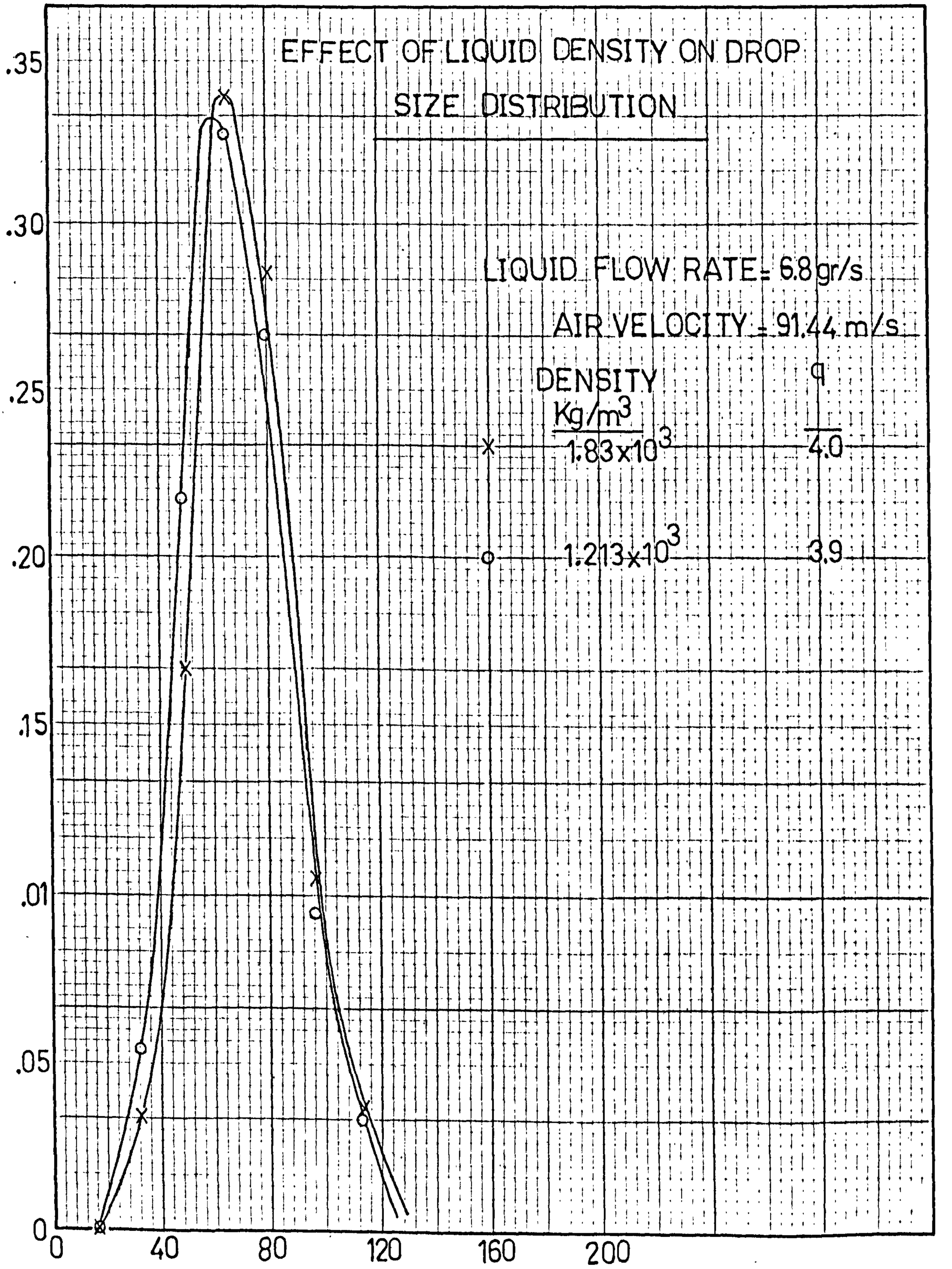
EFFECT OF LIQUID DENSITY ON DROP SIZE DISTRIBUTION
LIQUID FLOW RATE = 6.8 gr/s
AIR VELOCITY = 91.44 m/s
DENSITY Kg/m3
1.83x10^3
1.213x10^3
q
4.0
3.9
FRACTION OF VOLUME (Δv)
.35
.30
.25
.20
.15
.01
.05
0
0
40
80
120
160
200
DROP DIAMETER, microns

TYPICAL $\log(\log \frac{1}{1-v})$ vs $\log X$ PLOTS

WATER

	AIR VELOCITY	q
x	54.86 m/s	3.21
o	91.44 m/s	3.41
Δ	121.92 m/s	3.57

m_l = 22.7 gr/s

1000
100
10
1

X, microns

10 1 .1 .01 .001 .0001

$\log \frac{1}{1-v}$

FIG. 32

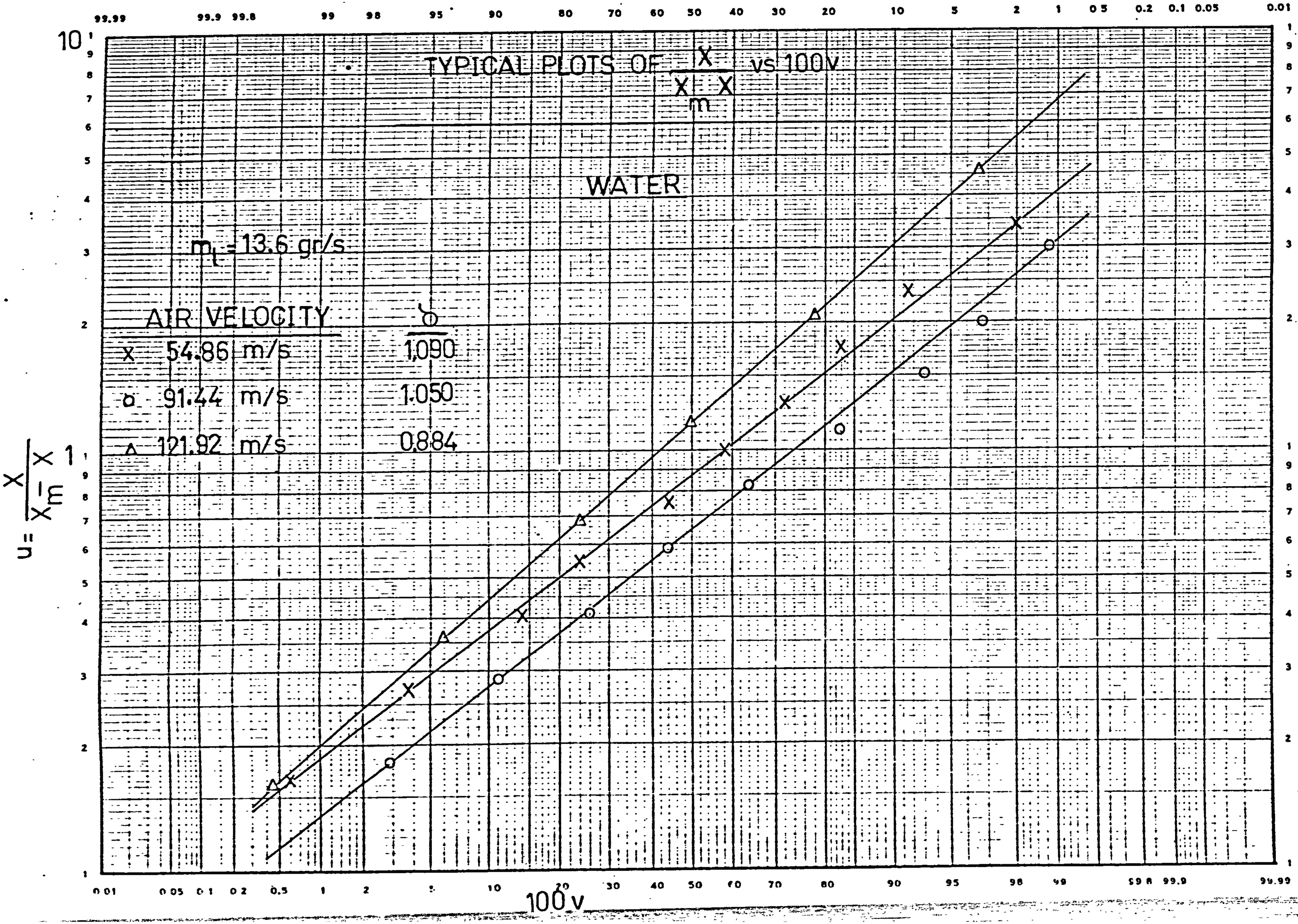
TYPICAL PLOTS OF X/X_m vs 100v
WATER
m_l = 13.6 gr/s
AIR VELOCITY
x 54.86 m/s
o 91.44 m/s
Δ 121.92 m/s
δ
1,090
1.050
0.884
u = X/X_m − 1
100 v
99.99 99.9 99.8 99 98 95 90 80 70 60 50 40 30 20 10 5 2 1 0.5 0.2 0.1 0.05 0.01
0.01 0.05 0.1 0.2 0.5 1 2 5 10 20 30 40 50 60 70 80 90 95 98 99 99.8 99.9 99.99

FIG.33

FIG.34

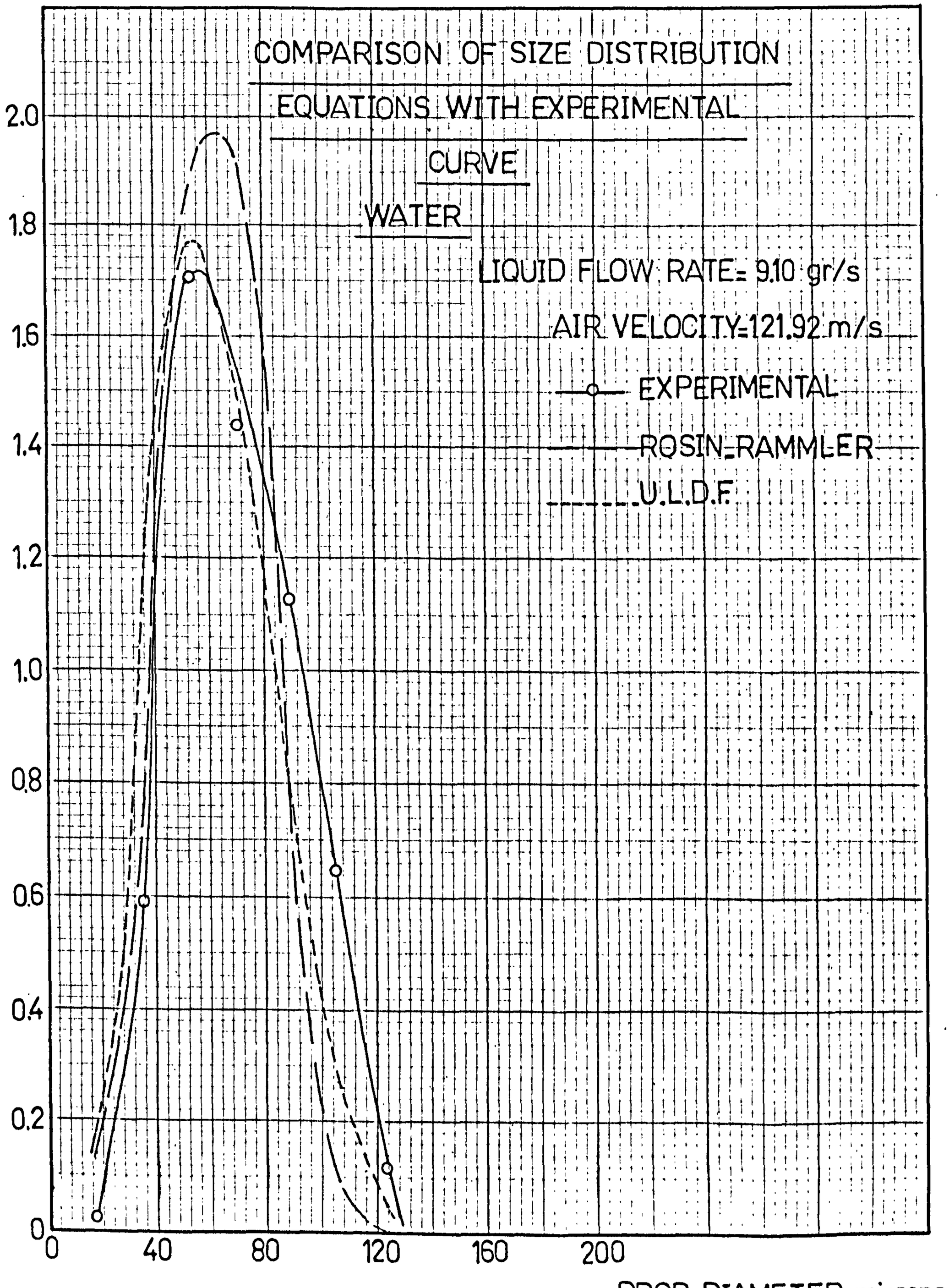
COMPARISON OF SIZE DISTRIBUTION
EQUATIONS WITH EXPERIMENTAL
CURVE
WATER
LIQUID FLOW RATE= 9.10 gr/s
AIR VELOCITY=121.92 m/s
EXPERIMENTAL
ROSIN-RAMMLER
U.L.D.F
100 dV/dX
2.0
1.8
1.6
1.4
1.2
1.0
0.8
0.6
0.4
0.2
0
0
40
80
120
160
200
DROP DIAMETER, microns

FIG.35

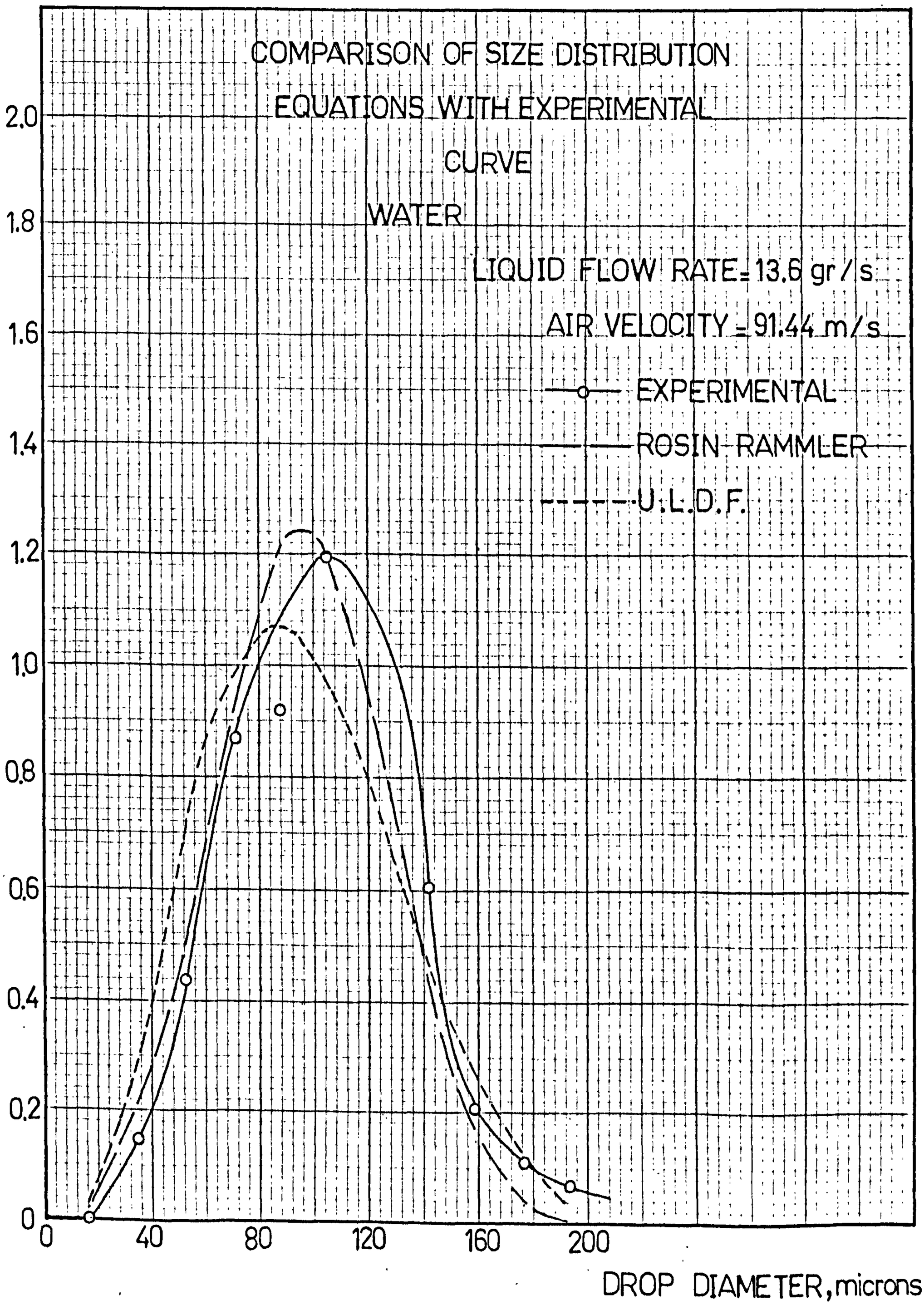
COMPARISON OF SIZE DISTRIBUTION EQUATIONS WITH EXPERIMENTAL CURVE
WATER
LIQUID FLOW RATE = 13.6 gr/s
AIR VELOCITY = 91.44 m/s
EXPERIMENTAL
ROSIN-RAMMLER
U.L.D.F.
100 dV/dX
2.0
1.8
1.6
1.4
1.2
1.0
0.8
0.6
0.4
0.2
0
0
40
80
120
160
200
DROP DIAMETER, microns

FIG.36

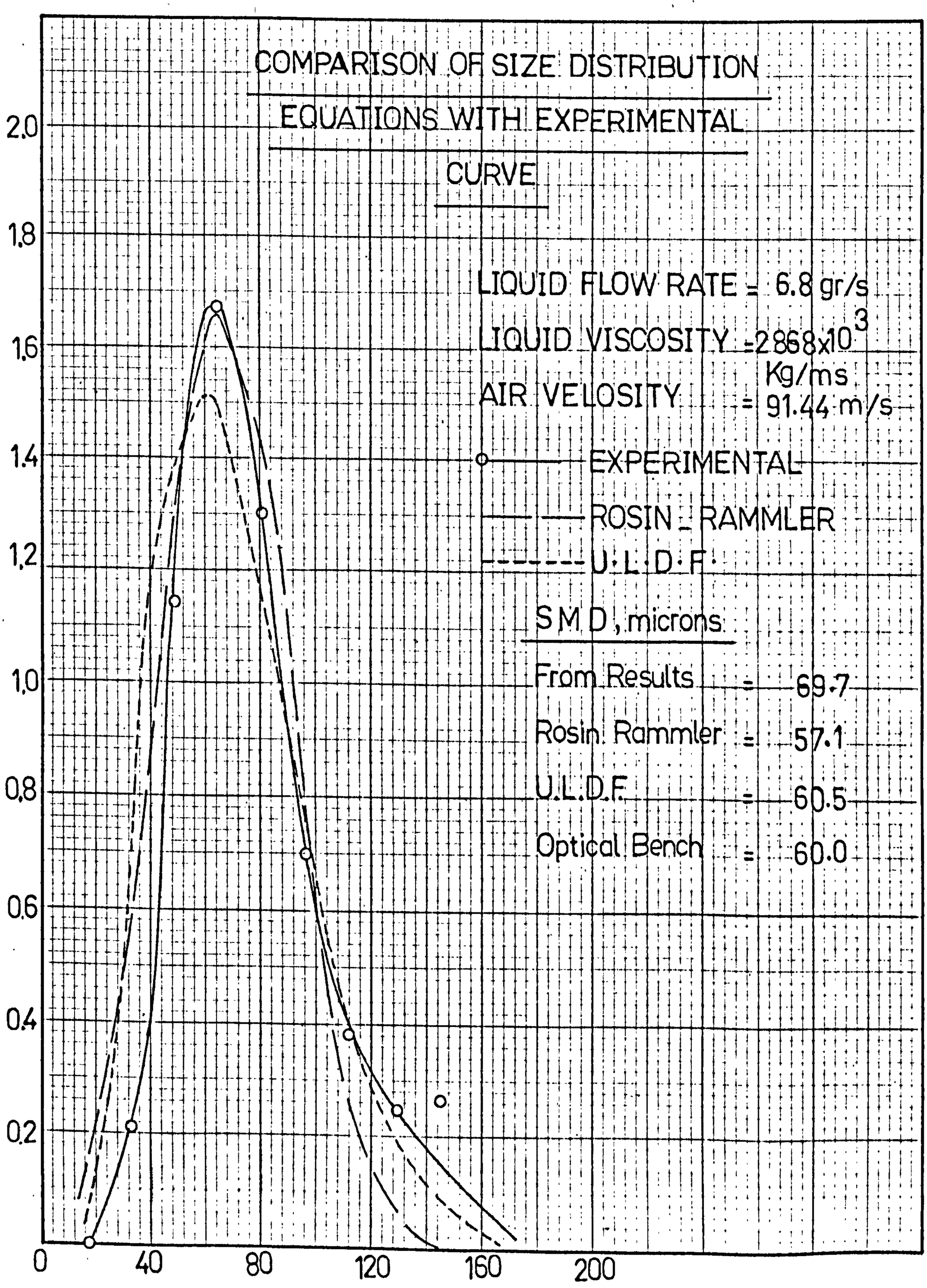
COMPARISON OF SIZE DISTRIBUTION EQUATIONS WITH EXPERIMENTAL CURVE
LIQUID FLOW RATE = 6.8 gr/s
LIQUID VISCOSITY = 2868x10^3 Kg/ms
AIR VELOSITY = 91.44 m/s
EXPERIMENTAL
ROSIN - RAMMLER
U.L.D.F.
SMD, microns
From Results = 69.7
Rosin Rammler = 57.1
U.L.D.F. = 60.5
Optical Bench = 60.0
100 dV/dX
2.0
1.8
1.6
1.4
1.2
1.0
0.8
0.6
0.4
0.2
0
40
80
120
160
200
DROP DIAMETER, microns

FIG.37

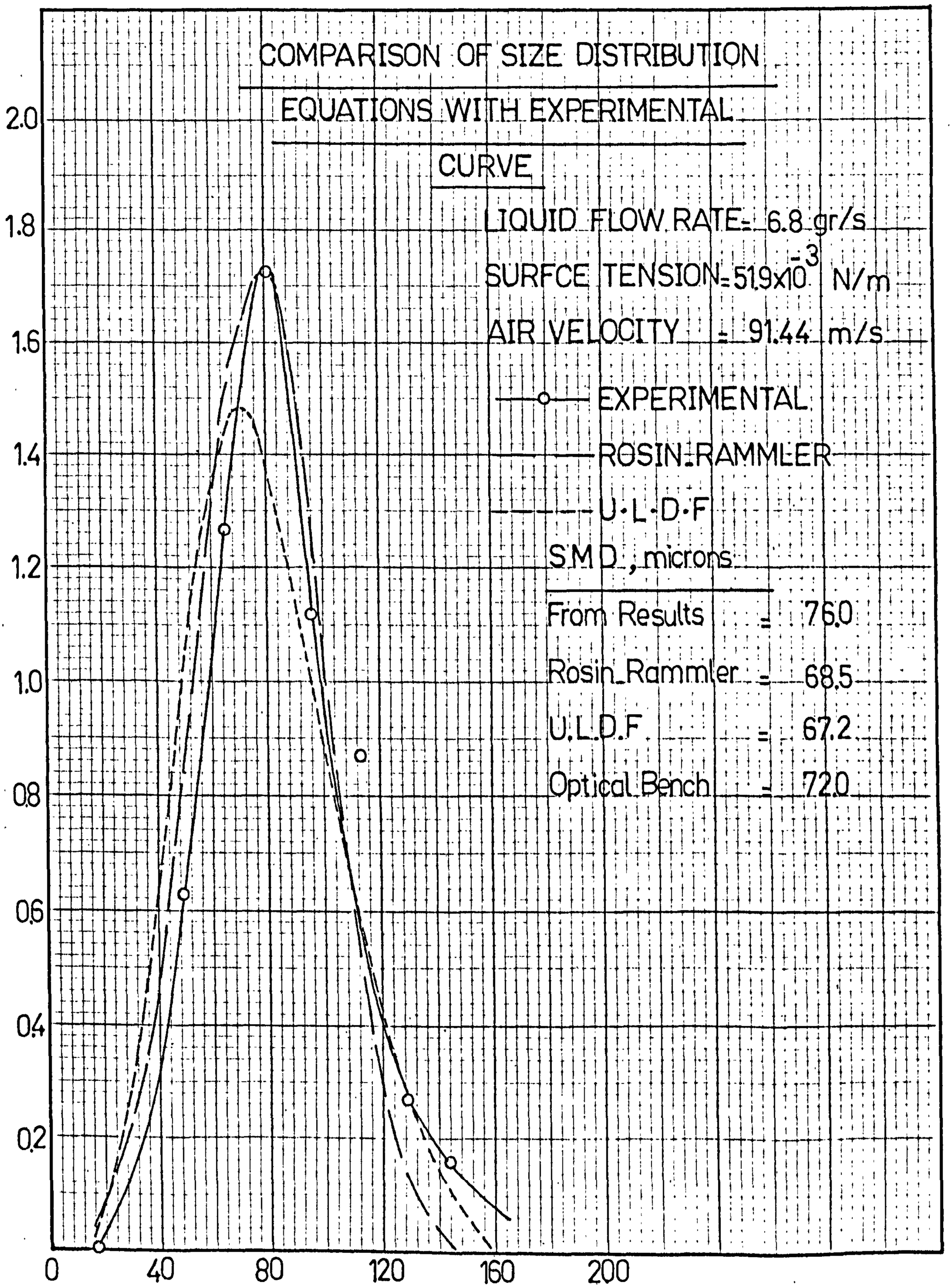
COMPARISON OF SIZE DISTRIBUTION
EQUATIONS WITH EXPERIMENTAL
CURVE
LIQUID FLOW RATE= 6.8 gr/s
SURFCE TENSION=51.9x10⁻³ N/m
AIR VELOCITY = 91.44 m/s
EXPERIMENTAL
ROSIN-RAMMLER
U·L·D·F
SMD, microns
From Results = 76.0
Rosin_Rammler = 68.5
U.L.D.F = 67.2
Optical Bench = 72.0
100 dv/dx
2.0
1.8
1.6
1.4
1.2
1.0
0.8
0.6
0.4
0.2
0
40
80
120
160
200
DROP DIAMETER microns

FIG.38

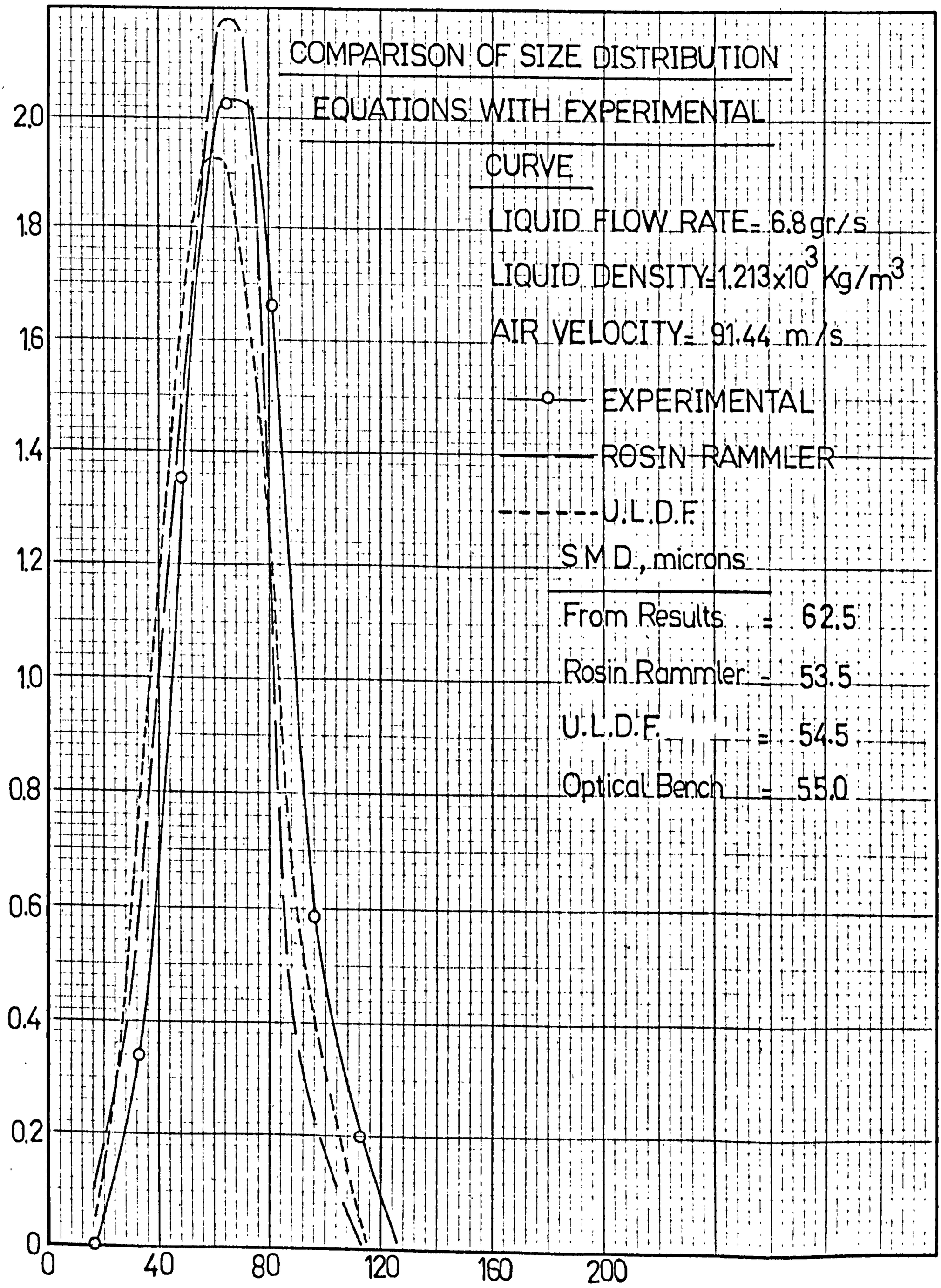
COMPARISON OF SIZE DISTRIBUTION
EQUATIONS WITH EXPERIMENTAL
CURVE
LIQUID FLOW RATE= 6.8 gr/s
LIQUID DENSITY=1.213x10^3 Kg/m^3
AIR VELOCITY= 91.44 m/s
EXPERIMENTAL
ROSIN RAMMLER
U.L.D.F.
S.M.D., microns
From Results = 62.5
Rosin Rammler = 53.5
U.L.D.F. = 54.5
Optical Bench = 55.0
100 dV/dX
2.0
1.8
1.6
1.4
1.2
1.0
0.8
0.6
0.4
0.2
0
0
40
80
120
160
200
DROP DIAMETER microns

COMPARISON OF PRESENT RESULTS WITH SIMMONS' CORRELATION

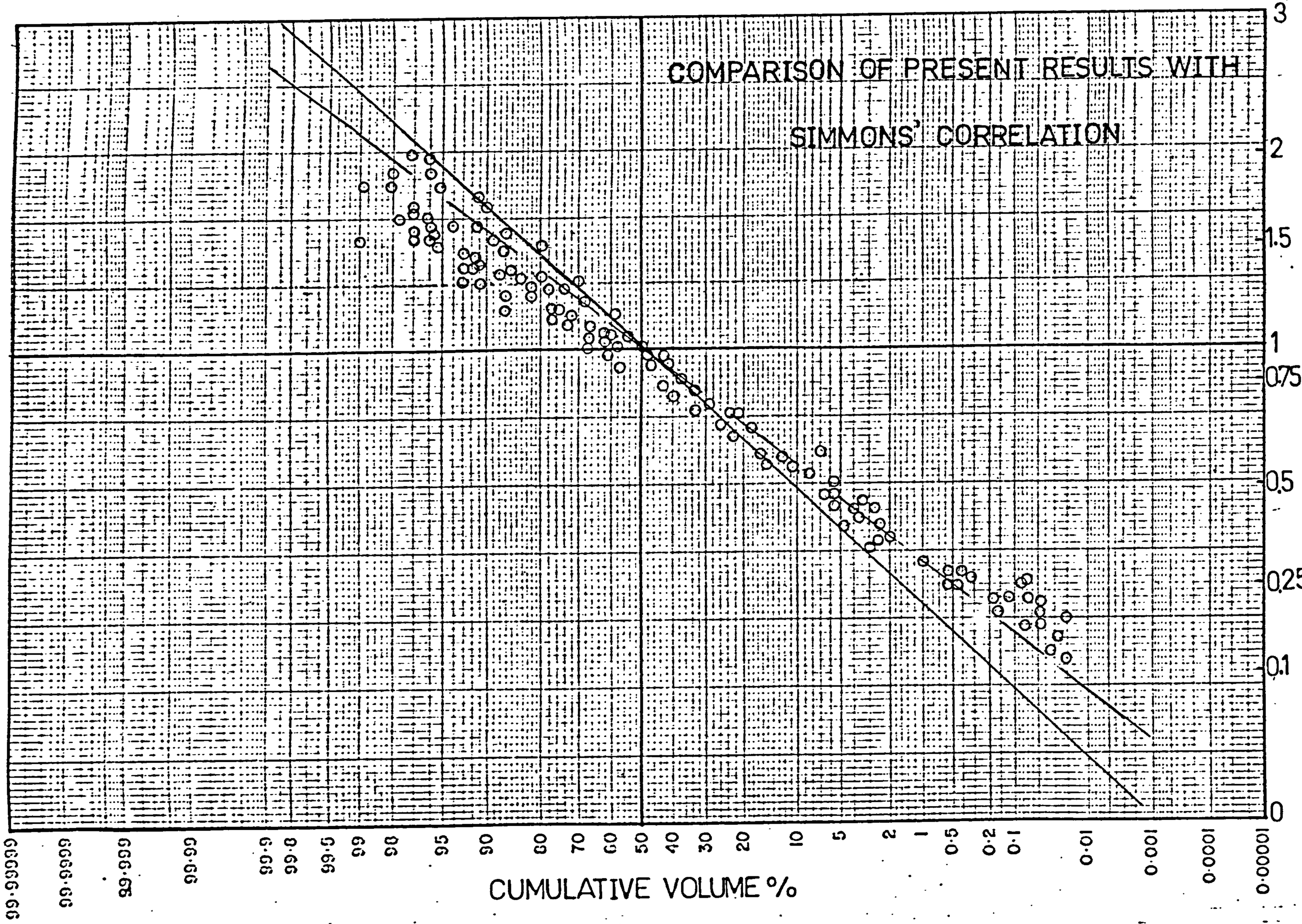

FIG.39

——— SIMMONS' CORRELATION ($\delta = 0.238$)

— — — EXPERIMENTAL LINE ($\delta = 0.200$)

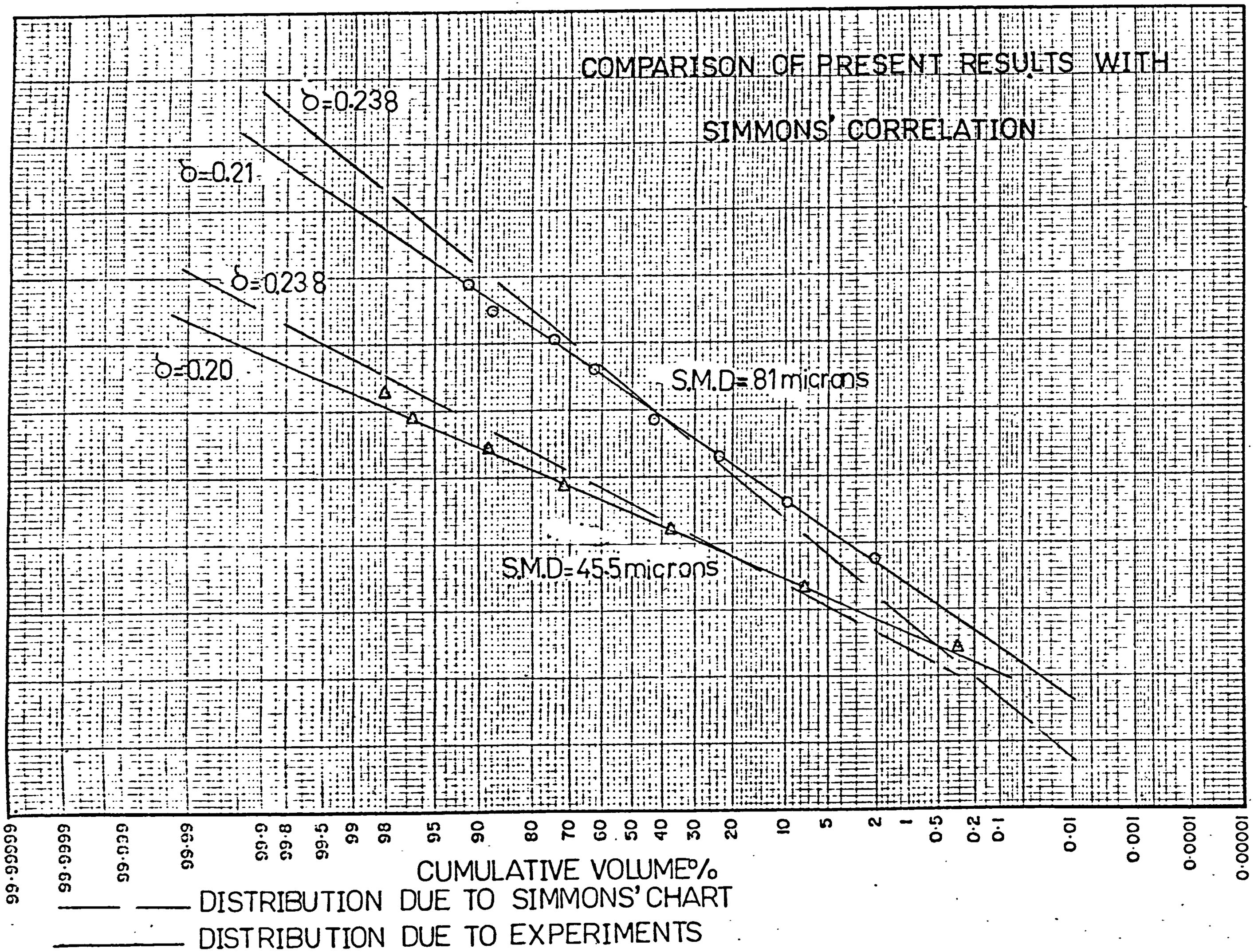
COMPARISON OF PRESENT RESULTS WITH SIMMONS' CORRELATION
δ=0.238
δ=0.21
δ=0.238
δ=0.20
S.M.D=81 microns
S.M.D=45.5 microns
99.9999
99.999
99.99
99.9
99.8
99.5
99
98
95
90
80
70
60
50
40
30
20
10
5
2
1
0.5
0.2
0.1
0.01
0.001
0.0001
0.00001
CUMULATIVE VOLUME%
DISTRIBUTION DUE TO SIMMONS' CHART
DISTRIBUTION DUE TO EXPERIMENTS

FIG.40

FIG.41

VARIATION OF LIQUID FILM THICKNESS WITH AIR VELOCITY AT DIFFERENT LIQUID FLOW RATES

EXPERIMENTAL TESTS ON ATOMIZER (A)

WATER

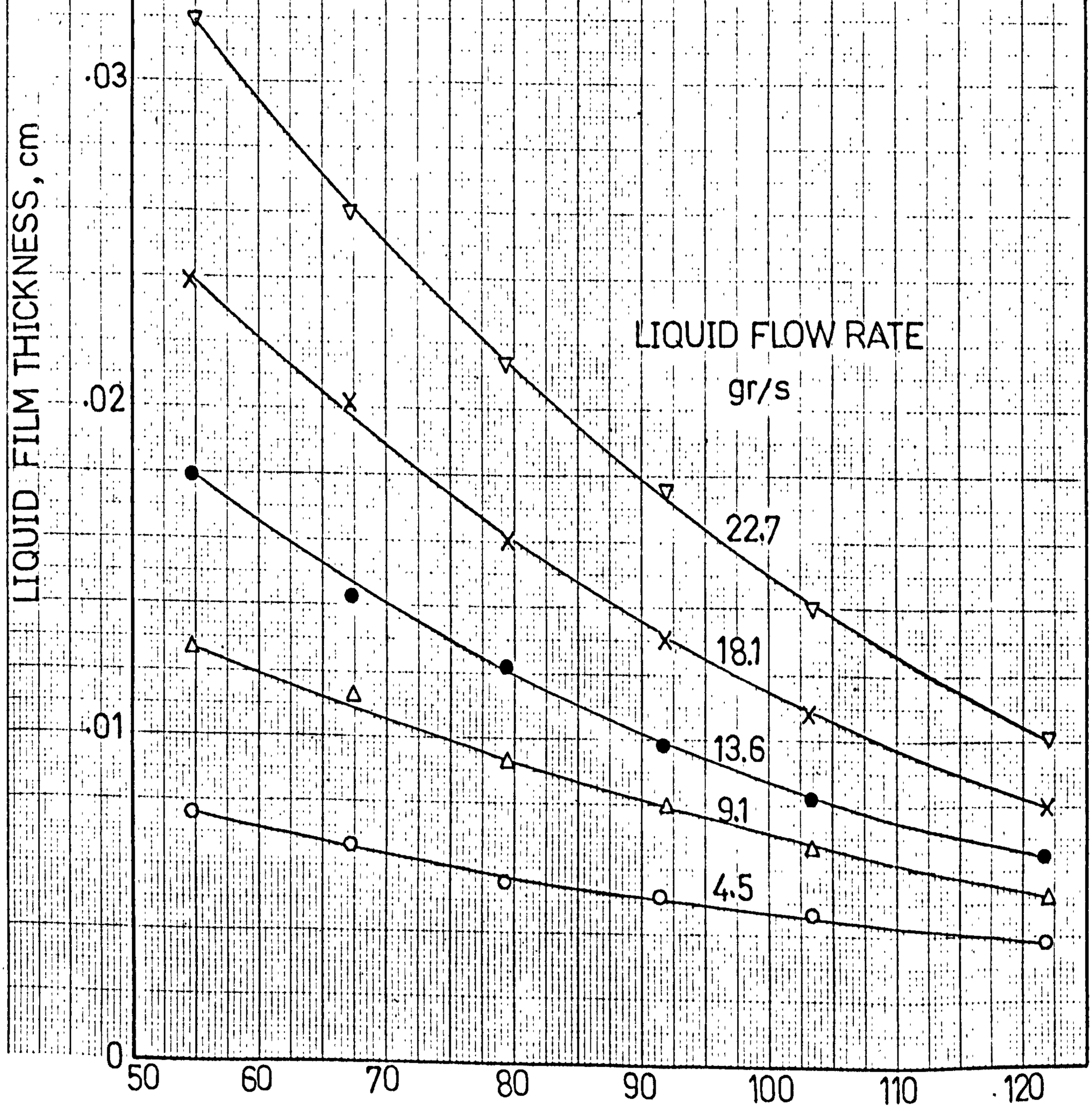

FIG.42

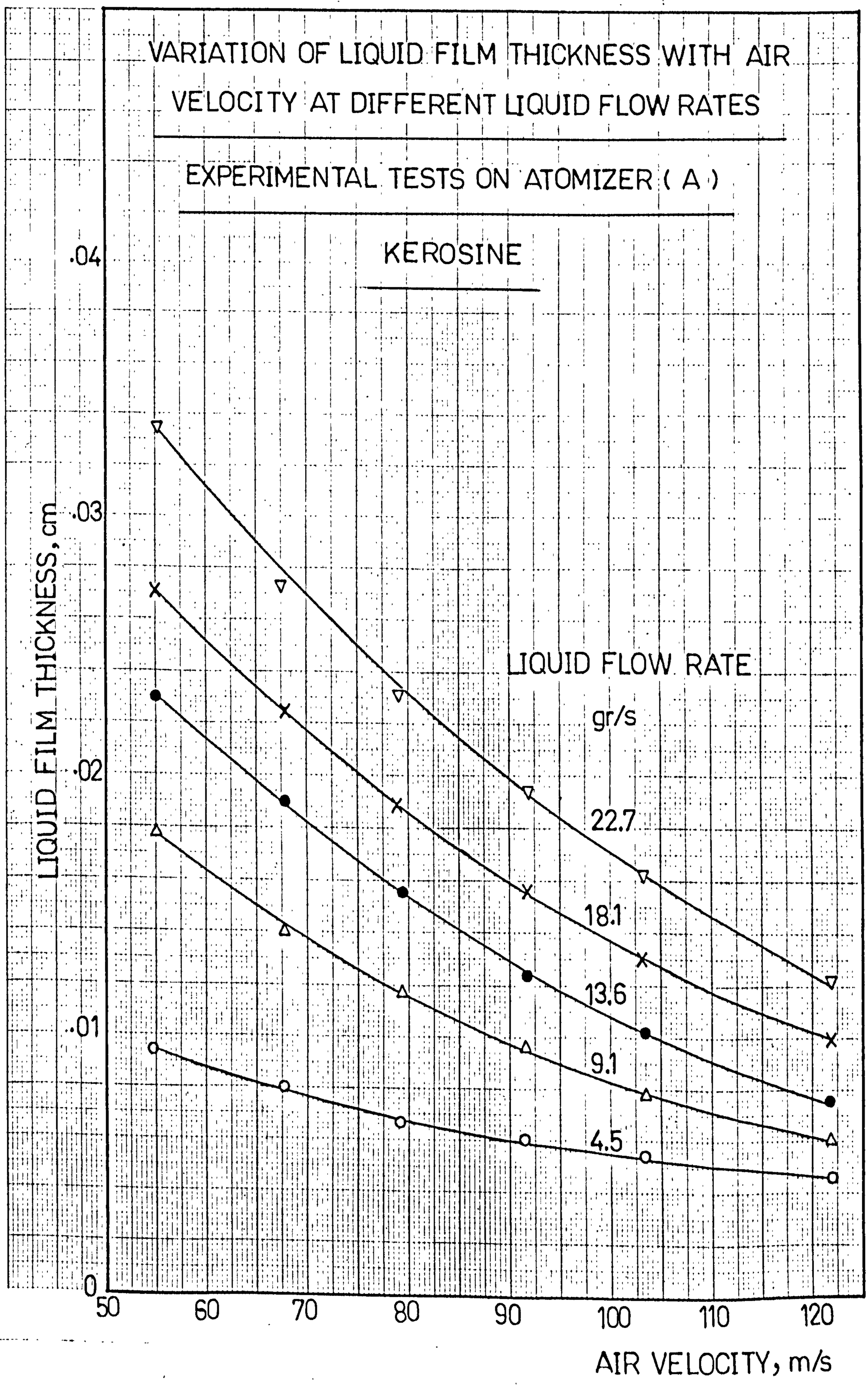
VARIATION OF LIQUID FILM THICKNESS WITH AIR VELOCITY AT DIFFERENT LIQUID FLOW RATES
EXPERIMENTAL TESTS ON ATOMIZER (A)
KEROSINE
LIQUID FILM THICKNESS, cm
.04
.03
.02
.01
0
LIQUID FLOW RATE
gr/s
22.7
18.1
13.6
9.1
4.5
50
60
70
80
90
100
110
120
AIR VELOCITY, m/s

FIG.43

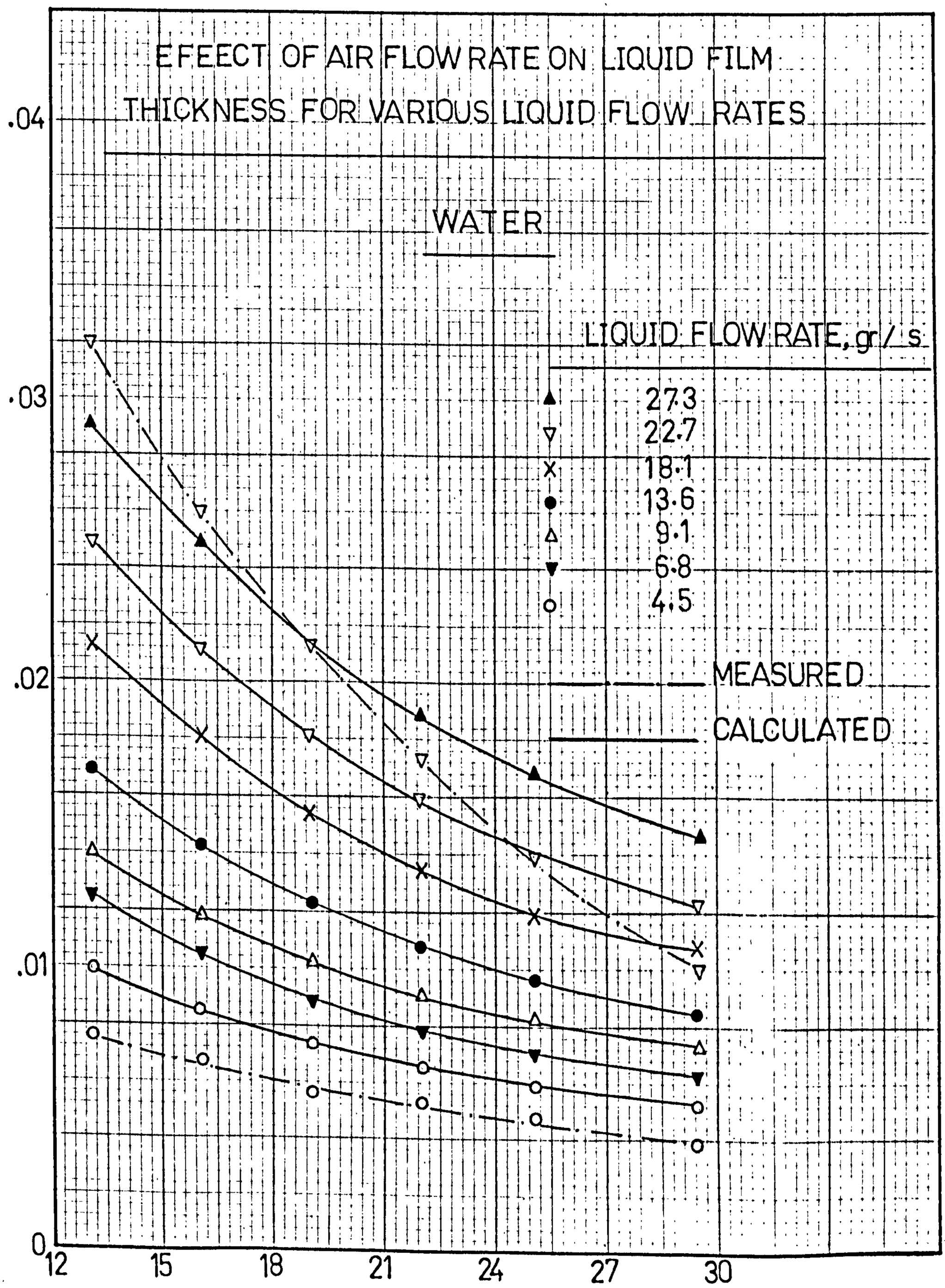
EFEECT OF AIR FLOW RATE ON LIQUID FILM THICKNESS FOR VARIOUS LIQUID FLOW RATES
WATER
LIQUID FLOW RATE, gr / s
27.3
22.7
18.1
13.6
9.1
6.8
4.5
MEASURED
CALCULATED
LIQUID FILM THICKNESS, cm
.04
.03
.02
.01
0
12
15
18
21
24
27
30
AIR FLOW RATE, gr/s

FIG.44

EFFECT OF AIR FLOW RATE ON LIQUID FILM THICKNESS FOR VARIOUS LIQUID FLOW RATES

KEROSINE

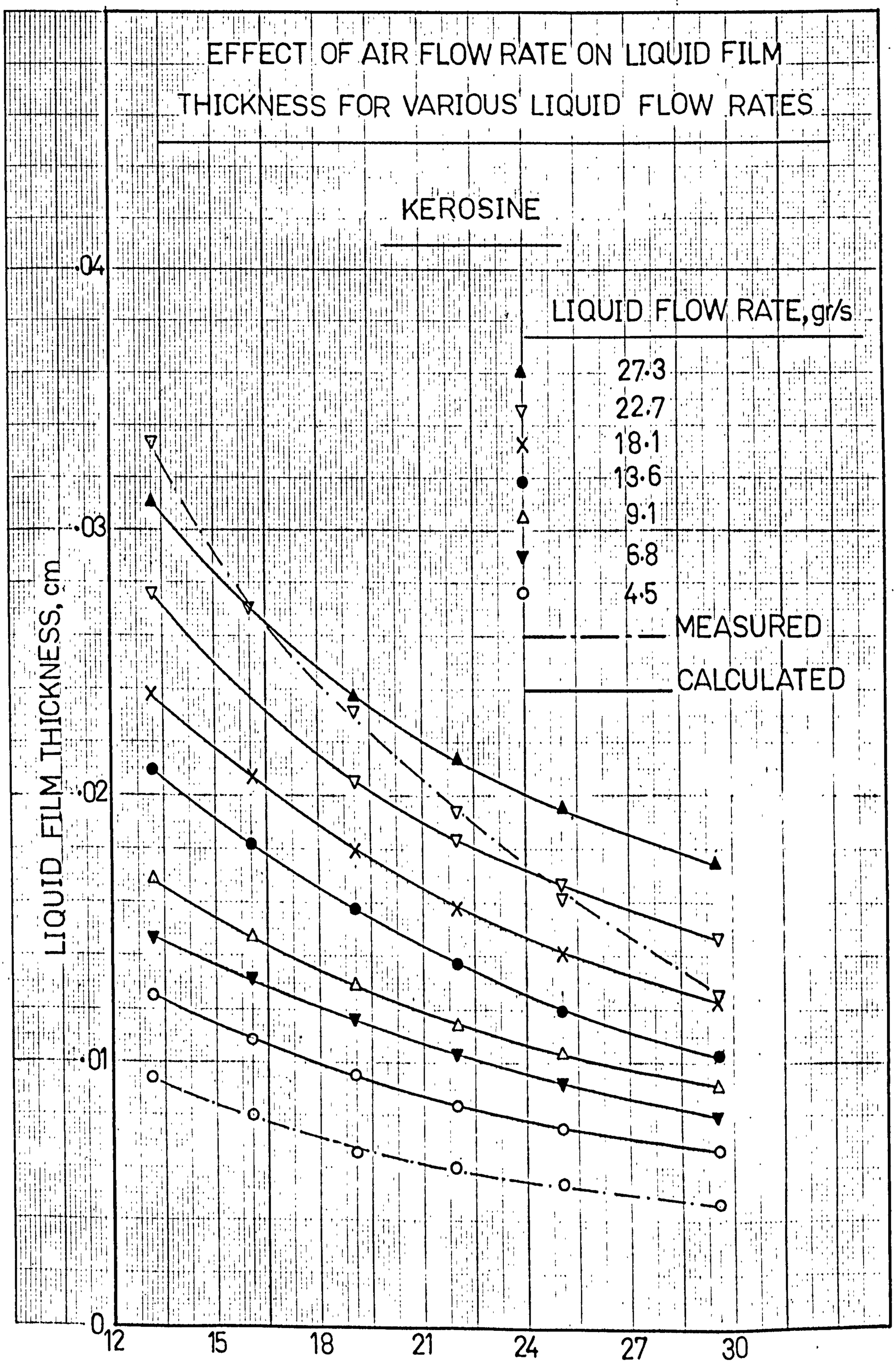

FIG.45

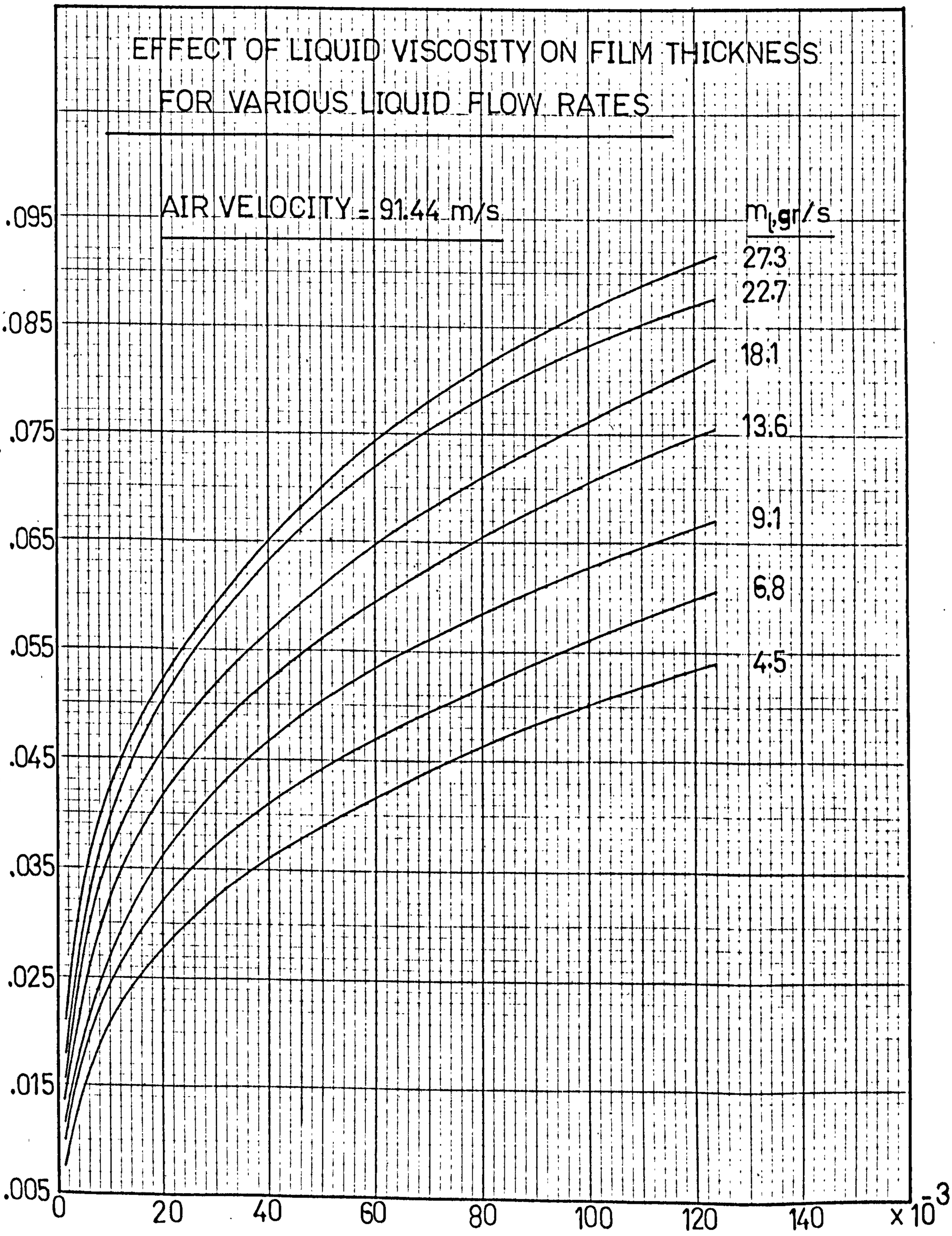
EFFECT OF LIQUID VISCOSITY ON FILM THICKNESS
FOR VARIOUS LIQUID FLOW RATES
AIR VELOCITY = 91.44 m/s
m_l, gr/s
27.3
22.7
18.1
13.6
9.1
6.8
4.5
LIQUID FILM THICKNESS, cm
.095
.085
.075
.065
.055
.045
.035
.025
.015
.005
0
20
40
60
80
100
120
140
x 10⁻³
LIQUID VISCOSITY
Kg/ms

FIG.46

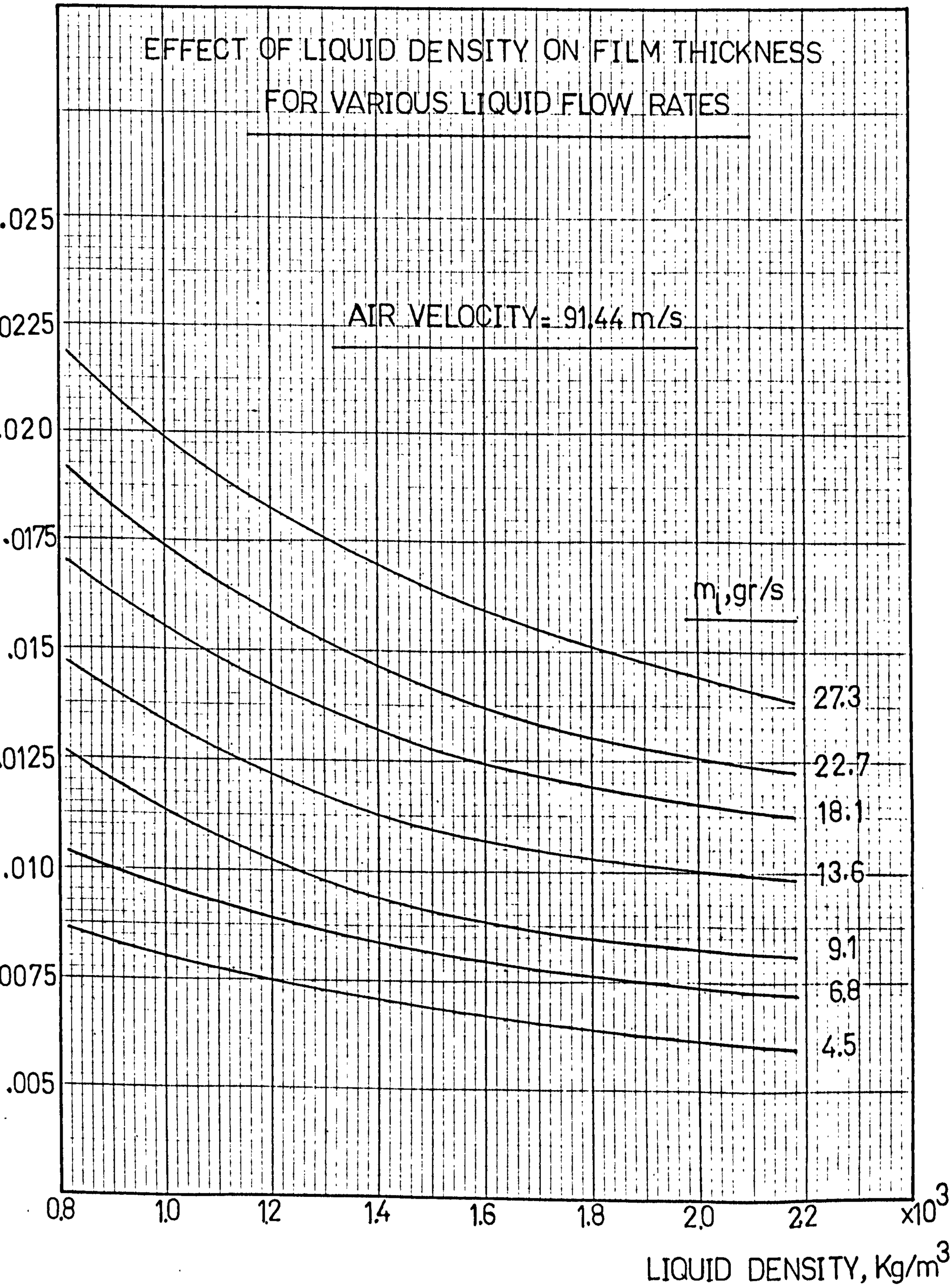
EFFECT OF LIQUID DENSITY ON FILM THICKNESS
FOR VARIOUS LIQUID FLOW RATES
AIR VELOCITY= 91.44 m/s
m_l, gr/s
27.3
22.7
18.1
13.6
9.1
6.8
4.5
LIQUID FILM THICKNESS, cm
.025
.0225
.020
.0175
.015
.0125
.010
.0075
.005
0.8
1.0
1.2
1.4
1.6
1.8
2.0
2.2
x10^3
LIQUID DENSITY, Kg/m^3

FIG.47

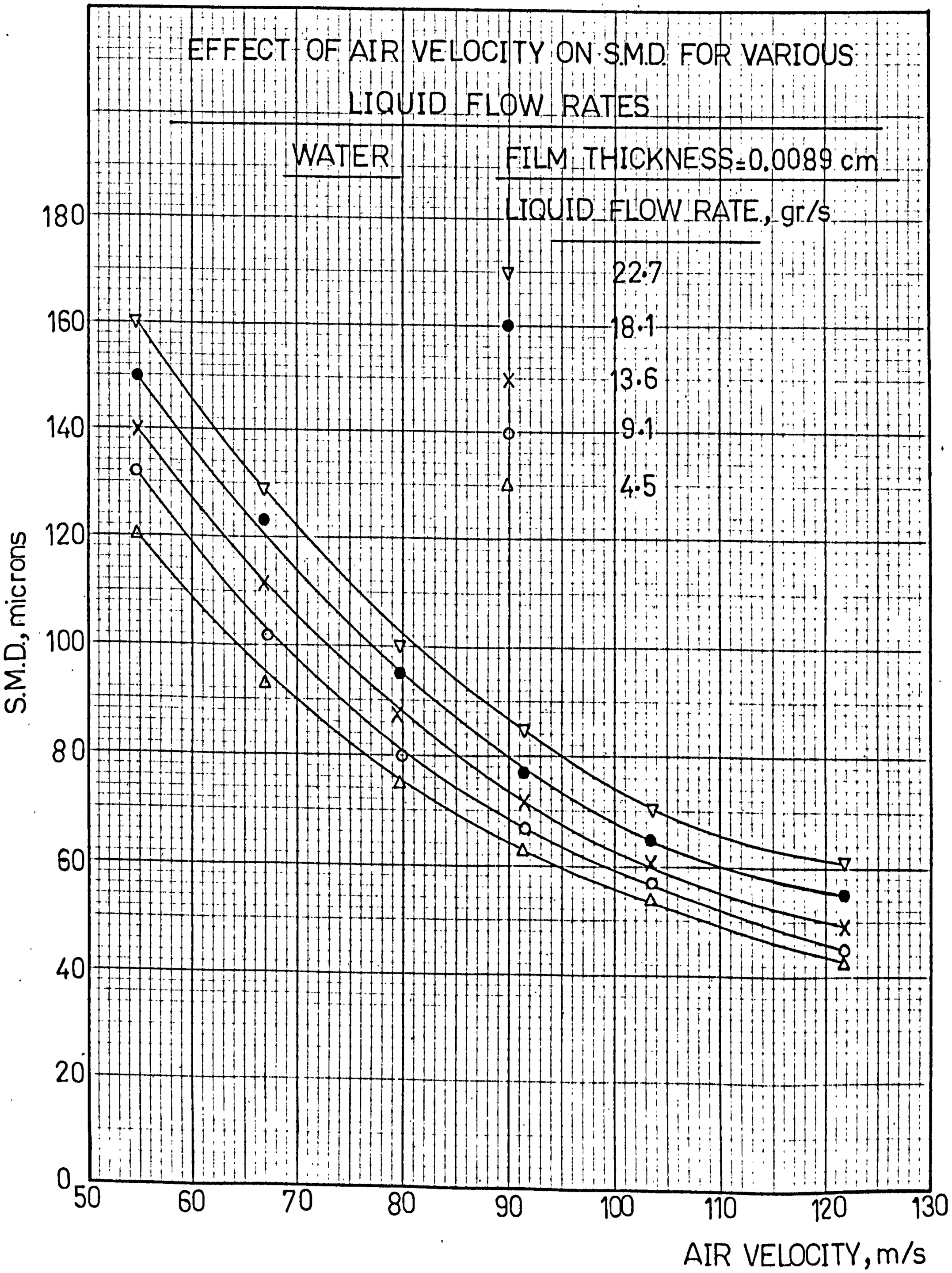
EFFECT OF AIR VELOCITY ON S.M.D. FOR VARIOUS LIQUID FLOW RATES
WATER
FILM THICKNESS=0.0089 cm
LIQUID FLOW RATE, gr/s
22.7
18.1
13.6
9.1
4.5
S.M.D., microns
0
20
40
60
80
100
120
140
160
180
50
60
70
80
90
100
110
120
130
AIR VELOCITY, m/s

FIG.48

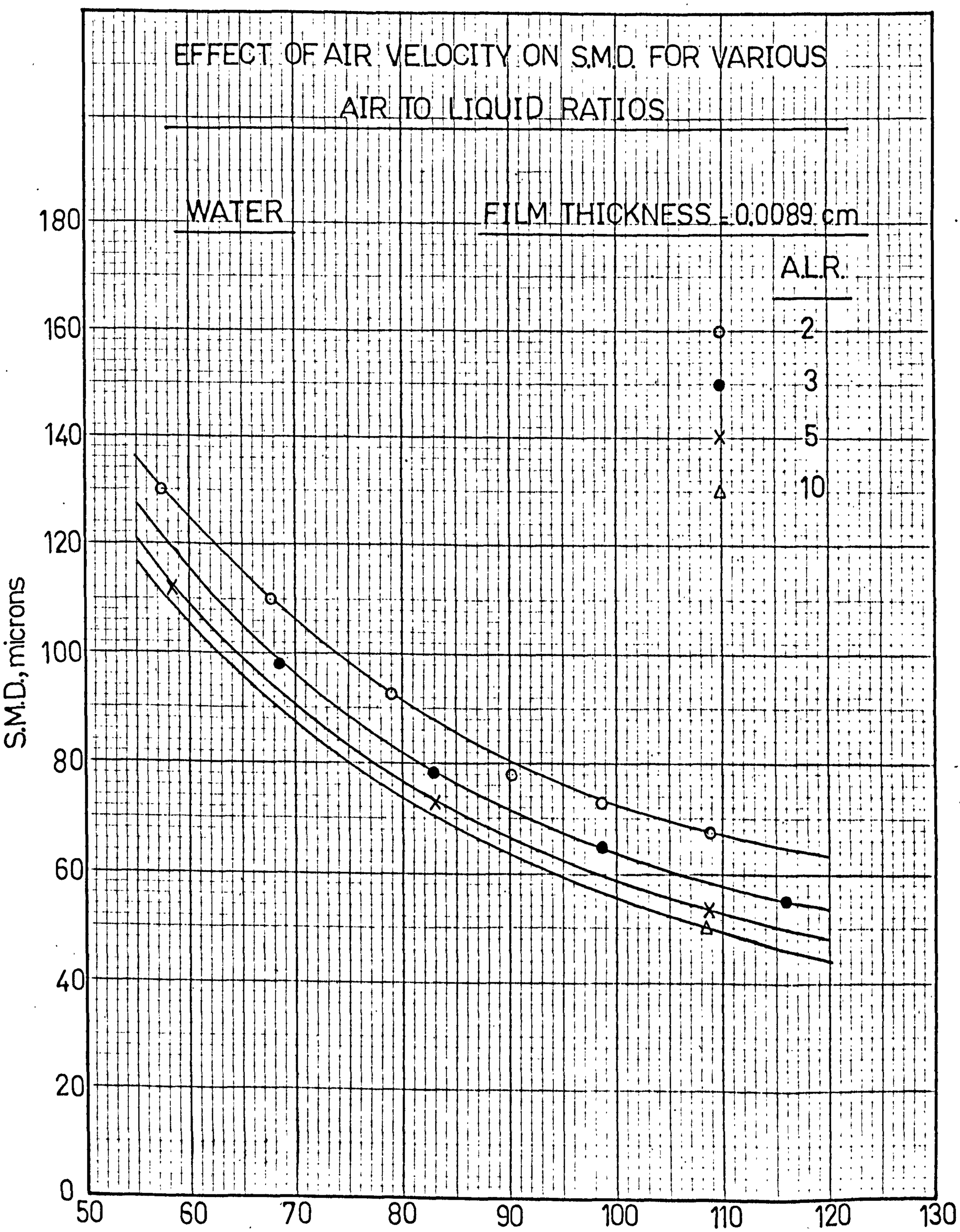
EFFECT OF AIR VELOCITY ON S.M.D. FOR VARIOUS AIR TO LIQUID RATIOS
WATER
FILM THICKNESS = 0.0089 cm
A.L.R.
2
3
5
10
S.M.D., microns
180
160
140
120
100
80
60
40
20
0
50
60
70
80
90
100
110
120
130
AIR VELOCITY, m/s

FIG.49

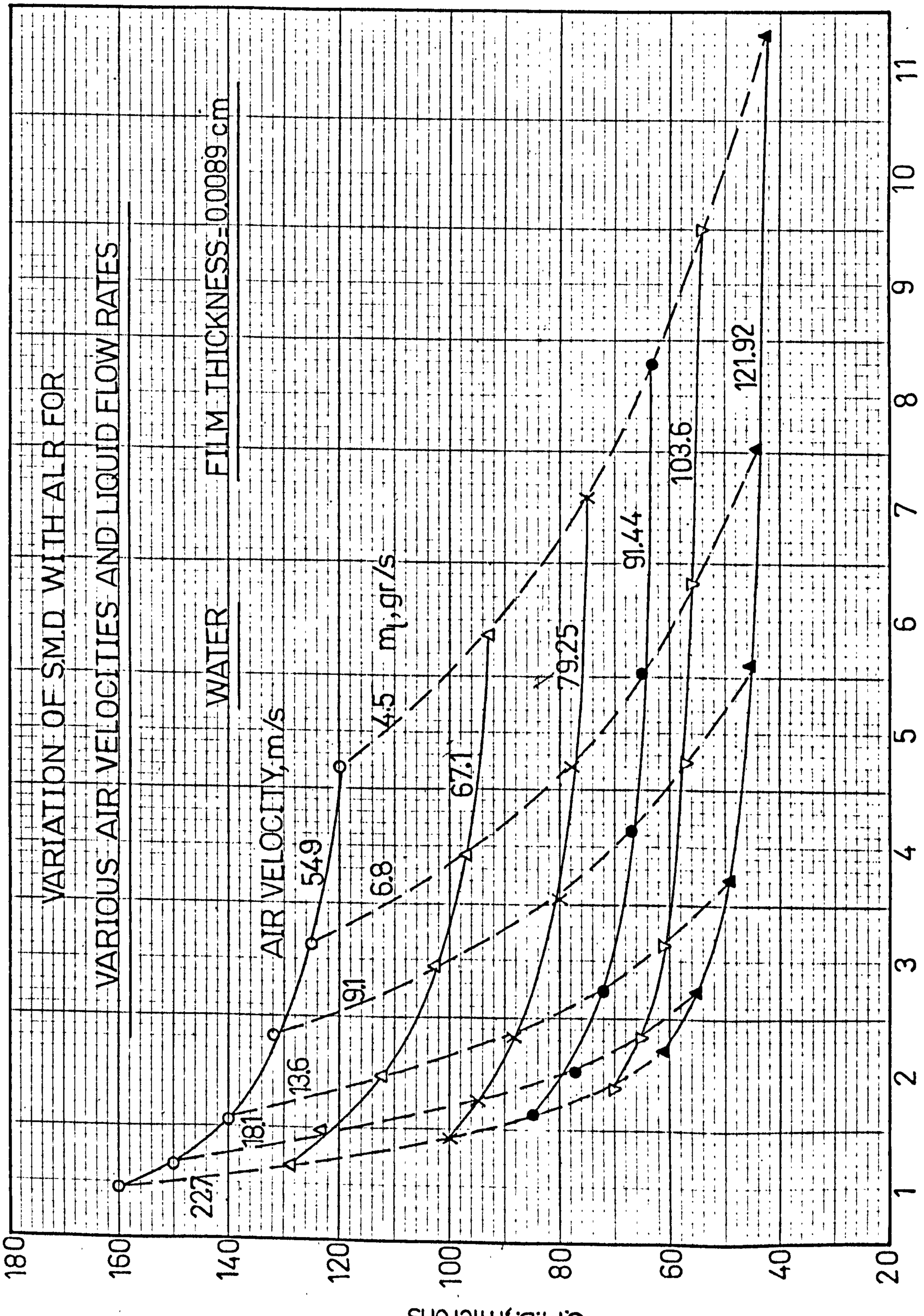
VARIATION OF SMD WITH ALR FOR
VARIOUS AIR VELOCITIES AND LIQUID FLOW RATES
WATER
FILM THICKNESS=0.0089 cm
AIR VELOCITY,m/s
22.7
18.1
13.6
9.1
6.8
5.49
4.5
m,gr/s
121.92
103.6
91.44
79.25
67.1
S.M.D.,microns
A.L.R
180
160
140
120
100
80
60
40
20
1
2
3
4
5
6
7
8
9
10
11

FIG.50

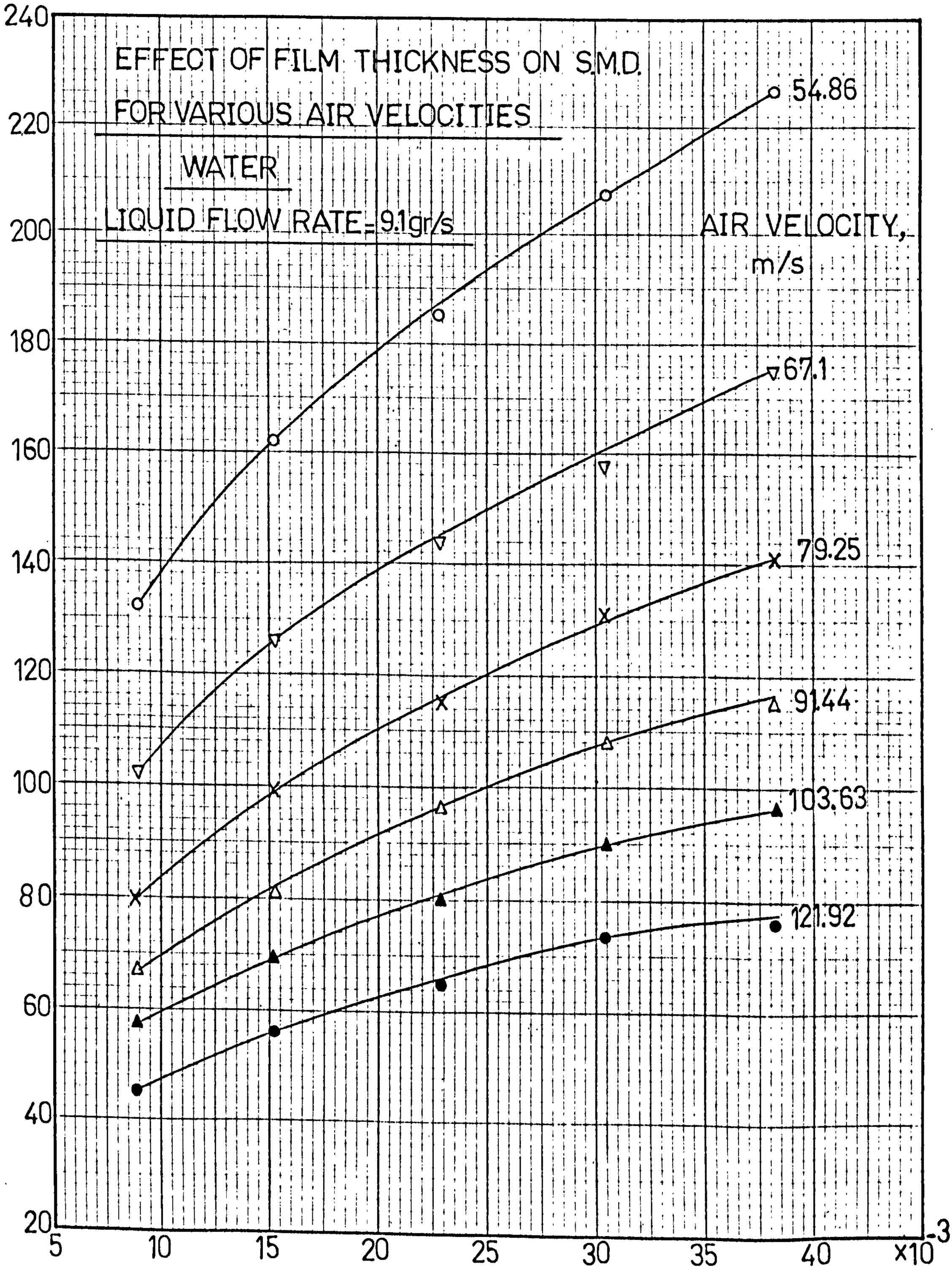
EFFECT OF FILM THICKNESS ON S.M.D.
FOR VARIOUS AIR VELOCITIES
WATER
LIQUID FLOW RATE=9.1gr/s
AIR VELOCITY, m/s
54.86
67.1
79.25
91.44
103.63
121.92
S.M.D., microns
240
220
200
180
160
140
120
100
80
60
40
20
5
10
15
20
25
30
35
40
x10-3
FILM THICKNESS, cm

FIG.51

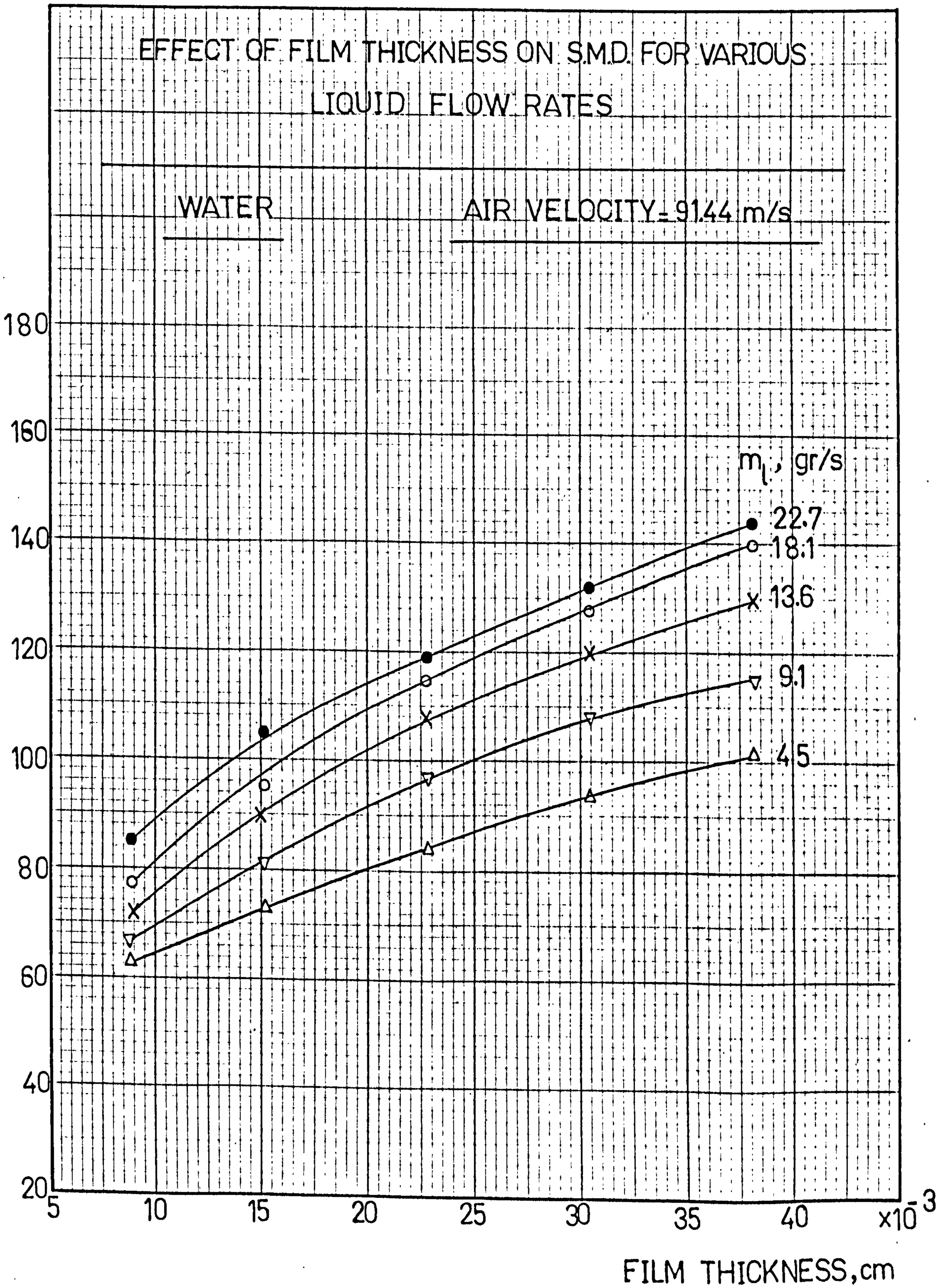
EFFECT OF FILM THICKNESS ON S.M.D. FOR VARIOUS LIQUID FLOW RATES
WATER
AIR VELOCITY = 91.44 m/s
m_l, gr/s
22.7
18.1
13.6
9.1
4.5
S.M.D., microns
180
160
140
120
100
80
60
40
20
5
10
15
20
25
30
35
40
x10⁻³
FILM THICKNESS, cm

FIG. 52

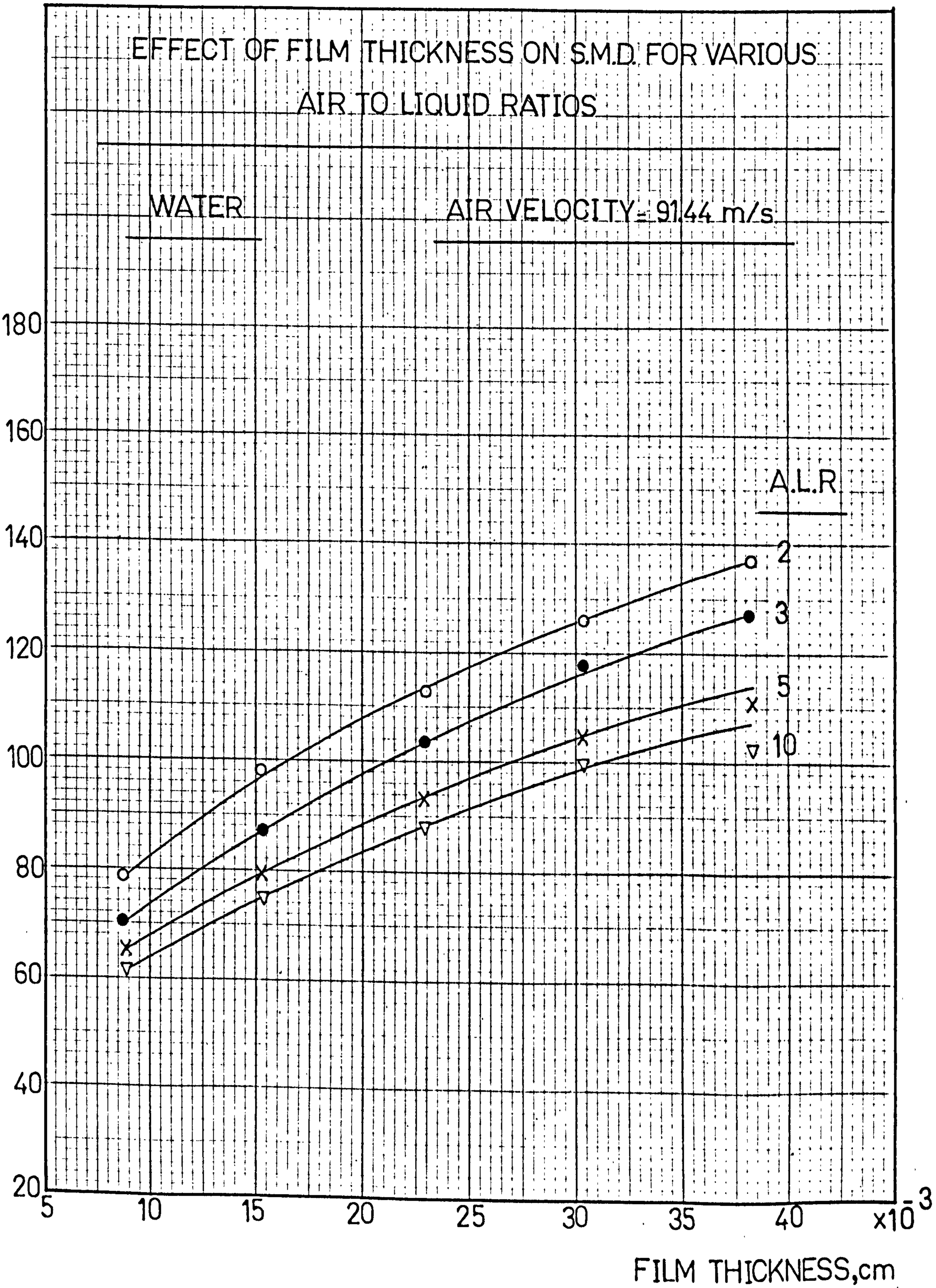
EFFECT OF FILM THICKNESS ON S.M.D. FOR VARIOUS AIR TO LIQUID RATIOS
WATER
AIR VELOCITY = 91.44 m/s
A.L.R
2
3
5
10
S.M.D., microns
180
160
140
120
100
80
60
40
20
5
10
15
20
25
30
35
40
x10⁻³
FILM THICKNESS, cm

FIG.53

EFFECT OF AIR VELOCITY ON S.M.D. FOR VARIOUS LIQUID FLOW RATES

KEROSINE

FILM THICKNESS = 0.0089 cm

LIQUID FLOW RATE, gr/s

- ▽ 22.7
- ● 18.1
- X 13.6
- ○ 9.1
- △ 4.5

S.M.D., microns

0
20
40
60
80
100
120
140
160

50 60 70 80 90 100 110 120 130

AIR VELOCITY, m/s

FIG.54

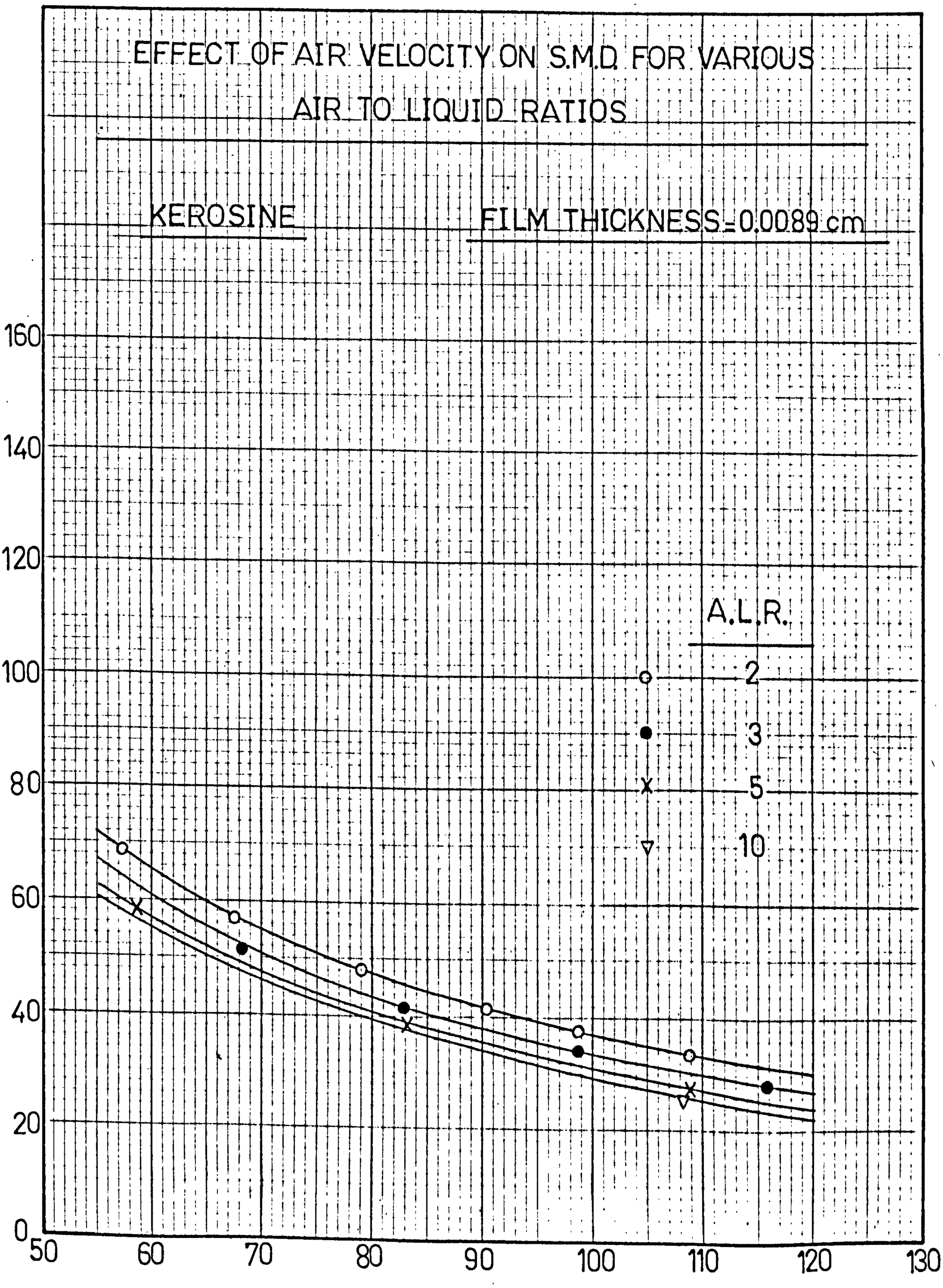
EFFECT OF AIR VELOCITY ON S.M.D. FOR VARIOUS AIR TO LIQUID RATIOS
KEROSINE
FILM THICKNESS=0.0089 cm
A.L.R.
2
3
5
10
S.M.D., microns
0
20
40
60
80
100
120
140
160
50
60
70
80
90
100
110
120
130
AIR VELOCITY, m/s

FIG.55

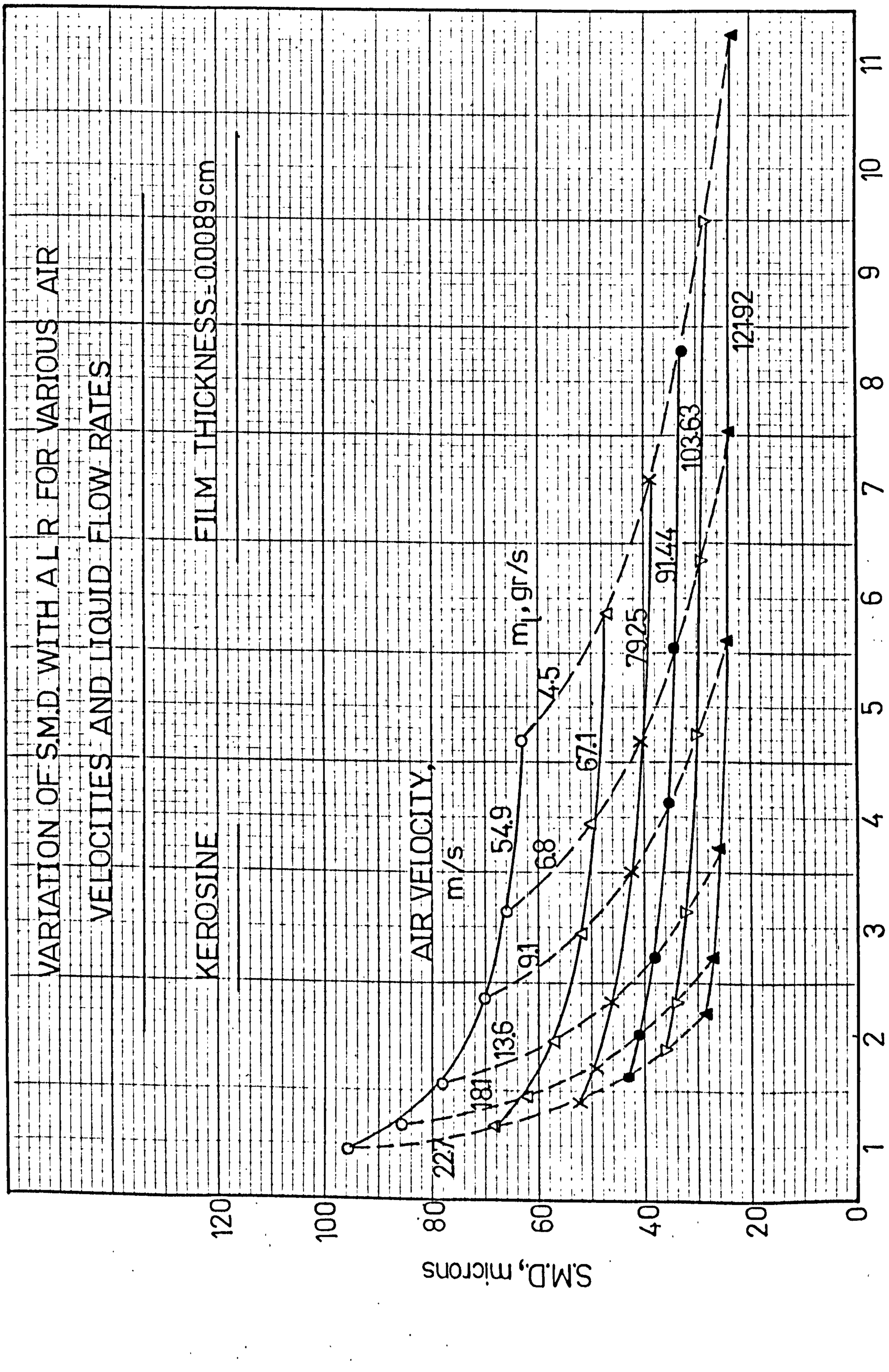
VARIATION OF S.M.D. WITH A.L.R. FOR VARIOUS AIR VELOCITIES AND LIQUID FLOW RATES
KEROSINE
FILM THICKNESS=0.0089cm
AIR VELOCITY, m/s
549
91
68
67.1
45
227
181
136
m_l, gr/s
91.44
103.63
121.92
79.25
S.M.D., microns
A.L.R.
120
100
80
60
40
20
0
1
2
3
4
5
6
7
8
9
10
11

FIG. 56

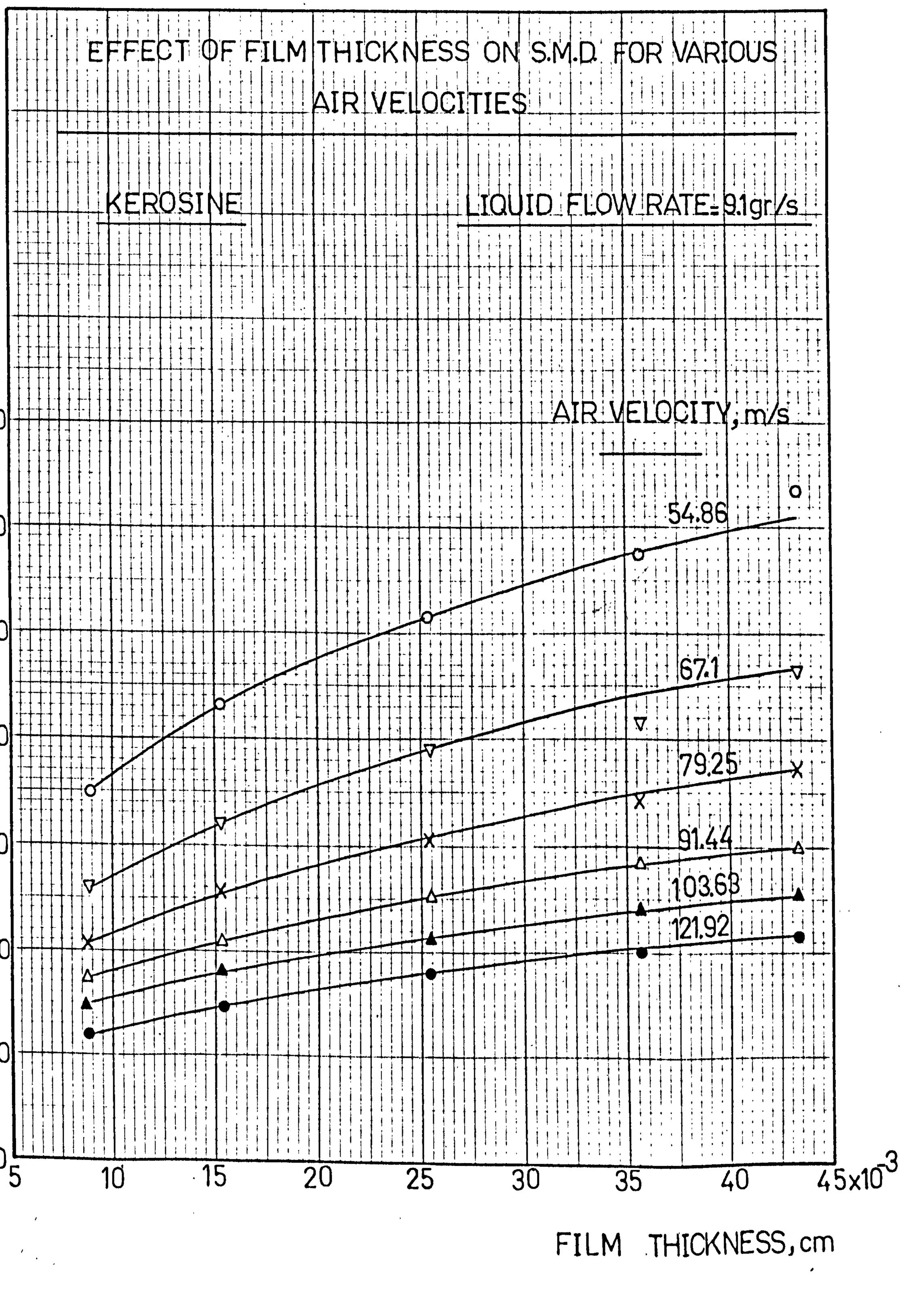
EFFECT OF FILM THICKNESS ON S.M.D. FOR VARIOUS AIR VELOCITIES
KEROSINE
LIQUID FLOW RATE = 9.1 gr/s
AIR VELOCITY, m/s
54.86
67.1
79.25
91.44
103.63
121.92
S.M.D., microns
0
20
40
60
80
100
120
140
5
10
15
20
25
30
35
40
45x10^-3
FILM THICKNESS, cm

FIG.57

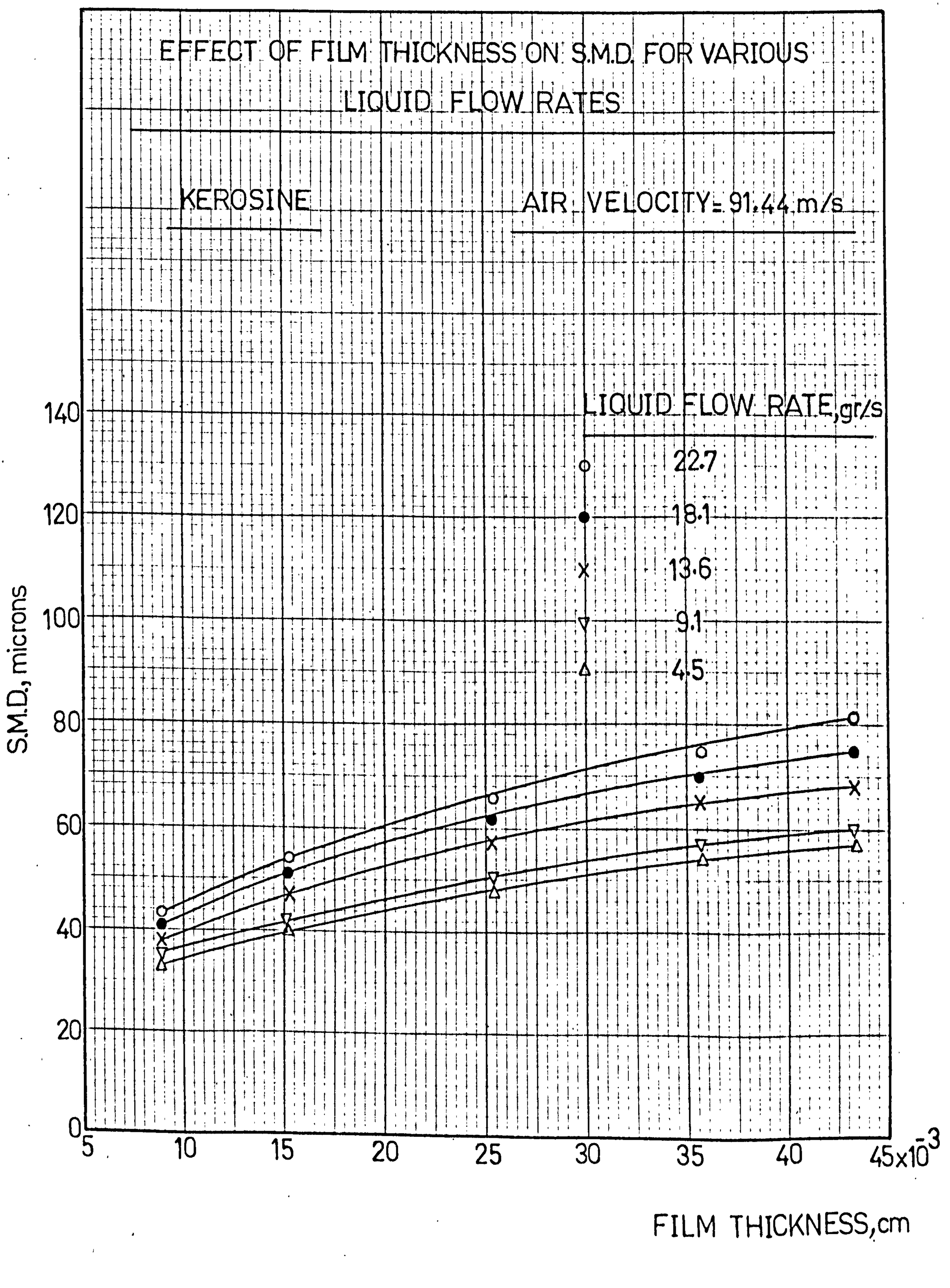
EFFECT OF FILM THICKNESS ON S.M.D. FOR VARIOUS LIQUID FLOW RATES
KEROSINE
AIR VELOCITY= 91.44 m/s
LIQUID FLOW RATE, gr/s
22.7
18.1
13.6
9.1
4.5
S.M.D., microns
140
120
100
80
60
40
20
0
5
10
15
20
25
30
35
40
45x10⁻³
FILM THICKNESS, cm

FIG 58

EFFECT OF FILM THICKNESS ON S.M.D. FOR VARIOUS AIR TO LIQUID RATIOS

KEROSINE AIR VELOCITY= 91.44 m/s

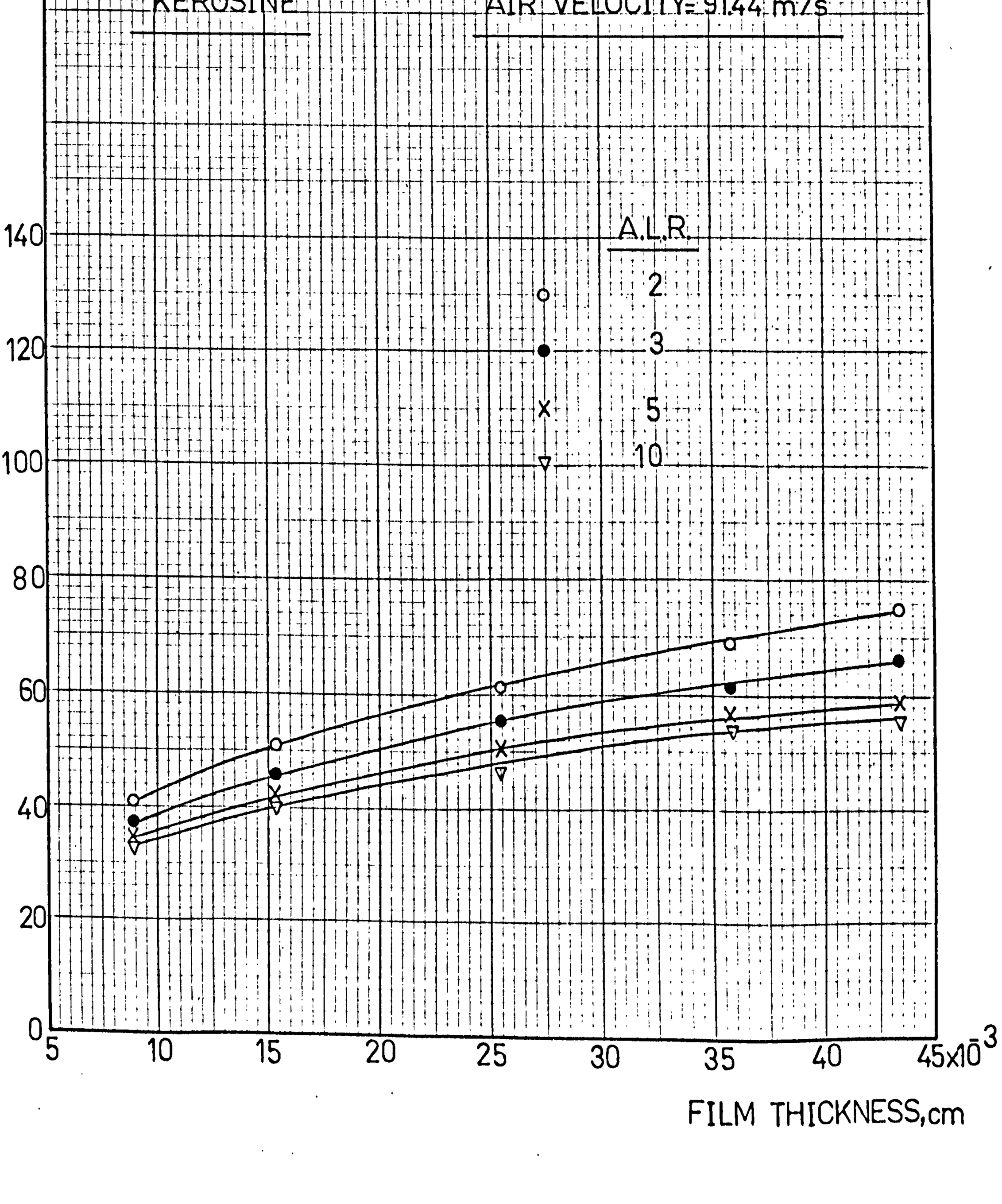

FIG. 59

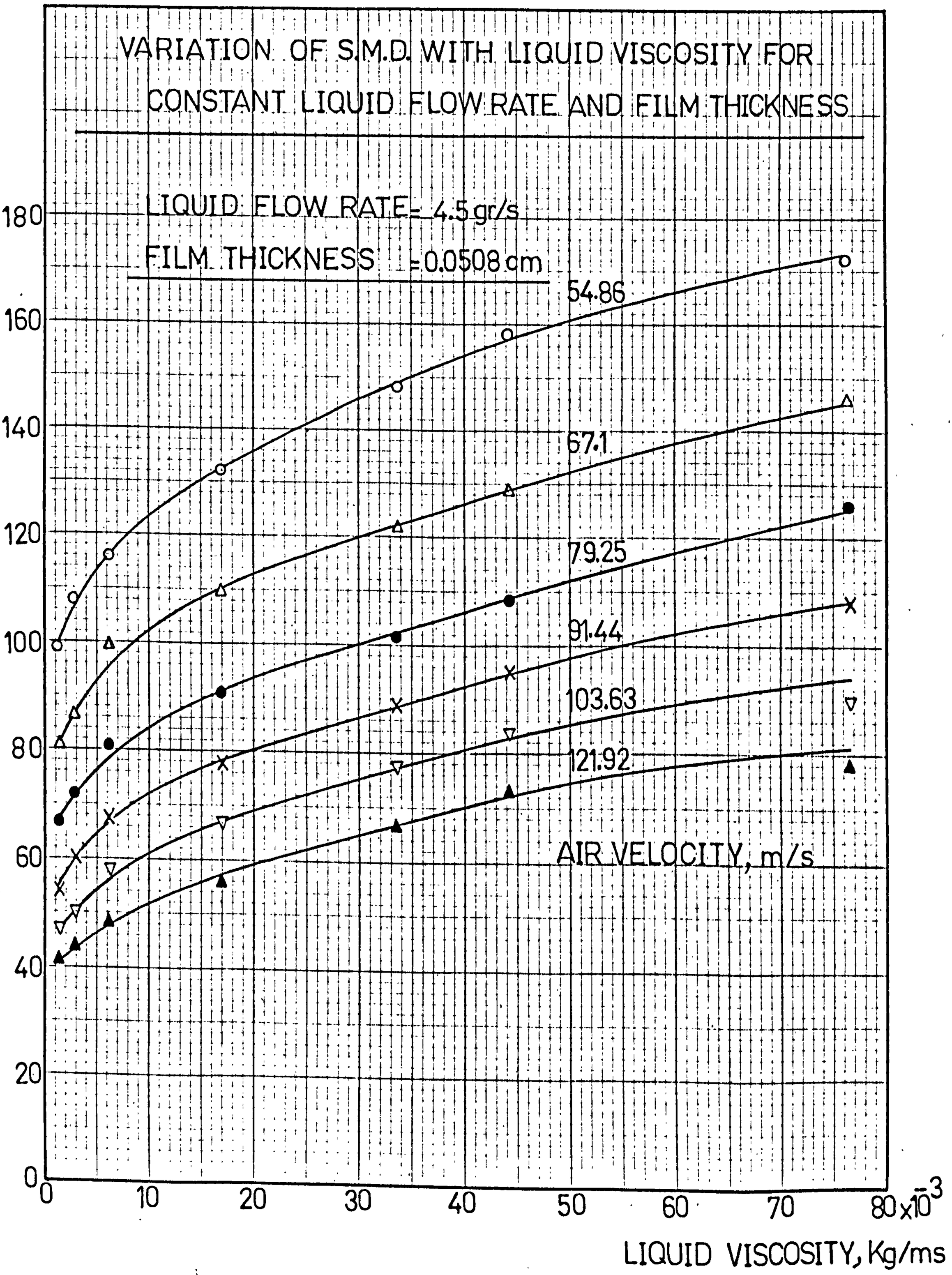
VARIATION OF S.M.D. WITH LIQUID VISCOSITY FOR CONSTANT LIQUID FLOW RATE AND FILM THICKNESS
LIQUID FLOW RATE= 4.5 gr/s
FILM THICKNESS =0.0508 cm
54.86
67.1
79.25
91.44
103.63
121.92
AIR VELOCITY, m/s
S.M.D., microns
LIQUID VISCOSITY, Kg/ms
0
20
40
60
80
100
120
140
160
180
0
10
20
30
40
50
60
70
80 x10^-3

FIG.60

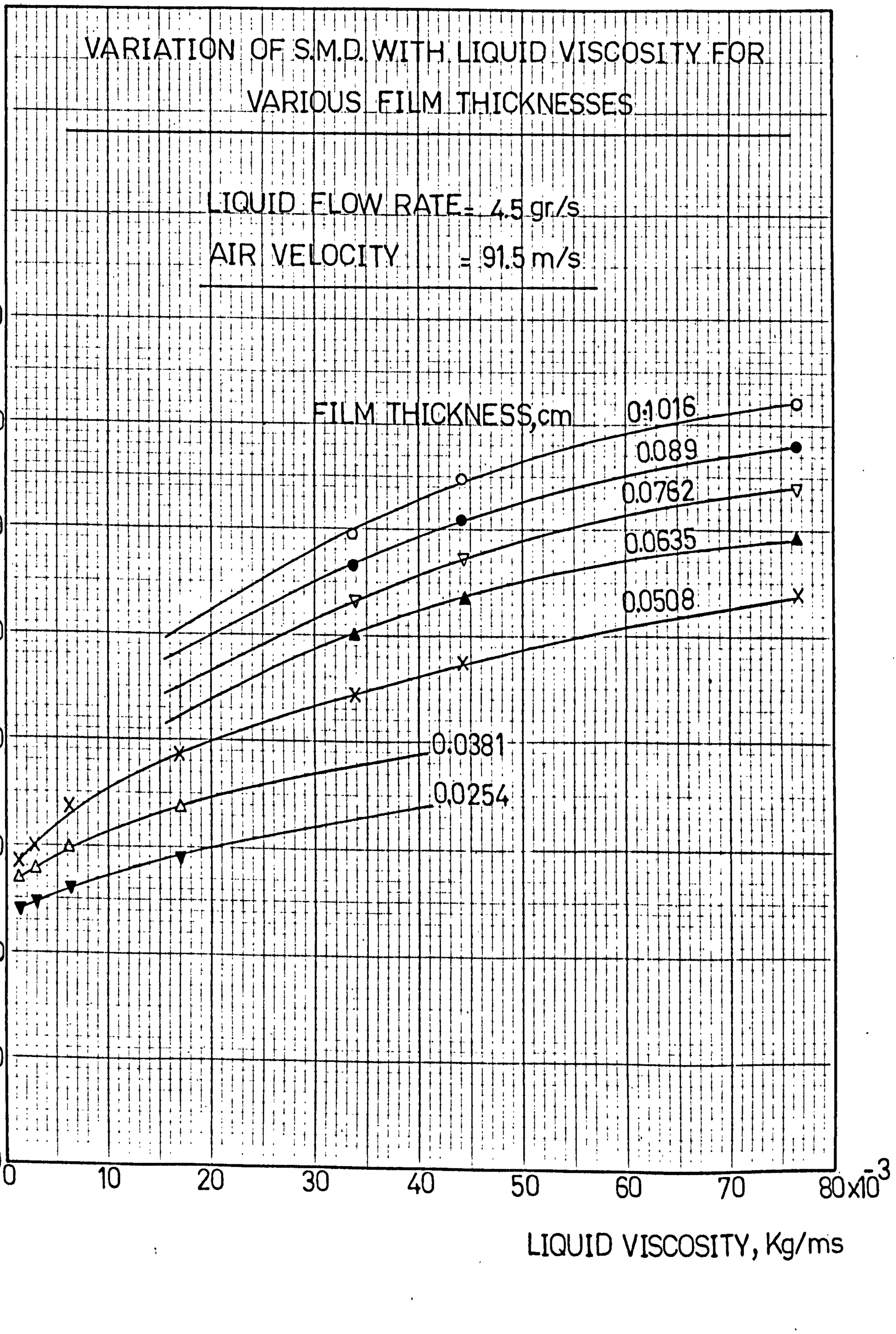
VARIATION OF S.M.D. WITH LIQUID VISCOSITY FOR VARIOUS FILM THICKNESSES
LIQUID FLOW RATE = 4.5 gr/s
AIR VELOCITY = 91.5 m/s
FILM THICKNESS, cm
0.1016
0.089
0.0762
0.0635
0.0508
0.0381
0.0254
S.M.D, microns
160
140
120
100
80
60
40
20
0
0
10
20
30
40
50
60
70
80 x10⁻³
LIQUID VISCOSITY, Kg/ms

FIG.61

EFFECT OF AIR TO LIQUID RATIO ON S.M.D. FOR HIGH VISCOSITY LIQUIDS

LIQUID FLOW RATE = 4.5 gr/s

FILM THICKNESS = 0.0508 cm

VISCOSITY, Kg/ms

- x — 76.54×10^{-3}
- ● — 44.10×10^{-3}
- △ — 17.01×10^{-3}
- ○ — 2.87×10^{-3}

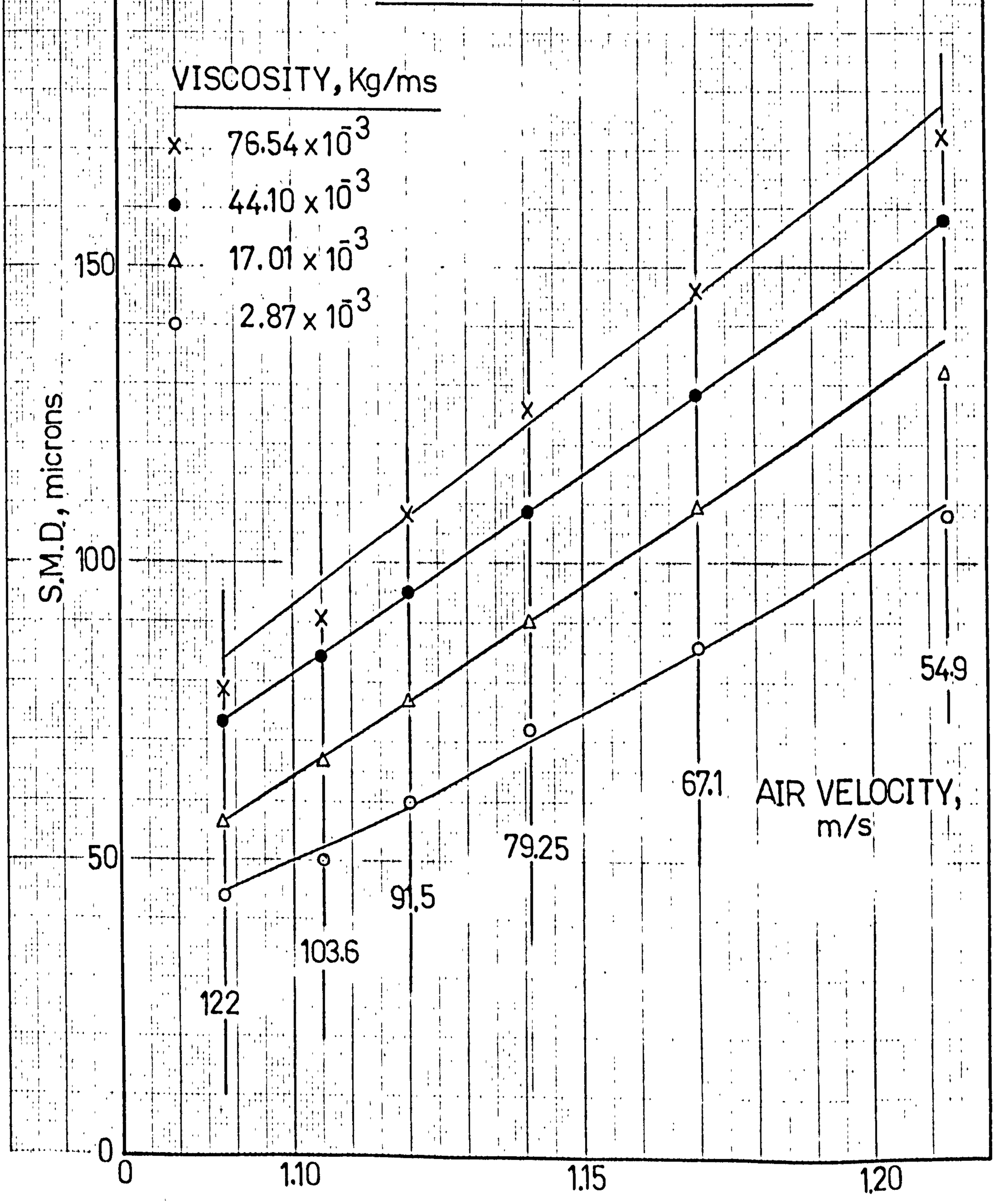

FIG.62

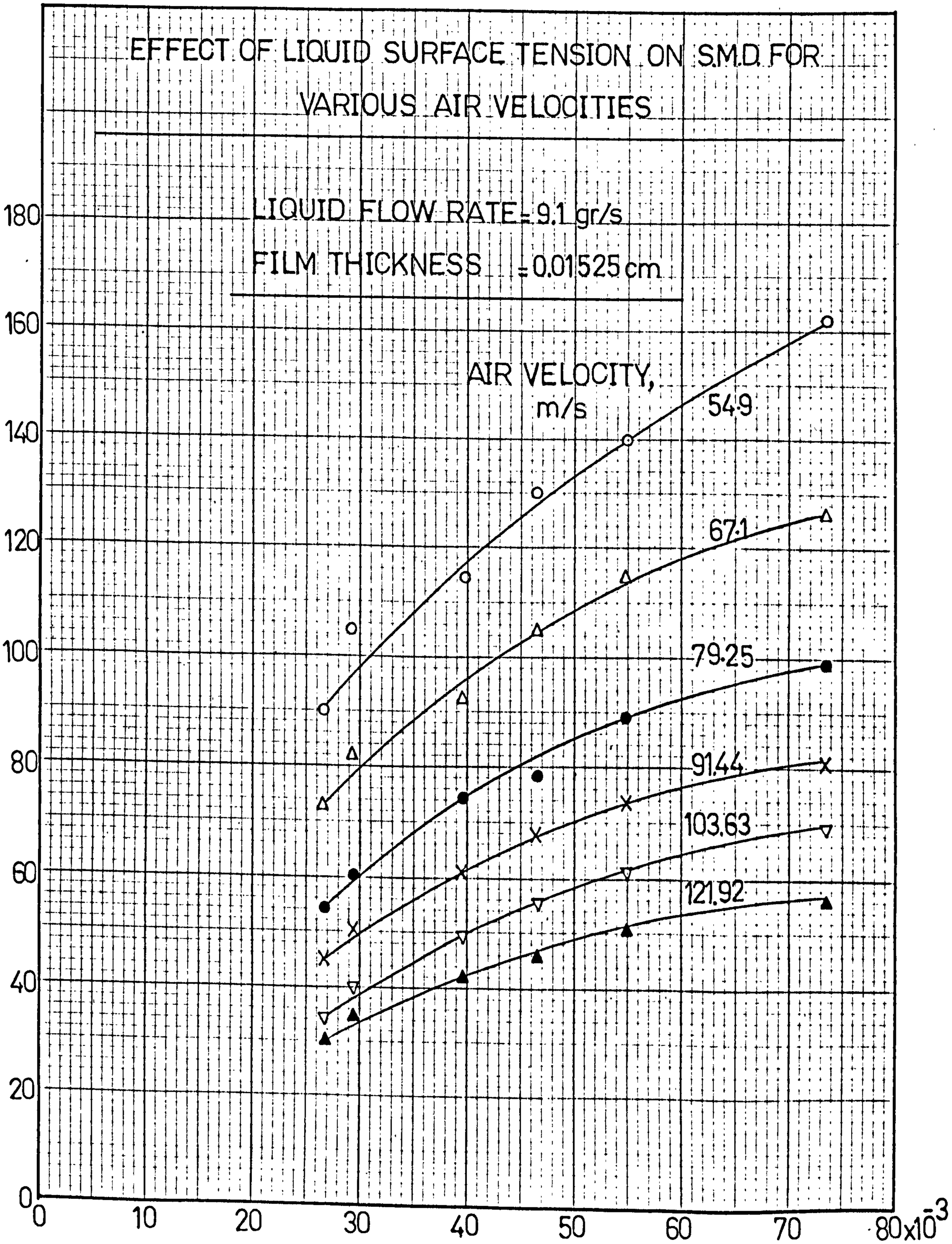
EFFECT OF LIQUID SURFACE TENSION ON S.M.D. FOR VARIOUS AIR VELOCITIES
LIQUID FLOW RATE = 9.1 gr/s
FILM THICKNESS = 0.01525 cm
AIR VELOCITY, m/s
54.9
67.1
79.25
91.44
103.63
121.92
S.M.D., microns
0
20
40
60
80
100
120
140
160
180
0
10
20
30
40
50
60
70
80x10⁻³
SURFACE TENSION, N/m

FIG.63

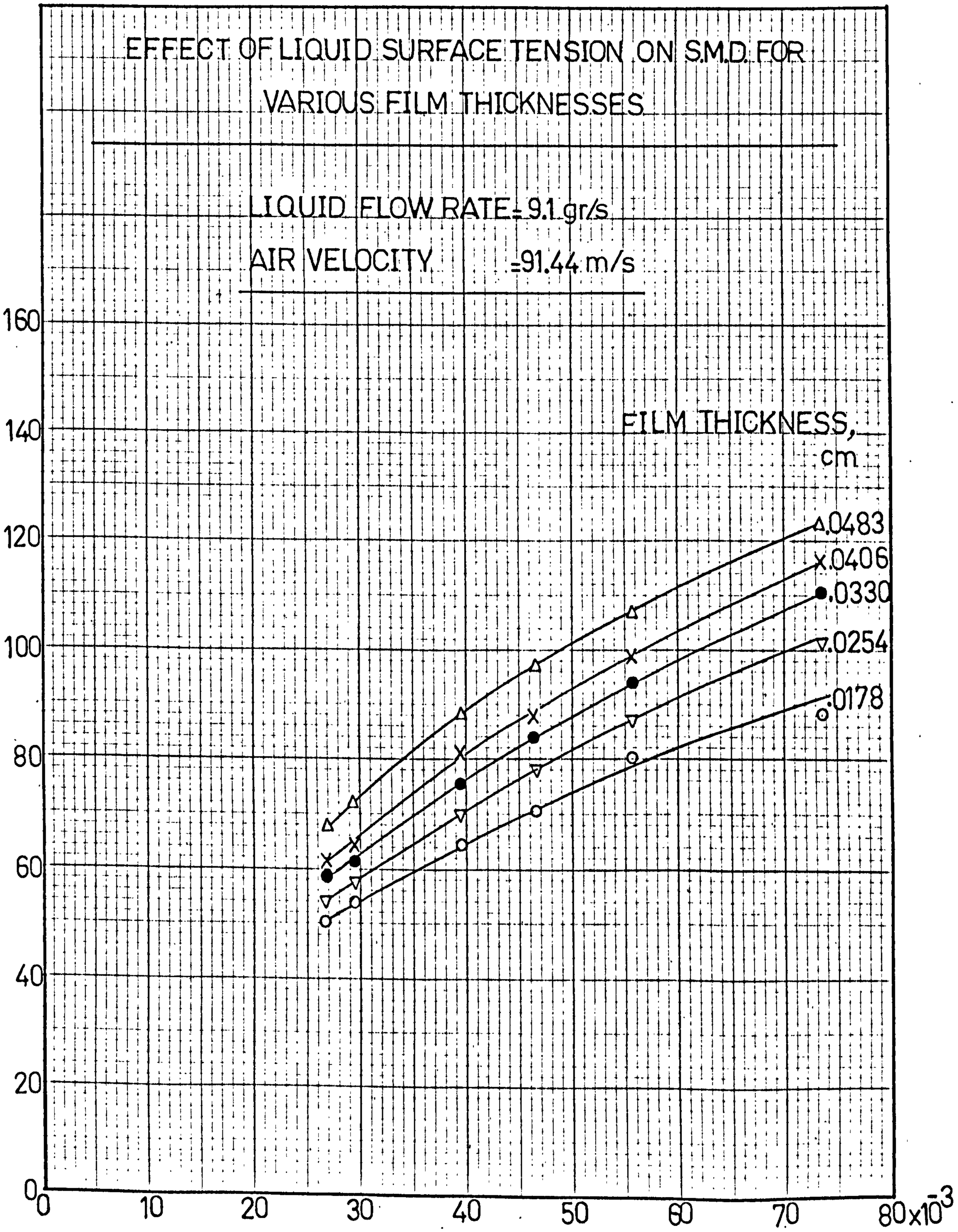
EFFECT OF LIQUID SURFACE TENSION ON S.M.D. FOR VARIOUS FILM THICKNESSES
LIQUID FLOW RATE = 9.1 gr/s
AIR VELOCITY = 91.44 m/s
S.M.D., microns
SURFACE TENSION, N/m
FILM THICKNESS, cm
.0483
.0406
.0330
.0254
.0178
0
20
40
60
80
100
120
140
160
10
20
30
40
50
60
70
80x10⁻³

FIG.64

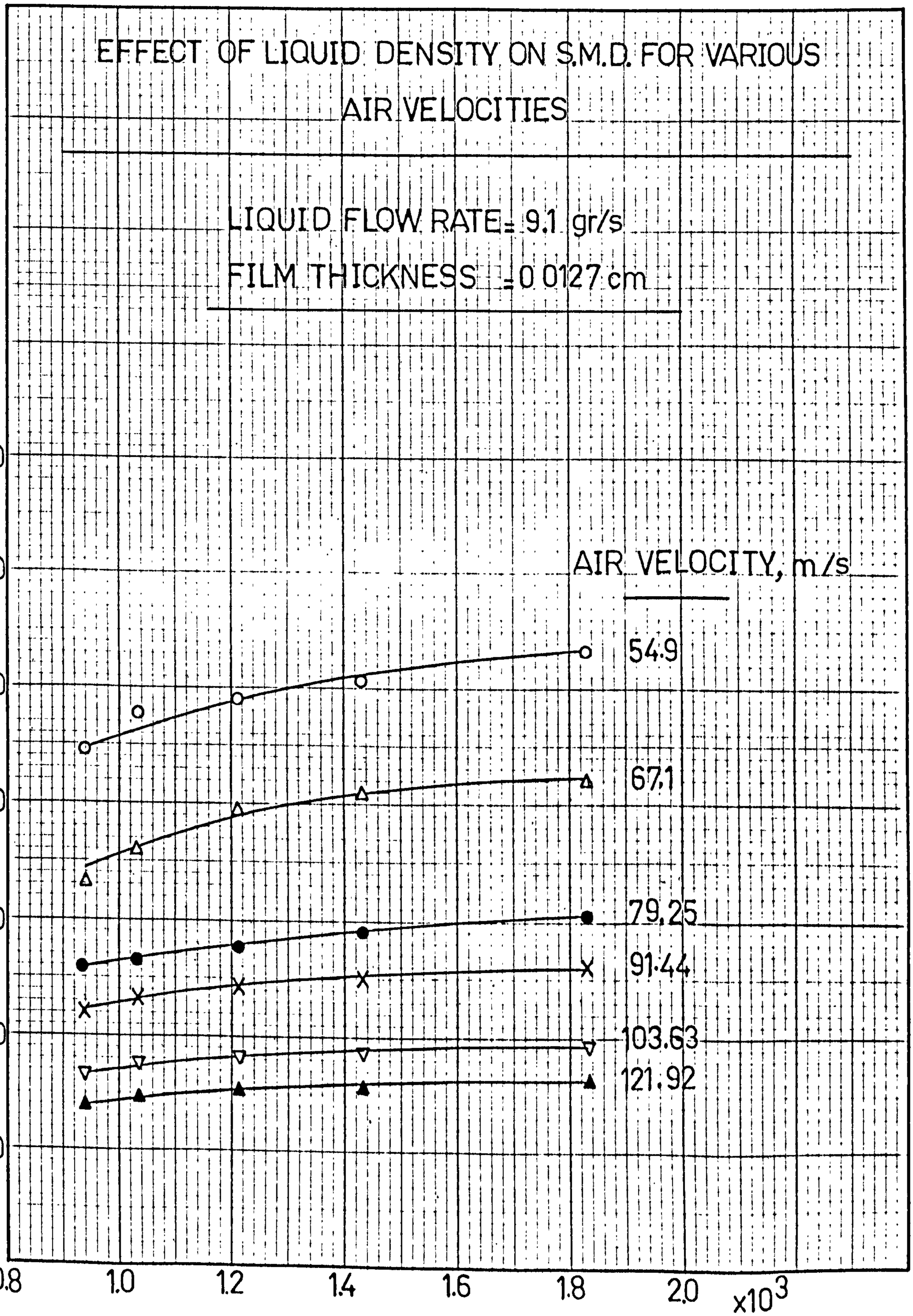
EFFECT OF LIQUID DENSITY ON S.M.D. FOR VARIOUS AIR VELOCITIES
LIQUID FLOW RATE = 9.1 gr/s
FILM THICKNESS = 0.0127 cm
AIR VELOCITY, m/s
54.9
67.1
79.25
91.44
103.63
121.92
S.M.D., microns
0
20
40
60
80
100
120
140
0.8
1.0
1.2
1.4
1.6
1.8
2.0
x10^3
LIQUID DENSITY Kg/m^3

FIG.65

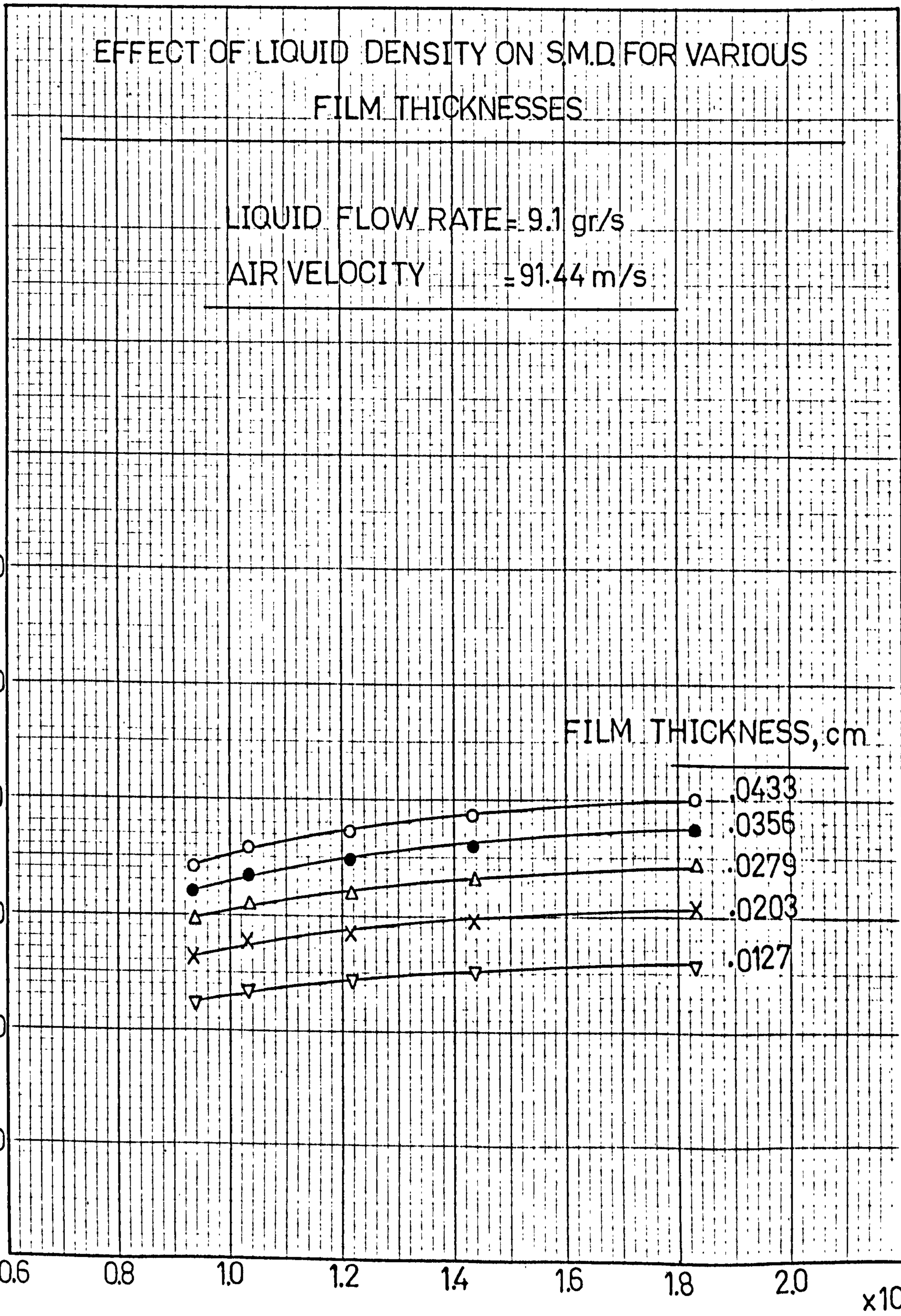
EFFECT OF LIQUID DENSITY ON S.M.D. FOR VARIOUS FILM THICKNESSES
LIQUID FLOW RATE = 9.1 gr/s
AIR VELOCITY = 91.44 m/s
S.M.D., microns
120
100
80
60
40
20
0
FILM THICKNESS, cm
.0433
.0356
.0279
.0203
.0127
0.6
0.8
1.0
1.2
1.4
1.6
1.8
2.0
x10^3
LIQUID DENSITY, Kg/m^3

PRESSURE DROP $\Delta P/P = 3.5\%$

WATER _____
KEROSINE _ _ _ _

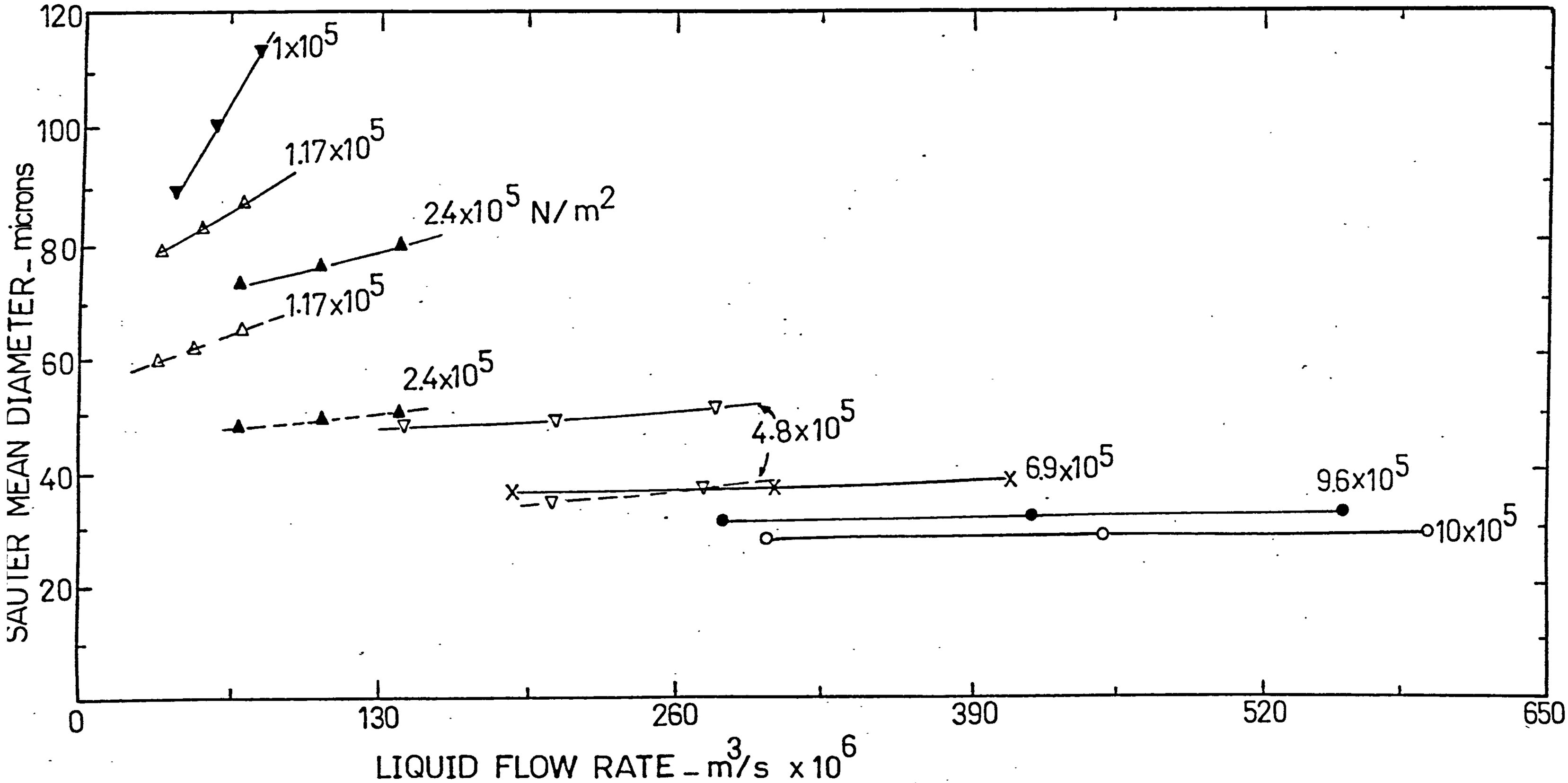

EFFECT OF AMBIENT PRESSURE ON S.M.D.

FIG.66

FIG.67

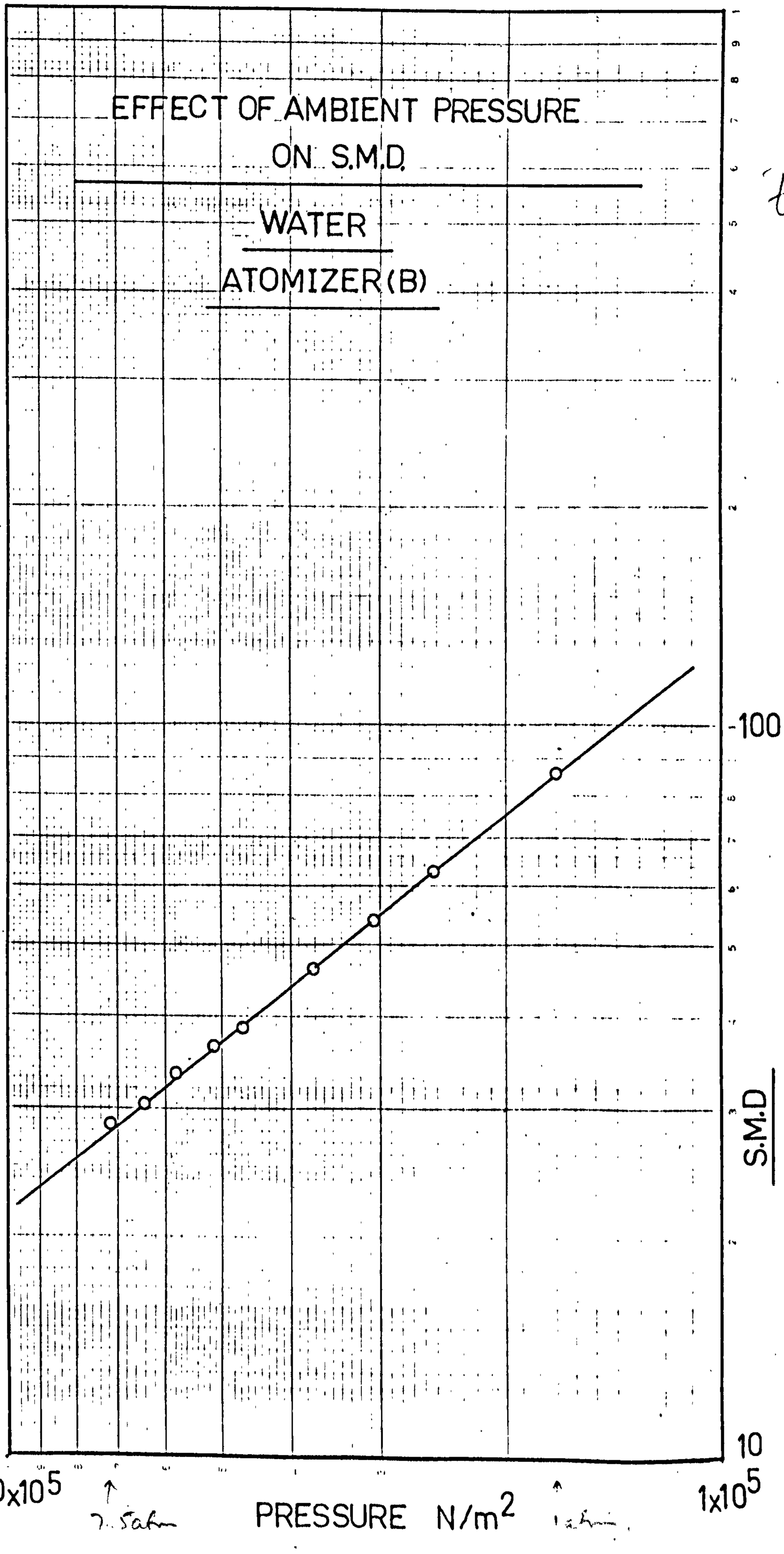
EFFECT OF AMBIENT PRESSURE
ON S.M.D.
WATER
ATOMIZER (B)
S.M.D / (1+W/W)^0.3
100
10
10x10^5
1x10^5
PRESSURE N/m^2

FIG. 68

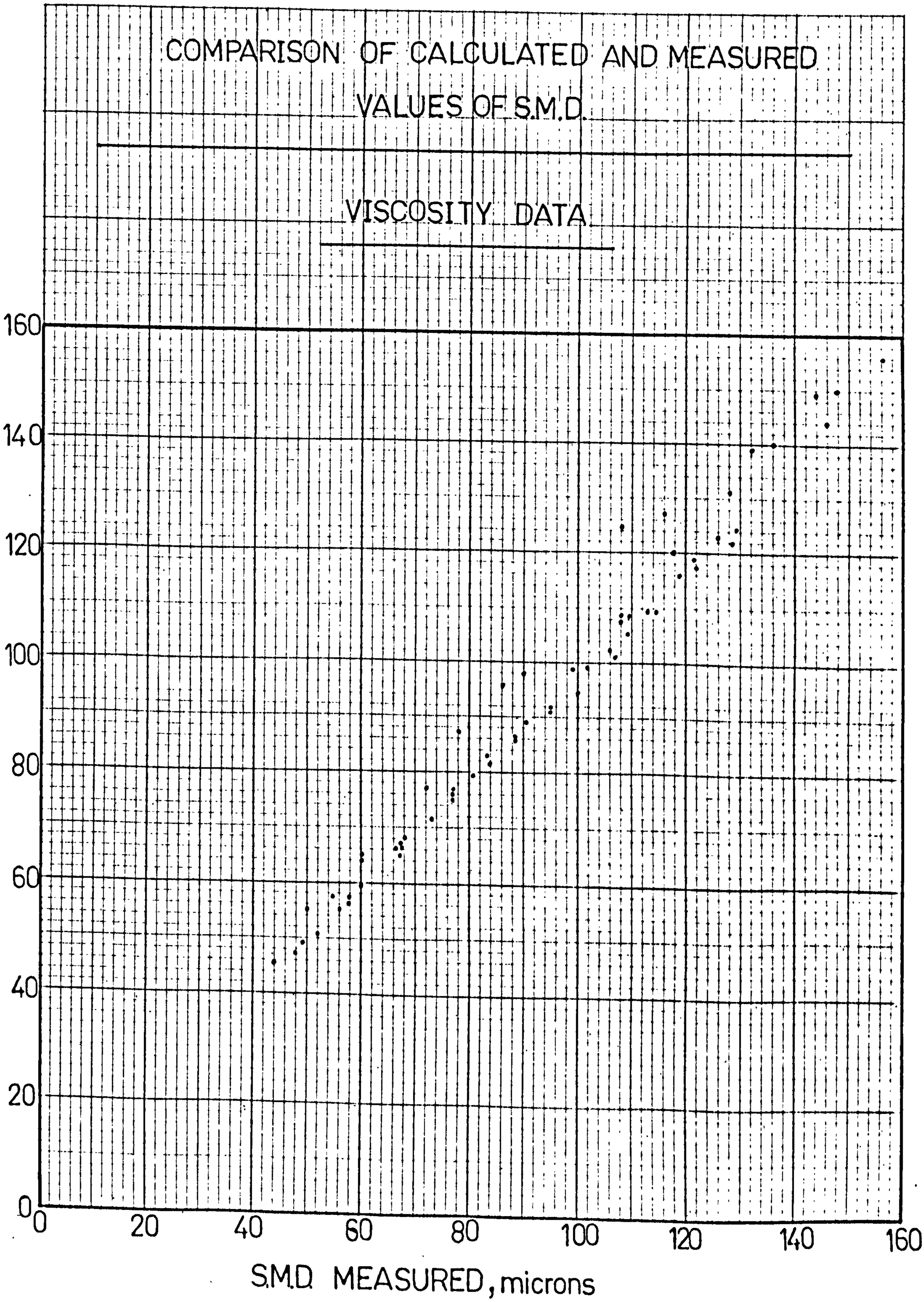
COMPARISON OF CALCULATED AND MEASURED VALUES OF S.M.D.
VISCOSITY DATA
S.M.D. CALCULATED, microns
S.M.D. MEASURED, microns
0
20
40
60
80
100
120
140
160

FIG. 69

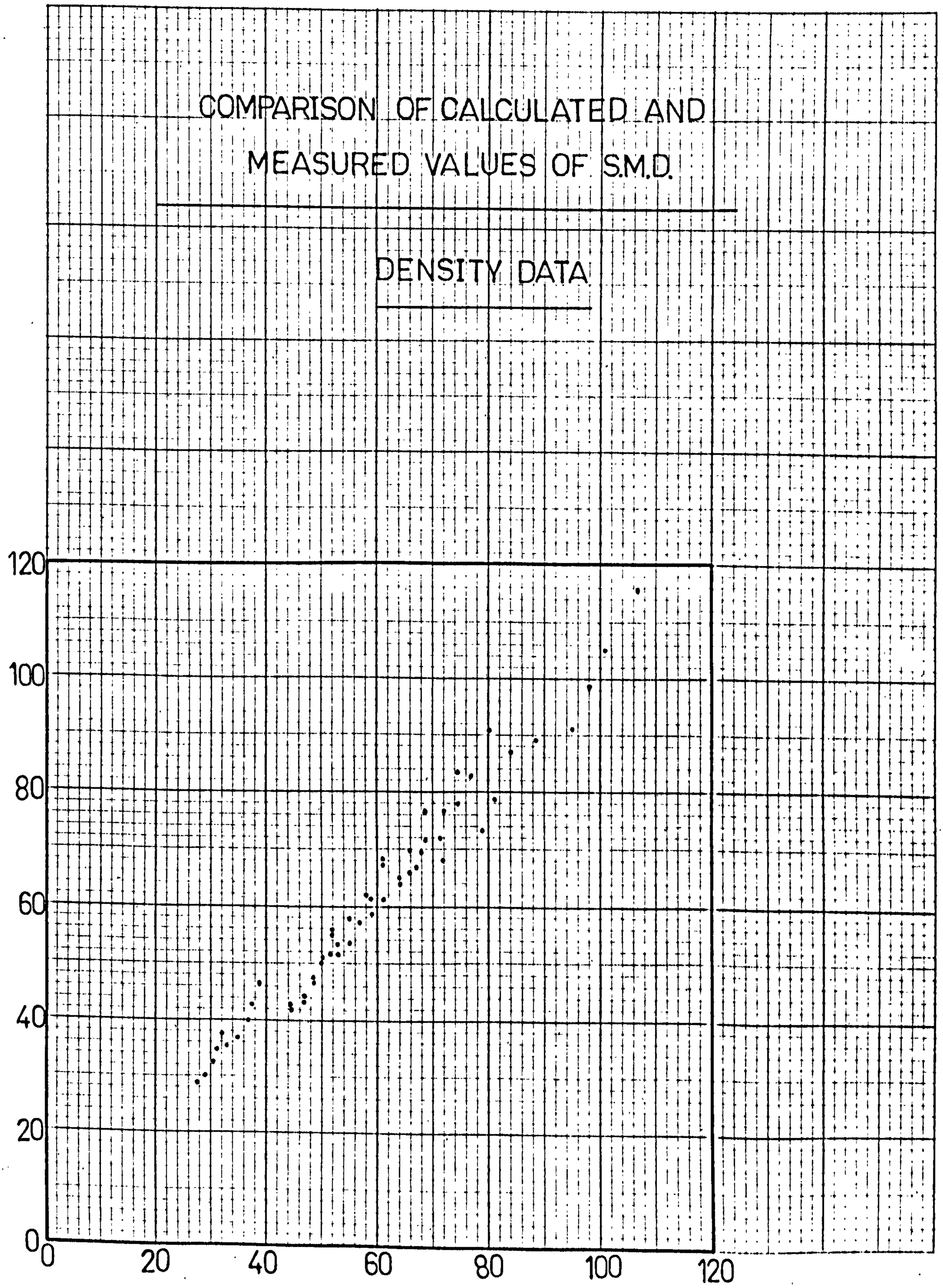
COMPARISON OF CALCULATED AND
MEASURED VALUES OF S.M.D.
DENSITY DATA
S.M.D. CALCULATED, microns
S.M.D. MEASURED, microns
0
20
40
60
80
100
120

FIG.70

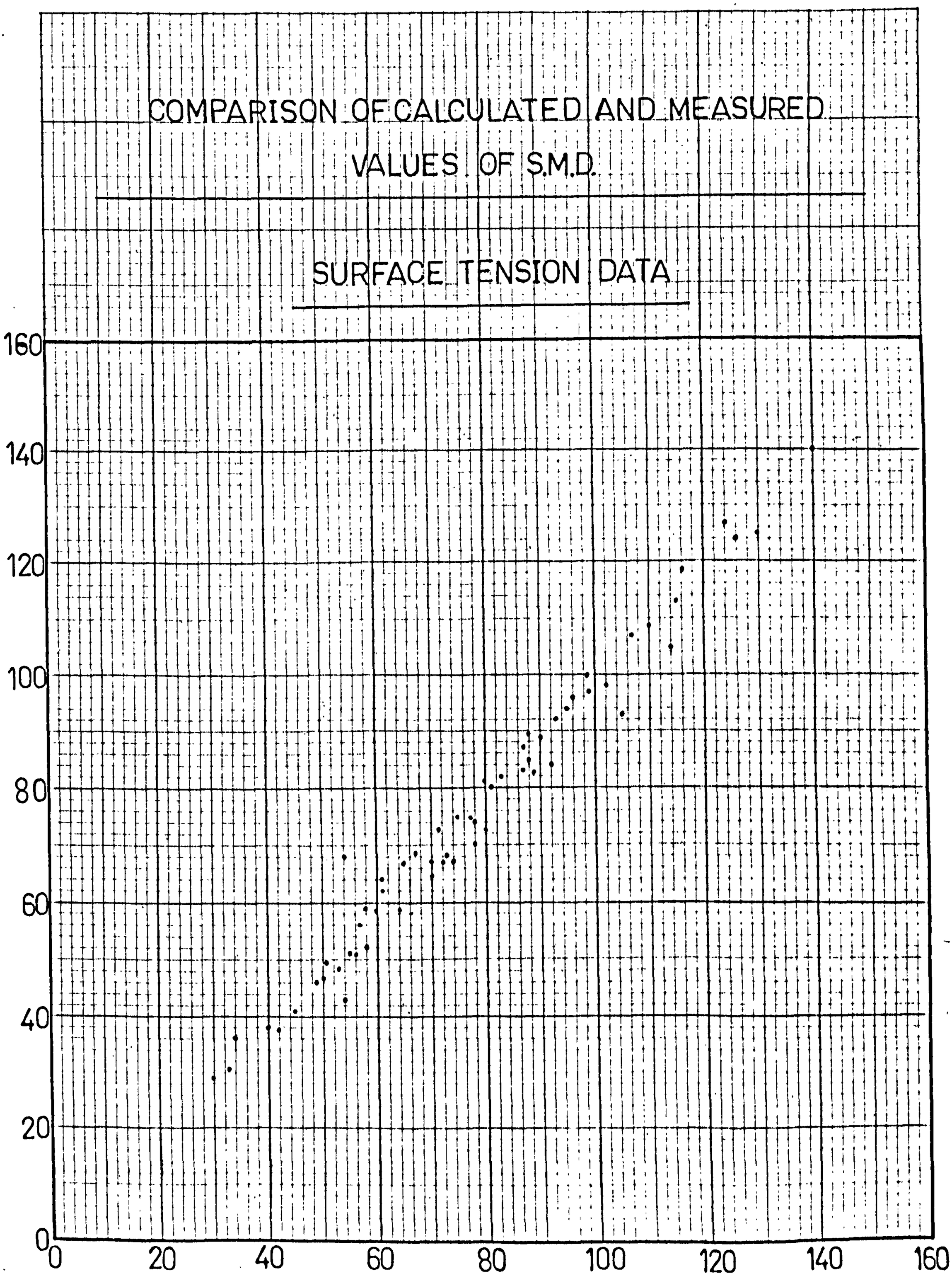
COMPARISON OF CALCULATED AND MEASURED
VALUES OF S.M.D.
SURFACE TENSION DATA
S.M.D. CALCULATED, microns
S.M.D. MEASURED, microns
0
20
40
60
80
100
120
140
160

FIG.71

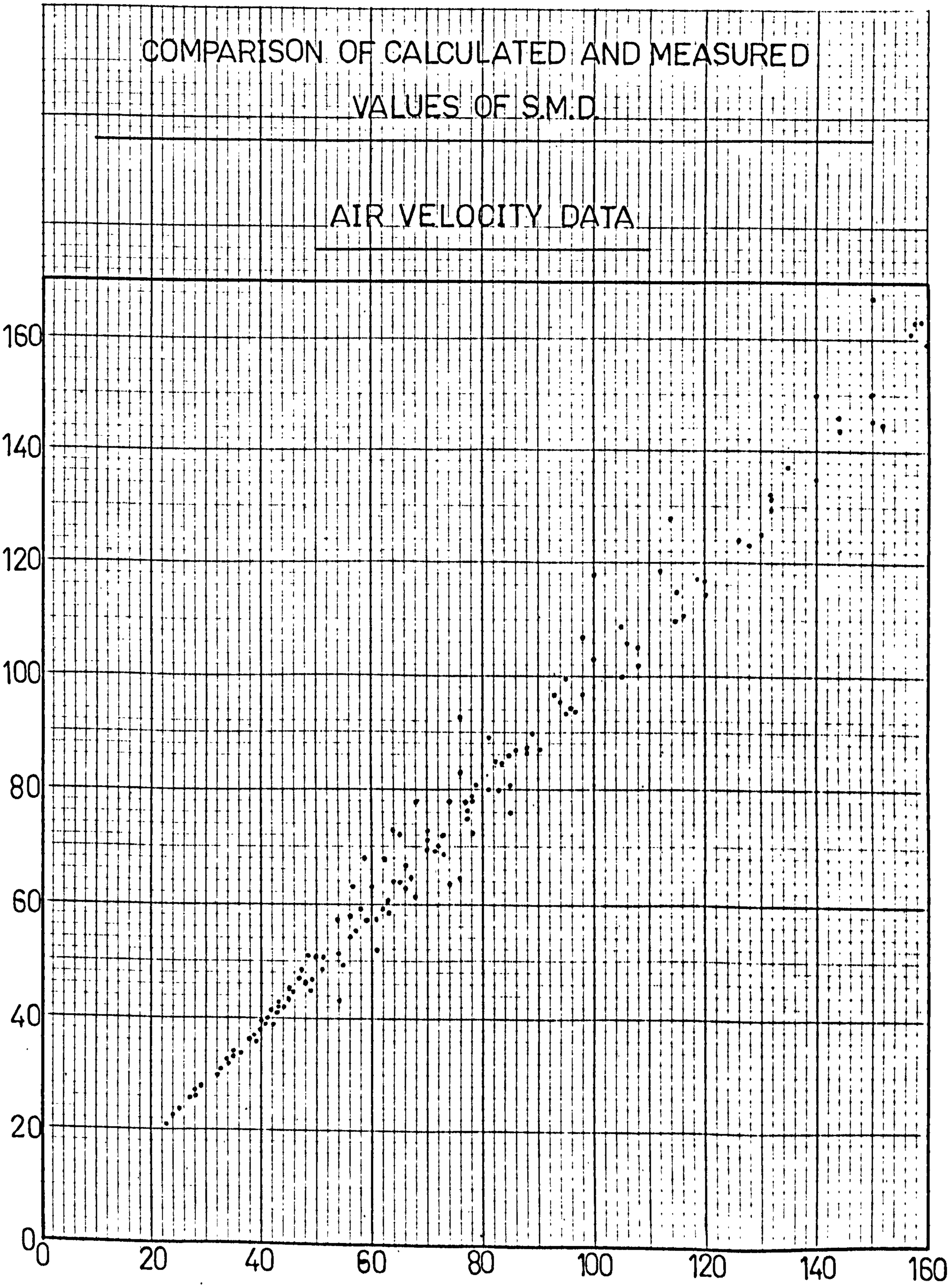
COMPARISON OF CALCULATED AND MEASURED VALUES OF S.M.D.
AIR VELOCITY DATA
S.M.D. CALCULATED, microns
S.M.D. MEASURED, microns
0
20
40
60
80
100
120
140
160

FIG.72

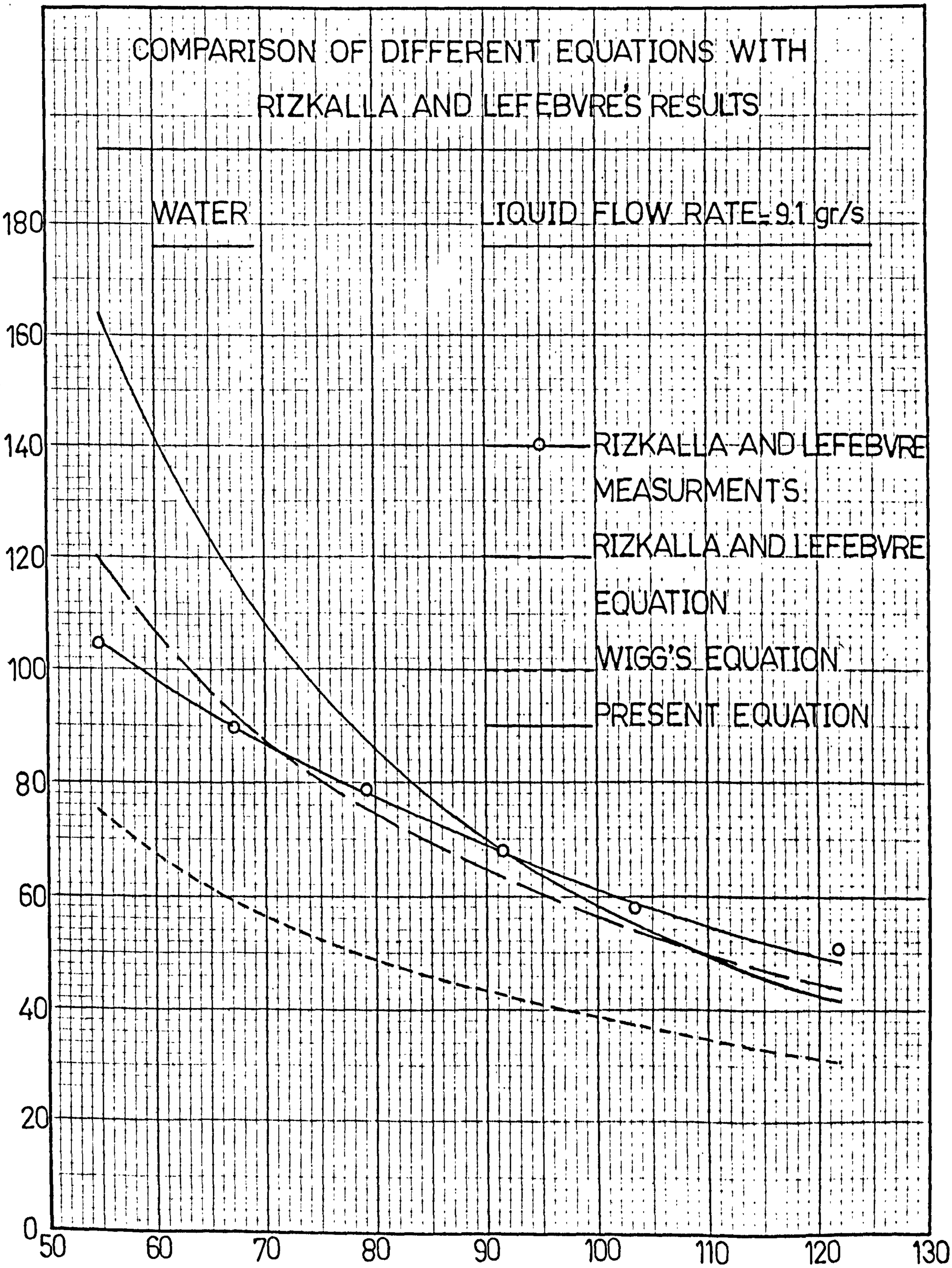
COMPARISON OF DIFFERENT EQUATIONS WITH
RIZKALLA AND LEFEBVRE'S RESULTS
WATER
LIQUID FLOW RATE= 9.1 gr/s
RIZKALLA AND LEFEBVRE
MEASURMENTS
RIZKALLA AND LEFEBVRE
EQUATION
WIGG'S EQUATION
PRESENT EQUATION
S.M.D., microns
AIR VELOCITY, m/s
180
160
140
120
100
80
60
40
20
0
50
60
70
80
90
100
110
120
130

FIG.73

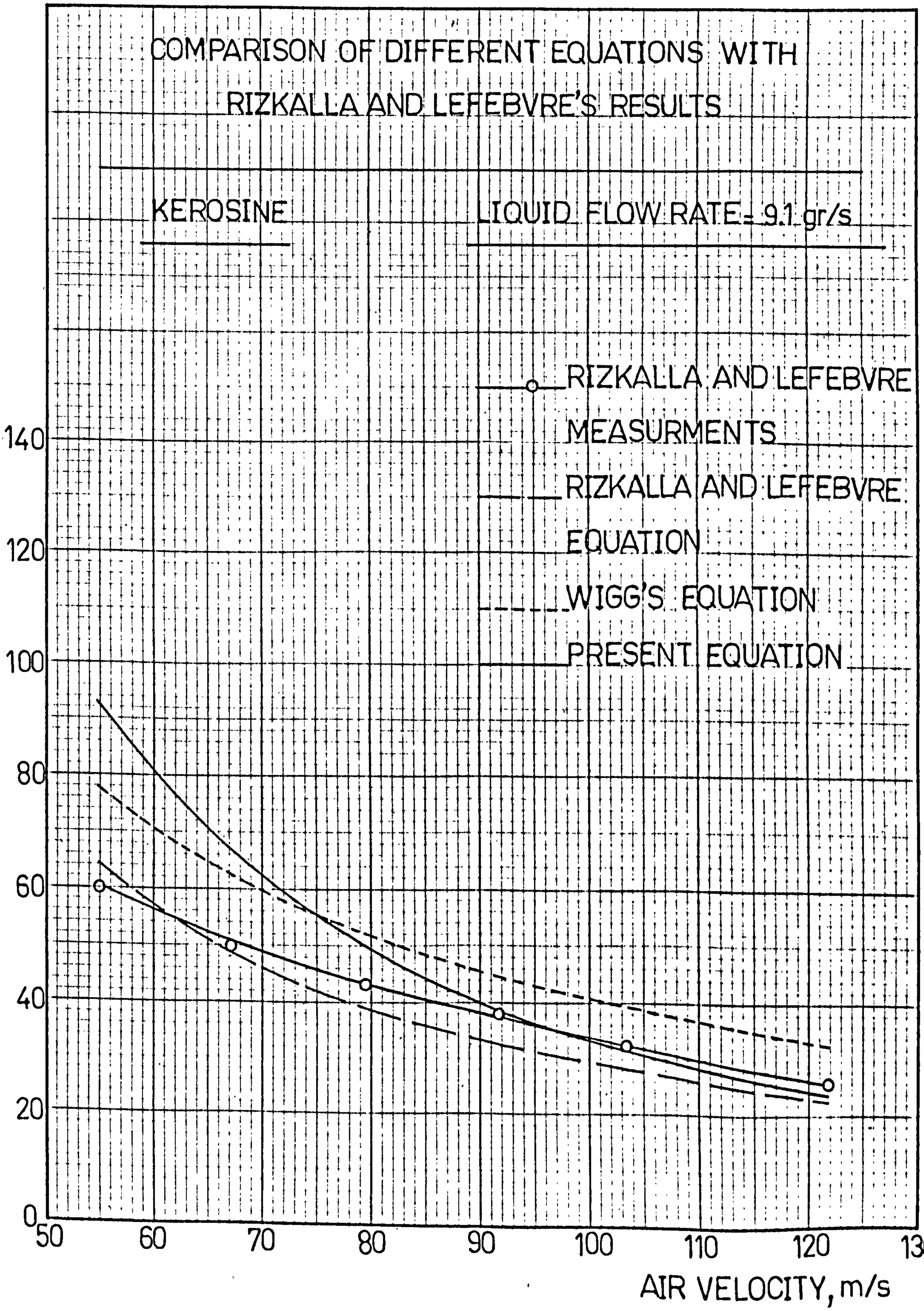
COMPARISON OF DIFFERENT EQUATIONS WITH RIZKALLA AND LEFEBVRE'S RESULTS
KEROSINE
LIQUID FLOW RATE = 9.1 gr/s
RIZKALLA AND LEFEBVRE MEASURMENTS
RIZKALLA AND LEFEBVRE EQUATION
WIGG'S EQUATION
PRESENT EQUATION
S.M.D., microns
0
20
40
60
80
100
120
140
50
60
70
80
90
100
110
120
130
AIR VELOCITY, m/s

FIG.74

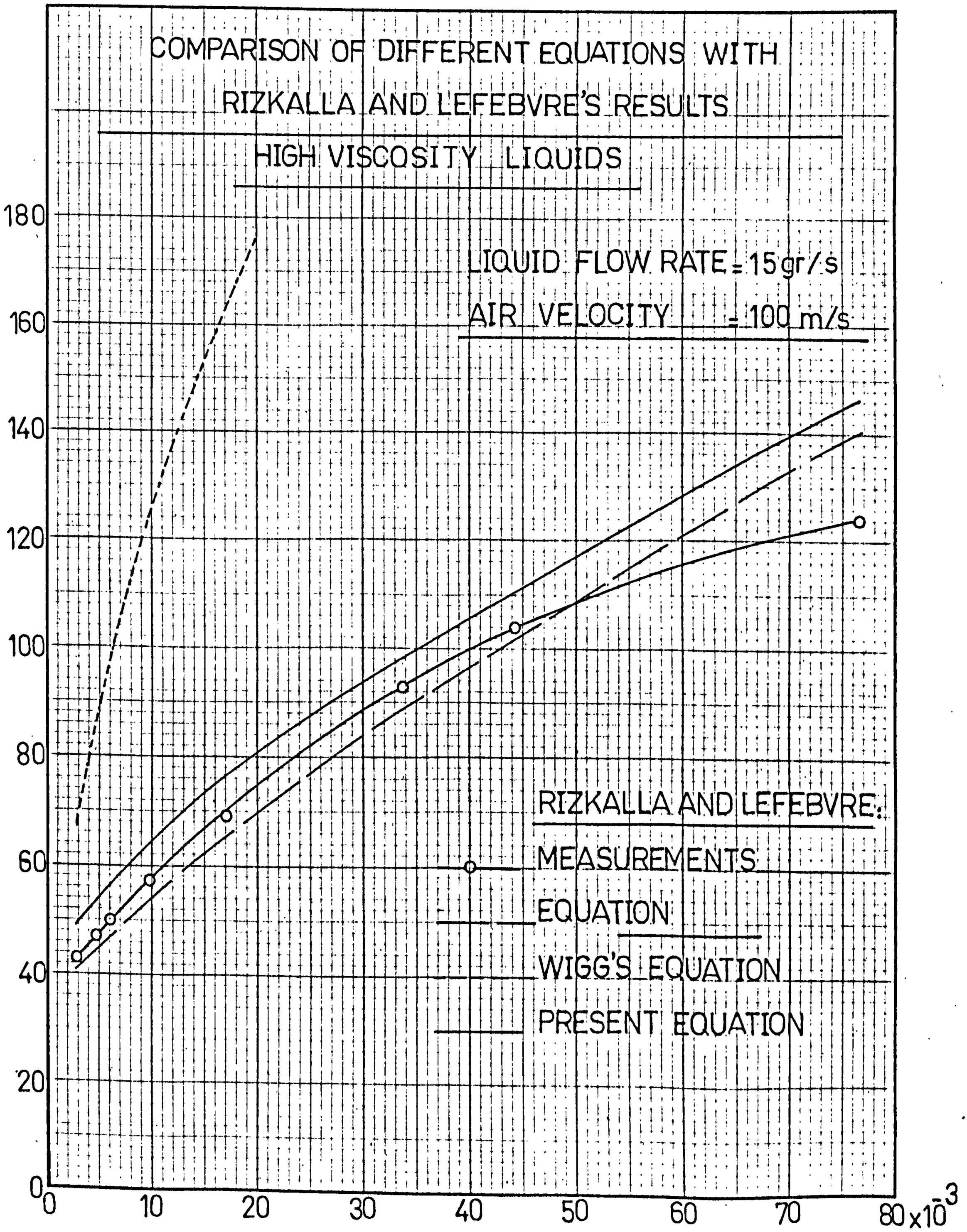
COMPARISON OF DIFFERENT EQUATIONS WITH RIZKALLA AND LEFEBVRE'S RESULTS
HIGH VISCOSITY LIQUIDS
LIQUID FLOW RATE = 15 gr/s
AIR VELOCITY = 100 m/s
S.M.D., microns
0
20
40
60
80
100
120
140
160
180
0
10
20
30
40
50
60
70
80 x 10⁻³
LIQUID VISCOSITY, Kg/ms
RIZKALLA AND LEFEBVRE:
MEASUREMENTS
EQUATION
WIGG'S EQUATION
PRESENT EQUATION

FIG. 75

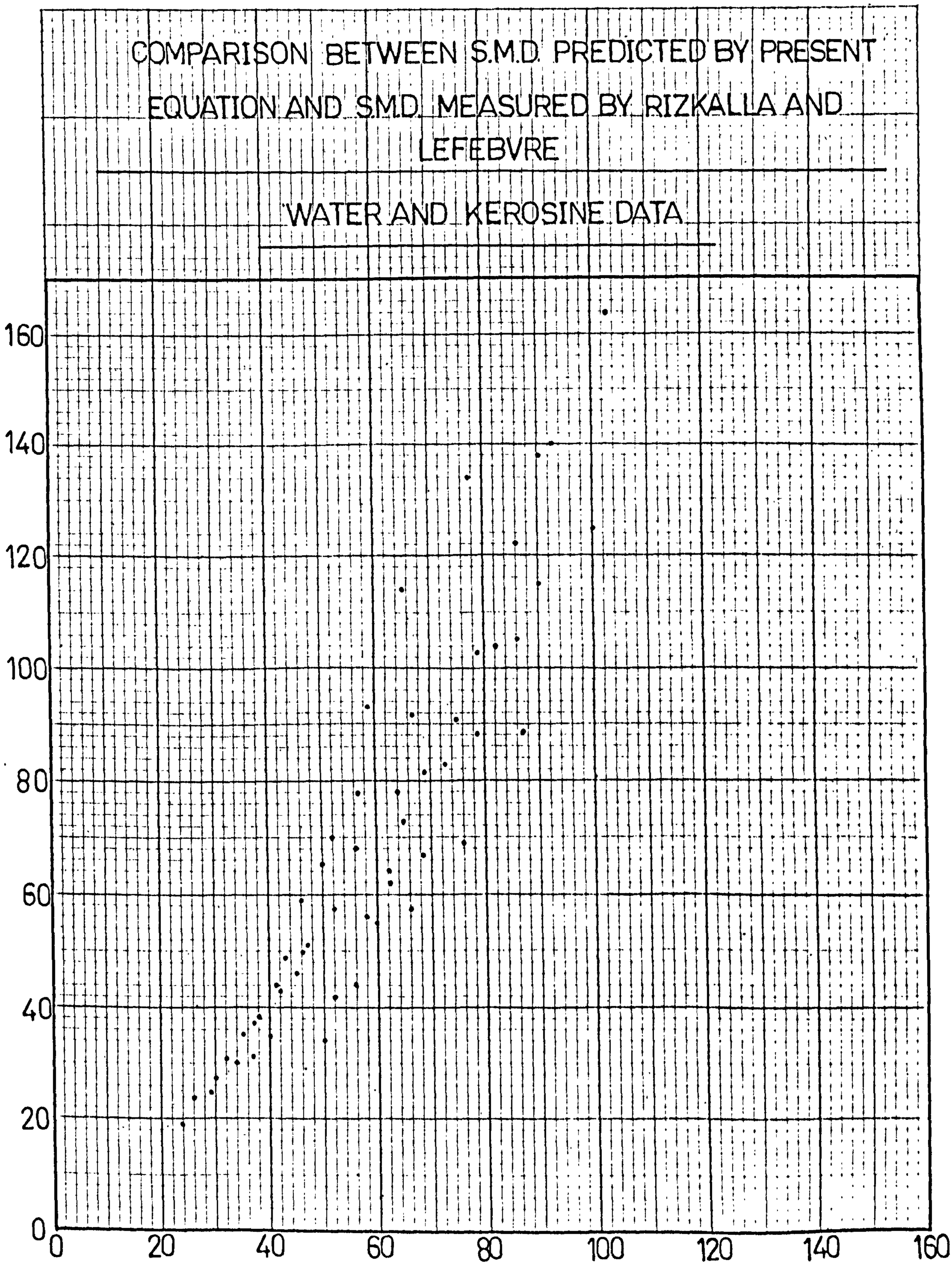
COMPARISON BETWEEN S.M.D. PREDICTED BY PRESENT EQUATION AND S.M.D. MEASURED BY RIZKALLA AND LEFEBVRE
WATER AND KEROSINE DATA
S.M.D. PREDICTED BY PRESENT EQUATION, microns
0
20
40
60
80
100
120
140
160
S.M.D. MEASURED BY RIZKALLA AND LEFEBVRE, microns

FIG.76

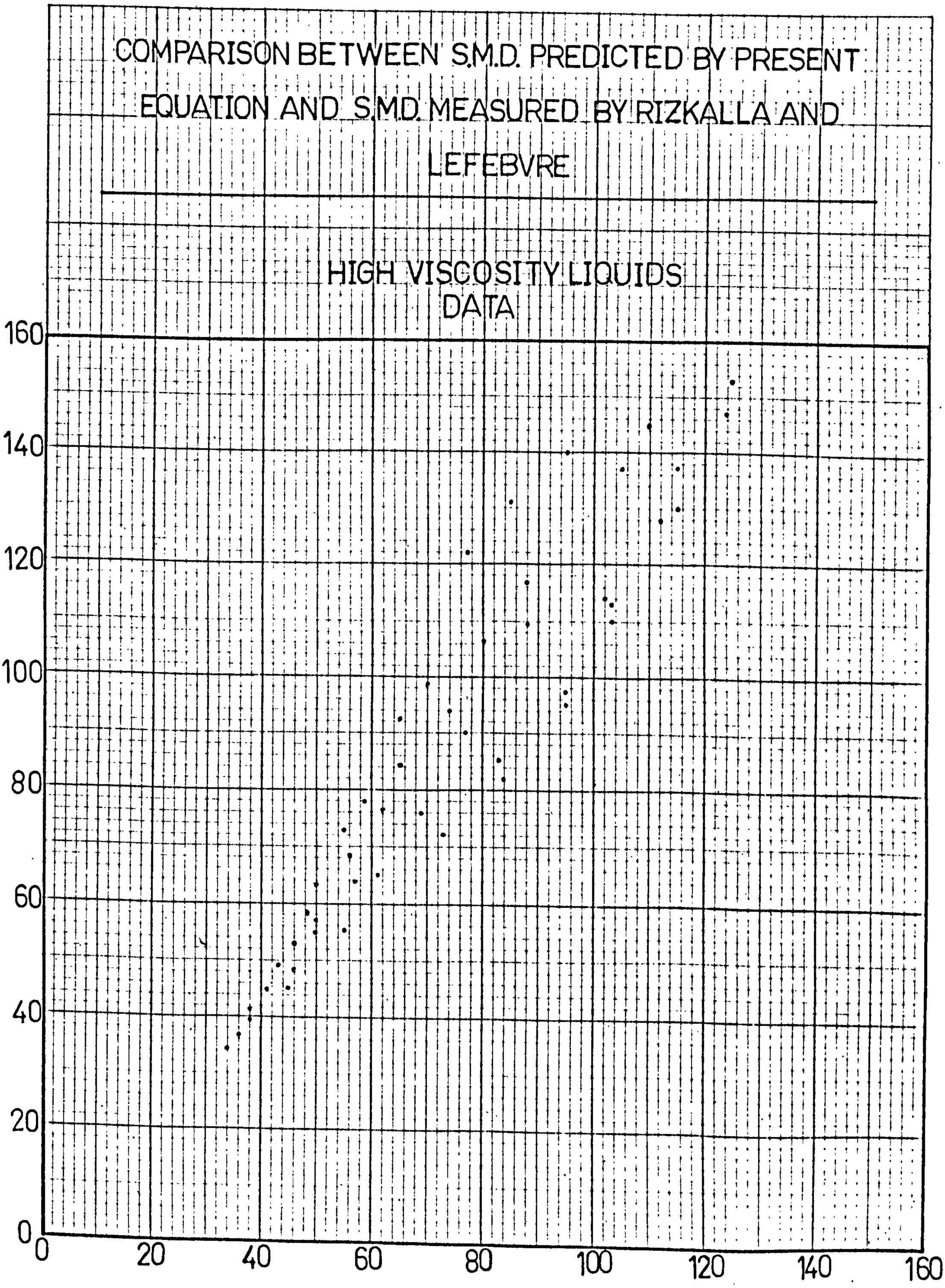
COMPARISON BETWEEN S.M.D. PREDICTED BY PRESENT EQUATION AND S.M.D. MEASURED BY RIZKALLA AND LEFEBVRE
HIGH VISCOSITY LIQUIDS DATA
S.M.D. PREDICTED BY PRESENT EQUATION, microns
S.M.D. MEASURED BY RIZKALLA AND LEFEBVRE, microns
0
20
40
60
80
100
120
140
160

LIST OF PHOTOGRAPHS

Magnification = 10.5

FIG.77

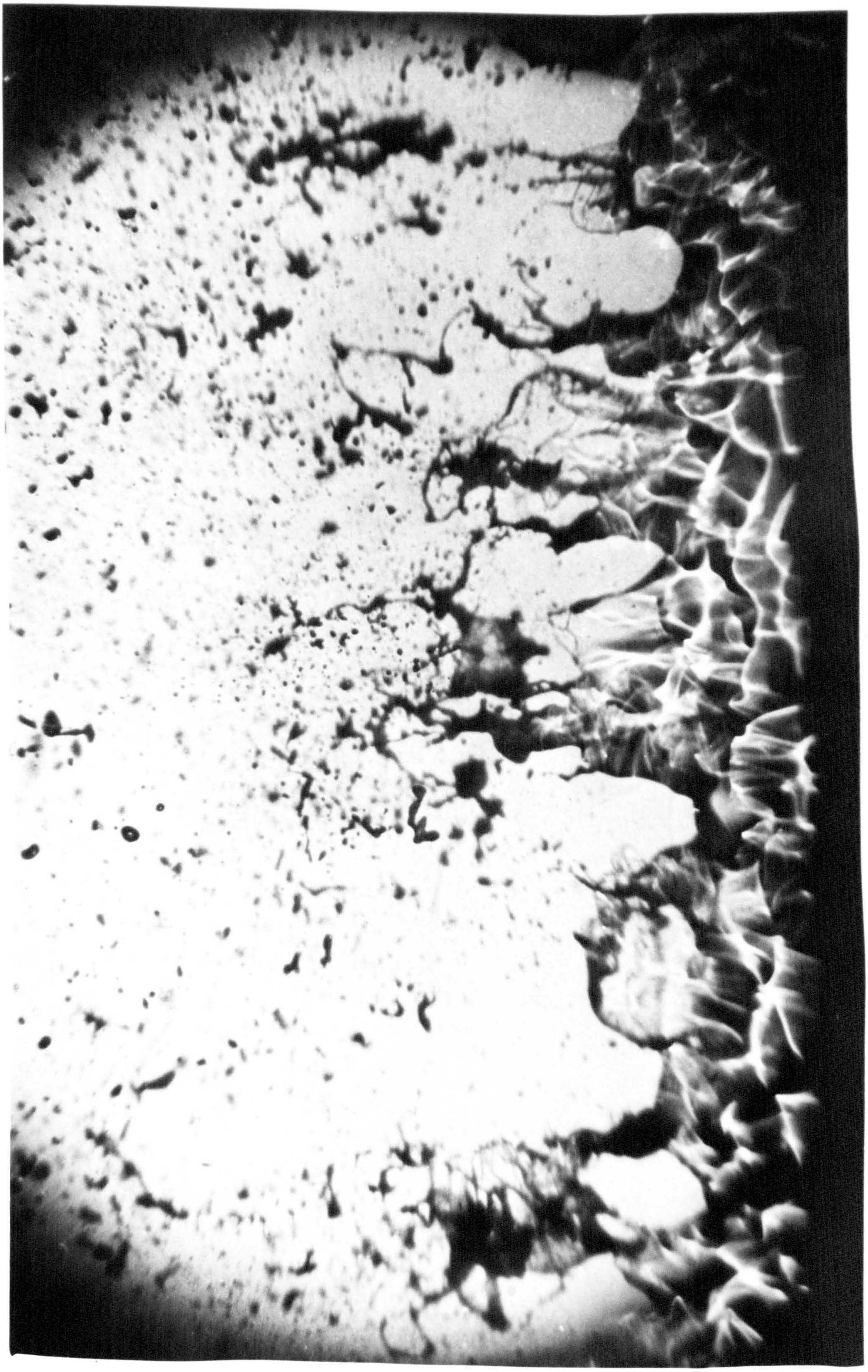

FIG. 78

FIG.79

WATER AIR VELOCITY = 54.9 m/s , LIQUID FLOW RATE = 9 gr/s

FIG.80

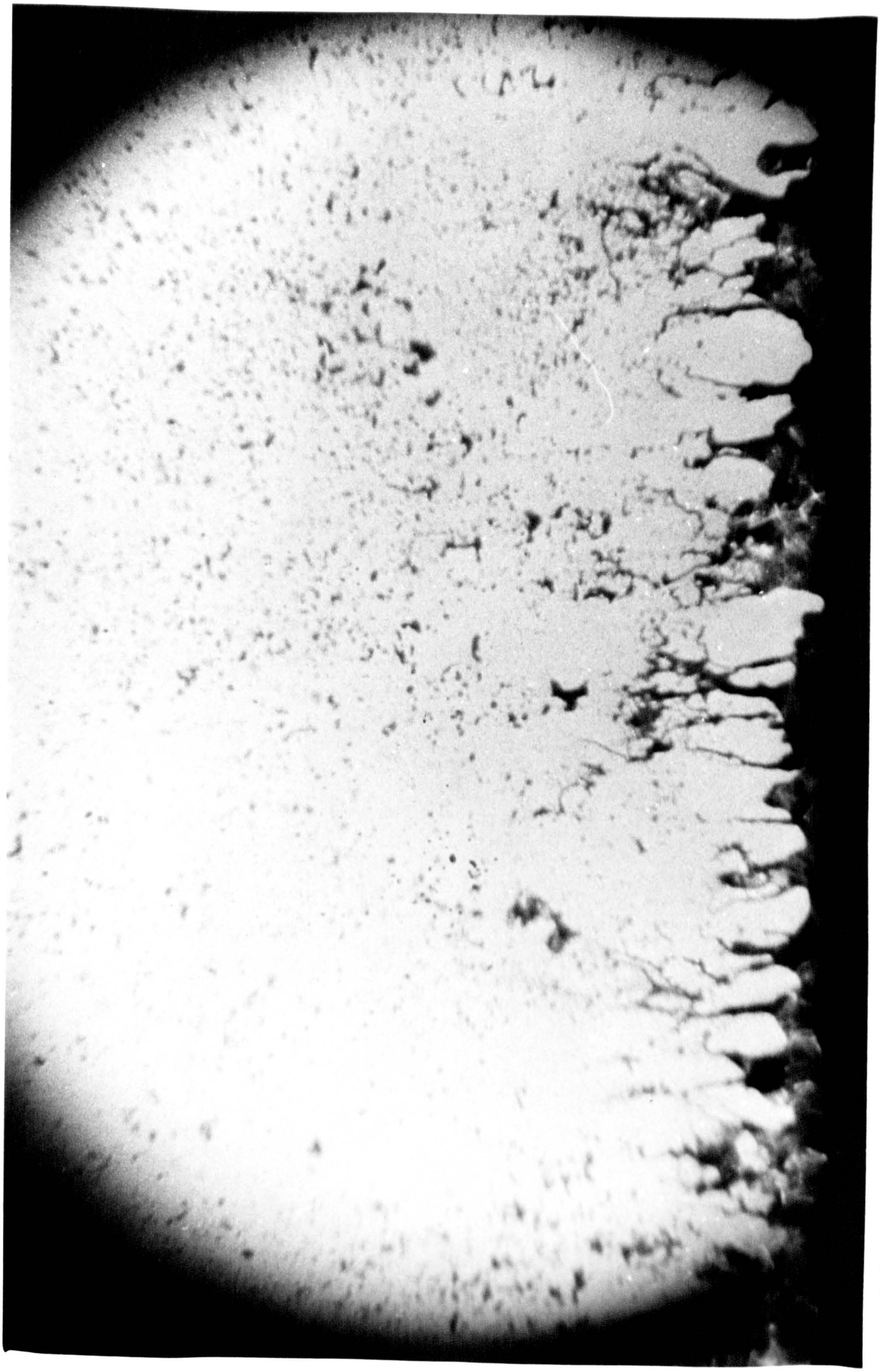

FIG.81

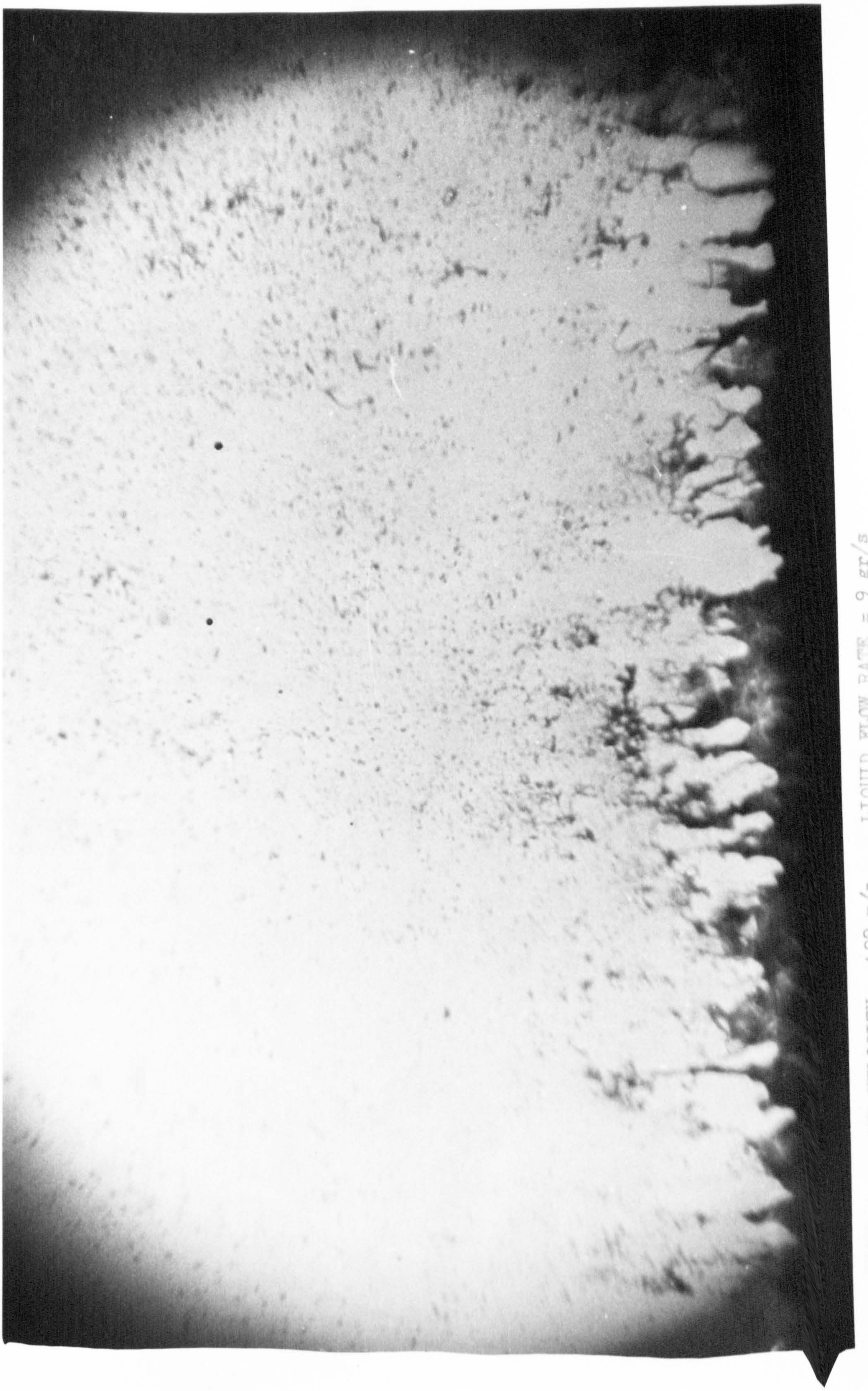

FIG.82

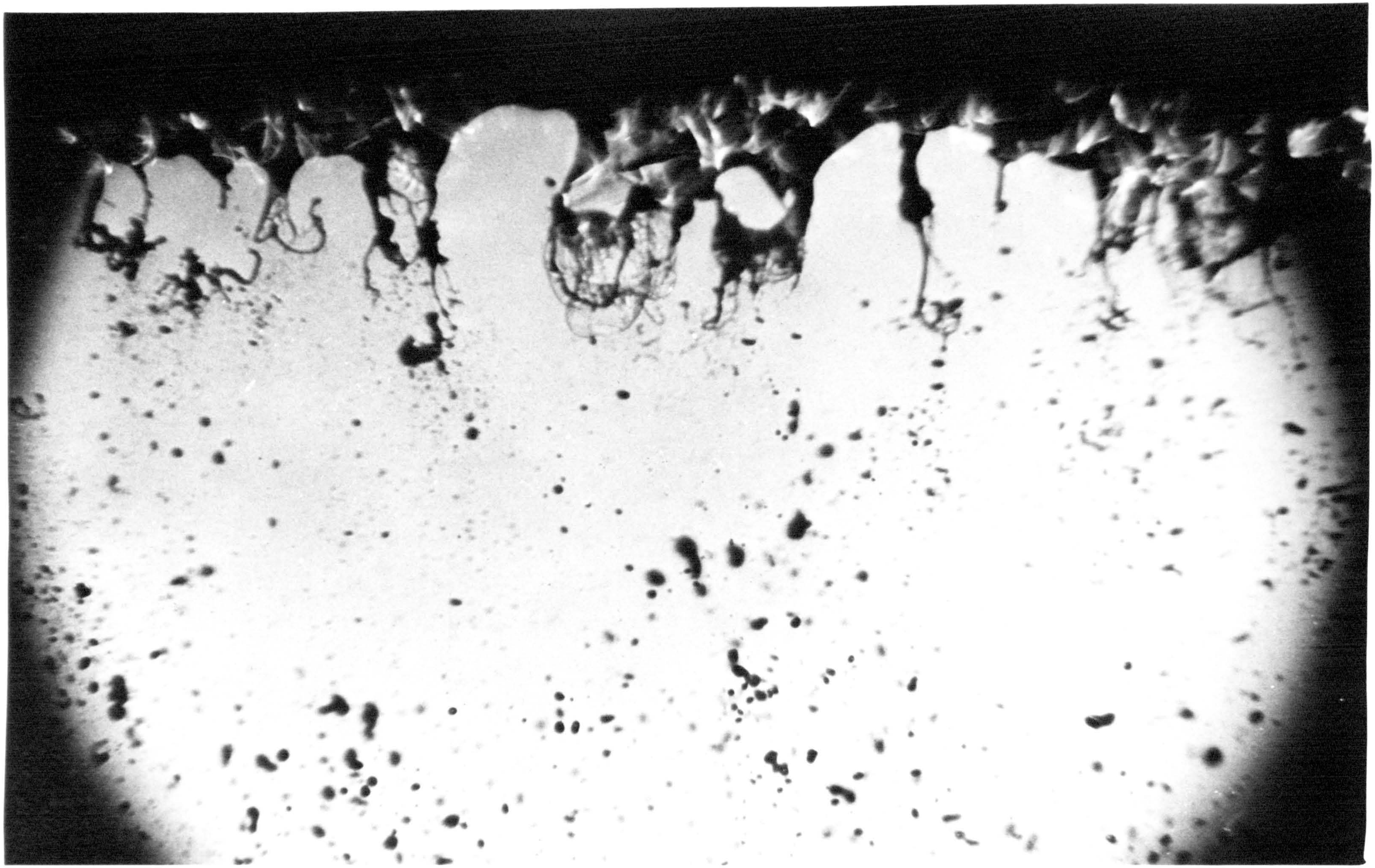

WATER AIR VELOCITY = 54.9 m/s , LIQUID FLOW RATE = 13.6 gr/s

FIG.83

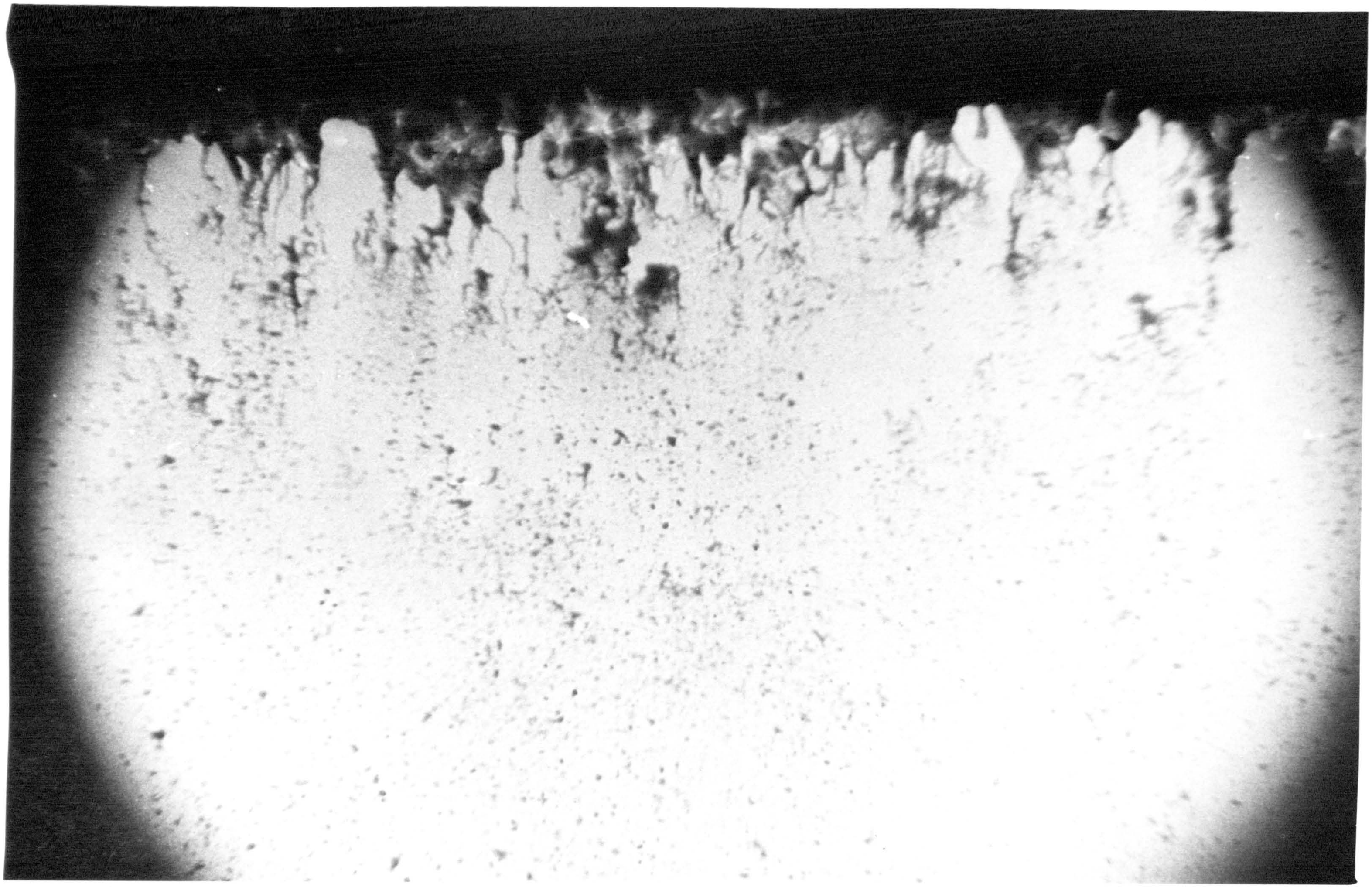

WATER AIR VELOCITY = 122 m/s , LIQUID FLOW RATE = 13.6 cm/s

KEROSINE AIR VELOCITY = 54.9 m/s , LIQUID FLOW RATE = 4.5 gr/s

FIG. 84

FIG. 85

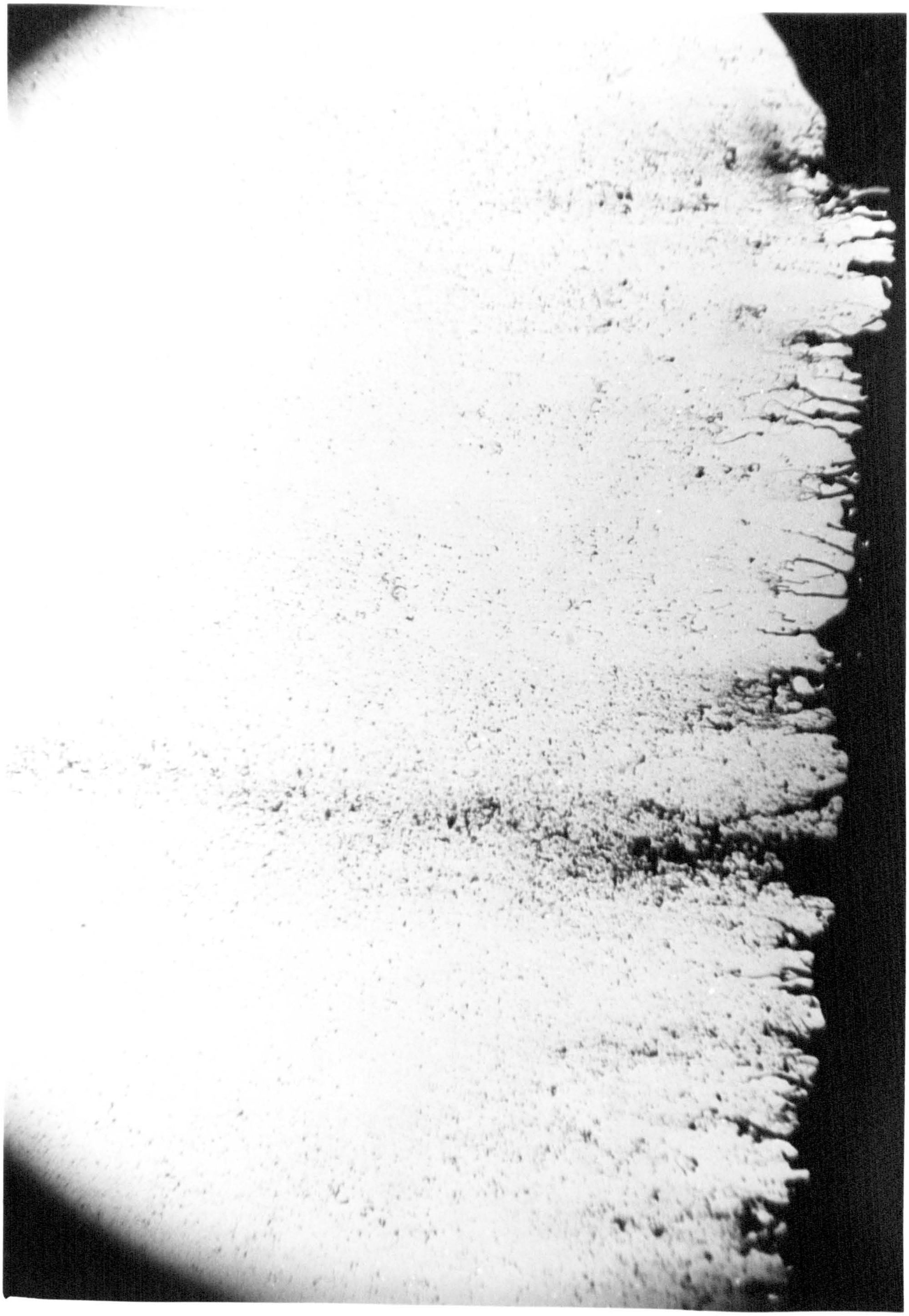

FIG. 86

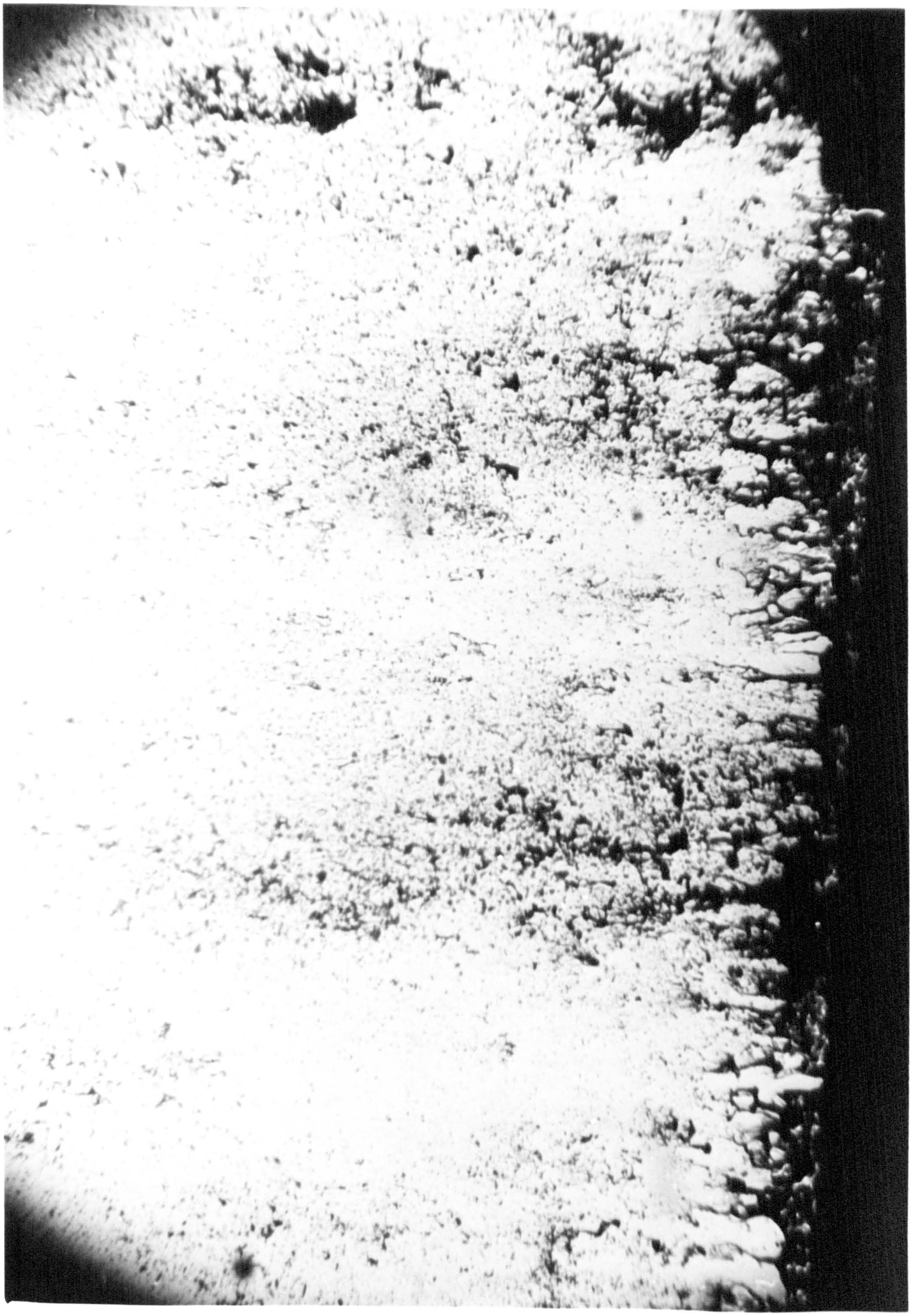

KEROSINE AIR VELOCITY = 122 m/s , LIQUID FLOW RATE = 13.6 gr/s

FIG.87


LIQUID PROPERTIES: SURFACE TENSION= 51.9x10^{-3} N/m , VISCOSITY= 1.13x10^{-3} Kg/ms
DENSITY = 0.988x10^{3} Kg/m^{3}
V_a = 91.5 m/s
m_1 = 9 m/s

FIG.88


LIQUID PROPERTIES: SURFACE TENSION =26.8x10^{-3} N/m , VISCOSITY= 2.34x10^{-3} Kg/ms
DENSITY = 0.968x10^{3} Kg/m^{3}
m_l=7.5 gr/s
V_a = 91.5 m/s

FIG.89

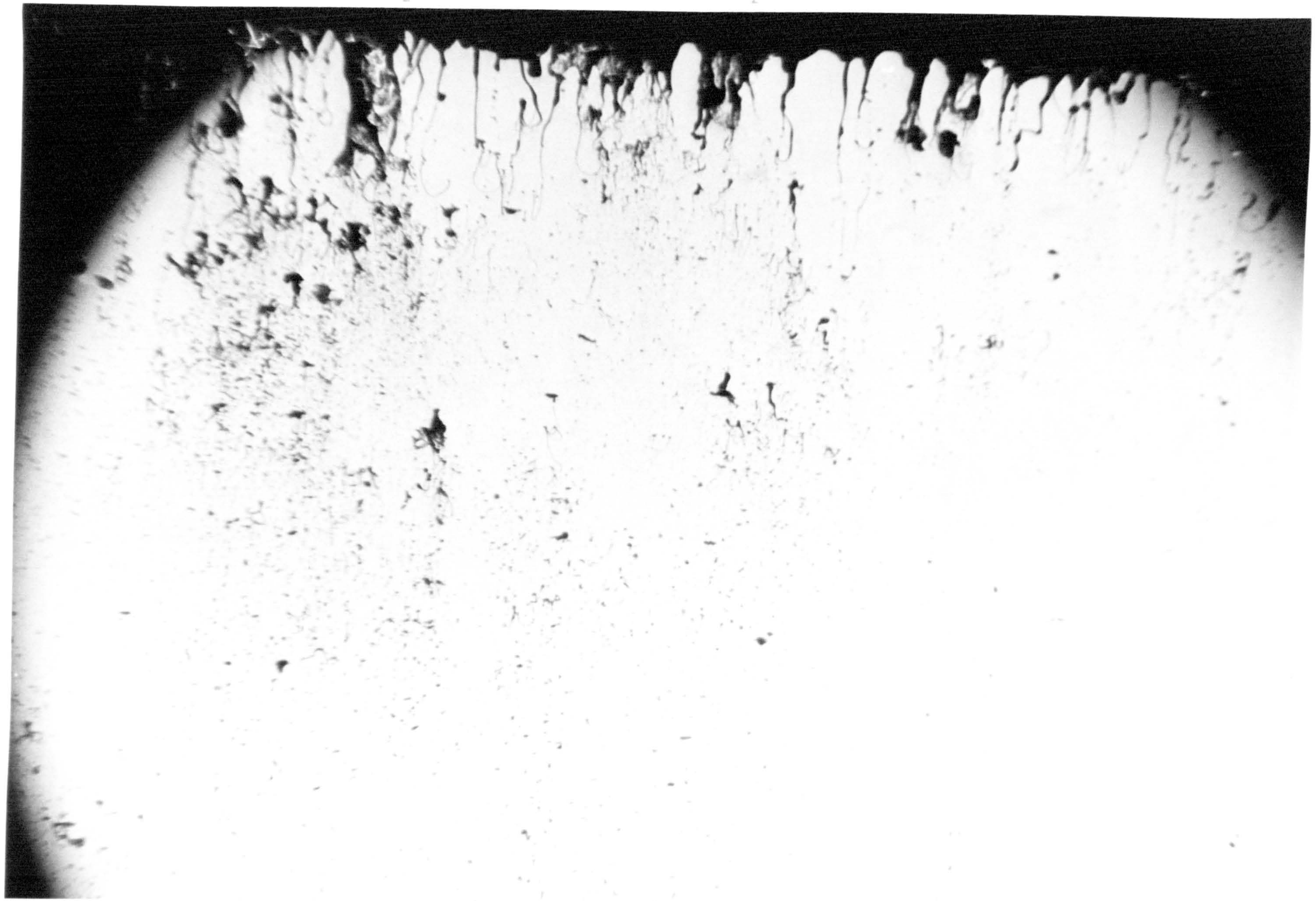

FIG.90


LIQUID PROPERTIES: SURFACE TENSION = 26.8x10^{-3} N/m , VISCOSITY = 2,34x10^{-3} Kg/ms
DENSITY =0.968x10^{3} Kg/m^{3}
V_a = 91.5 m/s
m_l = 12.5 gr/s

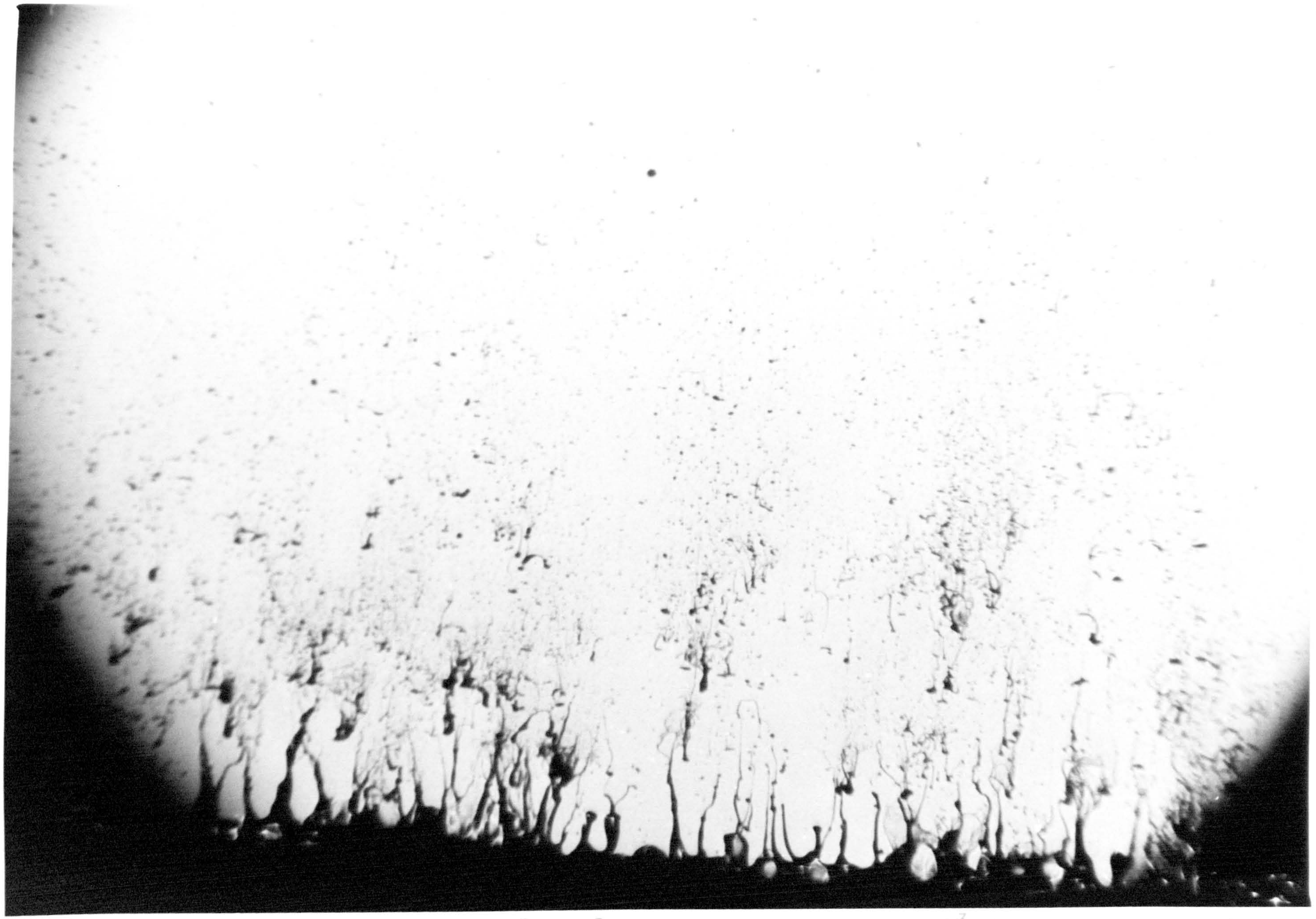

LIQUID PROPERTIES: DENSITY = 1.213×10^{3} Kg/m^{3} , SURFACE TENSION = 31.6×10^{-3} N/m V_a = 91.5 m/s

VISCOSITY = 1.6×10^{-3} Kg/ms m_l = 4.5 gr/s

FIG.91

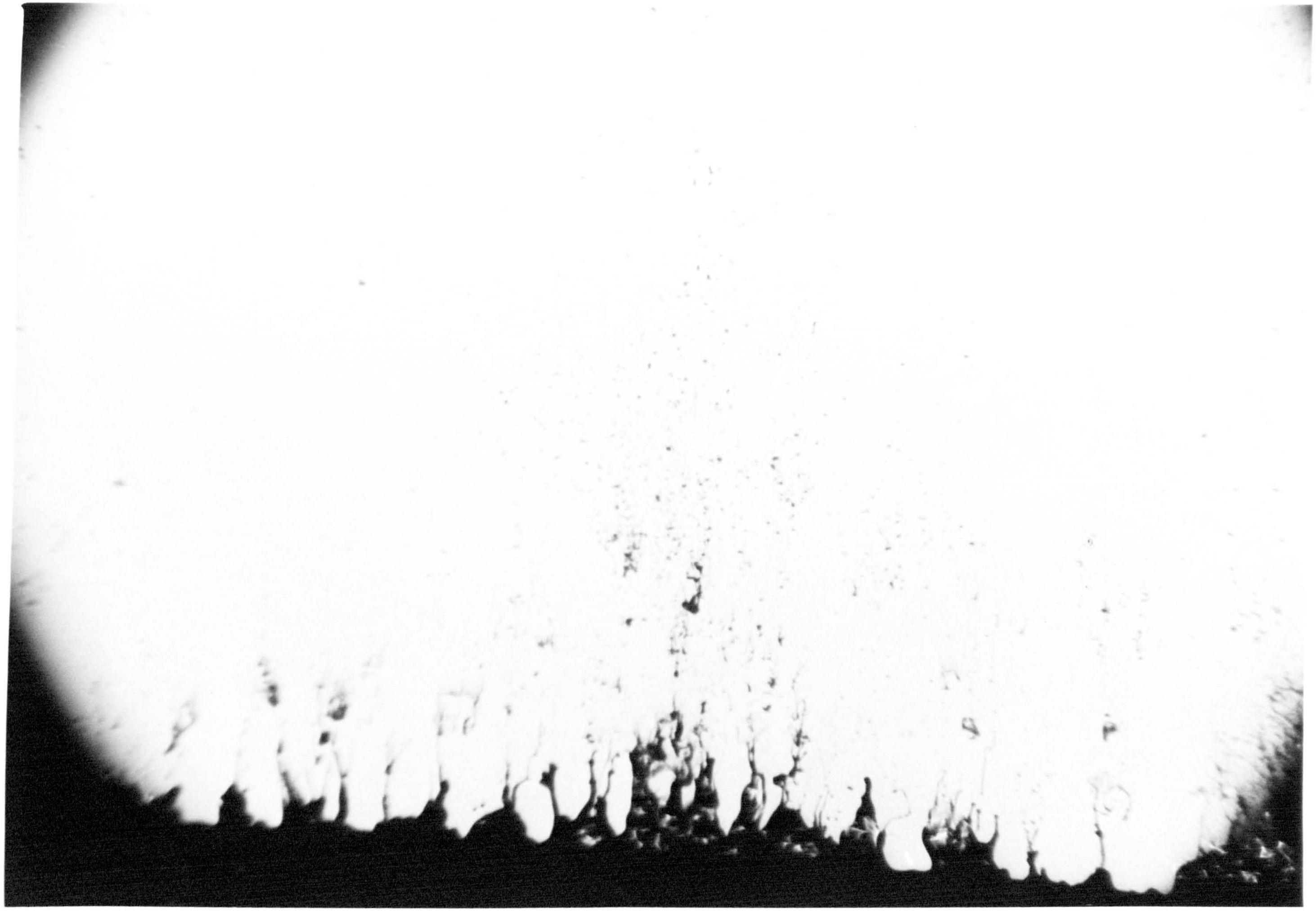

LIQUID PROPERTIES: DENSITY = 1.83×10^{3} Kg/m^{3}, SURFACE TENSION = 33.7×10^{-3} N/m
VISCOSITY = 1.6×10^{-3} Kg/ms

V_a = 91.5 m/s
m_l = 4.5 gr/s

FIG. 92

LIQUID PROPERTIES: DENSITY = 1.213×10^{3} Kg/m^{3}, SURFACE TENSION = 31.6×10^{-3} N/m V_a = 91.5 m/s
VISCOSITY = 1.6×10^{-3} Kg/ms m_l = 6.8 gr/s

FIG.93

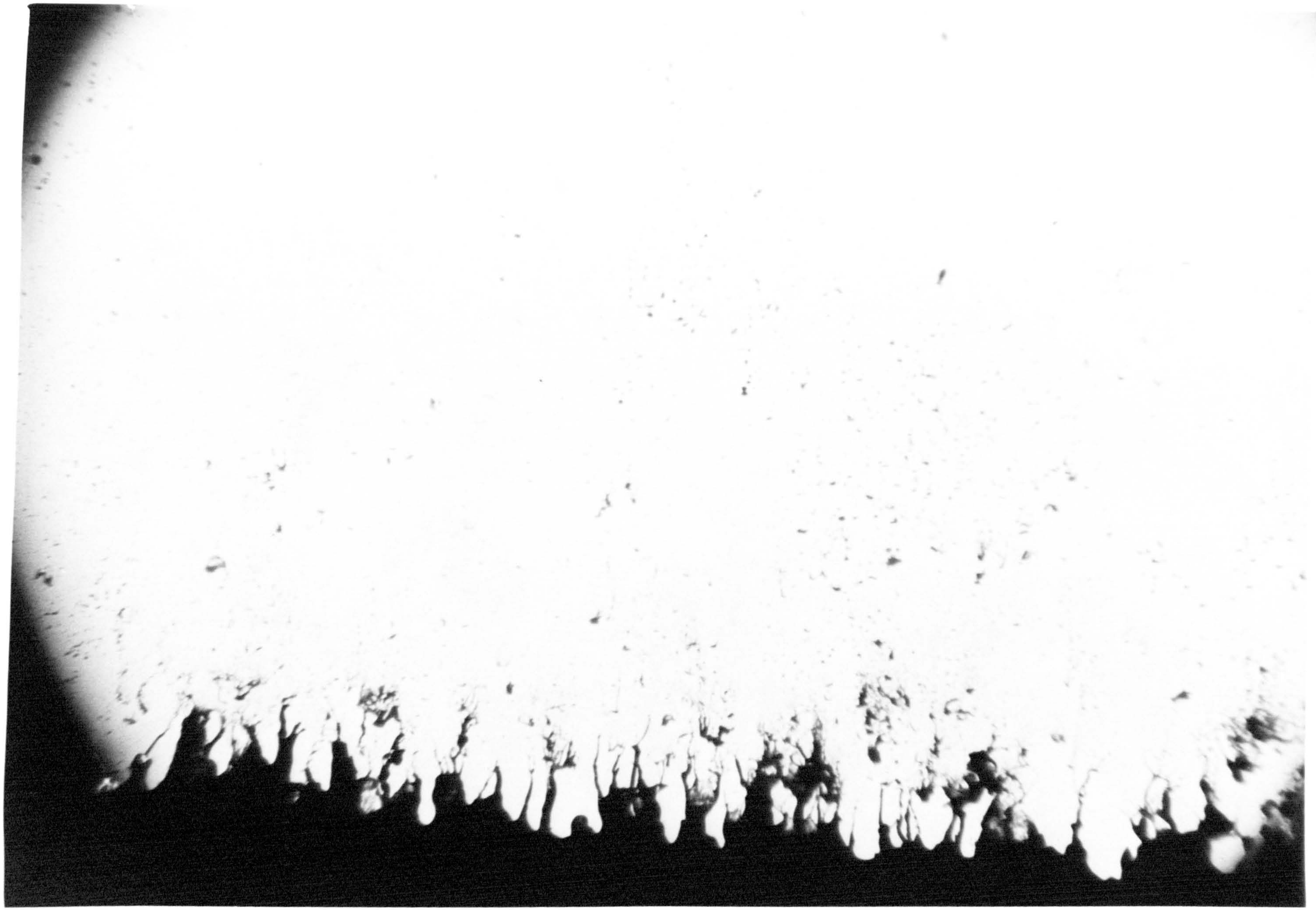

LIQUID PROPERTIES: DENSITY = 1.83×10^{3} Kg/s, SURFACE TENSION = 33.7×10^{-3} N/m $V_a = 91.5$ m/s

VISCOSITY = 1.6×10^{-3} Kg/ms $m_l = 6.8$ gr/s

FIG.94

FIG.95


LIQUID PROPERTIES: DENSITY = 1.213x10^3 Kg/m^3 , SURFACE TENSION = 31.6x10^-3 N/m
VISCOSITY = 1.6x10^-3 Kg/ms
V_a = 91.5 m/s
m_l = 12.5 gr/s

FIG.96

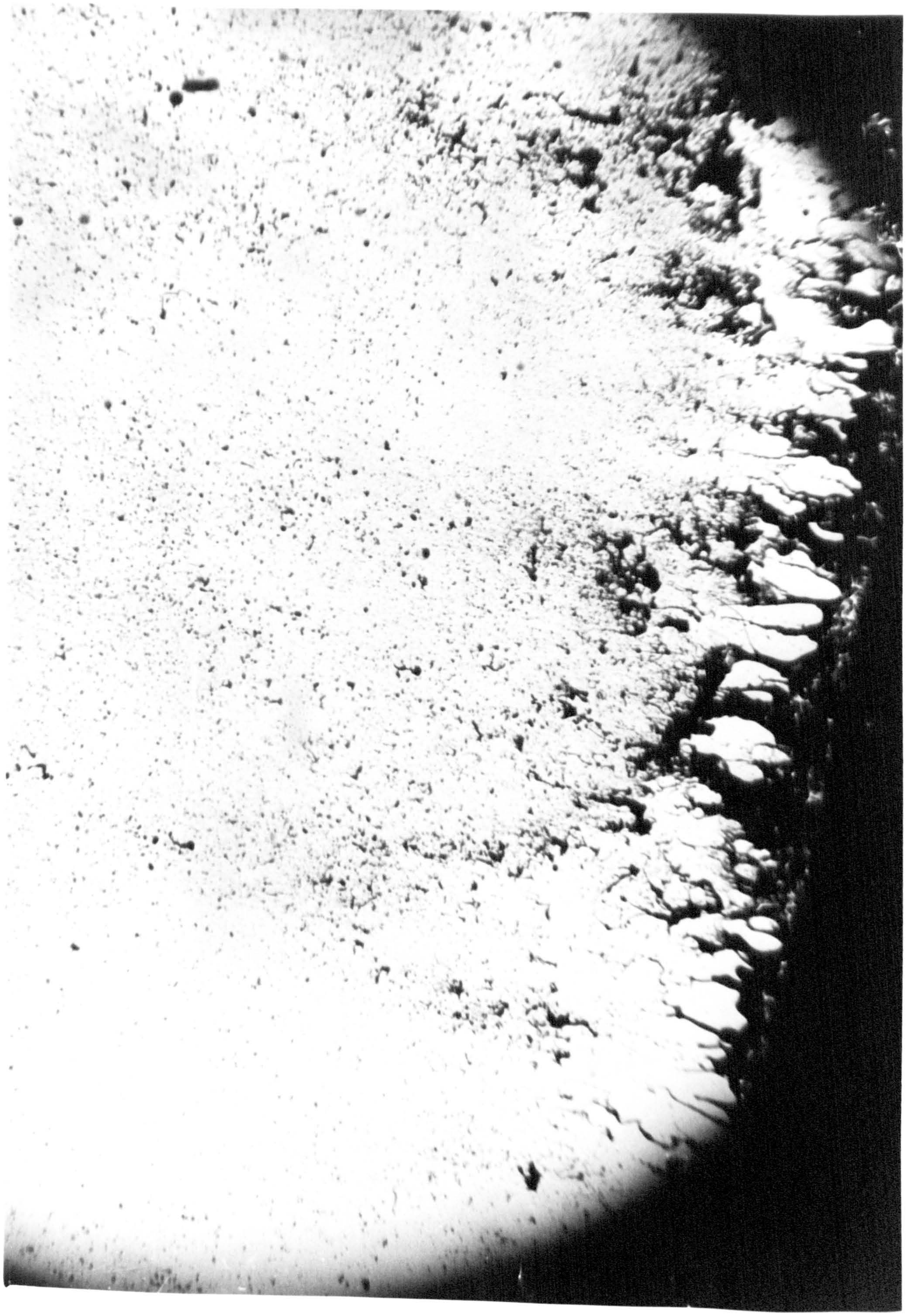
LIQUID PROPERTIES: DENSITY = 1.83x10^3 Kg/m^3 , SURFACE TENSION = 33.7x10^-3 N/m
VISCOSITY = 1.6x10^-3 Kg/ms
V_a = 91.5 m/s
m_l = 12.5 gr/s

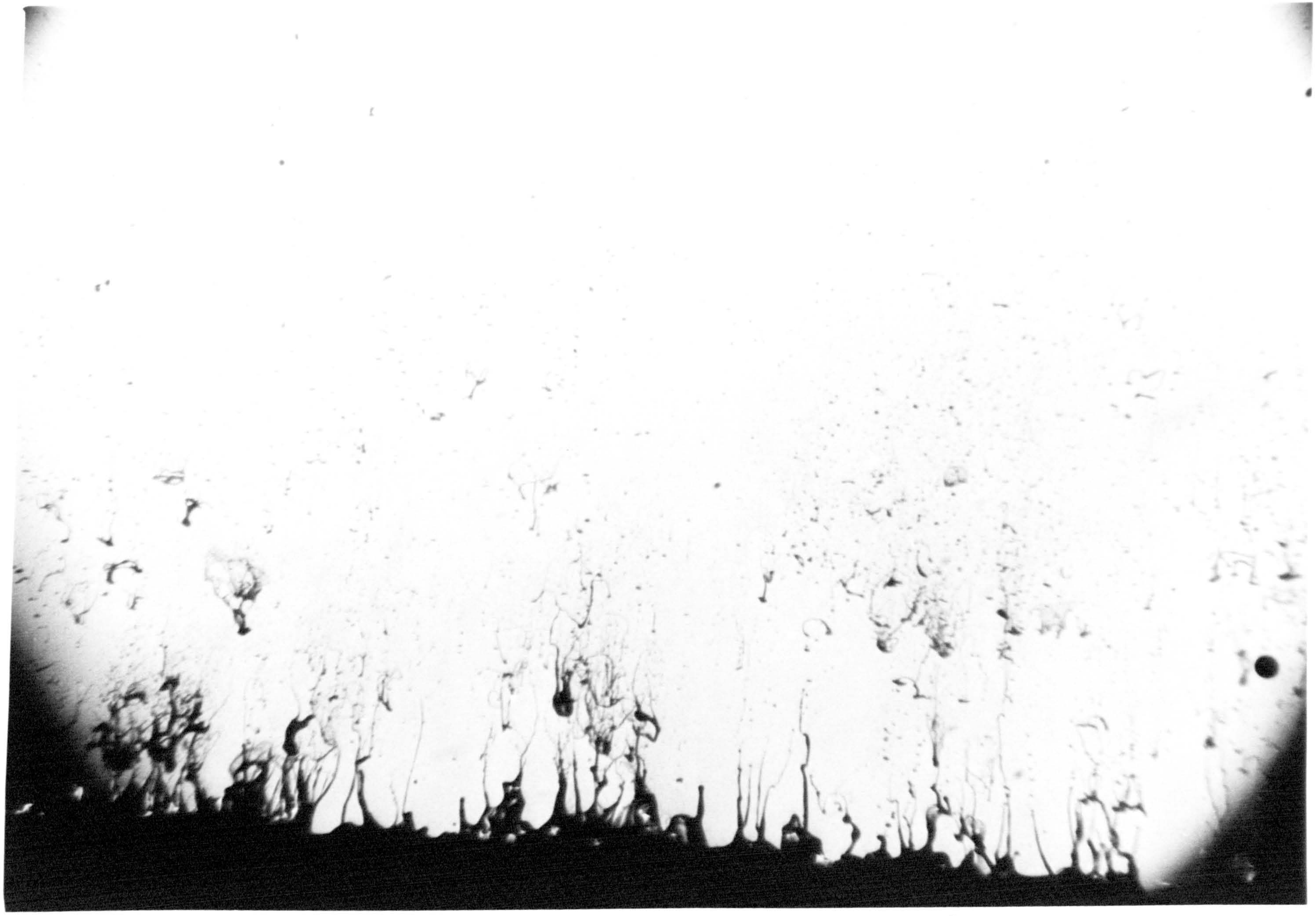

LIQUID PROPERTIES: VISCOSITY = 2.87×10^{-3} Kg/ms , SURFACE TENSION = 28.7×10^{-3} N/m V_a = 91.5 m/s

DENSITY = 0.80×10^{3} Kg/m^3 m_l = 4.5 gr/s

FIG. 97

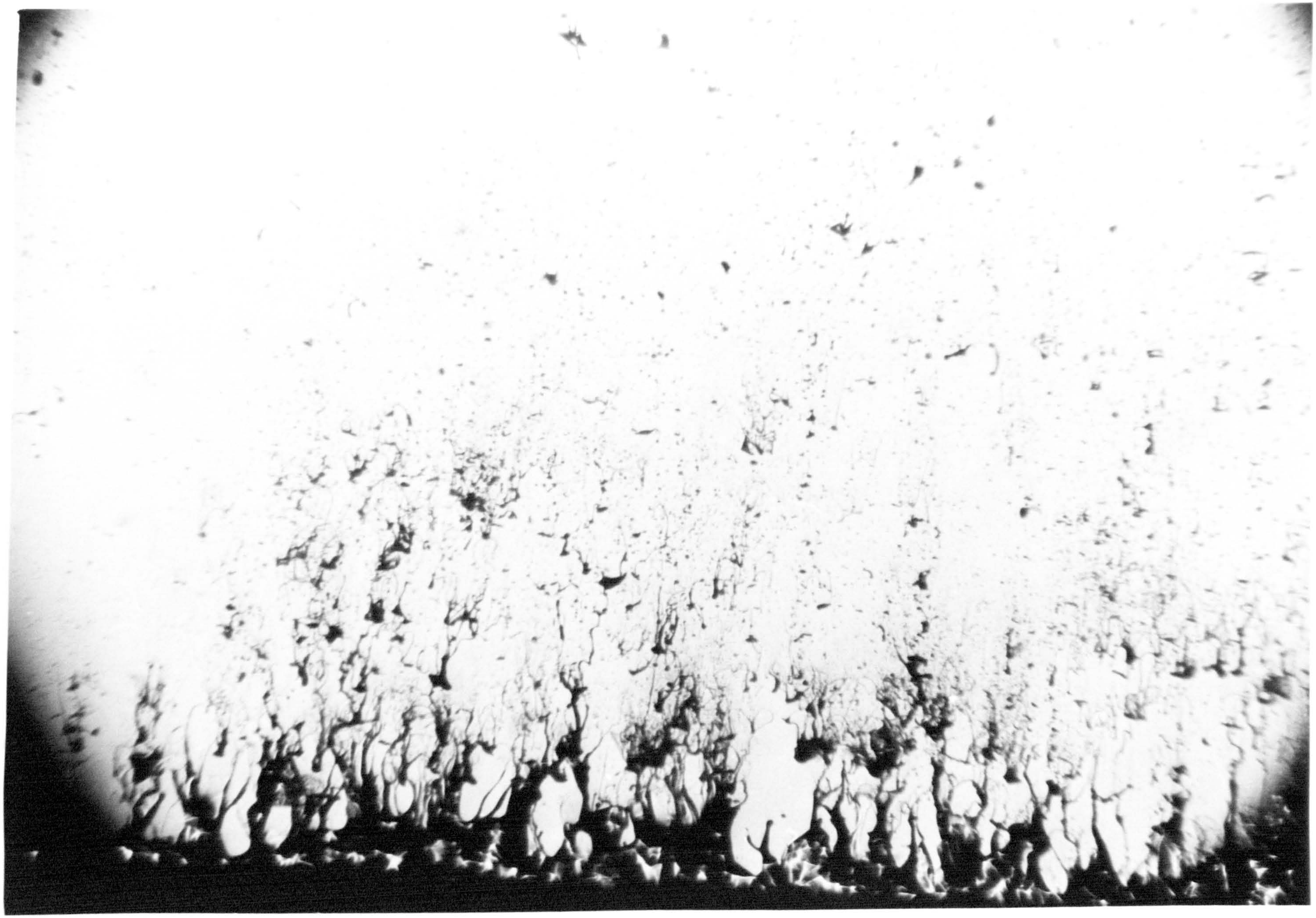

LIQUID PROPERTIES: VISCOSITY = 2.87×10^{-3} Kg/ms, SURFACE TENSION = 28.7×10^{-3} N/m $V_a = 91.5$ m/s

DENSITY = 0.80×10^{3} Kg/m^3 $m_l = 6.8$ gr/s

FIG. 98

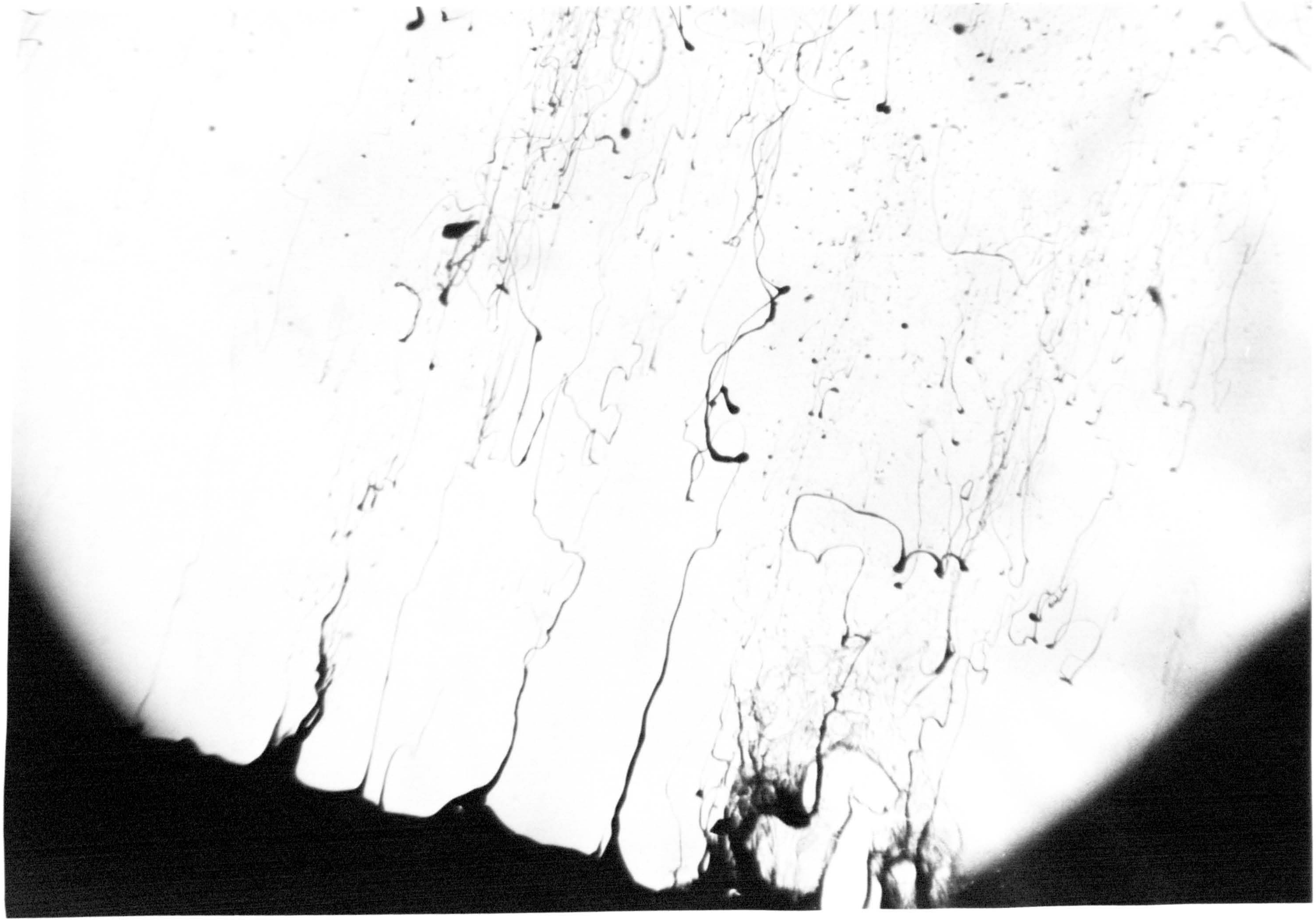

LIQUID PROPERTIES: VISCOSITY = 17×10^{-3} Kg/ms, SURFACE TENSION = 30.1×10^{-3} N/m
DENSITY = 0.823×10^{3} Kg/m^3

V_a = 91.5 m/s
m_l = 4.5 gr/s

FIG. 99

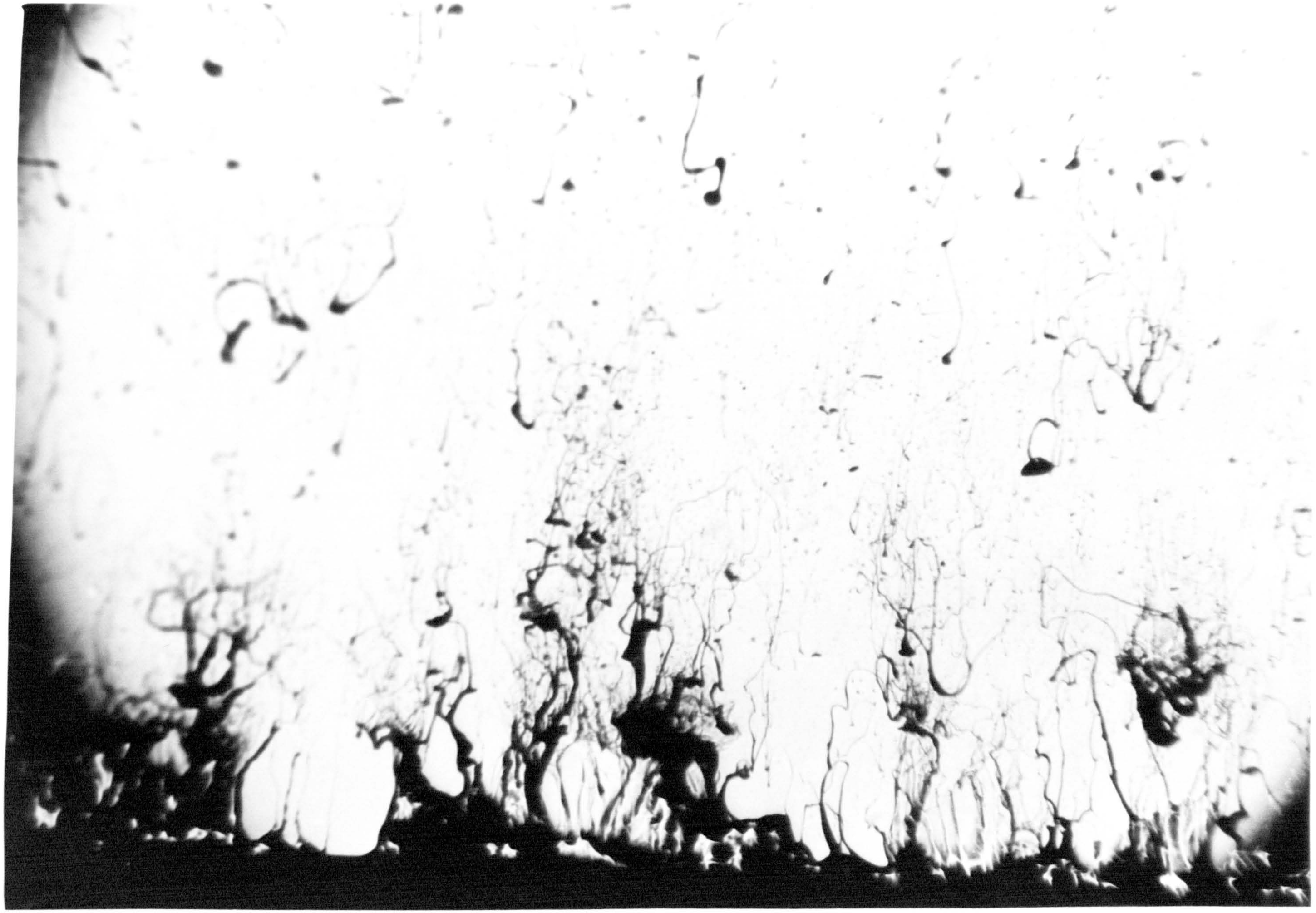

LIQUID PROPERTIES: VISCOSITY = 17×10^{-3} Kg/ms , SURFACE TENSION = 30.1×10^{-3} N/m V_a = 91.5 m/s

DENSITY = 0.823×10^{3} Kg/m^3 m_l = 4.5 gr/s

FIG.100

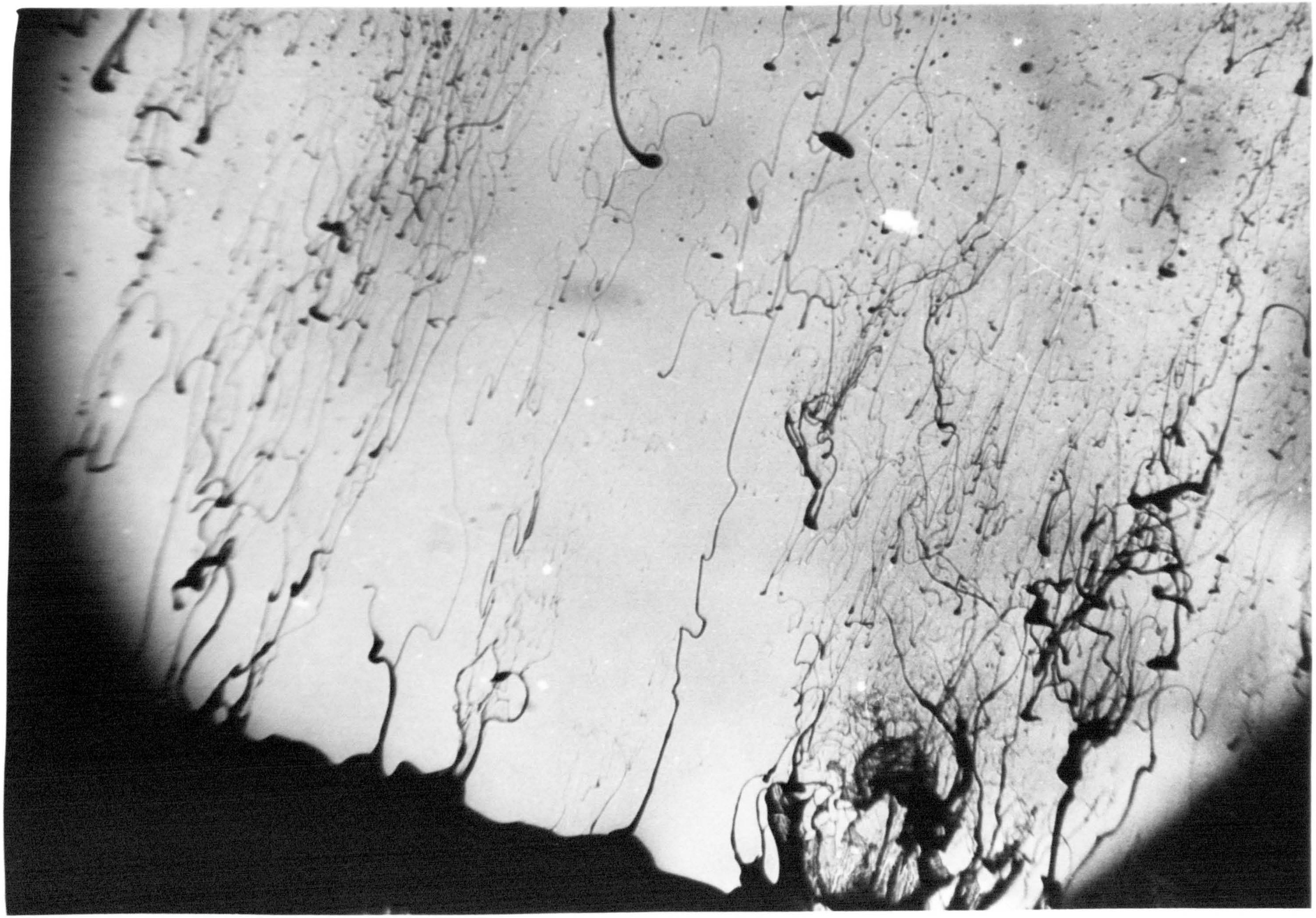

LIQUID PROPERTIES: VISCOSITY = 17×10^{-3} Kg/ms, SURFACE TENSION = 30.1×10^{-3} N/m
DENSITY = 0.823×10^{3} Kg/m^3

V_a = 91.5 m/s
m_l = 6.8 gr/s

FIG.101

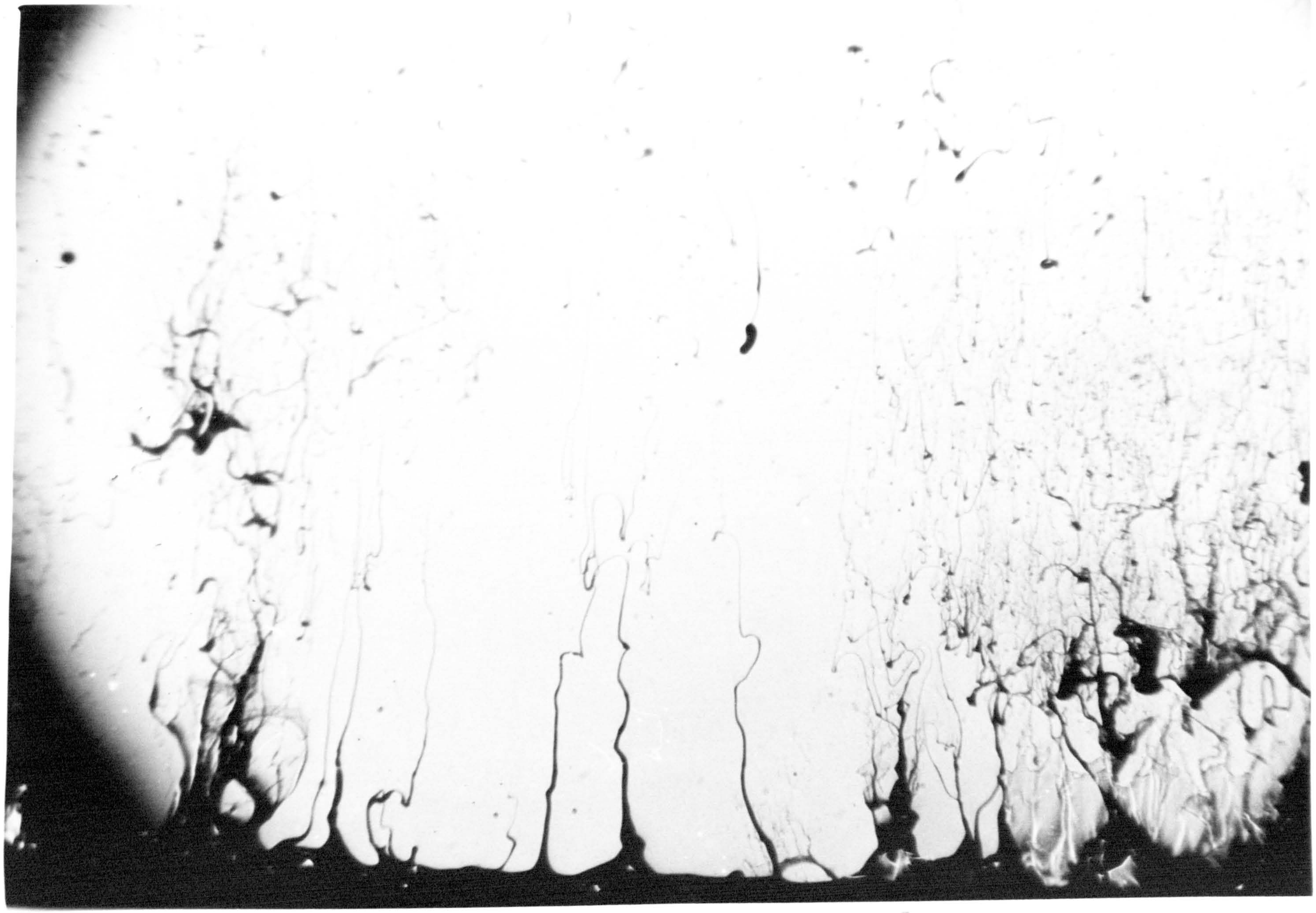

LIQUID PROPERTIES: VISCOSITY = 17×10^{-3} Kg/ms, SURFACE TENSION = 30.1×10^{-3} N/m $V_a = 91.5$ m/s

DENSITY $= 0.823 \times 10^{3}$ Kg/m^3 $m_l = 6.8$ gr/s

FIG.102

FIG.103

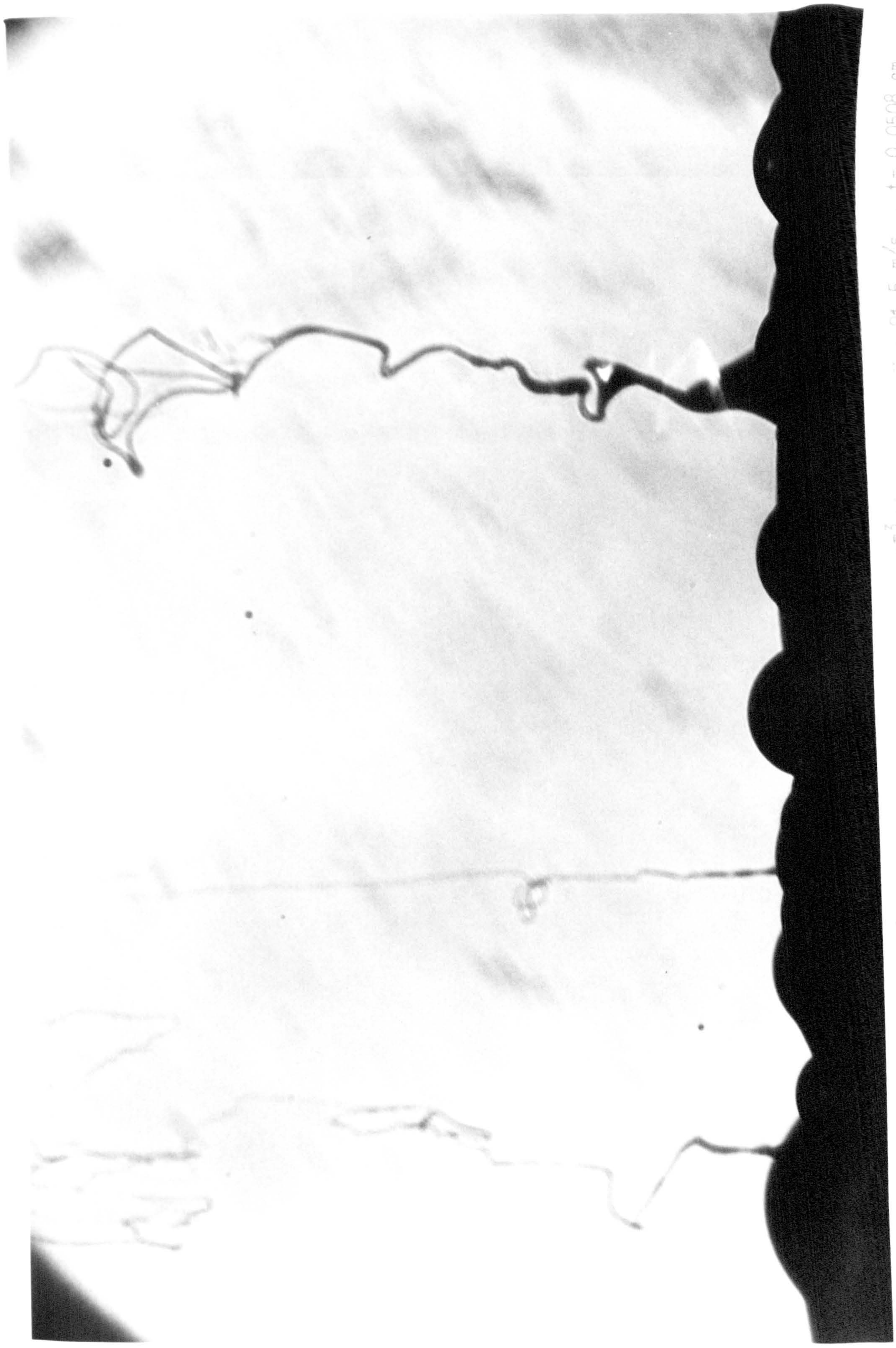
LIQUID PROPERTIES: VISCOSITY = 44x10^-4 Kg/m.s, SURFACE TENSION = 30.3x10^-3 N/m V_g = 91.5 m/s
DENSITY = 0.83x10^3 Kg/m^3 n_1 = 4 pr/s
t= 0.0508 cm

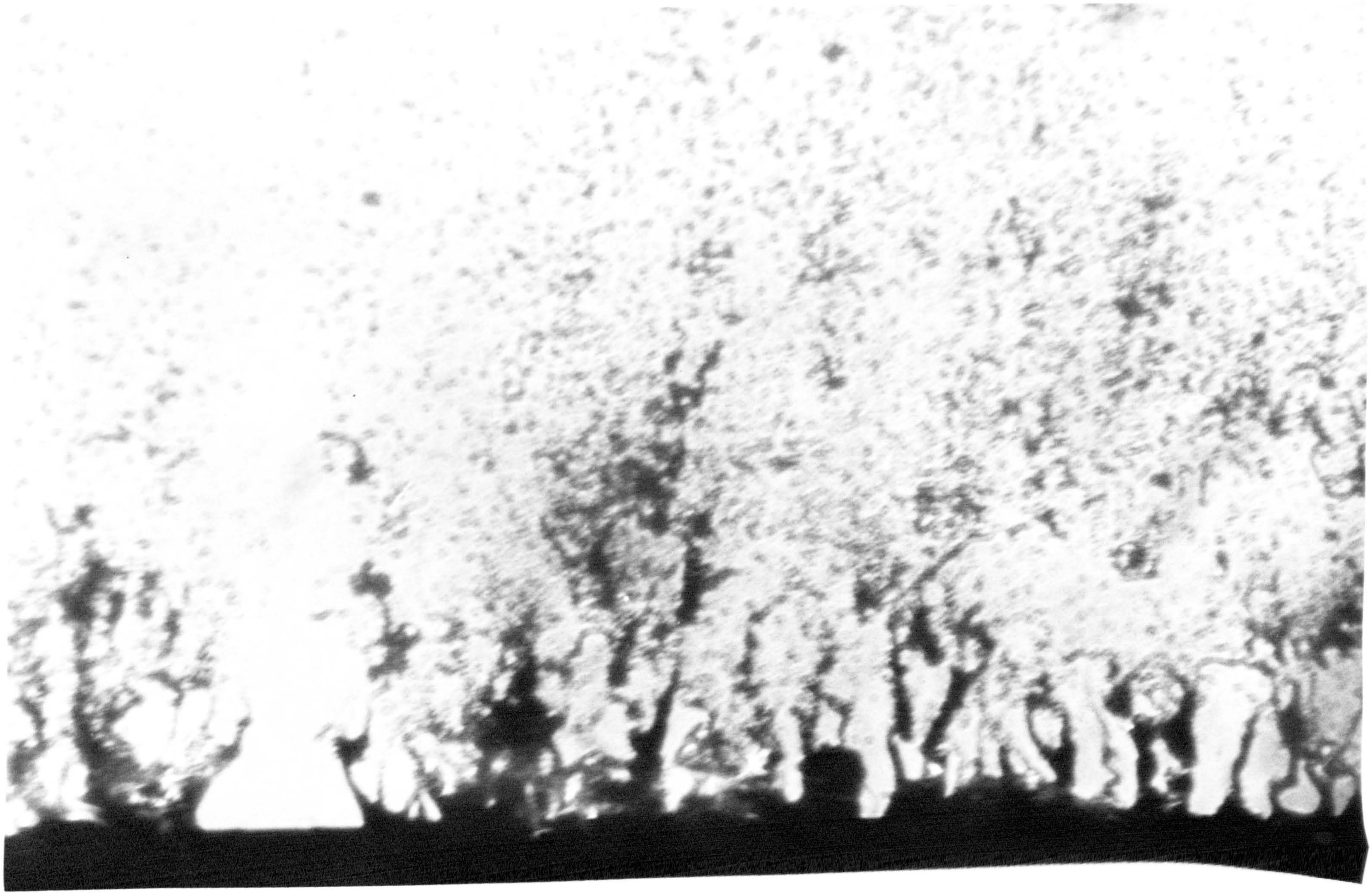

WATER FILM THICKNESS = 0.0178 cm V_a = 91.5 m/s m_l = 16.4 gr/s

FIG.104

FIG.105

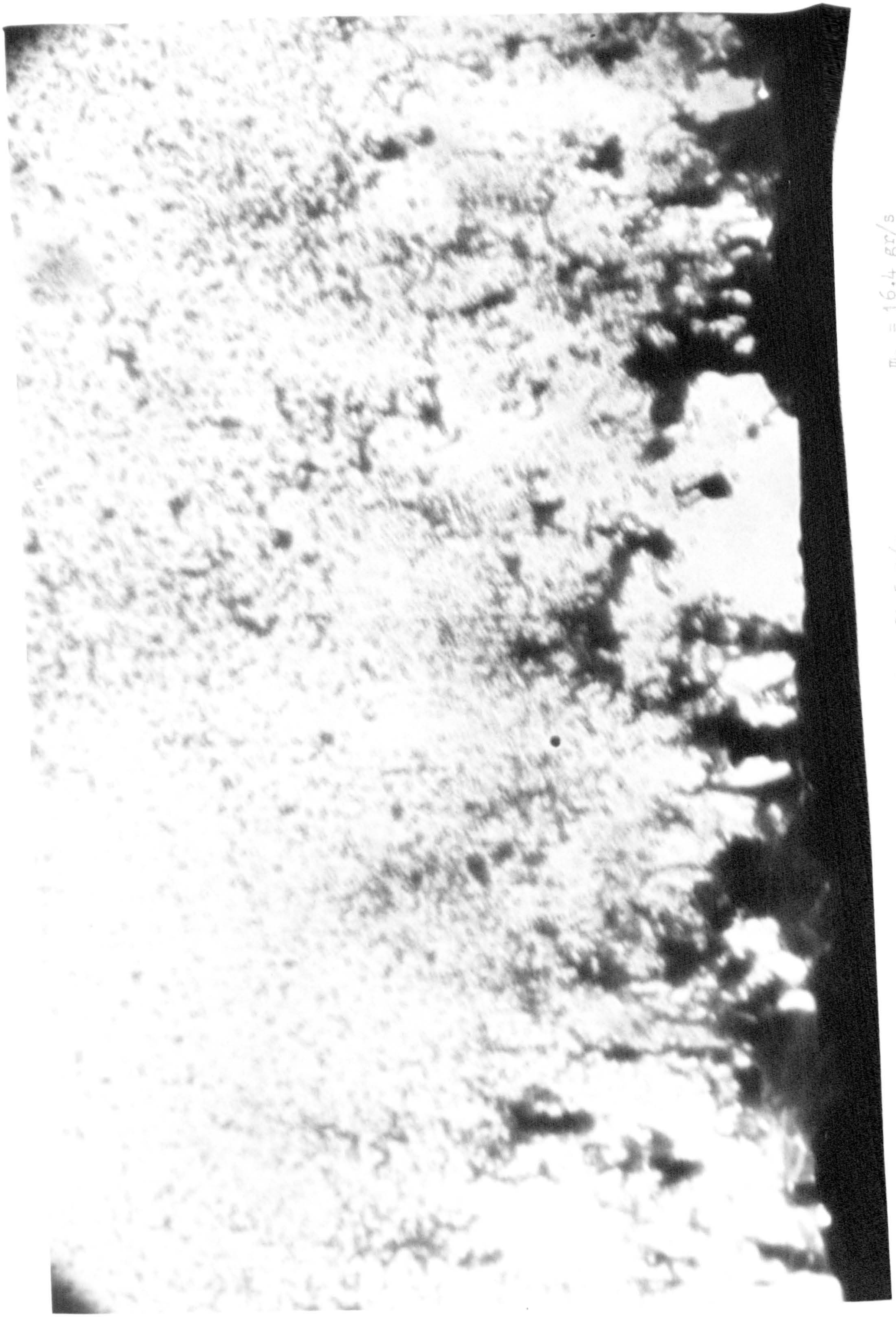

PLATES

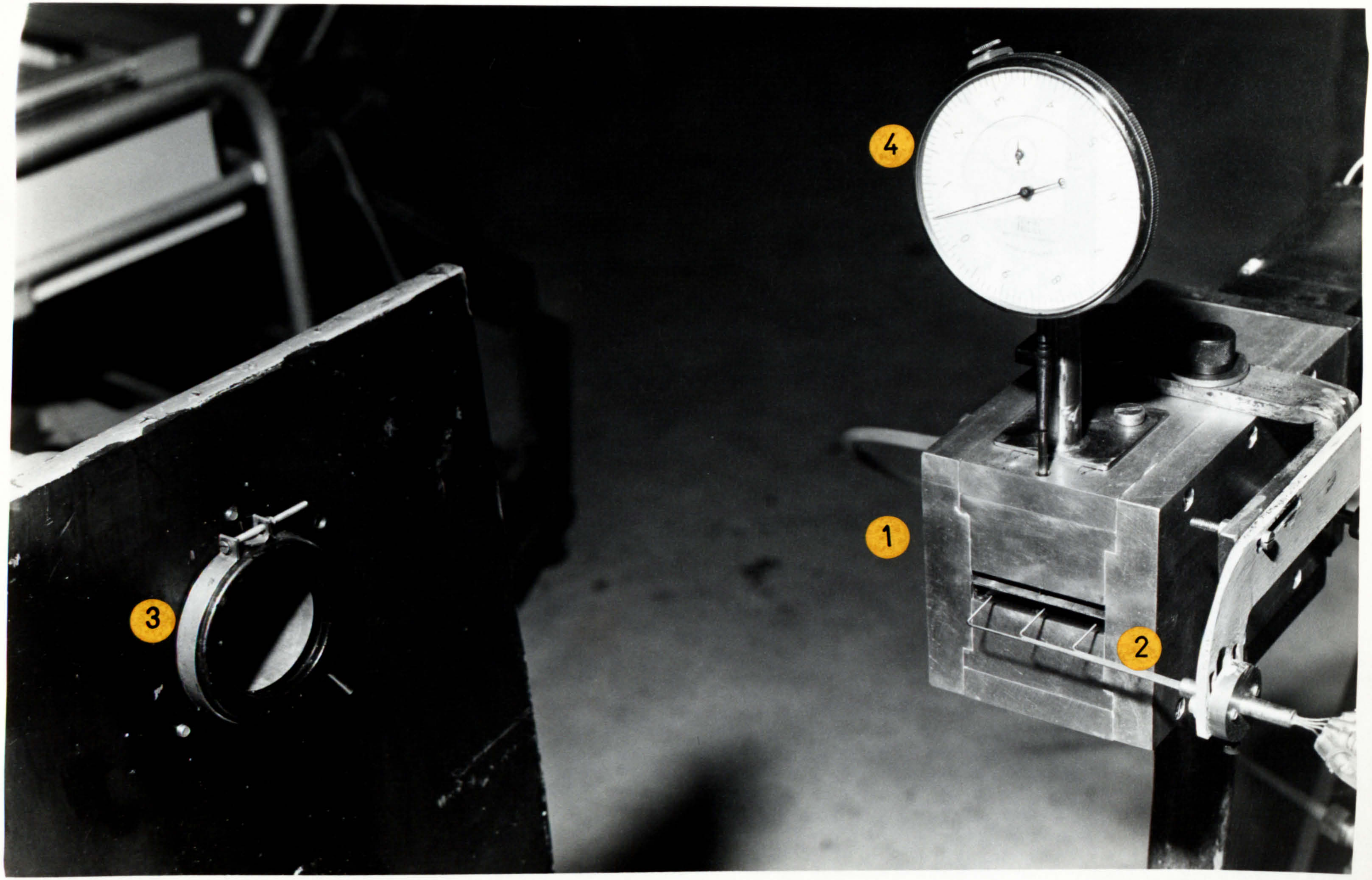

1_AIRBLAST ATOMIZER(B)
2_PITOT TUBE RAKE
3_RECEIVING SIDE OF OPTICAL BENCH
4_DIAL TEST INDICATOR

PLATE 1

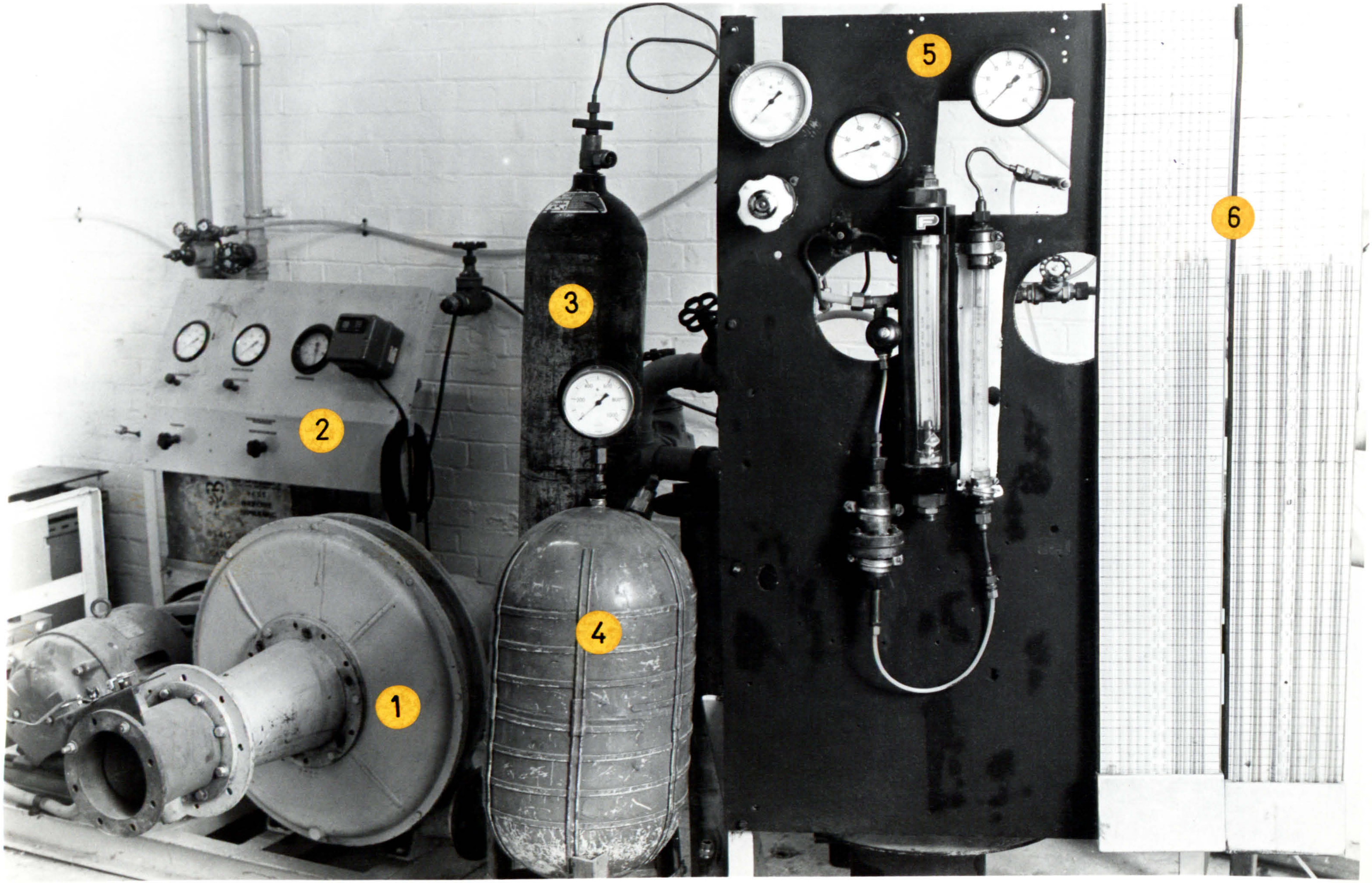

1_ AIR BLOWER
2_ WATER PUMP
3_ NITROGEN BOTTLE
4_ LIQUID TANK
5_ LIQUID CONTROL PANEL
6_ MANOMETERS SET_UP

PLATE 2

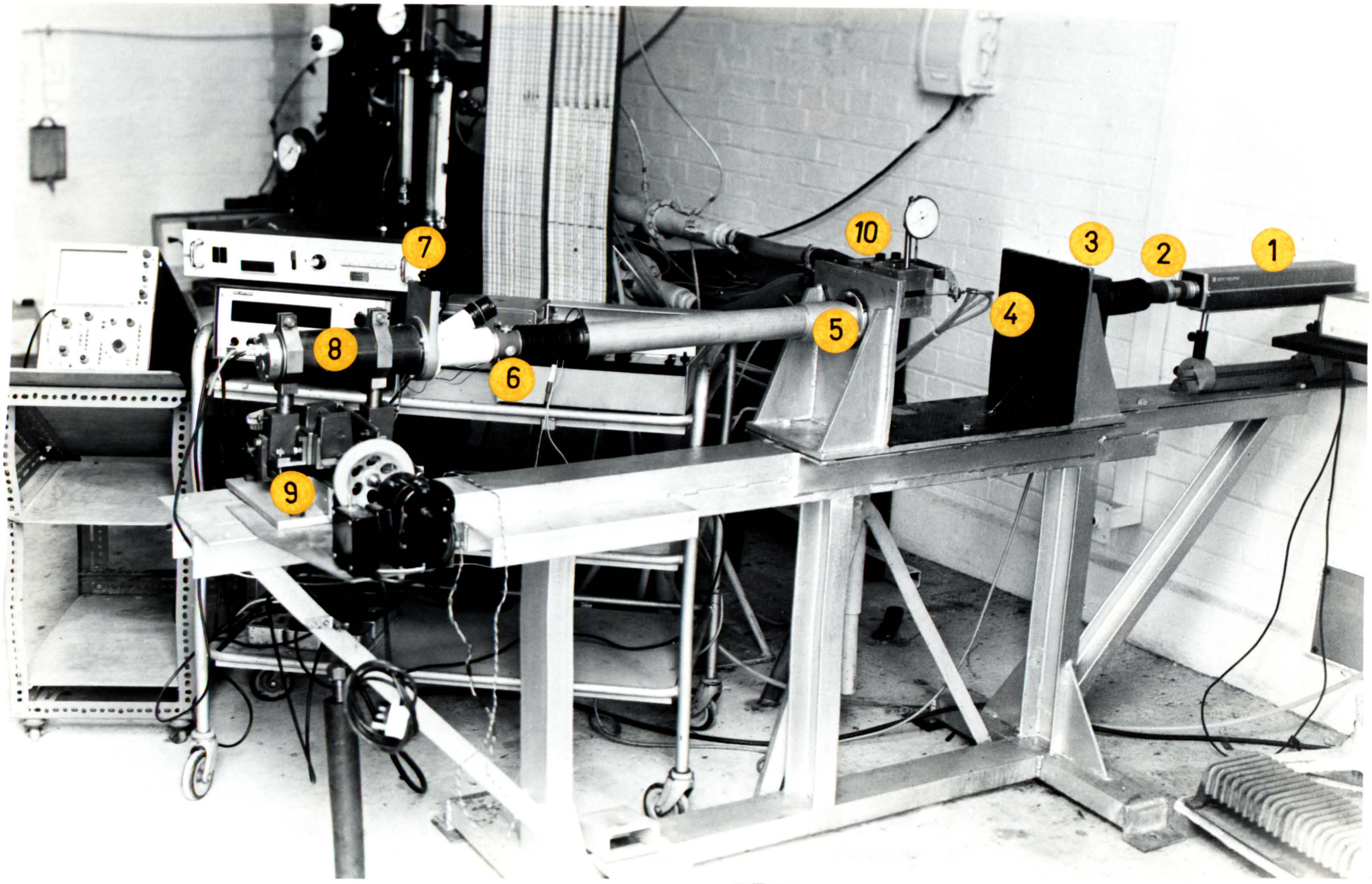

1_LASER
2_TELESCOPE
3_LIGHT CHOPPER
4_TEST SECTION
5_RECEIVER LENS
6_APERTURE
7_SHUTTER
8_PHOTOMULTIPLIER
9_TRAVERSING SYSTEM
10_AIRBLAST ATOMIZER

PLATE 3

PLATE 4

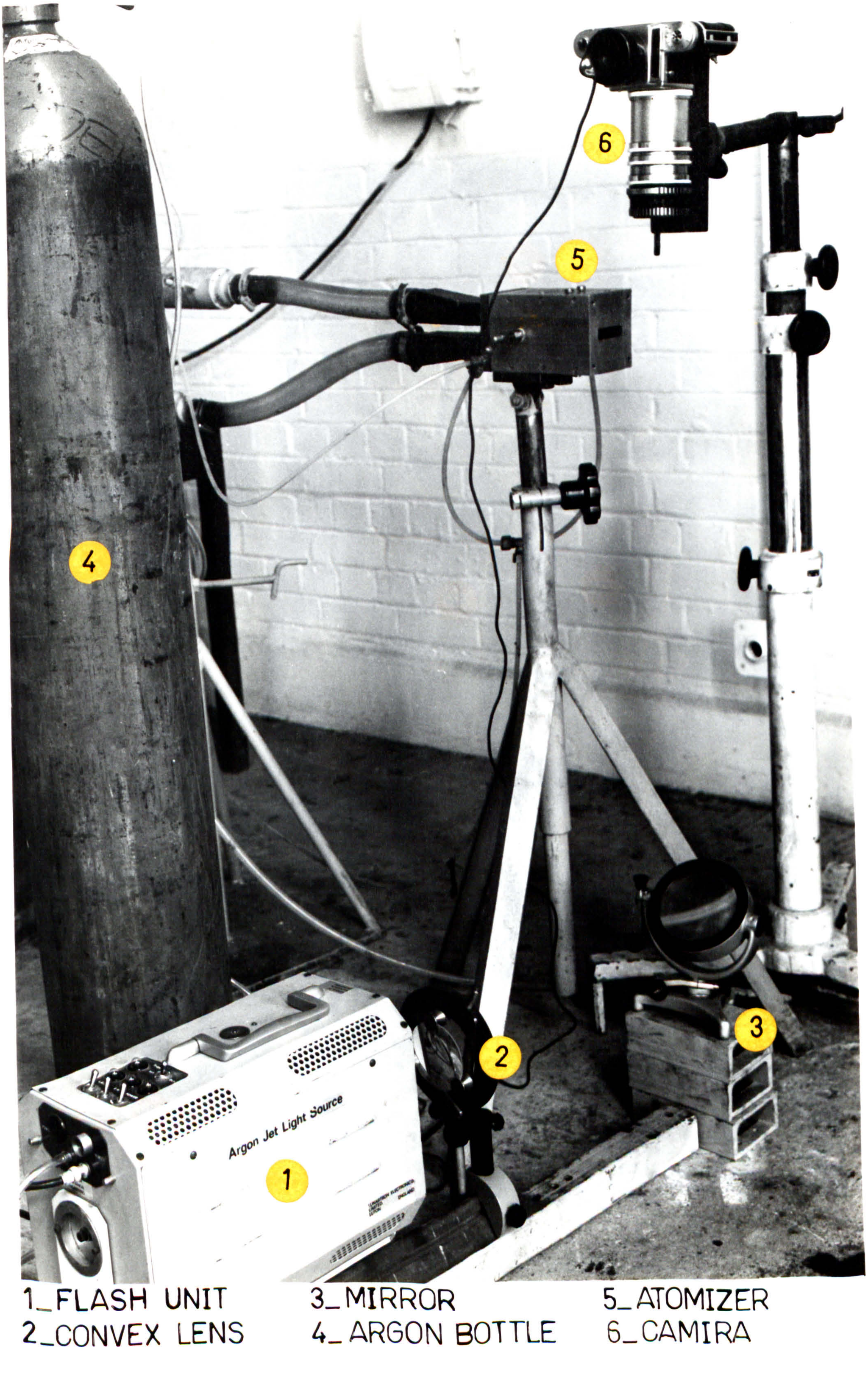

1_FLASH UNIT
2_CONVEX LENS
3_MIRROR
4_ARGON BOTTLE
5_ATOMIZER
6_CAMIRA

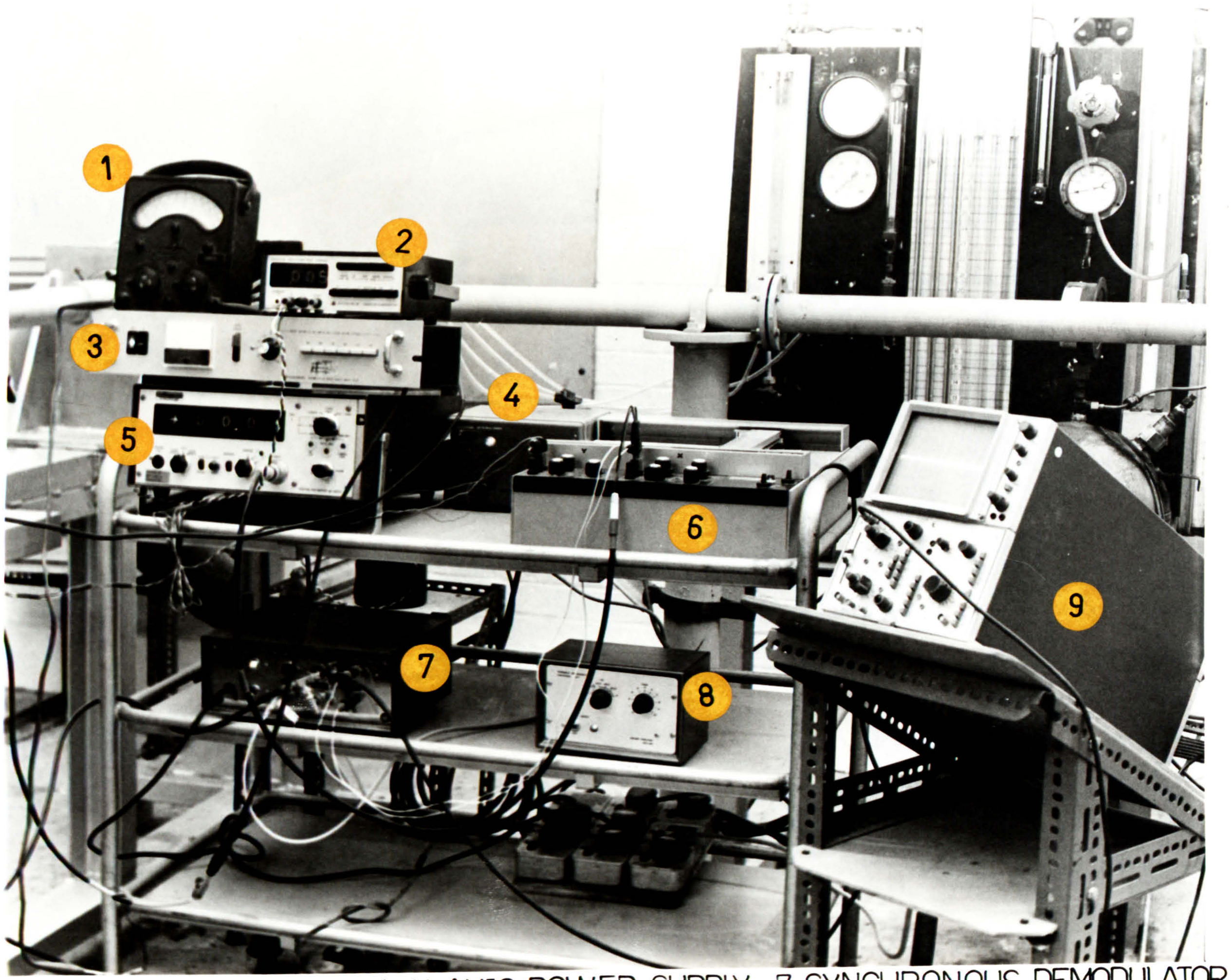

1_ A.V.O.
2_ D.V.M.
3_ H.T. SUPPLY TO P.M.
4_X-AXIS POWER SUPPLY
5_D.V.M.
6_LOG. AMPLIFIER
7_SYNCHRONOUS DEMODULATOR
8_CHOPPER FREQ. CONTROL
9_OSCILLOSCOPE

PLATE 5

PLATE 6

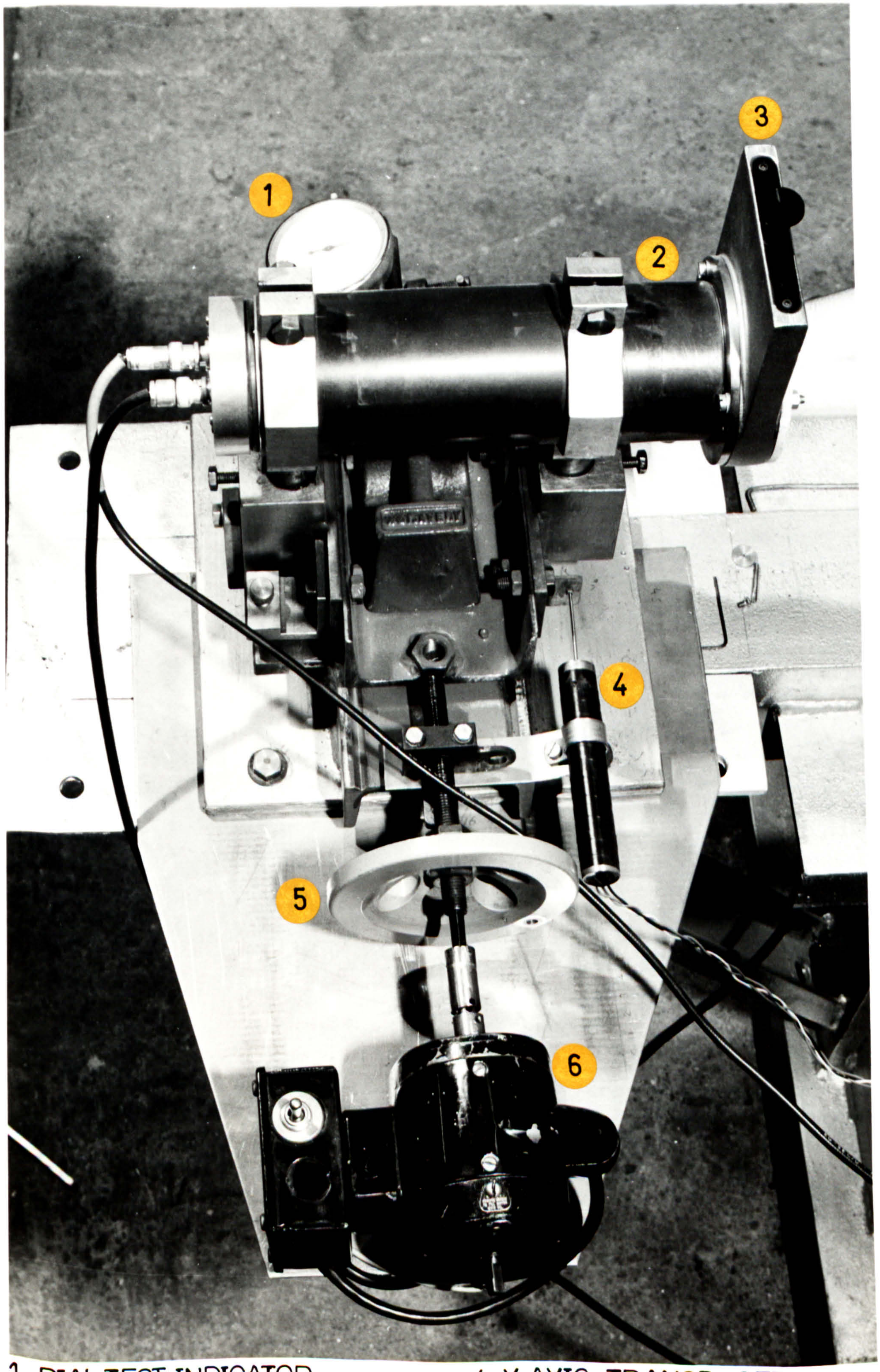

1_DIAL TEST INDICATOR
2_PHOTOMULTIPLIER
3_SHUTTER
4_X-AXIS TRANSDUCER
5_TRAVERSING WHEEL
6_TRAVERSING MOTOR